

Pertanika Journal of
**SCIENCE &
TECHNOLOGY**

JST

VOL. 32 (S2) 2024

*A Special Issue devoted to
Sustainable Design and Manufacturing*

Guest Editor
Mastura Mohammad Taha



A scientific journal published by Universiti Putra Malaysia Press

PERTANIKA JOURNAL OF SCIENCE & TECHNOLOGY

About the Journal

Overview

Pertanika Journal of Science & Technology is an official journal of Universiti Putra Malaysia. It is an open-access online scientific journal. It publishes original scientific outputs. It neither accepts nor commissions third party content.

Recognised internationally as the leading peer-reviewed interdisciplinary journal devoted to the publication of original papers, it serves as a forum for practical approaches to improve quality on issues pertaining to science and engineering and its related fields.

Pertanika Journal of Science & Technology currently publishes 6 issues a year (*January, March, April, July, August, and October*). It is considered for publication of original articles as per its scope. The journal publishes in **English** and it is open for submission by authors from all over the world.

The journal is available world-wide.

Aims and scope

Pertanika Journal of Science & Technology aims to provide a forum for high quality research related to science and engineering research. Areas relevant to the scope of the journal include: bioinformatics, bioscience, biotechnology and bio-molecular sciences, chemistry, computer science, ecology, engineering, engineering design, environmental control and management, mathematics and statistics, medicine and health sciences, nanotechnology, physics, safety and emergency management, and related fields of study.

History

Pertanika Journal of Science & Technology was founded in 1993 and focuses on research in science and engineering and its related fields.

Vision

To publish a journal of international repute.

Mission

Our goal is to bring the highest quality research to the widest possible audience.

Quality

We aim for excellence, sustained by a responsible and professional approach to journal publishing. Submissions can expect to receive a decision within 90 days. The elapsed time from submission to publication for the articles averages 180 days. We are working towards decreasing the processing time with the help of our editors and the reviewers.

Abstracting and indexing of Pertanika

Pertanika Journal of Science & Technology is now over 27 years old; this accumulated knowledge and experience has resulted the journal being abstracted and indexed in SCOPUS (Elsevier), Clarivate Web of Science (ESCI), EBSCO, ASEAN CITATION INDEX, Microsoft Academic, Google Scholar, and MyCite.

Citing journal articles

The abbreviation for Pertanika Journal of Science & Technology is *Pertanika J. Sci. & Technol.*

Publication policy

Pertanika policy prohibits an author from submitting the same manuscript for concurrent consideration by two or more publications. It prohibits as well publication of any manuscript that has already been published either in whole or substantial part elsewhere. It also does not permit publication of manuscript that has been published in full in proceedings.

Code of Ethics

The *Pertanika* journals and Universiti Putra Malaysia take seriously the responsibility of all of its journal publications to reflect the highest in publication ethics. Thus, all journals and journal editors are expected to abide by the journal's codes of ethics. Refer to *Pertanika*'s **Code of Ethics** for full details, or visit the journal's web link at http://www.pertanika.upm.edu.my/code_of_ethics.php

Originality

The author must ensure that when a manuscript is submitted to *Pertanika*, the manuscript must be an original work. The author should check the manuscript for any possible plagiarism using any program such as Turn-It-In or any other software before submitting the manuscripts to the *Pertanika* Editorial Office, Journal Division.

All submitted manuscripts must be in the journal's acceptable similarity index range:
≤ 20% – PASS; > 20% – REJECT.

International Standard Serial Number (ISSN)

An ISSN is an 8-digit code used to identify periodicals such as journals of all kinds and on all media—print and electronic.

Pertanika Journal of Science & Technology: e-ISSN 2231-8526 (Online).

Lag time

A decision on acceptance or rejection of a manuscript is reached in 90 days (average). The elapsed time from submission to publication for the articles averages 180 days.

Authorship

Authors are not permitted to add or remove any names from the authorship provided at the time of initial submission without the consent of the journal's Chief Executive Editor.

Manuscript preparation

For manuscript preparation, authors may refer to *Pertanika*'s **INSTRUCTION TO AUTHORS**, available on the official website of *Pertanika*.

Editorial process

Authors who complete any submission are notified with an acknowledgement containing a manuscript ID on receipt of a manuscript, and upon the editorial decision regarding publication.

Pertanika follows a **double-blind peer-review** process. Manuscripts deemed suitable for publication are sent to reviewers. Authors are encouraged to suggest names of at least 3 potential reviewers at the time of submission of their manuscripts to *Pertanika*, but the editors will make the final selection and are not, however, bound by these suggestions.

Notification of the editorial decision is usually provided within 90 days from the receipt of manuscript. Publication of solicited manuscripts is not guaranteed. In most cases, manuscripts are accepted conditionally, pending an author's revision of the material.

The journal's peer review

In the peer-review process, 2 to 3 referees independently evaluate the scientific quality of the submitted manuscripts. At least 2 referee reports are required to help make a decision.

Peer reviewers are experts chosen by journal editors to provide written assessment of the **strengths** and **weaknesses** of written research, with the aim of improving the reporting of research and identifying the most appropriate and highest quality material for the journal.

Operating and review process

What happens to a manuscript once it is submitted to *Pertanika*? Typically, there are 7 steps to the editorial review process:

1. The journal's Chief Executive Editor and the Editor-in-Chief examine the paper to determine whether it is relevance to journal needs in terms of novelty, impact, design, procedure, language as well as presentation and allow it to proceed to the reviewing process. If not appropriate, the manuscript is rejected outright and the author is informed.
2. The Chief Executive Editor sends the article-identifying information having been removed, to 2 to 3 reviewers. They are specialists in the subject matter of the article. The Chief Executive Editor requests that they complete the review within 3 weeks.

Comments to authors are about the appropriateness and adequacy of the theoretical or conceptual framework, literature review, method, results and discussion, and conclusions. Reviewers often include suggestions for strengthening of the manuscript. Comments to the editor are in the nature of the significance of the work and its potential contribution to the research field.

3. The Editor-in-Chief examines the review reports and decides whether to accept or reject the manuscript, invite the authors to revise and resubmit the manuscript, or seek additional review reports. In rare instances, the manuscript is accepted with almost no revision. Almost without exception, reviewers' comments (to the authors) are forwarded to the authors. If a revision is indicated, the editor provides guidelines for attending to the reviewers' suggestions and perhaps additional advice about revising the manuscript.
4. The authors decide whether and how to address the reviewers' comments and criticisms and the editor's concerns. The authors return a revised version of the paper to the Chief Executive Editor along with specific information describing how they have addressed the concerns of the reviewers and the editor, usually in a tabular form. The authors may also submit a rebuttal if there is a need especially when the authors disagree with certain comments provided by reviewers.
5. The Chief Executive Editor sends the revised manuscript out for re-review. Typically, at least 1 of the original reviewers will be asked to examine the article.
6. When the reviewers have completed their work, the Editor-in-Chief examines their comments and decides whether the manuscript is ready to be published, needs another round of revisions, or should be rejected. If the decision is to accept, the Chief Executive Editor is notified.
7. The Chief Executive Editor reserves the final right to accept or reject any material for publication, if the processing of a particular manuscript is deemed not to be in compliance with the S.O.P. of *Pertanika*. An acceptance letter is sent to all the authors.

The editorial office ensures that the manuscript adheres to the correct style (in-text citations, the reference list, and tables are typical areas of concern, clarity, and grammar). The authors are asked to respond to any minor queries by the editorial office. Following these corrections, page proofs are mailed to the corresponding authors for their final approval. At this point, **only essential changes are accepted**. Finally, the manuscript appears in the pages of the journal and is posted on-line.

Pertanika Journal of
**SCIENCE
& TECHNOLOGY**

A Special Issue devoted to
Sustainable Design and Manufacturing

Vol. 32 (S2) 2024
(Special Issue)

Guest Editor
Mastura Mohammad Taha



A scientific journal published by Universiti Putra Malaysia Press

EDITOR-IN-CHIEF

Luqman Chuah Abdullah
Chemical Engineering

CHIEF EXECUTIVE EDITOR

Mohd Sapuan Salit

UNIVERSITY PUBLICATIONS COMMITTEE

CHAIRMAN

Zamberi Sekawi

EDITORIAL STAFF

Journal Officers:

Ellyianur Puteri Zainal
Kanagamalar Silvarajoo
Siti Zuhaila Abd Wahid
Tee Syin Ying

Editorial Assistants:

Ku Ida Mastura Ku Baharom
Siti Juridah Mat Arip
Zulinaardawati Kamarudin

English Editor:

Norhanizah Ismail

PRODUCTION STAFF

Pre-press Officers:

Nur Farrah Dila Ismail
Wong Lih Jiun

WEBMASTER

IT Officer:

Illi Najwa Mohamad Sakri

EDITORIAL OFFICE

JOURNAL DIVISION

Putra Science Park
1st Floor, IDEA Tower II
UPM-IMTDC Technology Centre
Universiti Putra Malaysia
43400 Serdang, Selangor Malaysia.

General Enquiry

Tel. No: +603 9769 1622 | 1616

E-mail:

executive_editor.pertanika@upm.edu.my

URL: www.journals-jd.upm.edu.my

PUBLISHER

UPM Press

Universiti Putra Malaysia
43400 UPM, Serdang, Selangor, Malaysia.
Tel: +603 9769 8851
E-mail: penerbit@putra.upm.edu.my
URL: <http://penerbit.upm.edu.my>



ASSOCIATE EDITOR

2023-2024

Adem Kilicman

Mathematical Sciences
Universiti Putra Malaysia, Malaysia

Miss Laiha Mat Kiah

Security Services Sn: Digital Forensic,
Steganography, Network Security,
Information Security, Communication
Protocols, Security Protocols
Universiti Malaya, Malaysia

Saidur Rahman

Renewable Energy, Nanofluids, Energy
Efficiency, Heat Transfer, Energy Policy
Sunway University, Malaysia

EDITORIAL BOARD

2022-2024

Abdul Latif Ahmad

Chemical Engineering
Universiti Sains Malaysia, Malaysia

Ho Yuh-Shan

Water research, Chemical Engineering
and Environmental Studies
Asia University, Taiwan

Mohd Zulkifly Abdullah

Fluid Mechanics, Heat Transfer,
Computational Fluid Dynamics (CFD)
Universiti Sains Malaysia, Malaysia

Ahmad Zaharin Aris

Hydrochemistry, Environmental
Chemistry, Environmental Forensics,
Heavy Metals
Universiti Putra Malaysia, Malaysia

Hsiu-Po Kuo

Chemical Engineering
National Taiwan University, Taiwan

Mohd. Ali Hassan

Bioprocess Engineering, Environmental
Biotechnology
Universiti Putra Malaysia, Malaysia

Azlina Harun@Kamaruddin

Enzyme Technology, Fermentation
Technology
Universiti Sains Malaysia, Malaysia

Ivan D. Rukhlenko

Nonlinear Optics, Silicon Photonics,
Plasmonics and Nanotechnology
The University of Sydney, Australia

Nor Azah Yusof

Biosensors, Chemical Sensor, Functional
Material
Universiti Putra Malaysia, Malaysia

Bassim H. Hameed

Chemical Engineering: Reaction
Engineering, Environmental Catalysis &
Adsorption
Qatar University, Qatar

Lee Keat Teong

Energy Environment, Reaction
Engineering, Waste Utilization,
Renewable Energy
Universiti Sains Malaysia, Malaysia

Norbahiah Misran

Communication Engineering
Universiti Kebangsaan Malaysia,
Malaysia

Biswajeet Pradhan

Digital image processing, Geographical
Information System (GIS), Remote
Sensing
University of Technology Sydney,
Australia

Mohamed Othman

Communication Technology and
Network, Scientific Computing
Universiti Putra Malaysia, Malaysia

Roslan Abd-Shukur

Physics & Materials Physics,
Superconducting Materials
Universiti Kebangsaan Malaysia,
Malaysia

Daud Ahmad Israf Ali

Cell Biology, Biochemical, Pharmacology
Universiti Putra Malaysia, Malaysia

Mohd Shukry Abdul Majid

Polymer Composites, Composite
Pipes, Natural Fibre Composites,
Biodegradable Composites, Bio-
Composites
Universiti Malaysia Perlis, Malaysia

Wing Keong Ng

Aquaculture, Aquatic Animal Nutrition,
Aqua Feed Technology
Universiti Sains Malaysia, Malaysia

INTERNATIONAL ADVISORY BOARD

2021-2024

CHUNG, Neal Tai-Shung

Polymer Science, Composite and
Materials Science
National University of Singapore,
Singapore

Mohamed Pourkashanian

Mechanical Engineering, Energy, CFD
and Combustion Processes
Sheffield University, United Kingdom

Yulong Ding

Particle Science & Thermal Engineering
University of Birmingham, United
Kingdom

Hiroshi Uyama

Polymer Chemistry, Organic
Compounds, Coating, Chemical
Engineering
Osaka University, Japan

Mohini Sain

Material Science, Biocomposites,
Biomaterials
University of Toronto, Canada

ABSTRACTING AND INDEXING OF PERTANIKA JOURNALS

The journal is indexed in SCOPUS (Elsevier), Clarivate-Emerging Sources Citation Index (ESCI), BIOSIS, National Agricultural Science (NAL), Google Scholar, MyCite, ISC. In addition, Pertanika JSSH is recipient of "CREAM" Award conferred by Ministry of Higher Education (MoHE), Malaysia.

The publisher of Pertanika will not be responsible for the statements made by the authors in any articles published in the journal. Under no circumstances will the publisher of this publication be liable for any loss or damage caused by your reliance on the advice, opinion or information obtained either explicitly or implied through the contents of this publication.

All rights of reproduction are reserved in respect of all papers, articles, illustrations, etc., published in Pertanika. Pertanika provides free access to the full text of research articles for anyone, web-wide. It does not charge either its authors or author-institution for refereeing/publishing outgoing articles or user-institution for accessing incoming articles.

No material published in Pertanika may be reproduced or stored on microfilm or in electronic, optical or magnetic form without the written authorization of the Publisher.

Copyright © 2021 Universiti Putra Malaysia Press. All Rights Reserved.

Pertanika Journal of Science & Technology
Vol. 32 (S2) 2024

Contents

Sustainable Design and Manufacturing

Preface	i
<i>Mastura Mohammad Taha</i>	
Flow Analysis and Shear Rate Comparison of Counter-rotating and Co-rotating Intermeshing Twin-screw Extruders for Filament Extrusion of Polypropylene-based Biocomposites	1
<i>Abdul Munir Hidayat Syah Lubis, Syahibudil Ikhwan Abdul Kudus, Ammar Syafi Amran, Nuzaimah Mustafa, Mastura Mohammad Taha and Mohd Adrinata Shahraruzaman</i>	
Conceptual Design and Materials Selection of the FDM Composites for Passenger Vehicle's Spoiler	21
<i>Mohd Adrinata Shahraruzaman, Syed Muhammad Ayyub Sayed Idros, Mastura Mohammad Taha, Muhd Ridzuan Mansor, Ridhwan Jumaidin and Hilmi Senan</i>	
Environmental Assessment on Fabrication of Bio-composite Filament Fused Deposition Modeling Through Life Cycle Analysis	37
<i>Muhammad Farhan, Mastura Mohammad Taha, Yusliza Yusuf, Syahrul Azwan Sundi and Nazri Huzaimi Zakaria</i>	
A Study on the Thermal Distribution of the Thermoforming Process for Polyphenylene Sulfite (Polyphenylene Sulfide) PPS Composites Towards Out of Autoclave Activity	49
<i>Bushra Rashid, Nadlene Razali, Mohamad Shukri Zakaria, Muhammad Zaid Harith Ramlan, Hasanudin Hamdan, Emy Aqillah Sharif, Noryani Muhammad and Syazwan Ahmad Rashidi</i>	
Material Selection of Natural Fibre Composite Webbing Sling Using Rule of Mixture	61
<i>Noryani Muhammad, Nur Ain Fatimah Roslan and Mohd Syahril Abd Rahman</i>	
The Influence of MAPP and MAPE Compatibilizers on Physical and Mechanical Properties of 3D Printing Filament Made of Wood Fiber/ Recycled Polypropylene	77
<i>Nuzaimah Mustafa, Yusliza Yusuf, Syahibudil Ikhwan Abdul Kudus, Nadlene Razali, Dwi Hadi Sulistyarini, Mohd Hafizi Halim and Aenderson Chaong Anak Ujih</i>	

Mechanical Properties of Thermoplastic Cassava Starch/Coconut Fibre Composites: Effect of Fibre Size	91
<i>Ridhwan Jumaidin, Ainin Sofiya Gazari, Zatil Hafila Kamaruddin, Zatil Hazrati Kamaruddin, Nazri Huzaimi Zakaria, Syahibudil Ikhwan Abdul Kudus, Mohd Shukri Yob, Fudhail Abd Munir and Meysam Keshavarz</i>	
Design Ideation and Selection of Under-Piston Door for a Two-stroke Marine Engine Using Hybrid TRIZ-biomimetic and MCDM Methods	115
<i>Yiow Ru Vern, Muhd Ridzuan Mansor, Mohd Adrinata Shahraruzaman and Basori</i>	
Effect of Cutting Speed and Feed Per Tooth on the Trimmed Surface Roughness and Tool Wear During Milling of CFRP: Aerostructural Part	135
<i>Syahrul Azwan Sundi, Izzat Afandi Abdul Hakim, Mohd Farid Mahadi, Noramin Nazar Shah, Raja Izamshah, Intan Sharhida Othman, Mohd Shahir Kasim and Mohd Nor Hafizi Noordin</i>	
The Mechanical and Physical Properties of 3D Printing Filament made from Recycled Polypropylene and Ground Tyre Rubber Treated with Alkali	151
<i>Yusliza Yusuf, Nuzaimah Mustafa, Yusra Fitri Yusoff and Dwi Hadi Sulistyarini</i>	

Preface

As we approach the advent of the next industrial revolution, the principle of sustainability has increased awareness among industrial players regarding the imperative to manage waste production and resource consumption through closed-loop life cycle processes. This approach aims to yield positive economic, environmental, and societal outcomes. Consequently, researchers have increasingly emphasized environmental sustainability by utilizing renewable resources, such as bio-composite materials, in product design innovation and manufacturing technology. These materials are widely used in automotive component design, consumer product design, medical instruments and the food and packaging industries due to their sustainability, renewability, comparable performance to traditional materials and cost-effectiveness. To further explore the potential of bio-composite materials, this special issue examines the effectiveness of integrating ecological systems, economic considerations, and social factors to achieve sustainable design and manufacturing processes.

In addition to emphasizing bio-composite materials for product innovation, this special issue also includes recent advancements in manufacturing processes and technology. It is widely recognized that most manufacturing methods for composite-based products involve moulds shaping the final products. However, regarding dimensional accuracy, products manufactured through this method typically achieve only approximate final dimensions, known as near-net-shape products. Therefore, addressing the need for additional processes to ensure final dimensional accuracy and surface finish is crucial. This special issue addresses recent challenges in manufacturing composite-based products.

We believe that all the papers published in this special issue will provide valuable insights to researchers in the related field, serving as an excellent platform for readers to access the latest findings in sustainable design and manufacturing technologies. We thank all the authors who contributed to this special issue.

Guest Editor

Mastura Mohammad Taha (*Dr.*)

Flow Analysis and Shear Rate Comparison of Counter-rotating and Co-rotating Intermeshing Twin-screw Extruders for Filament Extrusion of Polypropylene-based Biocomposites

Abdul Munir Hidayat Syah Lubis¹, Syahibudil Ikhwan Abdul Kudus^{2*}, Ammar Syafi Amran², Nuzaimah Mustafa², Mastura Mohammad Taha² and Mohd Adrinata Shaharuzaman³

¹Department of Mechanical Engineering, Faculty of Engineering, Universitas Muhammadiyah, Surakarta, Indonesia

²Fakulti Teknologi dan Kejuruteraan Industri dan Pembuatan, Universiti Teknikal Malaysia Melaka, Hang Tuah Jaya, 76100 Durian Tunggal Melaka, Malaysia

³Fakulti Teknologi dan Kejuruteraan Mekanikal, Universiti Teknikal Malaysia Melaka, Hang Tuah Jaya, 76100 Durian Tunggal Melaka, Malaysia

ABSTRACT

This study investigates and compares the performance of counter-rotating and co-rotating intermeshing twin-screw designs in filament extruder machines. The research sought to determine whether the counter-rotating intermeshing design with its opposite flow direction offers advantages over the co-rotating intermeshing design in terms of flow analysis and shear rates. Flow analysis was conducted to examine the velocity of the polypropylene-based biocomposite material inside the barrel. Shear rate data was obtained by evaluating the relationship between shear rate and screw speed to assess the stability

and maximum shear rate of the twin-screw extruders. The results revealed that the counter-rotating intermeshing twin-screw extruders exhibited higher shear rates and more consistent pressure compared to the co-rotating intermeshing design. The superiority of the counter-rotating extruder was attributed to its opposite flow direction and distinct thread shapes, facilitating efficient material compression and improved dispersion of polymer-based biocomposite materials. The study suggested the potential for further exploration and refinement of

ARTICLE INFO

Article history:

Received: 16 August 2023

Accepted: 09 May 2024

Published: 14 June 2024

DOI: <https://doi.org/10.47836/pjst.32.S2.01>

E-mail addresses:

amh612@ums.ac.id (Abdul Munir Hidayat Syah Lubis)

syahibudil@utem.edu.my (Syahibudil Ikhwan Abdul Kudus)

ammrsyfii@gmail.com (Ammar Syafi Amran)

nuzaimah@utem.edu.my (Nuzaimah Mustafa)

mastura.taha@utem.edu.my (Mastura Mohammad Taha)

adrinata@utem.edu.my (Mohd Adrinata Shaharuzaman)

* Corresponding author

the counter-rotating intermeshing twin-screw extruder design, particularly in producing polypropylene-based biocomposite filaments for Fused Deposition Modeling (FDM) machines.

Keywords: Counter-rotating intermeshing, filament extruder machines, flow analysis, twin-screw designs, shear rates

INTRODUCTION

The use of natural fibers in producing biocomposite filaments has gained increasing popularity due to their environmental friendliness and potential for economic benefit. The integration of additive manufacturing (AM) technology has revolutionized the production of biocomposite filaments for Fused Deposition Modelling (FDM), which provides opportunities for developing sustainable, biodegradable products. To produce FDM filament, twin-screw extruders have played a significant role in the formulation and production of biocomposite filaments by providing excellent shear mixing to ensure uniform dispersion of natural fibers (Khalid & Billa, 2022; Yang et al., 2018).

Biocomposite filaments are made up of natural fibers combined with a polymer matrix. Natural fibers such as kenaf, coconut, corn, and hemp are renewable and biodegradable, making them an ideal choice for producing sustainable consumer products (Cali et al., 2020; Deb & Jafferson, 2021; Rett et al., 2021; Xiao et al., 2019). The polymer matrix is usually composed of synthetic materials such as polypropylene (PP), which are biodegradable, and some others are readily recyclable.

Manufacturing biocomposite filaments presents challenges due to the distinct properties of natural fibers and the polymer matrix (Balla et al., 2019). Achieving homogeneity in the mixture is crucial but can be difficult. Twin-screw extruder technology has emerged as an effective solution for addressing these issues (Liu et al., 2021; Ren et al., 2023). The versatility of twin-screw extruders makes them suitable for various industrial applications, including producing biocomposite filaments (Bauer et al., 2022; Senturk-Ozer et al., 2011; Zheng et al., 2022). Incorporating different natural fibers and polymer types can be easily achieved, ensuring a wide range of material combinations.

Moreover, twin-screw extruders offer high efficiency, enabling high throughput rates and ensuring repeatability, which is vital for industrial-scale production (Hejna et al., 2021). Twin-screw extruders find applications beyond compounding plastics; they are also used in food production (e.g., breakfast cereals and chocolates), pharmaceutical manufacturing, and chemical production. Continuous advancements in twin-screw extruder technology further enhance their efficiency and versatility, addressing the challenges of extruding biocomposite-reinforced polymer filaments.

On the other hand, AM, commonly known as 3D printing, has revolutionized the production of biocomposite filaments. 3D printing allows for developing sustainable

products with intricate designs, making it ideal for customized and personalized product development. FDM works by melting a thermoplastic filament and depositing it layer-by-layer to create a 3D object. Natural fibers biocomposite filaments can be utilized in FDM to create sustainable products, such as consumer product designs, biomedical devices, and biodegradable packaging. These materials can reduce carbon footprint, minimize waste, and improve the environmental impact of the manufacturing process. As the technology continues to develop, more applications of these materials are expected in AM, particularly in FDM.

The increasing demand for sustainable materials drives the need for more environmentally friendly alternatives. Growing market demand for biodegradable polymer and natural fiber composites presents a significant opportunity for twin-screw extruders to play a key role in meeting these needs. Henceforth, twin-screw extruder technology is significant for producing sustainable and eco-friendly materials to meet the demand for more environmentally friendly products.

The study presents an investigation comparing the performance of co-rotating and counter-rotating twin-screw extruders in terms of their capability to effectively mix biocomposite-reinforced polypropylene (PP) for producing FDM filament. The study involved a comprehensive analysis that included designing the twin screws using SolidWorks software and evaluating them through simulation analysis using computational fluid dynamics (CFD) software. The primary objective of the investigation is to determine which type of screw extruder demonstrates superior performance in terms of mixing efficiency and the quality of the resulting filament. By utilizing advanced design and simulation techniques, the study aims to provide valuable insights into the selection and optimization of screw extruders to produce high-quality biocomposite-reinforced PP filaments for FDM-based AM applications.

Literature Review

FDM 3D printers use thermoplastic filament to make 3D printed parts by adding layers from materials such as acrylonitrile butadiene styrene (ABS), polylactic acid (PLA), polypropylene (PP), and polycarbonate (PC). In recent years, researchers have increased the effort to develop alternative biocomposite filaments available for FDM by mixing the thermoplastic material with natural fibers (Han et al., 2019; Kariz et al., 2018; Mastura et al., 2020; Mazzanti et al., 2019). In Malaysia, sources of natural fibers such as kenaf, sugar palm, wood dust, and oil palm fruit bunch are cheap and abundant; therefore, they are ready to be exploited (Aida et al., 2021). The utilization of natural fiber-reinforced polymer composite as a filament in FDM is a subject that has not been widely explored. Nonetheless, incorporating them in FDM presents advantages such as accelerated prototyping processes when dealing with these materials.

The production process for natural fiber-reinforced polymer composite filaments is similar to that of conventional filaments, typically made from a single material such as PP or ABS. However, adding natural fiber to the composite filaments introduces another step of mixing the fibers with the thermoplastic polymer. Generally, the production process for filaments involves several steps. The natural fibers, which can come from kenaf, sugar palm, wood, or coconut, are cleaned and dried to remove impurities. They are then mixed with the thermoplastic polymer pellets.

During filament extrusion, materials in pellet form are fed from a hopper to the barrel. Rod heaters melt the materials, and a screw moves them longitudinally along the barrel through three zones, which are: feed, melt, and metering (Pitayachaval & Watcharamaisakul, 2019). Compression, shearing, and heating will liquefy the granules. The melted plastic moves through the metering zone into the die, which will be pumped out in a 1.75 mm or 3 mm diameter filament. The hot filament is cooled down by water or a cooling fan system and wound onto a spool. The resulting filament is a biocomposite material with the strength and durability of natural fibers combined with the thermoplastic polymer's flexibility and ease of use. Figure 1 shows the schematic diagram of the filament extruder setting.

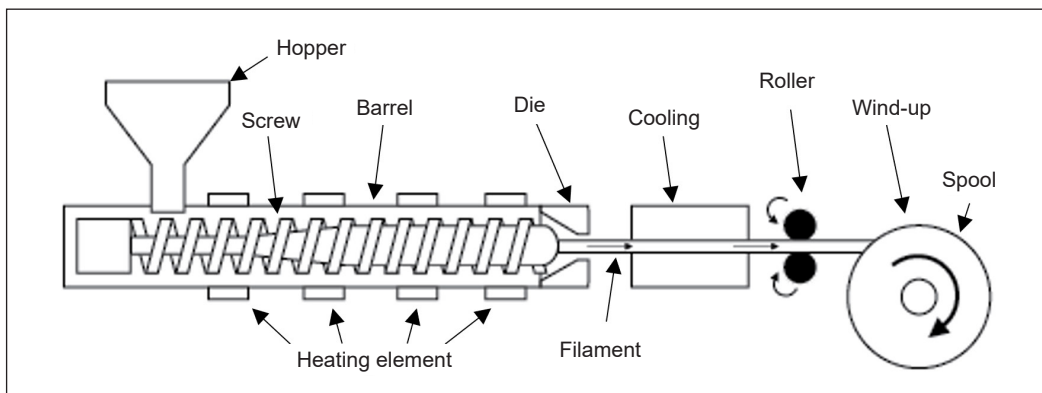


Figure 1. Schematic diagram of filament extruder setting

Natural fiber tends to be clumped, resulting in poor mechanical properties and inconsistencies. Another challenge in extruding natural fiber-reinforced polymer composites is achieving a uniform fiber orientation throughout the material. The orientation of the fibers can also greatly affect the mechanical properties of the filament, and achieving consistent orientation can be difficult due to the complex rheological behavior of the materials during extrusion. Several techniques have been developed to improve the dispersion of natural fibers in the polymer matrix, such as using a twin-screw extruder, which is able to provide better mixing capabilities to address this issue (Royan et al., 2021).

Generally, there are two types of filament extruder machines, which can be categorized based on the screw used in a barrel. They are single-screw and twin-screw extruders. Twin-

screw extruders have two screws that rotate within a barrel. As the material moves through the barrel, it is heated and mixed using various heating and mixing elements. The pressure created by the rotation of the screw forces the material through the die, which shapes the material into desired form. The screws are designed to intermesh, creating a self-wiping action that mixes and shears the material as it moves through the barrel. The intermeshing action of the screws allows better mixing and processing of the material compared to a single-screw extruder (Netto et al., 2022). The twin-screw extruder has certain benefits over the single twin-screw extruder as it does not need to use drag force to move the material. This results in lower shear heat, more effective mixing, and reduced flexibility for slow-speed tasks (Pitayachaval & Watcharamaisakul, 2019). Therefore, the advantages of twin-screw extruders make them a popular choice in industries where precise control over the manufacturing process is essential.

The intermeshing system is a key feature of twin-screw extruders that enables them to process materials effectively. There are three types of intermeshing twin-screw extruders: (1) non-intermeshing twin-screw extruders, (2) partially intermeshing twin-screw extruders, and (3) fully-intermesh twin-screw extruders. Opposed to fully intermeshing twin-screw extruders, non- and partially intermeshing twin-screw extruders have a gap between the screws. In contrast to non-intermeshing twin-screw extruders, fully intermeshing twin-screw extruders typically have a more complex screw design with kneading and mixing elements that enhance the mixing and shearing of materials. Therefore, fully intermeshing twin-screw extruders are designed for high-shear and high-mixing applications, while non-intermeshing twin-screw extruders are typically used for low-shear applications.

In this system, the screws rotate in either co-rotating or counter-rotating directions in the barrel. According to Rauwendaal's classic literature (1981), intermeshing counter-rotating extruders are screw characters that are good at moving material through the barrel quickly and evenly, which is important when working with heat-sensitive materials like PVC. They are operated at low speeds, typically between 10 to 30 rpm. By using these screw designs, heat exposure can be minimized, and the risk of damage to the material can be reduced. Therefore, a fully intermeshing, counter-rotating twin-screw extruder can achieve the highest positive conveying. Figure 2 shows the cylindrical, fully-intermeshing, counter-rotating twin-screw extruder. In contrast, Figure 3 shows the cylindrical, fully-intermeshing, co-rotating twin-screw extruder, and Figure 4 shows the extrusion screw geometry parameter guideline (Pitayachaval & Watcharamaisakul, 2019).

Understanding critical factors is essential for guaranteeing filament quality. Three pivotal parameters stand out: screw design, temperature control, and material feed rate (Chen et al., 2017; Kittikunakorn et al., 2020; Yacu, 2020). Screw design influences mixing, shearing, and conveying through the barrel, encompassing parameters such as diameter, pitch, length-to-diameter ratio (L/D ratio), flight depth, and helix angle. Larger

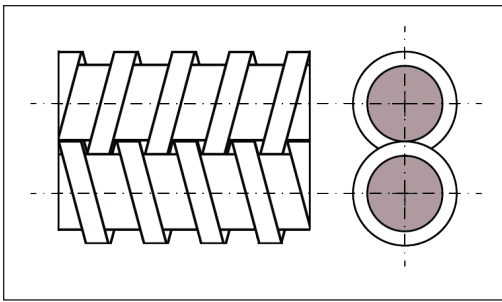


Figure 2. Cylindrical, fully intermeshing, counter-rotating twin-screw extruder

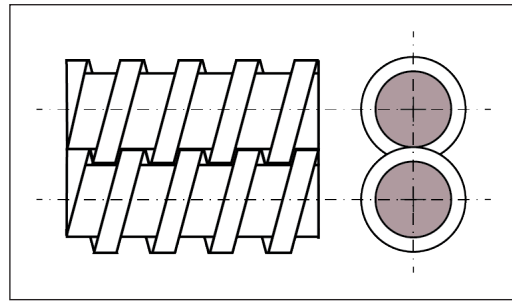


Figure 3. Cylindrical, fully-intermeshing, co-rotating twin-screw extruder

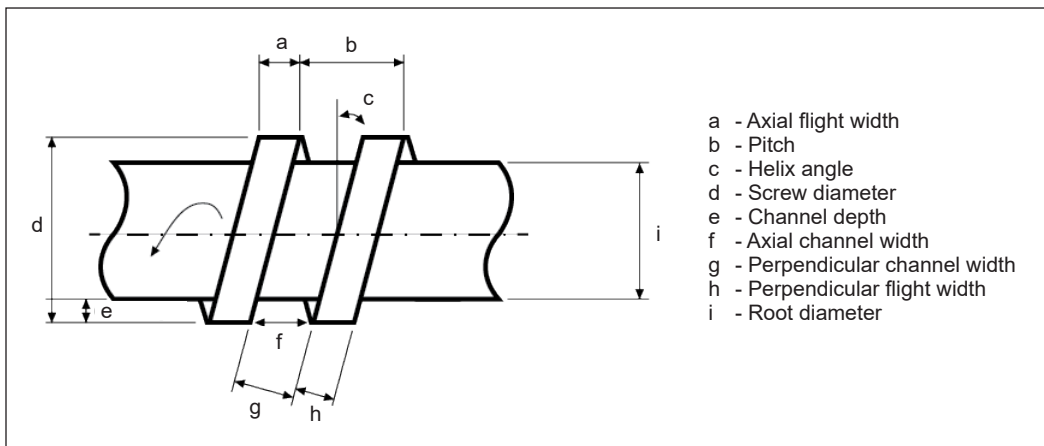


Figure 4. Extrusion screw geometry parameter guideline

screw diameters provide a greater surface area for heat transfer and mixing, which can be advantageous for materials that require extensive melting and mixing. The pitch of the screw, the distance between two flights along the axis, affects the residence time of the material in the barrel. A larger pitch produces faster material conveyance and a shorter residence time, which can be useful for heat-sensitive materials. The L/D ratio determines the residence time and the degree of mixing the material undergoes. Typically, a higher L/D ratio allows for more prolonged interaction between the material and the screws, leading to better mixing and homogenization (Irfan et al., 2021; Wang et al., 2023). Twin-screw extruders often have L/D ratios ranging from 20:1 to 40:1 (Dhaval et al., 2022; Jacobs et al., 2022).

According to Nandi et al. (2021), the flight depth, which is the distance from the screw core to the top of the flight, can be varied. Shallow flights create high shear and intensive mixing, while deeper flights result in gentle conveying with less shear. The appropriate flight depth depends on the material properties and the desired characteristics of the end product. On the other hand, the helix angle, the angle between the screw flight and the axis

of the screw, affects the forward conveying efficiency. A larger helix angle leads to better conveying efficiency, which is crucial for materials with poor flow properties.

Temperature control affects material viscosity, flow behavior, and final product properties, while precise control in heating and cooling zones is vital (Pitayachaval & Watcharamaisakul, 2019). The extruder barrel is divided into different heating and cooling zones; precise temperature control in each zone is essential. Material feed rate directly impacts output rate, residence time, and process stability (Rao et al., 2022; Zhuang et al., 2023). A consistent and uniform feed rate ensures steady conditions in the barrel. Fluctuations in feed rate can lead to variations in product dimensions, mechanical properties, and surface finish. The feed rate also influences the barrel's shear forces and mixing efficiency. A higher feed rate resulted in increased shear forces that benefit materials that require intense mixing. However, this can also cause overheating and material degradation if not properly managed (Thyashan et al., 2024; Wang et al., 2022). It is important to balance the material feed rate with the screw speed to ensure optimal processing conditions. A mismatch can lead to poor mixing, surging, or even blockages in the barrel.

Common extruder issues include screw wear, damage, and fouling, each affecting performance and output (Corleto et al., 2021; Demirci et al., 2021; Liu et al., 2021). Screw wear occurs over time due to the abrasion of the material being processed caused by exposure to certain chemicals or moisture, resulting in reduced performance and output. Screw damage can occur if foreign objects, such as hard plastics, enter the extruder. The damage can cause misalignment, leading to reduced performance, inconsistent output, or even failure of the extruder. Screw fouling, on the other hand, results from the accumulation of material on the screws and other surface within the extruder. It leads to reduced efficiency and output as well as increased wear and tear on the machine.

Co-rotating extruders excel in efficiency and material handling but require higher maintenance due to increased wear. In contrast, counter-rotating extruders offer lower initial investment and maintenance costs but with limited throughput and mixing capabilities. Table 1 provides a comparative table of co-rotating and counter-rotating fully intermeshing twin-screw extruders, focusing on various operational and performance aspects.

Recent studies have focused on twin-screw extruders to understand the material flow, mixing, and melting dynamics for both common polymers and polymer-based biocomposites (Dong et al., 2020; Irfan et al., 2021; Mysiukiewicz et al., 2020; Schall et al., 2023; Vergnes et al., 2022). Investigations delve into various performance aspects, including melting efficiency, pressure and temperature profiles, viscosity considerations, and the influence of processing conditions and screw design. Researchers explore how parameters like screw speed, feed rate, profile, pellet size, and extruder size affect melting efficiency and effectiveness (Lewandowski & Wilczyński, 2022; Stritzinger et al., 2021).

Table 1

Comparative table of co-rotating and counter-rotating fully intermeshing twin-screw extruders

Aspect	Co-rotating twin-screw extruder	Counter-rotating twin-screw extruder
Efficiency	High (excellent for complex and high output).	Moderate (better for low-shear, simple mixing)
Material Handling	Versatile (handles diverse and difficult materials).	Limited (best for less complex materials).
Maintenance	Higher cost (due to high-shear wear).	Lower cost (due to simpler design and lower wear).
Ease of operation	Complex (requires specialized knowledge).	Simpler (easier to operate and maintain).
Initial investment	Higher (reflected by advanced capabilities).	Lower (more cost-effective).
Throughput	High (suitable for high-volume production).	Lower (less suitable for high-volume production).
Mixing ability	Excellent (high shear and intensive kneading).	Less effective (due to lower shear force).
Degassing	Adequate.	Efficient.
Suitability	High-end applications (e.g., specialty plastic).	Straightforward tasks (e.g., PVC compounding).

Additionally, different screw configurations are examined to understand their role in shaping melting behavior and overall extruder performance. Computational Fluid Dynamics (CFD) analysis provides a comprehensive approach to evaluating extruder performance, allowing visualization of flow patterns, pressure gradients, and heat transfer characteristics (Prashanth et al., 2019). Through CFD simulations, researchers can identify areas for optimization and explore various design configurations and operational parameters to enhance filament fabrication technology.

MATERIALS AND METHODS

This study investigated two types of twin-screw filament extruders: counter-rotating intermeshing and co-rotating intermeshing. The dimensions of the twin-screw designs, including barrel diameter, screw tip diameter, screw root diameter, centerline distance, and screw pitch, are presented in Table 2. The schematic of the screw design is shown in Figure 5.

In the counter-rotating intermeshing design, one screw has a left-sided thread while the other screw has right-handed threads, enabling them to rotate in opposing

Table 2

Dimensions of twin-screw filament extruder

Item	Dimension
Barrel diameter (mm)	25
Screw tip diameter (mm)	25
Screw root diameter (mm)	15
Centerline distance (mm)	20
Screw pitch (mm)	6
Nozzle diameter (mm)	2

directions. Contrariwise, the co-rotating twin-screw design features identical right-handed threads, causing them to rotate in the same direction and speed. However, both designs have the same configuration in terms of the thread position, with the threads overlapping each other. The cross-sectional views of both twin-screw designs are depicted in Figure 6. Figures 7 and 8 show the twin-screw counter-rotating and co-rotating intermeshing orientation.

SolidWorks CFD software was utilized to analyze the material’s behavior as it flowed inside the barrel. PP was chosen as the polymer for the analysis, representing a copolymerized type that exhibits favorable characteristics for extrusion applications. Furthermore, PP serves as the polymer matrix in the natural fiber filament used in this study. The specific PP grade employed in the study possesses a melt flow rate of 1.8 g/10 min at 230°C and 2.16 kg, conforming to the ISO 1133 standard (Vincent et al., 2020).

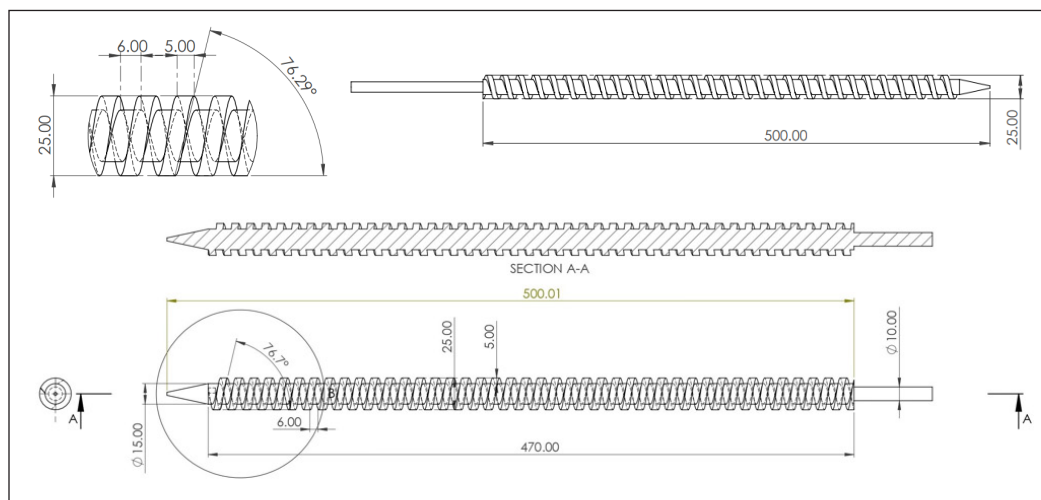


Figure 5. Dimension of the screw design

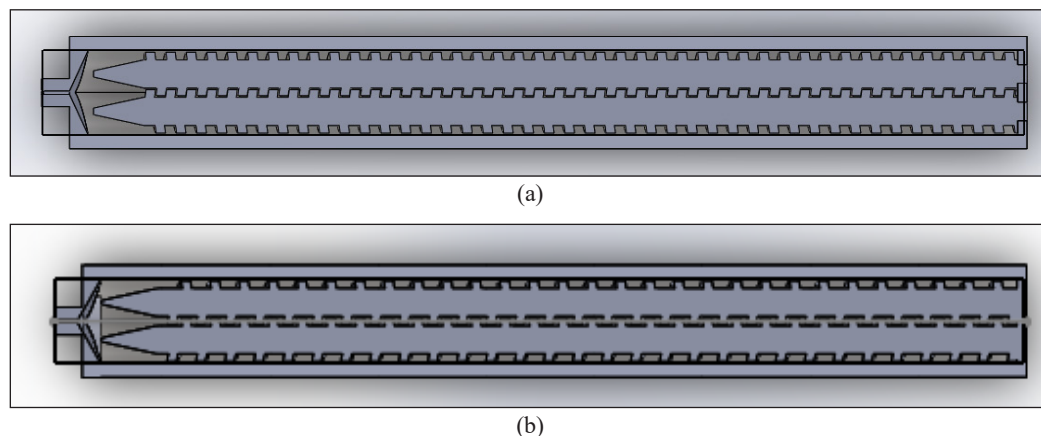


Figure 6. Cross-sectional view of (a) counter-rotating and (b) co-rotating, intermeshing twin-screws

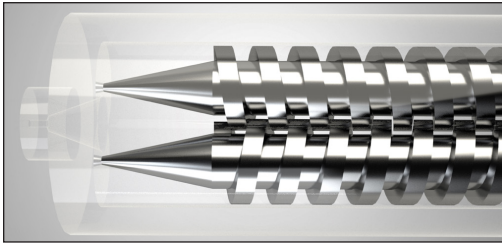


Figure 7. Twin-screw counter-rotating intermeshing orientation

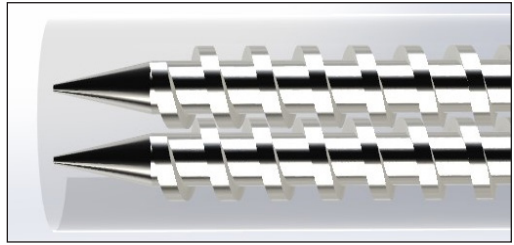


Figure 8. Twin-screw co-rotating intermeshing orientation

The extrusion screw's length-to-diameter (L/D) ratio needs to be considered to run the CFD analysis. The L/D ratio is a parameter used to describe the geometry of screws, especially in plastic-based extrusion screw machines. It represents the ratio of the flighted length of the screw to its outside diameter (Bauer et al., 2022). The L/D ratio was specified to be 20:1, which is the most standard ratio used in the industry. Both the counter-rotating and co-rotating extruder designs shared common specific parameters, including a screw diameter of 25 mm and a screw length of 500 mm. In conjunction with the L/D ratio calculation of $500/25=20:1$, these values were chosen to ensure accurate analysis of the material behavior within the barrel using SolidWorks CFD software. Additionally, a temperature setting of 190°C and a revolution-per-minute (rpm) speed of 26 rpm were applied to both the counter-rotating and co-rotating extruders. During the analysis, these operating conditions were maintained consistently for both extruder designs, facilitating a direct comparison of their performance.

RESULTS AND DISCUSSION

Velocity Flow Analysis on Counter-rotating Twin-screw Extruder

Figure 9 depicts the cross-sectional cut plot pressure flow inside the counter-rotating twin-screw chamber. In pressure analysis, the color scale visually represents pressure distribution and magnitude within a system, ranging from cooler colors for lower pressures to warmer colors for higher pressures. Researchers use this scale to identify pressure variations and pinpoint potential issues. The visualization facilitates quick interpretation of pressure data and enables comparative analysis under different conditions.

Observation from the simulation has shown that the pressure build-up build-up was consistent as the molten polymer spread across every corner of the screw threads. The counter-rotating design, along with the different shapes of screw threads, caused the pressure build-up at the intermesh section to overlap. Consequently, this increased drag on the material, especially when mixing composite materials.

Figure 10 shows the velocity analysis of the counter-rotating twin-screw extruder. Based on the analysis of velocity flow, the PP exhibited a flow through the barrel chamber

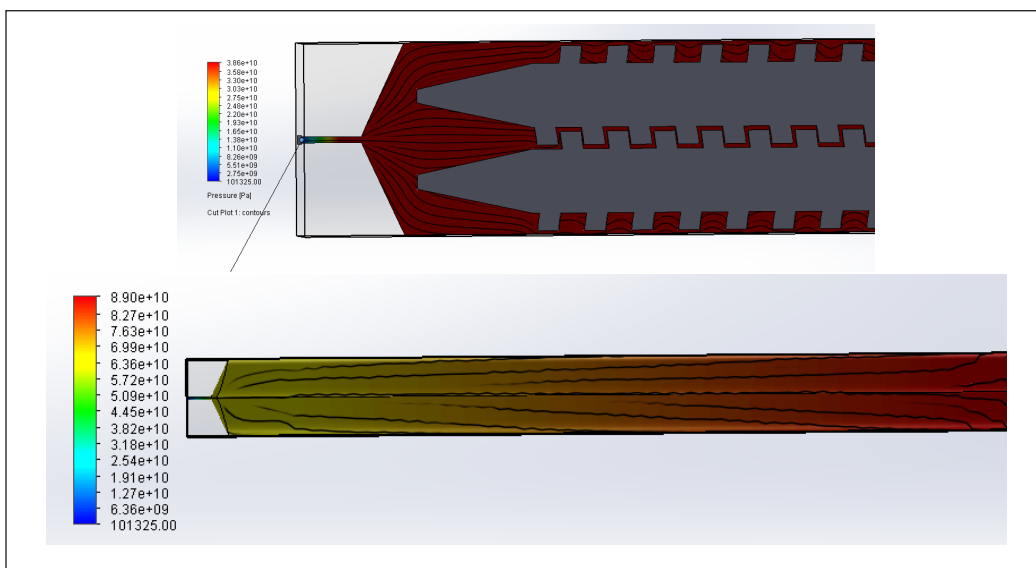


Figure 9. Cross-sectional cut plot pressure flow of counter-rotating twin-screw

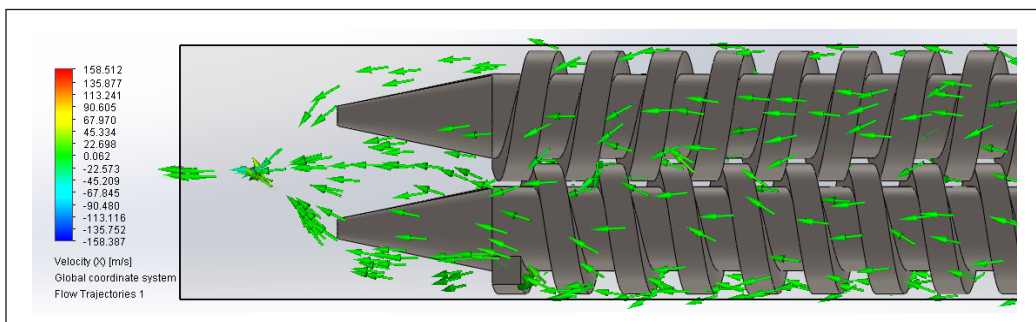


Figure 10. Velocity flow trajectory

at a temperature of 190°C. The counter-rotating twin screw compressed the material towards the nozzle exit, resulting in the resistance caused by the screw threads. This resistance led to a more complex flow pattern with multiple directions. The collision of the flow at the intermeshing section significantly increased the shear rate of the PP. Consequently, this enhanced the mixing of the material, allowing for better binding.

Figure 11 illustrates the relationship between velocity (m/s) and screw length (m), showcasing notable initial flow instability within the melting and mixing zones. The findings indicated that the molten PP attained stability at 0.0237 m or 23.78 mm from the melting initiation point, exhibiting a velocity of 0.0542 m/s or 54.2 mm/s. However, as the material progressed towards the nozzle exit, the flow was stabilized further.

Figure 12 presents the pressure variation with respect to the screw length. The findings demonstrated initial flow instability during the melting initiation and mixing zones.

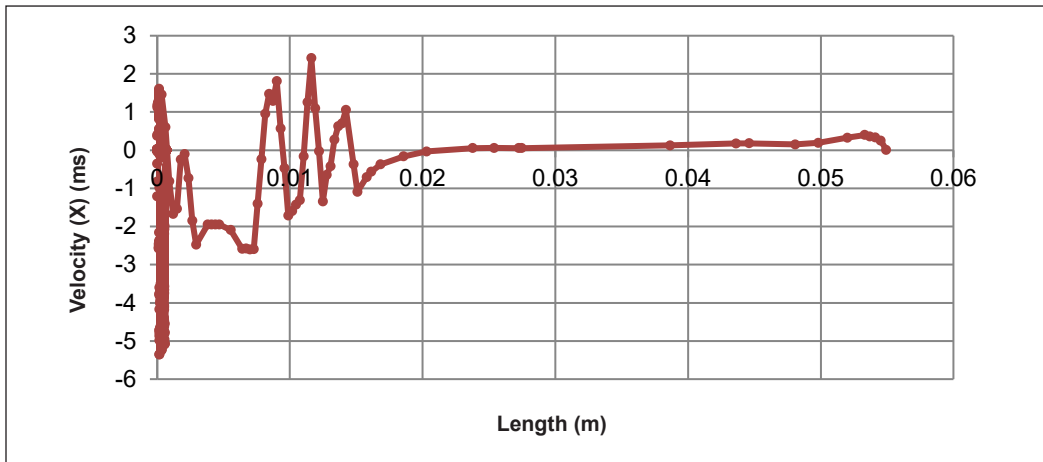


Figure 11. Velocity vs. screw length

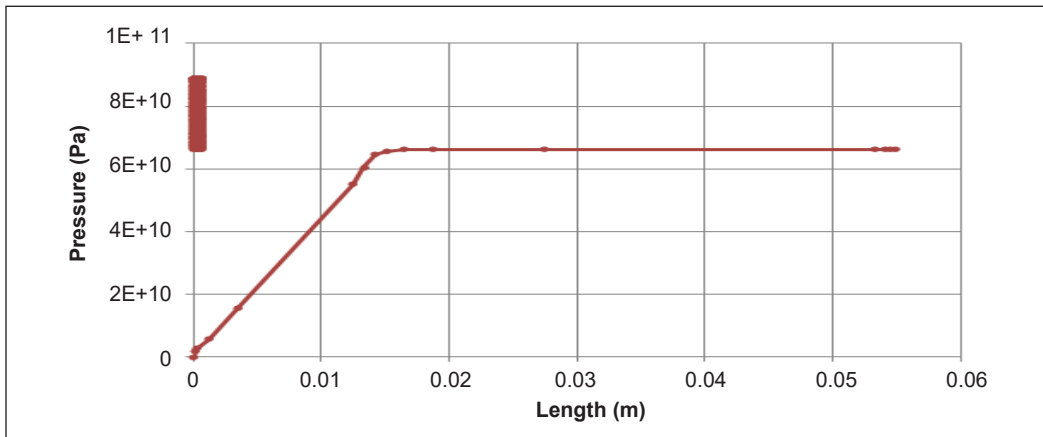


Figure 12. Pressure vs. screw length

However, as the flow advanced toward the nozzle exit, it exhibited enhanced stability. Examination of the accompanying chart revealed that the pressure within the extrusion melting zone initiated at 0.0164 m or 16.40 mm from the melting inlet, with a pressure reading of 6.6×10^{10} Pa.

Velocity Flow Analysis on Co-rotating Twin-screw Extruder

Figure 13 presents the cross-sectional view of the co-rotating twin screw, providing insight into the pressure build-up within the compression chamber. The color variations observed in the figures indicated increased pressure as the material approached the exit or nozzle. The nozzle itself was designed with 2.00 mm diameter holes. Notably, despite setting the initial pressure at 90 Pa from the starting point of the melting zone, there was a continuous increase in pressure.

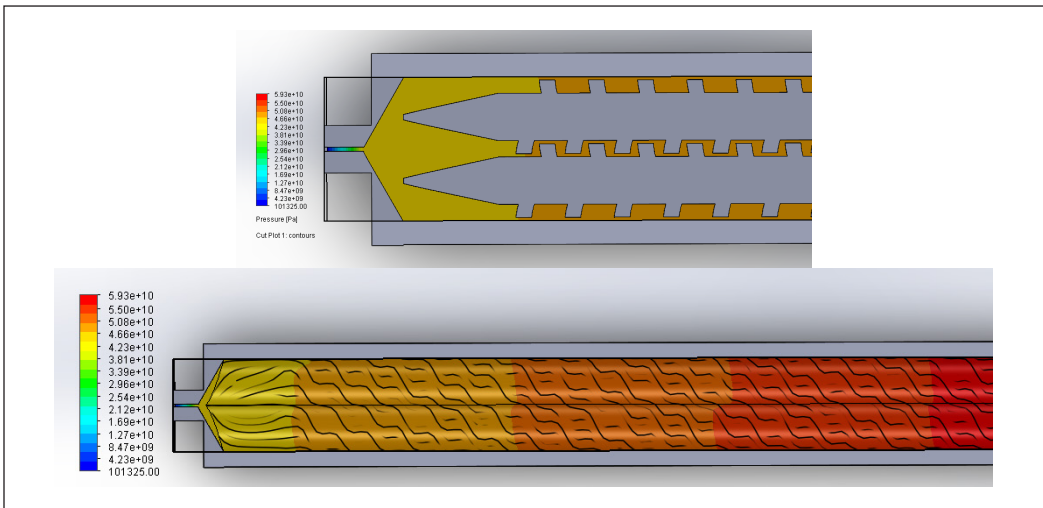


Figure 13. Cross-sectional cut plot pressure flow of co-rotating twin-screw

A further test was performed to determine the trajectory or flow of the molten PP when it was compressed by using the co-rotating and intermeshing twin-screw type. The results in Figure 14 showed that the flow was much more towards one direction, which means the flow was somehow much identical to the single screw extruder, as it did not flow against each other. Thus, the mixing capability did not reach the maximum potential in this case.

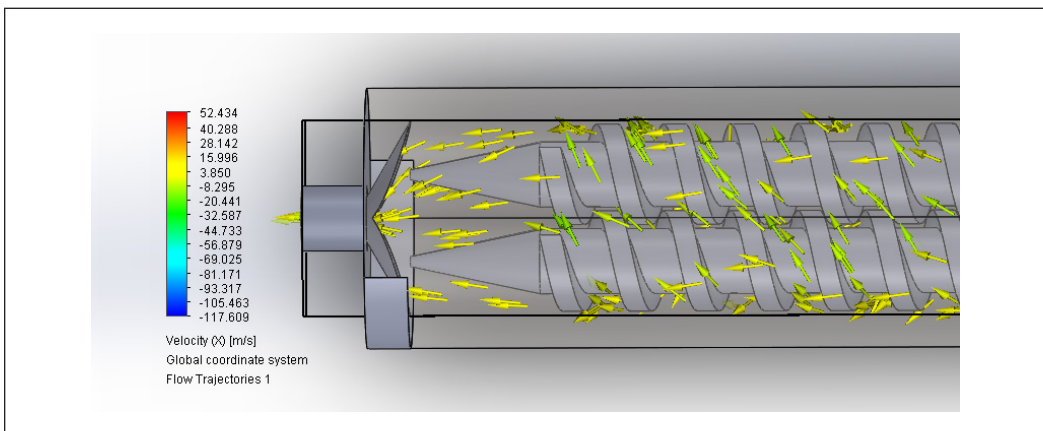


Figure 14. Flow trajectory of co-rotating twin-screw

Figure 15 depicts the relationship between velocity (m/s) and screw length (m), revealing the presence of initial flow instability within the melting and mixing zones. However, as the material progressed toward the nozzle, the flow stabilized. The results indicated that the material attained stability at 0.0297 m or 29.74 mm from the melting point, with a velocity of 0.0597 m/s or 59.72 mm/s.

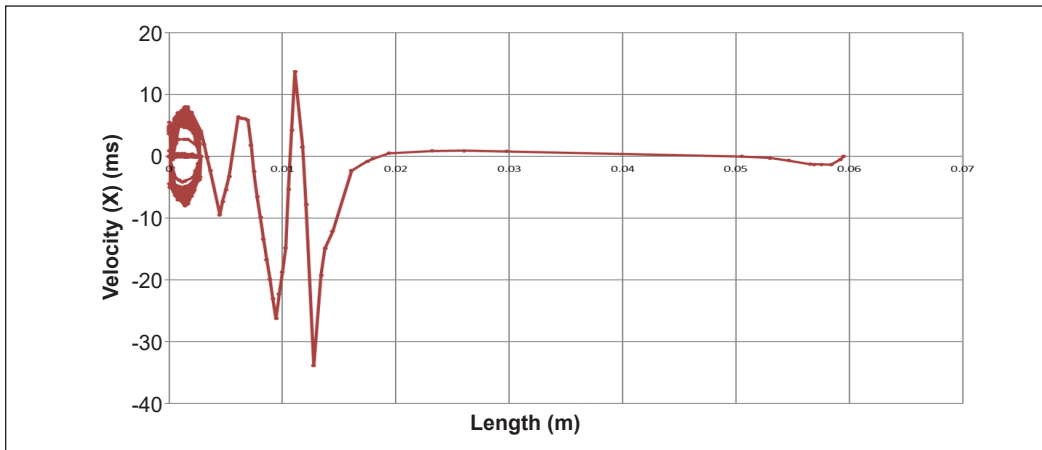


Figure 15. Co-rotating intermeshing screw fluid velocity vs screw length

Figure 16 illustrates the pressure variation along the screw length in the co-rotating intermeshing twin-screw design. The findings demonstrated enhanced flow stability as the material advanced toward the nozzle. The pressure inside the extrusion melting zone initiated at 0.0148 m or 14.80 mm from the melting inlet, with a recorded pressure value of 4.7×10^{10} Pa.

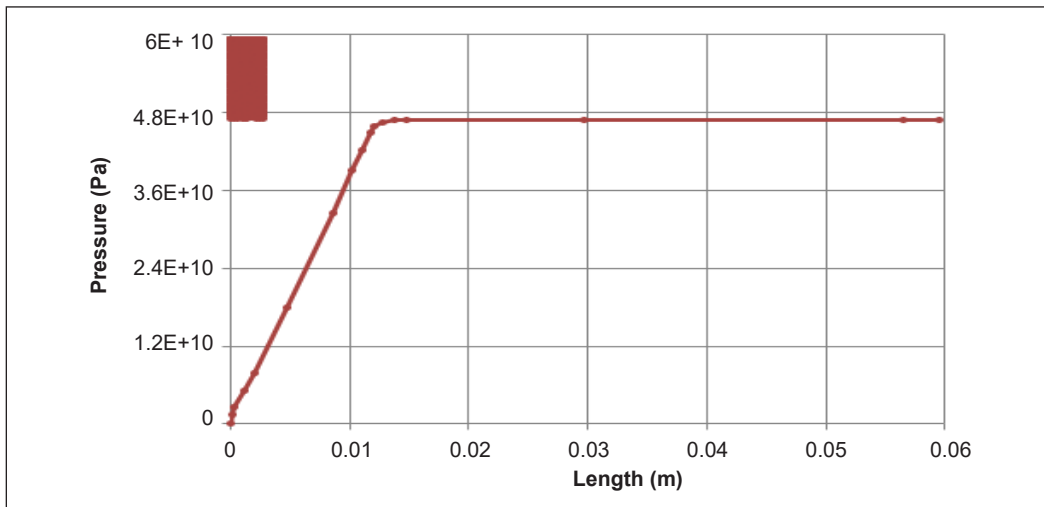


Figure 16. Co-rotating intermeshing screw pressure vs screw length

Based on the results above, comparing the counter-rotating and co-rotating intermeshing twin-screw designs revealed distinctive characteristics. The counter-rotating intermeshing configuration exhibited elevated shear stress and pressure build-up in the intermesh section. It can be attributed to the polymer's opposite-direction flow, which facilitated improved material compression and dispersion, resulting in superior mixing capabilities. Conversely,

the co-rotating intermeshing screw design demonstrated controlled shear stress and high-pressure build-up in the screw tip section. Compared to the counter-rotating design, the PP's flow in the same direction within this configuration limited the extent of mixing. These findings underscored the advantages of the counter-rotating intermeshing design in terms of shear stress, pressure build-up, flow direction, and mixing performance, establishing it as a desirable choice for applications requiring effective material processing and blending.

Shear Rates Analysis on Counter-rotating and Co-rotating Twin-screw Extruders

The shear rate vs. screw speed relationship was examined to assess the stability and identify the extruder with the highest mixing capability. The design that exhibited the maximum shear rate value indicated superior mixing performance. Throughout the tests, a fixed pressure of 90 Pa and a temperature of 190°C were maintained, while the screw speeds were varied between the range of 26 to 130 rpm. Figure 17 presents a comparative analysis of shear rates between the counter-rotating and co-rotating twin-screw designs at various screw speeds.

Based on Figure 16, the results demonstrated that the counter-rotating screw consistently exhibited higher shear rates compared to the co-rotating screw at each tested speed. At a screw speed of 26 rpm, the counter-rotating screw achieved a shear rate of 3 707, 408.15 1/s, while the co-rotating screw demonstrated a significantly lower shear rate of 1 936, 038.88 1/s. This initial comparison highlighted the substantial disparity in shear rates between the two designs, favoring the counter-rotating screw. As the screw speed increased to 52 rpm, the counter-rotating screw continued to outperform the co-rotating screw in terms of shear rate. The counter-rotating screw attained a shear rate of 3 960, 697.87 1/s, whereas the co-rotating screw recorded a shear rate of 1 973, 441.97 1/s.

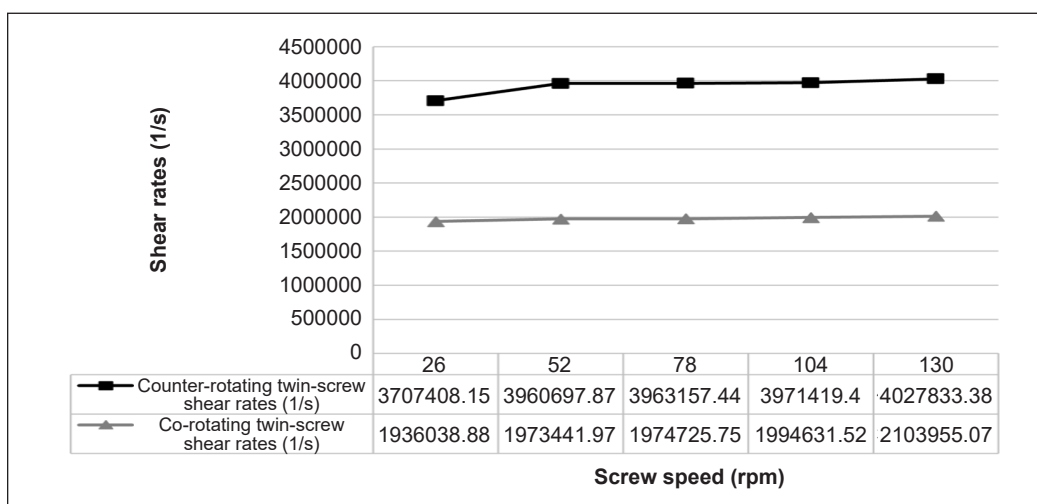


Figure 17. Comparative results of shear rates

Similar trends were observed at higher screw speeds. At 78 rpm, the counter-rotating screw achieved a shear rate of 3 963, 157.44 1/s, while the co-rotating screw lagged at 1 974, 725.75 1/s. At 104 rpm, the counter-rotating screw yielded a shear rate of 3 971, 419.4 1/s, while the co-rotating screw attained a shear rate of 1 994, 631.52 1/s. Lastly, at a screw speed of 130 rpm, the counter-rotating screw displayed a significantly higher shear rate of 4, 027, 833.38 1/s compared to the co-rotating screw's shear rate of 2, 013, 955.07 1/s.

The comparison of shear rates between the counter-rotating and co-rotating twin-screw designs has consistently demonstrated the superior performance of the counter-rotating screw in generating higher shear rates across all tested screw speeds. This clear disparity in shear rates emphasized the advantageous characteristics of the counter-rotating design, enabling enhanced material processing, dispersion, and mixing capabilities.

CONCLUSION

This study has investigated and compared the performance of counter-rotating intermeshing and co-rotating intermeshing twin-screw extruders in terms of velocity flow and shear rates for filament extruder machines. The analysis utilized SolidWorks CFD software to examine the behavior of polypropylene material inside the barrel, focusing on velocity and shear rates.

Based on the discussions and data presented above, the study concluded that the counter-rotating intermeshing twin-screw design outperformed the co-rotating intermeshing design in terms of shear rates and mixing capabilities for filament extruder machines. The shear rate data indicated that the counter-rotating screw consistently generated significantly higher shear rates compared to the co-rotating screw at various tested screw speeds. For instance, at a screw speed of 26 rpm, the counter-rotating screw exhibited a shear rate of 3 707, 408.15 1/s, while the co-rotating screw achieved a shear rate of 1 936, 038.88 1/s. This trend continued at higher screw speeds as well, further highlighting the superior performance of the counter-rotating screw. Nevertheless, the velocity flow analysis showed that as the material approached the nozzle exit, the flow became more stable for both twin-screw extruder configurations.

The results suggested that the counter-rotating intermeshing twin-screw design is more effective in material processing, compression, and dispersion, improving mixing capabilities. The opposite flow direction of the polymer in the counter-rotating design enables better material compression and dispersion, contributing to the enhanced shear rates observed. The incorporation of dual screw configurations and the screw designs of the counter-rotating and co-rotating intermeshing twin-screw extruders for biocomposite filament extrusion represents a significant advancement in this study. These elements contribute to enhanced mixing efficiency, a better understanding of material behavior,

improved extruder performance, and the utilization of innovative technologies for producing high-quality polypropylene-based biocomposite filaments.

Further studies can explore and refine the counter-rotating intermeshing design to optimize its performance and expand its application in producing biocomposite filaments. Investigations could focus on studying the influence of other operational parameters, such as temperature and pressure settings, on the performance of the twin-screw designs. The impact of different polymer materials and fillers on the shear rates and mixing capabilities could be explored to broaden the understanding of the counter-rotating intermeshing twin-screw design in various material extrusion processes. These findings contribute to optimizing twin-screw designs in AM and suggest avenues for further research and development in enhancing the counter-rotating intermeshing design to produce biocomposite filaments.

ACKNOWLEDGEMENT

The authors thank Universiti Teknikal Malaysia Melaka (PJP/2020/FTKMP/PP/S01735) and the Ministry of Higher Education Malaysia (FRGS/1/2020/TK0/UTEM/02/26) for providing the research grant scheme that supports this project.

REFERENCES

- Aida, H. J., Nadlene, R., Mastura, M. T., Yusriah, L., Sivakumar, D., & Ilyas, R. A. (2021). Natural fibre filament for Fused Deposition Modelling (FDM): A review. *International Journal of Sustainable Engineering*, 14(6), 1988–2008. <https://doi.org/10.1080/19397038.2021.1962426>
- Balla, V. K., Kate, K. H., Satyavolu, J., Singh, P., & Tadimeti, J. G. D. (2019). Additive manufacturing of natural fiber reinforced polymer composites: Processing and prospects. *Composites Part B: Engineering*, 174, Article 106956. <https://doi.org/10.1016/j.compositesb.2019.106956>
- Bauer, H., Matić, J., Evans, R. C., Gryczke, A., Ketterhagen, W., Sinha, K., & Khinast, J. (2022). Determining local residence time distributions in twin-screw extruder elements via smoothed particle hydrodynamics. *Chemical Engineering Science*, 247, Article 117029. <https://doi.org/10.1016/j.ces.2021.117029>
- Cali, M., Pascoletti, G., Gaeta, M., Milazzo, G., & Ambu, R. (2020). A new generation of bio-composite thermoplastic filaments for a more sustainable design of parts manufactured by FDM. *Applied Sciences (Switzerland)*, 10(17), Article 5852. <https://doi.org/10.3390/app10175852>
- Chen, B., Zhu, L., Zhang, F., & Qiu, Y. (2017). Process development and scale-up: Twin-screw extrusion. In Y. Qiu, Y. Chen, G. Z. Zhang, L. Yu & R. V. Mantri (Eds.), *Developing Solid Oral Dosage Forms: Pharmaceutical Theory and Practice*. (2nd ed.: pp. 821-868). Academic Press. <https://doi.org/10.1016/B978-0-12-802447-8.00031-5>
- Corleto, C. R., Briscoe, M., & Knight, C. T. (2021). Failure analysis of twin screw extruder shaft. *Journal of Failure Analysis and Prevention*, 21(5), 1622–1629. <https://doi.org/10.1007/s11668-021-01208-5>
- Deb, D., & Jafferson, J. M. (2021). Natural fibers reinforced FDM 3D printing filaments. *Materials Today: Proceedings*, 46, 1308–1318. <https://doi.org/10.1016/j.matpr.2021.02.397>

- Demirci, A., Teke, I., Polychronopoulos, N. D., & Vlachopoulos, J. (2021). The role of calender gap in barrel and screw wear in counterrotating twin screw extruders. *Polymers*, *13*(7), Article 990. <https://doi.org/10.3390/polym13070990>
- Dhaval, M., Sharma, S., Dudhat, K., & Chavda, J. (2022). Twin-screw extruder in pharmaceutical industry: History, working principle, applications, and marketed products: An in-depth review. *Journal of Pharmaceutical Innovation*, *17*(2), 294–318. <https://doi.org/10.1007/s12247-020-09520-7>
- Dong, T., Jiang, S., Wu, J., Liu, H., & He, Y. (2020). Simulation of flow and mixing for highly viscous fluid in a twin screw extruder with a conveying element using parallelized smoothed particle hydrodynamics. *Chemical Engineering Science*, *212*, Article 115311. <https://doi.org/10.1016/j.ces.2019.115311>
- Han, S. N. M. F., Mastura, M. T., & Mansor, M. R. (2019). Thermal and melt flow behaviour of kenaf fibre reinforced acrylonitrile butadiene styrene composites for fused filament fabrication. *Defence S&T Technical Bulletin*, *12*(2), 238–246.
- Hejna, A., Barczewski, M., Skórczewska, K., Szulc, J., Chmielnicki, B., Korol, J., & Formela, K. (2021). Sustainable upcycling of brewers' spent grain by thermo-mechanical treatment in twin-screw extruder. *Journal of Cleaner Production*, *285*, Article 124839. <https://doi.org/10.1016/j.jclepro.2020.124839>
- Irfan, M. S., Umer, R., & Rao, S. (2021). Optimization of compounding parameters for extrusion to enhance mechanical performance of kenaf-polypropylene composites. *Fibers and Polymers*, *22*(5), 1378–1387. <https://doi.org/10.1007/s12221-021-0676-8>
- Jacobs, E., Qian, K., Pietsch, V. L., Richter, M., Jones, D. S., Andrews, G. P., & Tian, Y. (2022). Design and scale-up of amorphous drug nanoparticles production via a one-step anhydrous continuous process. *International Journal of Pharmaceutics*, *628*, Article 122304. <https://doi.org/10.1016/j.ijpharm.2022.122304>
- Kariz, M., Sernek, M., & Kuzman, M. K. (2018). Effect of wood content in FDM filament on properties of 3D printed parts. *Materials Today Communication*, *14*, 135–140. <https://doi.org/10.1016/j.mtcomm.2017.12.016>
- Khalid, G. M., & Billa, N. (2022). Solid dispersion formulations by FDM 3D printing—A review. *Pharmaceutics*, *14*(4), Article 690. <https://doi.org/10.3390/pharmaceutics14040690>
- Kittikunakorn, N., Liu, T., & Zhang, F. (2020). Twin-screw melt granulation: Current progress and challenges. *International Journal of Pharmaceutics*, *588*, Article 119670. <https://doi.org/10.1016/j.ijpharm.2020.119670>
- Lewandowski, A., & Wilczyński, K. (2022). Modeling of twin screw extrusion of polymeric materials. *Polymers*, *14*(2), Article 274. <https://doi.org/10.3390/polym14020274>
- Liu, T., Kittikunakorn, N., Zhang, Y., & Zhang, F. (2021). Mechanisms of twin screw melt granulation. *Journal of Drug Delivery Science and Technology*, *61*, Article 102150. <https://doi.org/10.1016/j.jddst.2020.102150>
- Mastura, M. T., Jumaidin, R., M. Razali, N., & Kudus, S. I. A. (2020). Green material for fused filament fabrication: A review. In M. T. Mastura & S. M. Sapuan (Eds.), *Implementation and Evaluation of Green Materials in Technology Development: Emerging Research and Opportunities* (pp. 1–27). IGI Global. <https://doi.org/10.4018/978-1-7998-1374-3.ch001>

- Mazzanti, V., Malagutti, L., & Mollica, F. (2019). FDM 3D printing of polymers containing natural fillers: A review of their mechanical properties. *Polymers*, *11*(7), Article 1094. <https://doi.org/10.3390/polym11071094>
- Mysiukiewicz, O., Barczewski, M., Skórczewska, K., & Matykiewicz, D. (2020). Correlation between processing parameters and degradation of different polylactide grades during twin-screw extrusion. *Polymers*, *12*(6), Article 1333. <https://doi.org/10.3390/POLYM12061333>
- Nandi, U., Trivedi, V., Ross, S. A., & Douroumis, D. (2021). Advances in twin-screw granulation processing. *Pharmaceutics*, *13*(5), Article 624. <https://doi.org/10.3390/pharmaceutics13050624>
- Netto, J. M. J., Sarout, A. I., Santos, A. L. G., Lucas, A. de A., Chinelatto, M. A., Alves, J. L., Gaspar-Cunha, A., Covas, J. A., & Silveira, Z. de C. (2022). Design and validation of an innovative 3D printer containing a co-rotating twin screw extrusion unit. *Additive Manufacturing*, *59*, Article 103192. <https://doi.org/10.1016/j.addma.2022.103192>
- Pitayachaval, P., & Watcharamaisakul, P. (2019). A review of a machine design of chocolate extrusion based co-rotating twin screw extruder. *IOP Conference Series: Materials Science and Engineering*, *703*(1), Article 012012. <https://doi.org/10.1088/1757-899X/703/1/012012>
- Prashanth, S. R., Arumugam, S. K., Gangradey, R., Mukherjee, S., Kasthurirengan, S., Behera, U., Pabbineedi, G., & Mugilan, M. (2019). CFD modelling and performance analysis of a twin screw hydrogen extruder. *Fusion Engineering and Design*, *138*, 151–158. <https://doi.org/10.1016/j.fusengdes.2018.11.014>
- Royan, N. R. R., Leong, J. S., Chan, W. N., Tan, J. R., & Shamsuddin, Z. S. B. (2021). Current state and challenges of natural fibre-reinforced polymer composites as feeder in FDM-based 3D printing. *Polymers*, *13*(14), Article 2289. <https://doi.org/10.3390/polym13142289>
- Rao, R. R., Pandey, A., Hegde, A. R., Kulkarni, V. I., Chincholi, C., Rao, V., Bhushan, I., & Mutalik, S. (2022). Metamorphosis of twin screw extruder-based granulation technology: Applications focusing on its impact on conventional granulation technology. *AAPS PharmSciTech*, *23*(1), 1–23. <https://doi.org/10.1208/s12249-021-02173-w>
- Rauwendaal, C. J. (1981). Analysis and experimental evaluation of twin screw extruders. *Polymer Engineering and Science*, *21*(16), 1092–1100. <https://doi.org/10.1002/pen.760211608>
- Ren, A., Koleng, J. J., Costello, M., Spahn, J. E., Smyth, H. D. C., & Zhang, F. (2023). Twin-screw continuous mixing can produce dry powder inhalation mixtures for pulmonary delivery. *Journal of Pharmaceutical Sciences*, *112*(1), 272–281. <https://doi.org/10.1016/j.xphs.2022.10.007>
- Rett, J. P., Traore, Y. L., & Ho, E. A. (2021). Sustainable materials for fused deposition modeling 3D printing applications. *Advanced Engineering Materials*, *23*(7), Article 2001472. <https://doi.org/10.1002/adem.202001472>
- Schall, C., Altepeter, M., Schöppner, V., Wanke, S., & Kley, M. (2023). Material-preserving extrusion of polyamide on a twin-screw extruder. *Polymers*, *15*(4), Article 1033. <https://doi.org/10.3390/polym15041033>
- Senturk-Ozer, S., Gevgilili, H., & Kalyon, D. M. (2011). Biomass pretreatment strategies via control of rheological behavior of biomass suspensions and reactive twin screw extrusion processing. *Bioresource Technology*, *102*(19), 9068–9075. <https://doi.org/10.1016/j.biortech.2011.07.018>

- Stritzinger, U., Roland, W., Albrecht, H., & Steinbichler, G. (2021, May 10-21). *Modeling fully intermeshing co-rotating twin-screw extruder kneading-blocks: Part A. conveying characteristics*. [Paper presentation]. Annual Technical Conference - ANTEC, Conference Proceedings, Online.
- Thyashan, N., Perera, Y. S., Xiao, R., & Abeykoon, C. (2024). Investigation of the effect of materials and processing conditions in twin-screw extrusion. *International Journal of Lightweight Materials and Manufacture*, 7(3), 353-361. <https://doi.org/10.1016/j.ijlmm.2023.09.003>
- Vergnes, B., Souveton, G., Delacour, M. L., & Ainsler, A. (2022). Experimental and theoretical study of polymer melting in a co-rotating twin screw extruder. *International Polymer Processing*, 16(4), 351–362. <https://doi.org/10.1515/ipp-2001-0006>
- Vincent, R., Langlotz, M., & Dungen, M. (2020). Viscosity measurement of polypropylene loaded with blowing agents (propane and carbon dioxide) by a novel inline method. *Journal of Cellular Plastics*, 56(1), 73–88. <https://doi.org/10.1177/0021955X19864400>
- Wang, J., Hu, X., Liu, F., Long, Z., & Shao, M. (2022). Gel-spinning of ultra-high molecular weight polyethylene by a twin-screw extruder with an ultra-large length-to-diameter ratio. *Polymer Engineering and Science*, 62(11), 3773–3785. <https://doi.org/10.1002/pen.26143>
- Wang, J., Zheng, K., Hu, X., Long, Z., & Chen, K. (2023). Application of a twin-screw extruder with an ultra-high length-to-diameter ratio in the dry-jet wet spinning process of polyacrylonitrile nascent fibers. *Industrial & Engineering Chemistry Research*, 62(21), 8477–8488. <https://doi.org/10.1021/acs.iecr.3c00509>
- Xiao, X., Chevali, V. S., Song, P., He, D., & Wang, H. (2019). Polylactide/hemp hurd biocomposites as sustainable 3D printing feedstock. *Composites Science and Technology*, 184, Article 107887. <https://doi.org/10.1016/j.compscitech.2019.107887>
- Yacu, W. (2020). Extruder screw, barrel, and die assembly: General design principles and operation. In G. M. Ganjyal (Ed.), *Extrusion Cooking: Cereal Grains Processing* (pp. 73-117). Woodhead Publishing. <https://doi.org/10.1016/b978-0-12-815360-4.00003-1>
- Yang, X., Wang, G., Miao, M., Yue, J., Hao, J., & Wang, W. (2018). The dispersion of Pulp-Fiber in high-density polyethylene via different fabrication processes. *Polymers*, 10(2), Article 122. <https://doi.org/10.3390/polym10020122>
- Zheng, C., Govender, N., Zhang, L., & Wu, C. Y. (2022). GPU-enhanced DEM analysis of flow behaviour of irregularly shaped particles in a full-scale twin screw granulator. *Particuology*, 61, 30–40. <https://doi.org/10.1016/j.partic.2021.03.007>
- Zhuang, Y., Saadatkhan, N., Morgani, M. S., Xu, T., Martin, C., Patience, G. S., & Ajji, A. (2023). Experimental methods in chemical engineering: Reactive extrusion. *The Canadian Journal of Chemical Engineering*, 101(1), 59–77. <https://doi.org/10.1002/cjce.24538>

Conceptual Design and Materials Selection of the FDM Composites for Passenger Vehicle's Spoiler

Mohd Adrinata Shaharuzaman^{1,3*}, Syed Muhammad Ayyub Sayed Idros^{1,4}, Mastura Mohammad Taha^{2,3}, Muhd Ridzuan Mansor^{1,3}, Ridhwan Jumaidin^{2,3} and Hilmi Senan¹

¹Fakulti Teknologi dan Kejuruteraan Mekanikal, Universiti Teknikal Malaysia Melaka, Hang Tuah Jaya, 76100 Durian Tunggal, Melaka, Malaysia

²Fakulti Teknologi dan Kejuruteraan Industri dan Pembuatan, Universiti Teknikal Malaysia Melaka, Hang Tuah Jaya, 76100 Durian Tunggal, Melaka, Malaysia

³Centre for Advanced Research on Energy, Universiti Teknikal Malaysia Melaka, Hang Tuah Jaya, 76100 Durian Tunggal, Melaka, Malaysia

⁴FoundPac Technologies Sdn Bhd, Plot 35, Hilir Sungai Keluang 2, Bayan Lepas Industrial Estate, Non-Free Industrial Zone Phase IV 11900 Bayan Lepas, Pulau Pinang, Malaysia

ABSTRACT

One of the additive manufacturing techniques available is Fused Deposition Modeling (FDM), which offers advantages in design flexibility, cost-effectiveness, and the ability to produce intricate designs. Therefore, FDM for the 3D-printed vehicle's car spoiler is a subject that can be explored. The FDM technology can significantly reduce time and cost before mass production, and the vehicle's car spoiler was used as the case study in this research. The research investigates the mechanical properties of various commercial PLA composite filaments, addressing the lack of specifications provided by manufacturers. Testing four types of filaments—PLA/bamboo, PLA/coconut, PLA/wood, and PLA/metal. This research also emphasizes the conceptual design generation and selection

for the passenger vehicle's spoiler. Five design concepts were generated using the morphological chart for the passenger vehicle's spoiler. The Technique for Order of Preference by Similarity to Ideal Solution (TOPSIS) method was used as the decision-making tool. As a result, PLA/metal, with 53.65 MPa and 70.23 MPa, showed the highest tensile and flexural strength values, respectively. Design concept 5 with the infill pattern of rib + I was the best from the

ARTICLE INFO

Article history:

Received: 16 August 2023

Accepted: 09 May 2024

Published: 14 June 2024

DOI: <https://doi.org/10.47836/pjst.32.S2.02>

E-mail addresses:

adrinata@utem.edu.my (Mohd Adrinata Shaharuzaman)

ayyub.syed90@gmail.com (Syed Muhammad Ayyub Sayed Idros)

mastura@utem.edu.my (Mastura Mohammad Taha)

muhd.ridzuan@utem.edu.my (Muhd Ridzuan Mansor)

ridhwan@utem.edu.my (Ridhwan Jumaidin)

hilmisenan96@gmail.com (Hilmi Senan)

* Corresponding author

finite element analysis (FEA) using SolidWorks simulation software. Finally, the TOPSIS technique revealed PLA/metal as the best PLA composite filament for car spoilers, scoring first in performance score with a value of 0.5774. This study demonstrates that by using a systematic approach, researchers may choose the best design concept and material choice by combining the conceptual design, experimental, simulation, and TOPSIS methods.

Keywords: 3D printing, fused deposition modeling, mechanical properties, pla composite filament, TOPSIS

INTRODUCTION

According to Rae and Binder (2023), the automotive industry involves the manufacturers of motorized vehicles, including major components like engines and bodies, but excluding items such as tires, batteries, and fuel. This industry originated in Europe during the late 19th century, initially with steam-powered vehicles, and later in the 1860s, gasoline engines were introduced, especially in France and Germany.

The automotive industry plays a very important role in the global economy, serving as a crucial catalyst for macroeconomic growth, stability, and technological advancements in both developed and developing nations (Klink et al., 2014). It encompasses a wide range of interconnected industries, upstream and downstream, supporting the core automotive sector of vehicle and parts manufacturers, as illustrated in Figure 1.

As in Figure 1, various parts and components are needed for a vehicle in the core automotive industry, such as an engine, gearbox transmission, chassis, steering wheel, brake system, dashboard, and side mirror. Some of the vehicles have spoilers. The purpose of a spoiler is to ‘spoil’ adverse air passage across a moving vehicle’s body. Johnston (2015) stated that a spoiler is a feature on the back of a car that reduces drag or turbulence caused by the vehicle. The spoiler improves the driving grip and is a decorative element

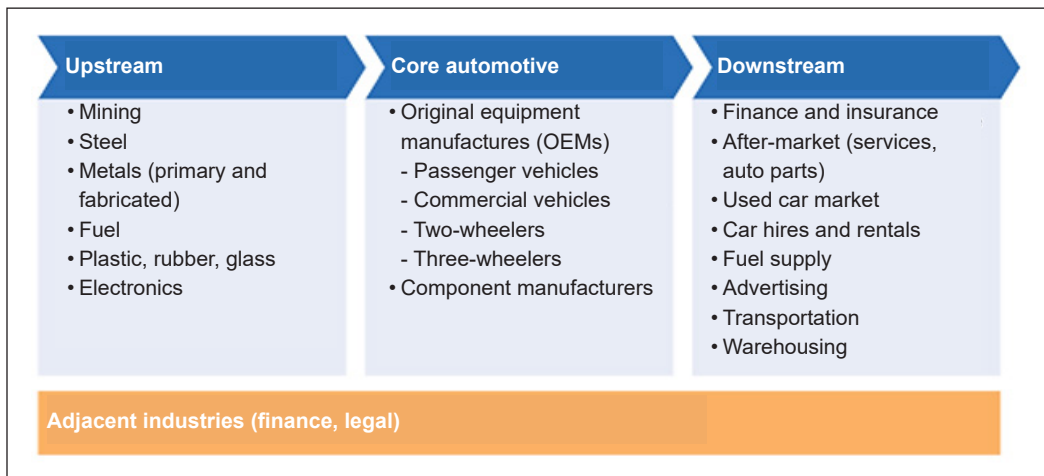


Figure 1. Automotive industries: Upstream, core automotive and downstream (Klink et al., 2014)

that makes the car look sportier (Suwanda, 2015). Figure 2 shows the type of spoiler chosen to be studied in this research (Idros, 2022).

In a study conducted by Irawan et al. (2020), the manufacturing process of woven rattan fiber composites was described as having dimensions of 220 cm in length and 70 cm in width. Prior to drying, the material underwent a 30-minute soaking in 90 % alcoholic liquid. The spoiler generated two positive mold pieces: one for the top and one for the bottom. These pieces were put together to create the finished product, which had the design on it. The mirror coating comprises the first layer of the spoiler, followed by the continuous layer of rattan fiber. After that, it was firmly sealed and laminated with a resin matrix until it dried. Subsequently, the positive molds were opened, the spoiler was removed, and the final touches were applied before it was ready to be used, as shown in Figure 2.

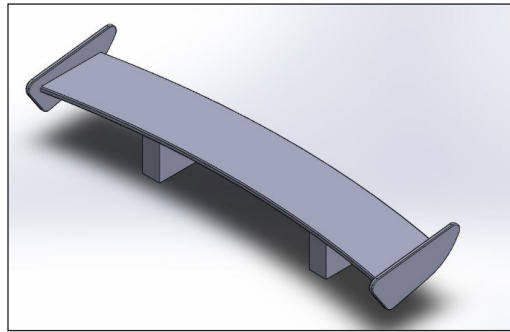


Figure 2. GT wing spoiler (Idros, 2022)

It can be seen from Figure 3 that the natural fiber composite spoiler was made manually using mold and human experts. Human experts depend on individual skills that differ from one another. Therefore, implementing additive manufacturing (AM) technology in this area is significant. AM can be referred to as the technologies that construct 3D objects by depositing the material layers one after another (Mahale et al., 2021). Pelz et al. (2021) stated that AM has ushered in a new era of digital manufacturing by revolutionizing engineering procedures. Metal, ceramic, and plastic components were easily produced using AM processes for prototypes and finished products. According to Bandyopadhyay and Heer (2018), the manufacturing industry is continually changing, and 3D printers can now produce multi-material systems with increased performance in user-defined places. The AM revolution has stimulated broad innovation using a single material.

The key principle of AM is forming three-dimensional parts by incrementally adding material, according to the ISO/ASTM standard 52900:2015(E). The method applies to most industrial fields. It makes use of a wide variety of substances, such as metallic, ceramic, and polymers, as well as mixtures in the form of composites, hybrid, and graded functional substances, and hydrogels, in a variety of physical states, such as solid, liquid, viscoelastic, and gels (Alghamdi et al., 2021).

Figure 4 shows the classification of AM processes from different perspectives. According to the ASTM, more than 50 technologies are based on the above processes (Alghamdi et al., 2021). As a result, ASTM has created a set of standards (ISO/ASTM 52900:2015) that divides the various AM processes into seven broad groups. AM methods were developed with seven families based on the product creation approach. These

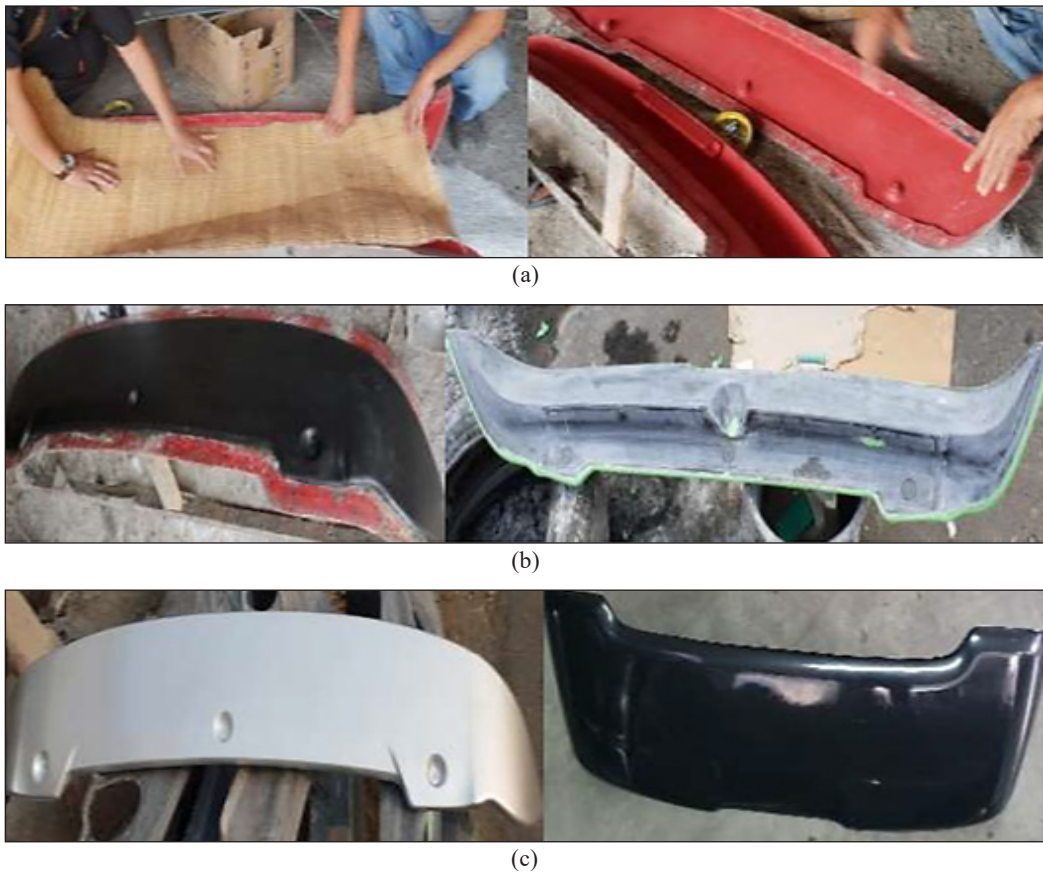


Figure 3. Methodology of car spoiler production using rattan fiber composite (Irawan et al., 2020): (a) Preparation of rattan fibers and positive mold; (b) Manufacturing process of car spoiler; and (c) Product prototype of spoiler

include vat photopolymerization, powder bed fusion, binder jetting, material jetting, sheet lamination, material extrusion, and directed energy deposition (Pelz et al., 2021). Material requirements, process parameters, development speed, performance and cost, dimensional precision, final product utilization, and applications all impact the material choice for AM (Sood et al., 2010).

One of the AM methods is Fused Deposition Modelling (FDM), which converts a CAD or digital three-dimensional (3D) model into a 3D object. FDM, also known as 3D printing, is a technique considered suitable for producing functional and aesthetic prototypes, also known as rapid prototyping. It is the most popular because of the simple concept that it does not require health-conscious solvents or glues. Besides that, all printing apparatus setups are cheap and require less space. The FDM or 3D printing technique can create parts or objects with large thicknesses or intricate shapes that are typically impossible to produce using conventional manufacturing techniques (Mazzanti et al., 2019). The material

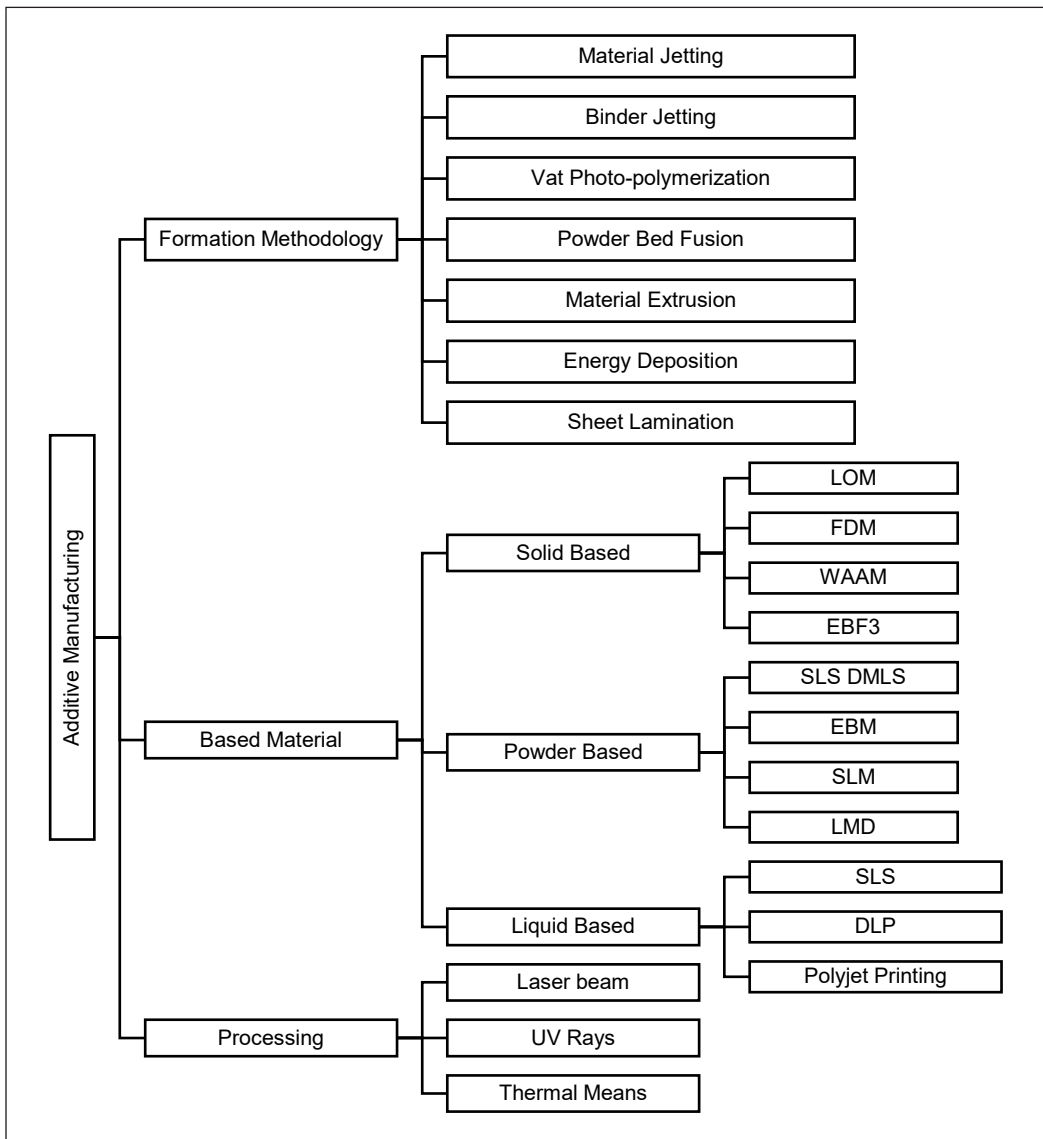


Figure 4. AM processes classification (Alghamdi et al., 2021)

starts to melt when the extruder of an FDM 3D printer is heated to a working temperature. The component is created by melting the filament over its glass transition temperature and forcing it through a narrow opening known as a heat break. This step is done on the printer bed, as shown in Figure 5 (Babagowda et al., 2018).

There are commercially available PLA composite filaments without information on their mechanical properties. This study provides mechanical testing of the available filaments for the users. Therefore, it is significant to this study to create car spoiler structures using natural composite material depending on their mechanical properties,

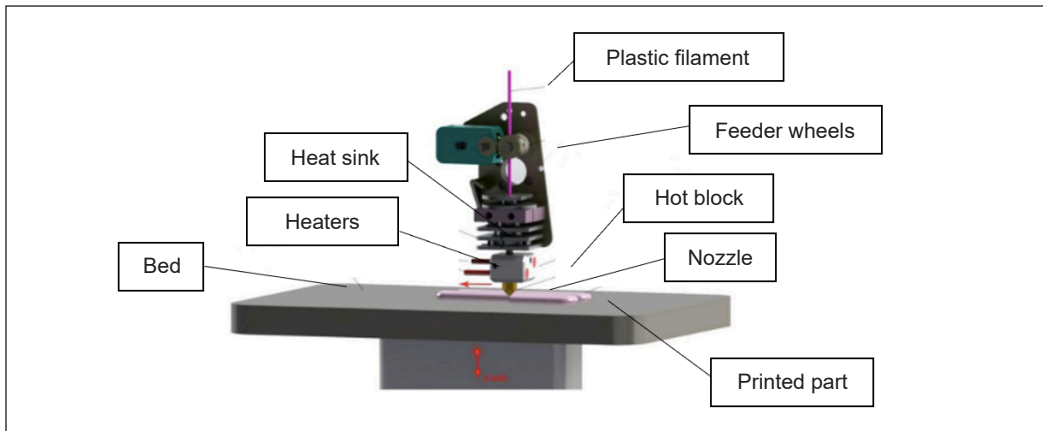


Figure 5. Schematic of 3D printer (Heidari-rarani et al., 2019)

physical properties, and hybridization of the conceptual design stages. This paper aims to analyze the mechanical properties of commercial PLA composite filaments using the Fused Deposition Modelling (FDM) technique to generate the conceptual design of a passenger vehicle’s spoiler and select the best conceptual design and best PLA composite filaments by Technique for Order of Preference by Similarity to Ideal Solution (TOPSIS) method.

MATERIALS AND METHODS

Figure 6 shows the research methodology, which can be divided into two sections: mechanical properties and conceptual design. The mechanical properties section analyzed the tensile and flexural strengths of the PLA composite filaments printed using the FDM technique. The conceptual design section generated the design concepts of the passenger vehicle’s spoiler using the morphological chart, performed analysis through the finite element analysis (FEA) method, and selected the best conceptual design by Technique for Order of Preference by Similarity to Ideal Solution (TOPSIS) method. Finally, the TOPSIS method was utilized to determine the best material of PLA composite filaments for the best design of a car spoiler.

The samples or specimens for the tensile and flexural strength analyses were printed using the Creality Ender 6 printer (Figure 7). The printing process started by setting

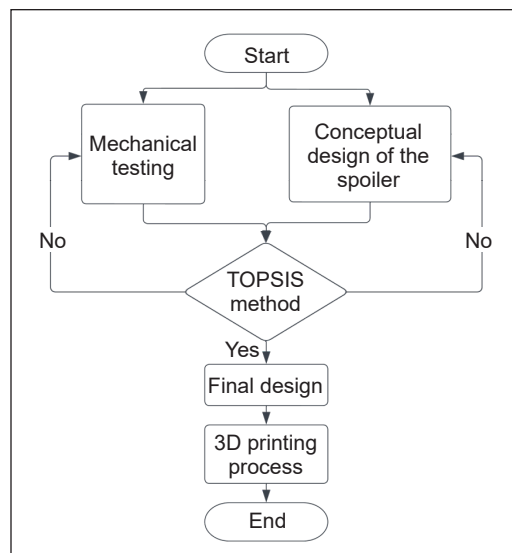


Figure 6. Methodology of the research

the nozzle temperature at 205, 210, and 215°C with the printer nozzle diameter of 0.6 mm and 1.75 mm filament diameter. The setting of bed temperature was from 50 to 60°C with the specimen's infill percent of 50%. The adhesive was added during the printing to support the specimen using a brim. The specimens were printed within 1 hour and 30 minutes. The infill pattern layer setup during the printing was lined, and the additional support of the plate adhesion for the specimens, such as brims, helped to improve bed adhesion and prevent warping. Also, 3D glue and 3D blue tape were used to support the bed adhesion. The setup parameters for Creality Ender 6 are shown in Table 1. Four types of PLA composite filaments (FDM) were printed in 3D, including polylactic acid (PLA)/bamboo, PLA/coconut, PLA/wood, and PLA/metal. The printed specimens followed ASTM D638 Type IV for tensile and ASTM D790 for flexural specimens (Ahmad et al., 2020).

The morphological chart method was applied at the beginning of the idea generation of the conceptual vehicle's car spoiler. The conceptual design was selected based on the morphological chart results (Asyraf et al., 2019), which focused on the five designs (Table 2). The design feature was divided into four main parts for the car spoiler: the spoiler frame type, end plate, frame body, and infill pattern structure. Kumar et al. (2017) inspired these rear spoiler design concepts including the spoiler frame, end plate and frame body. Additionally, in FDM, the infill pattern can be chosen by the designer from the slicer software to reduce the filament usage, simultaneously reduce the printing cost and improve the mechanical properties of the products (Kadhun et al., 2023).

The morphological chart method in Table 2 was applied in this study, and the proposed design concepts shown in Table 3 indicate that five design concepts were generated. Table 3 simplified the design generated using the morphological chart in Table 2.

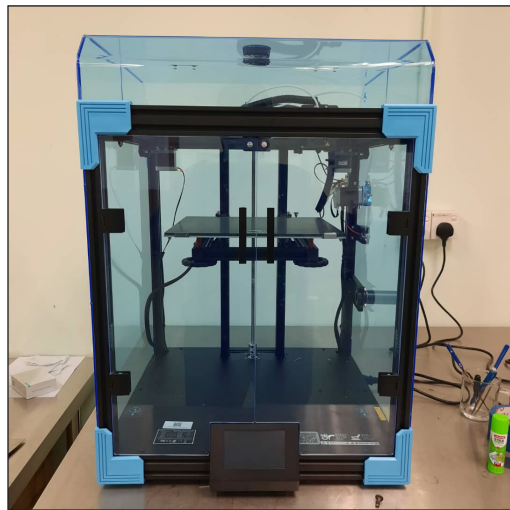


Figure 7. Creality Ender 6 3D printer

Table 1
Printing parameters

Parameter	Value
Nozzle temperature (°C)	205–240
Bed temperature (°C)	50–100
Percent infill (%)	100, 80, 50
Printing speed (mm/s)	100
Raster angle (°)	45
Layer height (mm)	0.2
Nozzle size (mm)	0.8 & 0.4
Adhesive	Glue, blue tape, and brim
Material type	Hybrid PLA/bamboo PLA/wood PLA/coconut PLA/metal

Table 2
 Morphological chart for conceptual design generation

Design features	Solution				
	1	2	3	4	5
Spoiler frame type	Curve	Straight	Pedestal		
End plates type	Type A	Type B	Type C	Type D	None
Spoiler frame body	Unibody	Separate parts			
Infill pattern	Rib + V	Honeycomb	Square lattice	Rib + square	Rib + I

Table 3
 Conceptual design generation from the morphological chart (Table 2)

Design concept	Solution			
	Spoiler frame type	End plates type	Spoiler frame body	Infill pattern
1	Straight	Type D 	Separate parts	Square lattice
2	Curve	Type C 	Separate parts	Honeycomb
3	Pedestal	Type A 	Separate parts	Rib + square
4	Straight	Type C 	Separate parts	Rib + V
5	Curve	Type D 	Separate parts	Rib + I

The mechanical properties data from the mechanical testing and the performance data from finite element analysis (FEA) were used in the TOPSIS method to determine the score rank of the best material for the best passenger vehicle's spoiler. The basic steps of the TOPSIS method formula and calculation (Mansor et al., 2014) are described below:

Step one: Construct standardized decision matrix A. For the comprehensive assessment questions with n evaluation units and m evaluation indexes, its decision matrix A is:

$$x_{ij} = \frac{x_{ij}}{\sqrt{\sum_{j=1}^n x_{ij}^2}} \quad (1)$$

Step two: Construct weighted and standardized decision matrix V, weight vector $W = (W_1, W_2, \dots, W_n)$:

$$\bar{x}_{ij} = \frac{x_{ij} \cdot W_j}{\sqrt{\sum_{j=1}^n x_{ij}^2 \cdot W_j^2}} \quad (2)$$

Step three: Determine the ideal solution X^+ and minus ideal solution X^- :

$$x^+ = \{ \max v_{ij} \mid j \in J, (\min v_{ij} \mid j \in J') \mid i = 1, 2, \dots, n \} = \{x_1^+, x_2^+, \dots, x_m^+\}$$

$$x^- = \{ \min v_{ij} \mid j \in J, (\max v_{ij} \mid j \in J') \mid i = 1, 2, \dots, n \} = \{x_1^-, x_2^-, \dots, x_m^-\}$$

Step four: Calculate distance. The distance of each project to the ideal solution X^+ is:

$$s_i^+ = \sqrt{\sum_{j=1}^m (v_{ij} - x_j^+)^2} \quad (3)$$

The distance of each project to the minus ideal solution X^- is:

$$s_i^- = \sqrt{\sum_{j=1}^m (v_{ij} - x_j^-)^2} \quad (4)$$

Step five: Calculate the relative proximity index of each project to the ideal solution C_i :

$$C_i = \frac{s_i^-}{(s_i^- + s_i^+)} \quad (5)$$

Step six: Rank the priority of the projects in descending order of C_i .

RESULTS AND DISCUSSION

Five design concepts were generated from the morphological chart (Table 3). All the design concepts were modeled using 3D software, SolidWorks (Figure 8). Design Concept 1 selected the straight spoiler frame with type D of the end plate, frame of a separate body, and infill pattern as a square lattice structure. Design Concept 2 chose the curved spoiler frame and the end plate of type C with a separate body of the frame. Design Concept 3 selected the pedestal frame type and Type A end plate of the car spoiler, which featured a separate spoiler body. In contrast, Design Concept 4 selected the spoiler's straight frame type and Type C end plate, featuring a separate spoiler body. Design Concept 5 chose the curved frame type with a Type D end plate and a separate body for the spoiler. Figure 9 shows the rib + I pattern for the infill in Design Concept 5. Figure 10 shows the fixed fixtures, external loads applied on the spoiler, and meshing of the car spoiler in Solidworks software. Figure 11 shows the results obtained from the simulation software and data for the Von-Mises stress, displacement, and strain,

Figure 10 shows the fixed fixtures, external loads applied on the spoiler, and meshing of the car spoiler in Solidworks software. Figure 11 shows the results obtained from the simulation software and data for the Von-Mises stress, displacement, and strain,

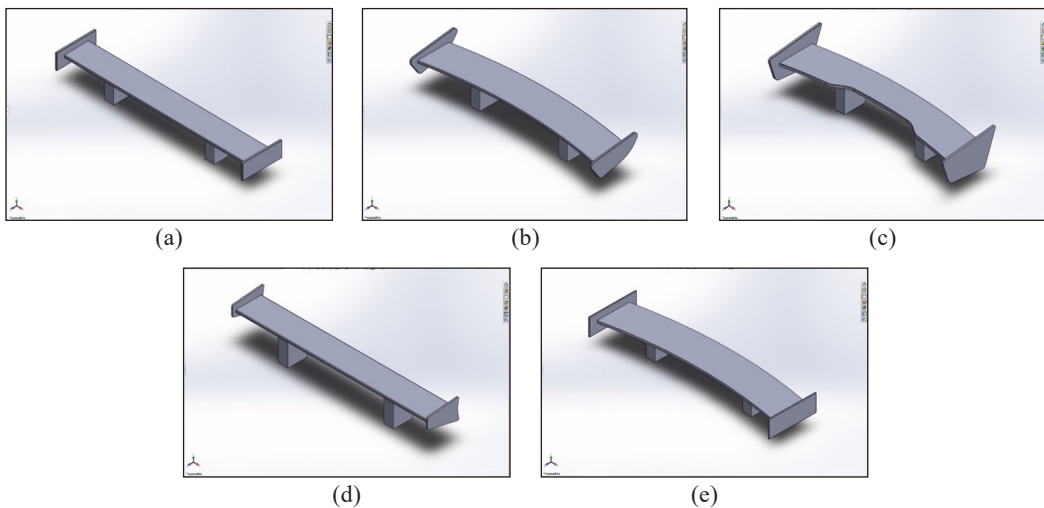


Figure 8. Five design concepts generated from the morphological chart: (a) Design concept 1; (b) Design concept 2; (c) Design concept 3; (d) Design concept 4; and (e) Design concept 5

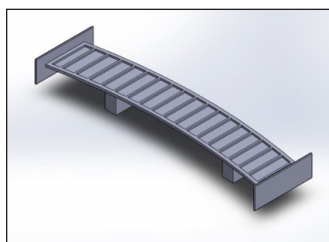


Figure 9. Design concept 5 with infill pattern rib + I

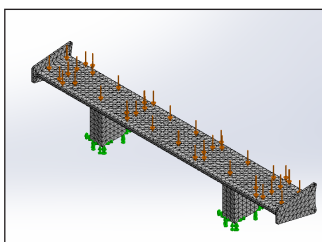


Figure 10. Boundary condition, external loads applied, and meshing for the spoiler

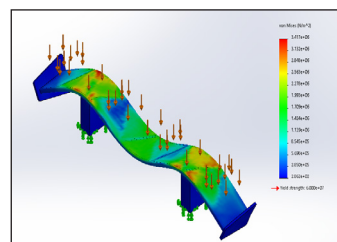


Figure 11. Simulation path coefficients and significance

which were recorded for the different material properties gained for the PLA composite filaments.

Figures 12 and 13 show the tensile and flexural test results, respectively, for the mechanical properties of the PLA composite filaments. Three specimens following the ASTM D638 standard were used for tensile testing, and the other three specimens following the ASTM D790 standard were used for flexural testing for each type of natural fiber filament. In the graph, the mechanical properties data of PLA composite were compared. As in Figure 8, the PLA/metal was the highest, with 53.65 MPa, followed by PLA/wood (36.62 MPa), PLA/bamboo (32.83 MPa), and PLA/coconut (30.70 MPa). The highest value for flexural stress shown in Figure 13 is PLA/metal with 70.23 MPa, followed by PLA/bamboo with 41.04 MPa, PLA/coconut with 39.36 MPa, and the lowest is PLA/wood with 37.18 MPa.

The mechanical property of the composite filament is important in utilizing the FDM method in 3D printing to ensure the materials the designer uses are the best for their product. Therefore, the data on mechanical properties helps designers and engineers select the appropriate materials for 3D printing based on the required mechanical performance. Besides that, it can be the early performance prediction for the engineers to analyze whether the printed part can withstand the required load without fail. This study used the TOPSIS method to select the best materials to help engineers and researchers.

From the finite element analysis (FEA) analysis of five design concepts of a passenger vehicle's spoiler (Table 4), Design Concept 5 had the lowest value of Von Mises stress. Design Concept 5, showing the lowest displacement and strain, was selected for FEA simulation by replacing the mechanical properties with the PLA composite filaments analyzed in the experimental analysis. The data from the FEA simulation of Design Concept 5 were combined with the data on mechanical properties from the first section, as illustrated

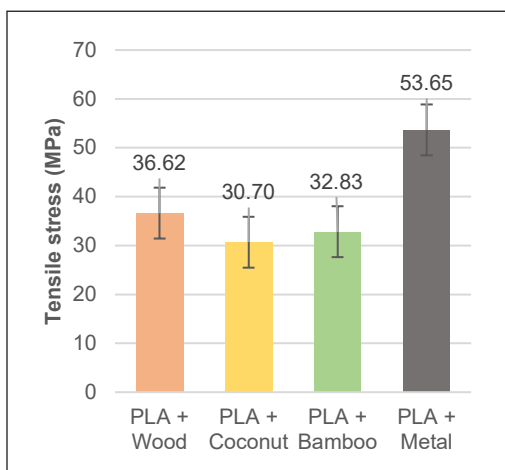


Figure 12. Tensile stress for PLA composite filaments

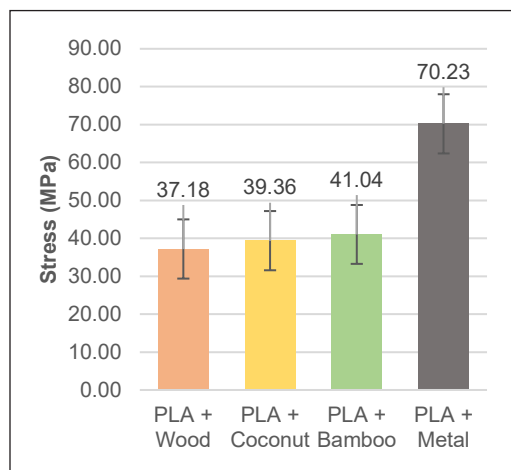


Figure 13. Flexural stress for PLA composite filaments

in Figures 12 and 13. From the findings, the best concept design and best material for the passenger vehicle’s spoiler were generated and ranked by using the TOPSIS method.

Table 4
 Simulation results for five design concepts

Design concept	Von Mises stress (Max) (N/m ²)	Displacement (Max) (mm)	Strain (Max)
Design concept 1	2.439	1.212	3.320
Design concept 2	2.381	1.418	3.455
Design concept 3	2.822	1.717	3.968
Design concept 4	3.417	1.639	4.882
Design concept 5	2.114	1.123	2.613

Table 5 compiles the data from the mechanical properties and data on the performance of Design Concept 5 from the FEA analysis for all PLA composite filaments. Data from Table 4 were used for the TOPSIS method and calculated using Equations 1 to 5. Through the TOPSIS method, the value of C_1 can be obtained, and the results are shown in Table 6.

Table 5
 Data of PLA composite filaments

Material	*TS (MPa)	YM (GPa)	FS (MPa)	FM (GPa)	Cost (RM/kg)	VMS (N/m ²)	DP (mm)
PLA/ Bamboo	32.83	4.88	41.04	1.07	156.90	2.114	1.333
PLA/ Coconut	30.70	5.20	39.36	1.46	152.94	2.114	1.25
PLA/ Wood	36.62	5.34	37.18	1.18	79.00	2.114	1.218
PLA/ Metal	53.65	6.26	70.23	2.71	245.96	2.114	1.039

*TS: Tensile Strength, YM: Young Modulus, FS: Flexural Strength, FM: Flexural Modulus, VMS: Von Mises stress, DP: Displacement

- (i) Decision matrix A was determined using Equation 1 and was shown in Table 5

$$A = \sqrt{\sum_{j=1}^n x_{ij}^2}$$

- (ii) The weighted vector and standardized matrix were calculated using Equation 2 and tabulated in Table 7.

$$\bar{x}_{ij} = \frac{x_{ij}}{\sqrt{\sum_{j=1}^n x_{ij}^2}}$$

- (iii) the standardized matrix V was calculated, and the ideal solution X^+ and minus ideal solution X^- were determined, as shown in Table 8.
- (iv) The distance of each material to the ideal solution, S_i^+ , and minus the ideal solution, S_i^- , were calculated using Equations 3 and 4.
- (v) Finally, the relative proximity index of each material to the ideal solution was computed using Equation 5 and tabulated in Table 9.

Table 6
Decision matrix for the criteria and composite filaments

Material	TS	YM	FS	FM	Cost	VMS	DP
PLA/ Bamboo	36.62	5341.53	37.18	1182.4	79.00	2.114	1.218
PLA/ Coconut	30.7	5203.03	39.36	1461.77	152.94	2.114	1.25
PLA/ Wood	32.83	4879.13	41.04	1071.33	156.90	2.114	1.333
PLA/ Metal	53.65	6261.77	70.23	2714.267	245.96	2.114	1.039
A	78.991	10891.241	97.714	3471.287	338.741	4.228	2.429

Table 7
Weighted vector and standardized matrix for the criteria and composite filaments

Material	TS	YM	FS	FM	Cost	VMS	DP
PLA/ Bamboo	0.46359	0.49044	0.38050	0.34062	0.23322	0.50	0.50134
PLA/ Coconut	0.38865	0.47773	0.40281	0.42110	0.45150	0.50	0.51451
PLA/ Wood	0.41561	0.44799	0.42000	0.30863	0.46319	0.50	0.54867
PLA/ Metal	0.67919	0.57494	0.71873	0.78192	0.72610	0.50	0.42766
Weightage	0.143	0.143	0.143	0.143	0.143	0.143	0.143

Table 8
Data of PLA composite filaments

Material	TS	YM	FS	FM	Cost	VMS	DP
PLA + Wood	0.06629	0.07013	0.05441	0.04871	0.03335	0.07150	0.07169
PLA + Coconut	0.05558	0.06831	0.05760	0.06022	0.06456	0.07150	0.07358
PLA + Bamboo	0.05943	0.06406	0.06006	0.04413	0.06624	0.07150	0.07846
PLA + Metal	0.09712	0.08222	0.10278	0.11181	0.10383	0.07150	0.06116
X+ (best)	0.09712	0.0822	0.10278	0.11181	0.03335	0.0715	0.06116
X- (worst)	0.05558	0.06406	0.05441	0.04413	0.10244	0.0715	0.07846

Table 9
Results of the TOPSIS method analysis

Material	S_i^+	S_i^-	Performance score		Rank
			$S_i^+ + S_i^-$	C_i	
PLA/bamboo	0.09765	0.03684	0.1345	0.2740	4
PLA/coconut	0.08803	0.04178	0.1298	0.3218	3
PLA/wood	0.08676	0.07065	0.1574	0.4488	2
PLA/metal	0.07048	0.09632	0.1668	0.5775	1

Figure 14 shows the best concept design of a car spoiler, which is Design Concept 5 fabricated via FDM 3D printing, and the PLA composite material of PLA/metal was determined to be the best material for the passenger vehicle's spoiler. As proposed in the morphological chart of Design Concept 5, the infill pattern inside the car spoiler has a rib + I structure pattern.



Figure 14. 3D printed spoiler for Design Concept 5 using PLA/metal composite filament

CONCLUSION

In conclusion, four types of PLA composite filaments were printed using the FDM 3D printing technique to determine their mechanical properties. The specimens were characterized via a tensile test (ASTM D638) and a flexural test (ASTM D790) to generate data on the material properties of the PLA composite filaments. The morphological chart approach enabled the solution in the conceptual design stage, and the idea developed was further refined to include particular design characteristics. For the simulation data of the von Mises stress value of 2.114, Design Concept 5 was chosen as the ultimate design concept for developing the product. The best design and material selection was finalized using the TOPSIS method based on the highest priority rank value. TOPSIS method validated that Design Concept 5 with PLA/metal filament was at the highest rank among all four materials with a value of 0.5775. This study used only four composite filaments to analyze their mechanical properties and select the best materials for the vehicle's spoiler. If there are databases for all commercially available filaments, it can help researchers and engineers select the filament for their products. It can be concluded that the hybrid morphological chart-TOPSIS method is proven to be able to be applied in performing the idea refinement, idea generation, conceptual design development, and conceptual design selection process approaches to achieving the desired solution in developing the conceptual design of the PLA composite filament of a passenger vehicle's car spoiler. This study proposes the hybrid method of producing the products using 3D printing to realize the conceptual design stage and assist the engineers in reducing the cost and choosing the best product materials.

ACKNOWLEDGMENT

The authors thank Universiti Teknikal Malaysia Melaka for the financial support from the Short-Term Grant (PJP/2020/FKM/PP/S01736) to the principal author to carry out this research project.

REFERENCES

- Ahmad, M. N., Wahid, M. K., Maidin, N. A., Ab Rahman, M. H., Osman, M. H., & Alis@Elias, I. F. (2020). Mechanical characteristics of oil palm fiber reinforced thermoplastics as filament for fused deposition modelling (FDM). *Advances in Manufacturing*, 8(1), 72–81. <https://doi.org/10.1007/s40436-019-00287-w>
- Alghamdi, S. S., John, S., Choudhury, N. R., & Dutta, N. K. (2021). Additive manufacturing of polymer materials: Progress, promise and challenges. *Polymers*, 13(5), Article 753. <https://doi.org/10.3390/polym13050753>
- Asyraf, M. R. M., Ishak, M. R., Sapuan, S. M., & Yidris, N. (2019). Conceptual design of creep testing rig for full-scale cross arm using TRIZ-Morphological chart-analytic network process technique. *Journal of Materials Research and Technology*, 8(6), 5647–5658. <https://doi.org/10.1016/j.jmrt.2019.09.033>
- Babagowda, Math, R. S. K., Goutham, R., & Prasad, K. R. S. (2018). Study of effects on mechanical properties of PLA Filament which is blended with recycled PLA materials. *IOP Conference Series: Materials Science and Engineering*, 310(1), Article 012103. <https://doi.org/10.1088/1757-899X/310/1/012103>
- Bandyopadhyay, A., & Heer, B. (2018). Additive manufacturing of multi-material structures. *Materials Science and Engineering R: Reports*, 129, 1–16. <https://doi.org/10.1016/j.msere.2018.04.001>
- Heidari-Rarani, M., Rafiee-Afarani, M., & Zahedi, A. M. (2019). Mechanical characterization of FDM 3D printing of continuous carbon fiber reinforced PLA composites. *Composites Part B: Engineering*, 175, Article 107147. <https://doi.org/10.1016/j.compositesb.2019.107147>
- Idros, S. M. A. S. (2022). *Conceptual design of the natural fiber composites of car spoiler using hybrid method* [Unpublish master thesis]. Universiti Teknikal Malaysia Melaka.
- Irawan, A. P., Adiando, & Sukania, I. W. (2020). Manufacturing process of car spoiler product using continuous rattan fiber composite materials. *International Journal of Mechanical Engineering and Technology (IJMET)*, 11(1), 9–15. <https://doi.org/10.34218/ijmet.11.1.2020.002>
- Johnston, V. (2015). *4 Essential things to know about your car's spoiler*. YourMechanic. <https://www.yourmechanic.com/article/4-essential-things-to-know-about-your-car-s-spoiler>
- Kadhum, A., Al-Zubaidi, S., & Abdulkareem, S. S. (2023). Effect of the infill patterns on the mechanical and surface characteristics of 3D printing of PLA, PLA+ and PETG materials. *ChemEngineering*, 7(3), Article 46. <https://doi.org/10.3390/chemengineering7030046>
- Klink, G., Mathur, M., Kidambi, R., & Sen, K. (2014). Contribution of the automobile industry to technology and value creation. *Auto Tech Review*, 3(7), 18–23. <https://doi.org/10.1365/s40112-014-0688-5>
- Kumar, M. V. S., Rao, B. A., & Mallaiah, G. (2017). Design, analysis and manufacturing of a car rear spoiler for drag reduction. *International Advanced Research Journal in Science, Engineering and Technology*, 4(6), 89-96. <https://doi.org/10.17148/iarjset.2017.4617>
- Mahale, R. S., Shamanth, V., Hemanth, K., Nithin, S. K., Sharath, P. C., Shashanka, R., Patil, A., & Shetty, D. (2021). Processes and applications of metal additive manufacturing. *Materials Today: Proceedings*, 54, 228–233. <https://doi.org/10.1016/j.matpr.2021.08.298>

- Mansor, M. R., Sapuan, S. M., Zainudin, E. S., Nuraini, A. A., & Hambali, A. (2014). Application of integrated AHP-TOPSIS method in hybrid natural fiber composites materials selection for automotive parking brake lever component. *Australian Journal of Basic and Applied Sciences*, 8(5), 431–439.
- Mazzanti, V., Malagutti, L., & Mollica, F. (2019). FDM 3D printing of polymers containing natural fillers: A review of their mechanical properties. *Polymers*, 11(7), Article 1094. <https://doi.org/10.3390/polym11071094>
- Pelz, J. S., Ku, N., Meyers, M. A., & Vargas-Gonzalez, L. R. (2021). Additive manufacturing of structural ceramics: A historical perspective. *Journal of Materials Research and Technology*, 15, 670–695. <https://doi.org/10.1016/j.jmrt.2021.07.155>
- Rae, J. B., & Binder, A. K. (2023). *Automotive industry*. Encyclopedia Britannica. <https://www.britannica.com/technology/automotive-industry>
- Sood, A. K., Ohdar, R. K., & Mahapatra, S. S. (2010). Parametric appraisal of mechanical property of fused deposition modelling processed parts. *Materials and Design*, 31(1), 287–295. <https://doi.org/10.1016/j.matdes.2009.06.016>
- Suwanda. (2015). Maker spoiler is car daihatsu use for kind polymer ingredient. *Science International (Lahore)*, 27(5), 4059–4065.

Environmental Assessment on Fabrication of Bio-composite Filament Fused Deposition Modeling Through Life Cycle Analysis

Muhammad Farhan¹, Mastura Mohammad Taha^{2*}, Yusliza Yusuf², Syahrul Azwan Sundi² and Nazri Huzaimi Zakaria²

¹Department of Mechanical Engineering, Faculty of Engineering, Integral University, Lucknow, 226026, Uttar Pradesh, India

²Fakulti Teknologi dan Kejuruteraan Industri dan Pembuatan, Universiti Teknikal Malaysia Melaka, Hang Tuah Jaya, 76100 Durian Tunggal, Melaka, Malaysia

ABSTRACT

The environmental effect of a manufacturing or service method is determined by the resource and energy inputs and outputs at each point of the product's life cycle. In Fused Deposition Modeling (FDM), generally, the material used for fabrication is plastic, and the raising of interest from different backgrounds of users could increase the issue of plastic pollution. Therefore, many scholars have proposed an initiative to employ bio-composite in FDM. In this study, an environmental assessment of global warming potential and fine particulate matter emission from the fabrication of bio-composite filament FDM was performed through its life cycle analysis using GaBi Software. Initially, data on resources and energy inputs and outputs were gathered. The functional unit in this study was the 1.0 kg wood/PLA composite filament extruded using a twin-screw extruder. All wastes were collected and recycled. The fabricated composite filaments were transported by container ship with a capacity of 5000 – 200 000 dwt gross weight for 100 km within Malaysia. Based on the results from the GaBi dashboard, the FDM process of bio-composite filament

has contributed as much as 138.7 kg CO₂ eq on the global warming potential and 1.71e⁻⁴ kg N eq. on fine particulate matter by the electricity power generation in extrusion and printing processes. The main factor for this issue is the consumption of coal in electric power generation, which is considered a non-renewable resource. Therefore, it is recommended that natural fibers such as wood fiber be employed in the filament of

ARTICLE INFO

Article history:

Received: 16 August 2023

Accepted: 09 May 2024

Published: 14 June 2024

DOI: <https://doi.org/10.47836/pjst.32.S2.03>

E-mail addresses:

mufarhan@iul.ac.in (Muhammad Farhan)

mastura.taha@utem.edu.my (Mastura Mohammad Taha)

yusliza@utem.edu.my (Yusliza Yusuf)

syahrul.azwan@utem.edu.my (Syahrul Azwan Sundi)

nazrihuzaimi@utem.edu.my (Nazri Huzaimi Zakaria)

* Corresponding author

FDM to reduce the environmental impact. As shown in the study, the materials contribute less to the impact. Further study is suggested to compare the FDM technology with conventional technology using similar materials.

Keywords: Bio-composite, environmental assessment, fused deposition modeling (FDM), life cycle analysis (LCA)

INTRODUCTION

Recently, three-dimensional (3D) printing, also known as additive manufacturing technology, has gained popularity as a technology widely used in everything from production and prototyping art to education. The applications can be found in the construction, automotive, and packaging industries, where the materials are varied according to the applications. The filament used to make the finished printed part is an essential feedstock of fused deposition modeling (FDM). Generally, the materials used as a feedstock of 3D printing are from polymer groups, specifically thermoplastic polymers. The advantages of this type of material are that it is cheaper, easy to process, has a better environmental impact, and has good material properties. Consequently, researchers' rising interest in computing their feedstock can be found in many research articles in the current year (Table 1).

Table 1
In-house FDM filament process

Materials	Process	Author
Polylactic acid (PLA)	Single screw extrusion	Harshit K. Dave, 2022
Secondary recycled Acrylonitrile Butadiene Styrene (ABS)	Twin screw extrusion	Kapil Chawla, 2021
Poly-ether-ether-ketone (PEEK)	Single screw extrusion	Bharath Tej Challa, 2022
SiC/Al ₂ O ₃ /recycled Low-Density Polyethylene (LDPE)	-	Piyush Bedi, 2020
Ceramic Thermoplastic composite	Melt extrusion	Kosamiya, 2023
Polyvinylidene Fluoride (PVDF)/graphene (Gr)/Barium Titanate (BTO)	Twin screw extrusion	Farina, 2020
Graphene /Acrylonitrile Butadiene Styrene (ABS)	Twin screw extrusion/ chemical dissolution	Gurleen Singh Sandhu, 2020
Nylon 6/Aluminum/Aluminum Oxide	Single screw extrusion	Jasvir Singh, 2022
Birch/Polylactic acid (PLA)	Filament maker	Mahdi Rafiee, 2021
Oil Palm/ABS composite	Hot Press	Ahmad, 2021
Corn Husk/Post-Used Expanded Polystyrene	-	Ariel Leong, 2021
Rice straw/Polylactic-acid (PLA)	Twin screw extrusion	Wangwang Yu, 2021
Kenaf/Acrylonitrile Butadiene Styrene (ABS)	Twin screw extrusion	Mastura MT, 2022
<i>Acacia Concinna</i> /Polylactic acid (PLA)	Single screw extrusion	Muthu, 2022

Filament extrusion is a process used for 3D printing to produce the filament that serves as the printing feedstock of FDM. Creating a long and continuous solid filament entails melting and extruding thermoplastic polymer granules, such as acrylonitrile butadiene styrene (ABS) or polylactic acid (PLA), through a nozzle with a particular diameter size. The extrusion process in producing the filament is used to heat and push the polymer granules that are typically fed into a hopper, as shown in Figure 1. There is a concern about energy consumption, where the process from filament production to printing using a 3D printer requires a significant amount of energy. Energy consumption may contribute to greenhouse gas emissions and climate change (Khosravani & Reinicke, 2020).

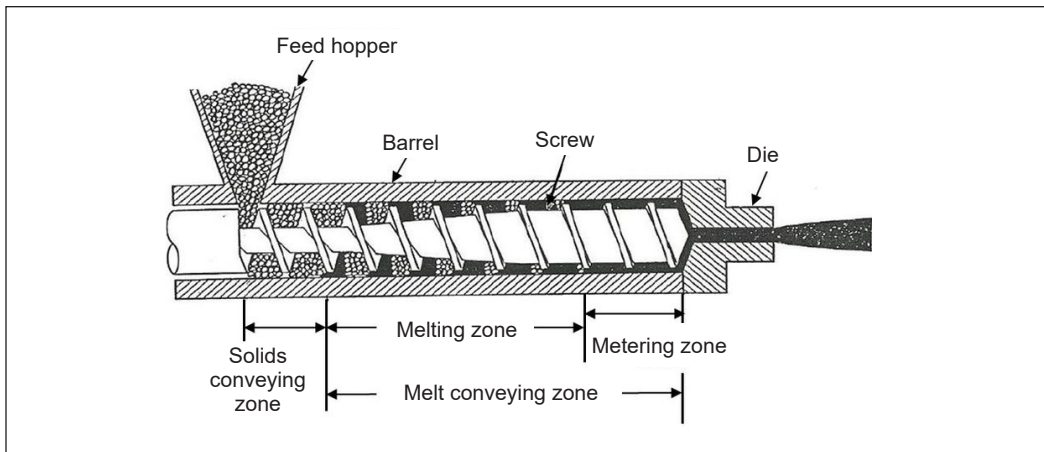


Figure 1. Schematic drawing of filament extrusion (Vlachopoulos & Polychronopoulos, 2019)

Typically, greenhouse gas emission is contributed by the manufacturing industry, where greenhouse gases (GHG) such as carbon dioxide (CO_2), methane (CH_4), and nitrous oxide (N_2O) are released into the atmosphere during various stages of the manufacturing process. These include the extraction of raw materials, the transportation of finished parts, and the disposal of waste products. Generally, GHG emissions are caused by burning fossil fuels such as coal, oil, and natural gas to generate energy for manufacturing processes. Consequently, the rise in energy consumption may increase the possibility of GHG emissions released into the atmosphere. A review study by Suárez and Domínguez (2020) focused on evaluating the environmental impact and sustainability of FDM technologies. They found that the largest environmental impact was from producing raw materials for FDM due to energy consumption and greenhouse gas emissions. Ulkir (2023), in his study, found the energy consumption of 3D printing associated with different types of materials, where recycled materials and bioplastics exhibited the most energy-efficient materials for 3D printing. These materials are recommended for sustainable 3D printing, which can reduce the environmental impact throughout its life cycle. Energy consumption in FDM

is broken down into four phases: raw material preparation, filament deposition or printing process, post-processing, and waste disposal.

At the beginning of the process, energy is required for extrusion, where heat is used to melt the polymer and produce the long and continuous profile filament. Energy is also required for the FDM machine to heat the nozzle and printing platform, move the printing head, and supply power to the various motors and mechanisms. Additional energy may be required for the post-processing process, such as polishing. At the disposal phase, energy is consumed to process the waste and may be used to transport the waste to the disposal facility. However, the amount of energy consumed during the process varies, depending on factors such as the type of FDM machine, materials used, and specific printing parameters. A study by Hopkins et al. (2021) suggested semi-empirical equations that can accurately predict the energy use for each printing process. The volumetric-specific energy use was 24.8–85.7 kJ/cm³.

Disposing of unneeded or failing FDM printed parts and support structures is the primary source of plastic waste pollution from FDM. Support structures are frequently used in FDM technology to support the printed object's position during printing. These support structures must be removed and disposed of after printing. As shown in Figure 2, errors or failed prints may produce discarded plastic parts during printing. It is suggested to recycle plastic waste. However, the recycling process could be difficult and may not always be possible. Anderson (2017) experienced using the recycled polylactic acid filament, and nozzle clogging occurred with decreased mechanical properties of the recycled filament compared with virgin filament. Pinho et al. (2020) supported this study and found some chain scission in the recycled polylactic acid filament. As a result, the semi-crystalline polymer experienced a 33% reduction in tensile stress and flexural strength. The polymer used in FDM is generally from non-renewable resources, such as petroleum, and once it is used, the leftover plastic spools may be discarded and end up in landfills.

Hence, plastic waste pollution from FDM can contribute to environmental issues without proper waste management and recycling processes. Several initiatives need to be taken to reduce pollution and improve the sustainable FDM process. Herianto et al. (2020) suggested an approach to recycle the filament of FDM using optimum parameters for the extrusion process. According to their findings, recycled polypropylene waste material can be effectively processed using extrusion to fabricate high-quality filament for FDM. This strategy could provide a sustainable and environmentally friendly solution for the manufacturing process of FDM.



Figure 2. Failed printed part

The growing interest in FDM technology has increased concerns about its environmental and human health impact. The emissions of hazardous particulate matter (PM) during the printing process are one of the key concerns. Particulate matter refers to microscopic particles that can be inhaled and cause respiratory issues, especially if they are fine enough to penetrate deep into the lungs. Studies have shown that 3D printing can generate significant matter, harming human health and the environment (Nyika et al., 2022). PM emissions can come from a variety of sources, such as the melting of the printing material, heating of the printing platform, and movement of the printer head. Yi et al. (2016) concluded that the impact of PM emissions is influenced by many factors, including the type of filament materials. They found that ABS generated bigger PM than PLA, possibly due to agglomeration. The geometric mean particle sizes, total particle number, and mass emissions varied significantly across the filament materials. The use of printer covers lowered PM emissions by a factor of 2. Lung deposition calculations revealed that PLA particle deposition in alveoli was three times that of ABS. Desktop 3D printers emit large quantities of ultrafine particles released into indoor spaces with insufficient ventilation (Khaki et al., 2021). Zhou et al. (2015) found that most of the particles emitted from the desktop 3D printers were less than 10 μm (PM₁₀). The particle concentrations increased in parallel with the distance from the printer. Furthermore, the smaller the particle size, the higher the particle concentration, with particle sizes ranging from 0.25 to 0.28 μm . The maximum particle concentration for a single printer was roughly $2.5 \times 10^4/\text{L}$ and $4 \times 10^4/\text{L}$ for two printers. Therefore, it is important to conduct further research on the potential impact of FDM technology on the environment and health hazards so that mitigation strategies can be implemented to minimize any negative effects.

MATERIALS AND METHODS

The primary purpose of this research is to investigate the potential environmental implications of wood composite printed FDM. The study assesses the environmental implications of wood/PLA composite prepared in-house and used for FDM technology. Three stages of product development were included, starting from the composite extrusion, printing, and delivery.

Goal and Scope Definition

In order to achieve the goals above, the life cycle analysis (LCA) of FDM was performed using GaBi software and Environmental Footprint 2.0 and ReCiPe 2016 v1.1 Midpoint (H) methodology. The impact categories investigated were global warming potential (GWP) and particulate matter emission. A functional unit, namely, 1 kg wood/PLA composite, was used in the analysis to measure the environmental impact of the composite. Thus, 1 kg wood/PLA composite was determined as the functional unit. Land transportation for the delivery of the product was assumed within a 100 km distance.

The transportation of materials was the starting point for each system analysis. The primary electricity from the grid mix was considered to provide the requisite amount of electric power to the extruder and 3D printing machine. The characteristics of this study are summarized in Table 2. This study aims to evaluate the environmental impact of bio-composite filament in FDM technology.

Table 2
Inputs and outputs of the system

Amount	Unit	Unit Process	Reference
<i>Inputs</i>			
Polylactic Acid	1.05	kg	
Cooling water	4	kg	
Wood fiber	0.1	kg	
Electricity	6	MJ	MY: Electricity grid mix
Truck 7.5t-12t gross	100	km	GLO: Truck Euro 5
<i>Outputs</i>			
Plastic extrusion profile	1.05	kg	-
Plastic waste	0.05	kg	-
Wood fiber waste	0.05	kg	-

Life Cycle Inventory

Life cycle inventory (LCI), defined by ISO 14040, entails gathering data and computation techniques to quantify the flows, inputs, and outputs. LCI includes information such as energy, raw material inputs, products and wastes, and air, soil, and water emissions. The accuracy of data provided in LCI significantly impacts the reliability and comprehensiveness of an LCA.

Extrusion of Wood/PLA Composite Filament

Construction of the extrusion of a 1.05 kg wood/PLA composite filament system is presented in Figure 3. It includes the transportation of the PLA granules as raw materials and supplying electricity for the extruder machine within the system boundaries.

FDM of Wood/PLA Composite Filament

After the wood/PLA composite filament is fabricated through the extrusion process, the filament will be used for the FDM technology as a feedstock in the FDM machine. A regular desktop FDM machine was used in this study, and a part was expected to print within 8 hours using 1 kg of composite filament. The printed part was expected to be delivered to the customer within a 100 km distance. The system is presented in Figure 4.

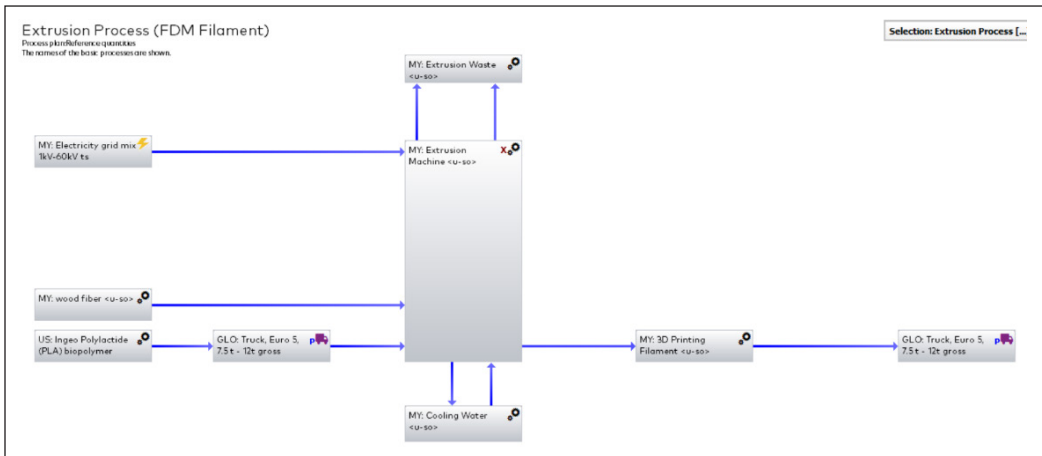


Figure 3. Extrusion process of FDM filament

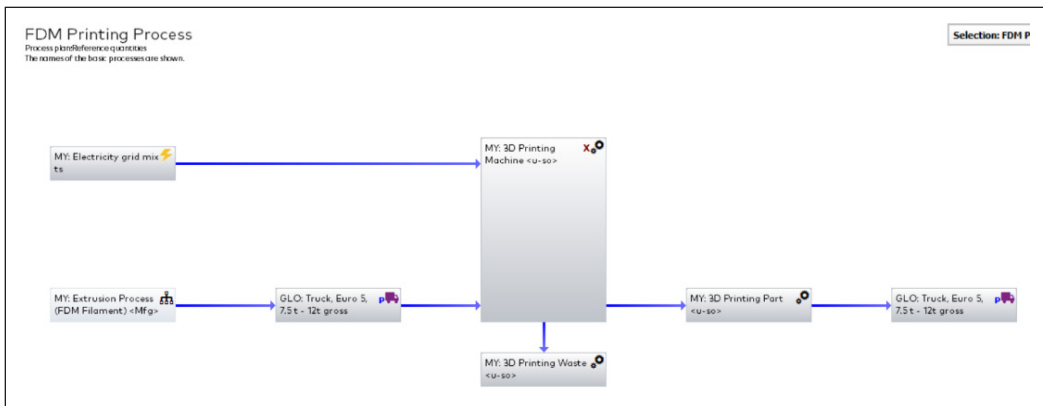


Figure 4. FDM printing system

RESULTS AND DISCUSSIONS

The impact assessment for this study was modeled and simulated using the LCA software, GaBi Professional v6.0 database, to measure the environmental burden and benefits.

Impact Assessment

Here, the results compared the total environmental impact of each wood/PLA composite FDM process for the evaluated impact categories contained in Environmental Footprint 2.0 and ReCiPe 2016 v1.1 Midpoint (H) methodology.

Global Warming Potential. From Figure 5, the total Global Warming Potential (GWP) value for an FDM printing of wood/PLA composite filament was 146 kg CO₂ eq. The values of the grid electricity mix from the FDM printing process that contributed to GWP

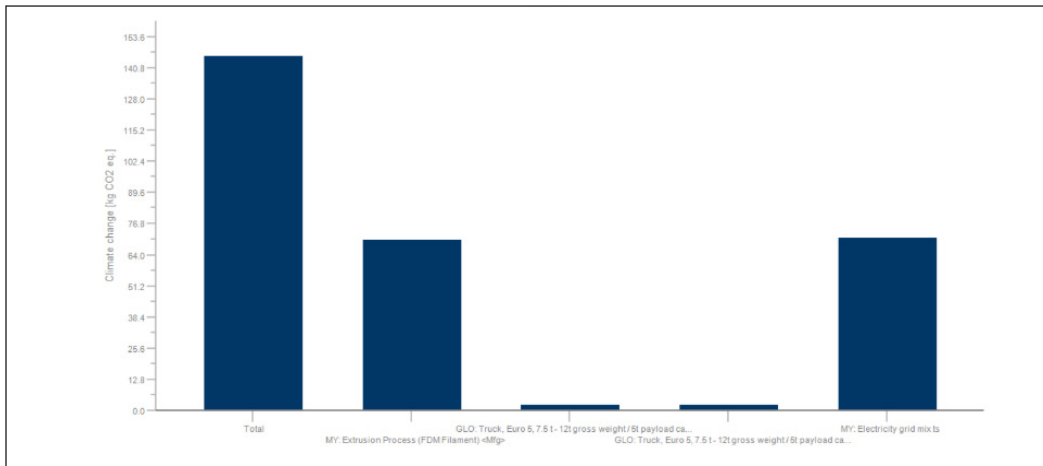


Figure 5. Total results for GWP

and from the extrusion process were 71.1 kg CO₂ eq and 67.6 kg CO₂ eq, respectively. Next, the value of PLA contributed to GWP was 0.708 kg CO₂ eq. The lowest contributor was transportation, with only 4.41 kg CO₂ eq.

Malaysian power generation is classified into five sources: oil, coal, natural gas, hydro, biomass, and others. Nearly 95 % of the electricity in Peninsular Malaysia is generated from coal (Rashid, 2021). Coal contains a large carbon content, and it releases greenhouse gases (GHG), mainly carbon dioxide, during the extraction, production, and combustion. When coal is used to generate energy in coal-fired power plants, a significant amount of CO₂ is released into the atmosphere. The combustion process involves the chemical reaction of carbon in coal with oxygen, which produces CO₂ as well as additional pollutants such as sulfur dioxide (SO₂), nitrogen oxides (NO_x), and particulate matter. Regarding this, coal significantly contributes to GWP. Hence, it produces the highest amount of CO₂ per unit of energy generated. In Malaysia, natural gas that emits lower levels of CO₂ and other pollutants compared to coal-fired power plants is likely to be steadily replaced by coal in the future.

Based on the results of GWP, no significant value was obtained from wood fiber production. Only 0.708 kg of CO₂ eq was contributed to the production of PLA. PLA is a biodegradable polymer made from renewable resources and has a prominent role in the bio-polymer market due to its inherent qualities. Papong et al. (2014) concluded that although biopolymers like PLA have a smaller impact on GWP and fossil fuel consumption than synthetic polymers, they may have greater environmental consequences due to eutrophication, carcinogens, and ozone layer depletion. This phenomenon is due to increased agricultural production necessitating fertilizers, pesticides, and land use changes. It has been supported by the results of this study, as shown in Figure 6. Similar results were

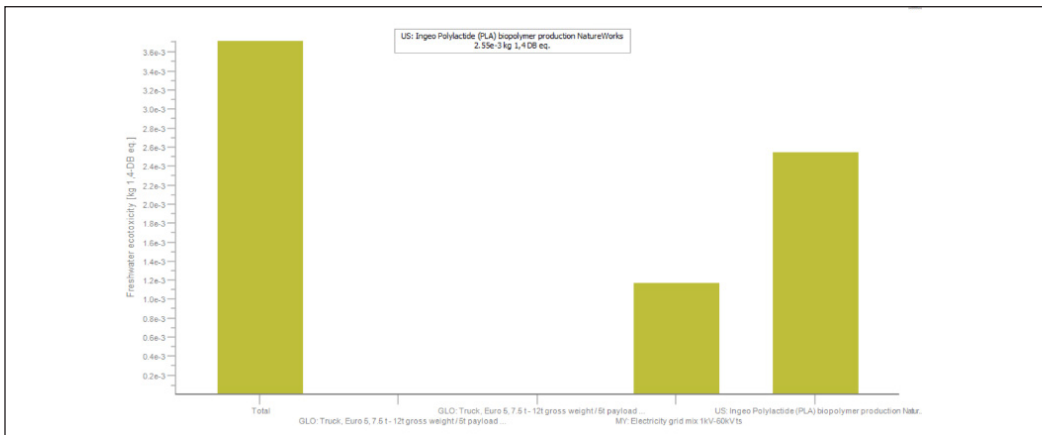


Figure 6. Results for freshwater ecotoxicity

obtained from the production of wood fibers. The demand for fertilizer and pesticides for agricultural production has contributed to the environmental impact discussed previously.

Particulate Matter Emissions. As seen in Figure 7, the biggest contributor to particulate matter emissions to produce bio-composite printed parts was during the extrusion of FDM filament, which stated as much as 2.02×10^{-4} kg N eq. The second largest contributor to PM emissions was the electricity grid mix, which recorded as much as 1.71×10^{-4} kg N eq. and the lowest contributor to PM emissions was PLA, which only contributed 3.93×10^{-5} kg N eq. The total fine PM emissions were determined to be 3.74×10^{-4} kg N eq.

Particulate matter emissions from PLA production probably consist of respirable particles harmful to the human body. The concentration and impact of particle emissions were influenced by the processing parameters that were set during the fabrication. Moreover,

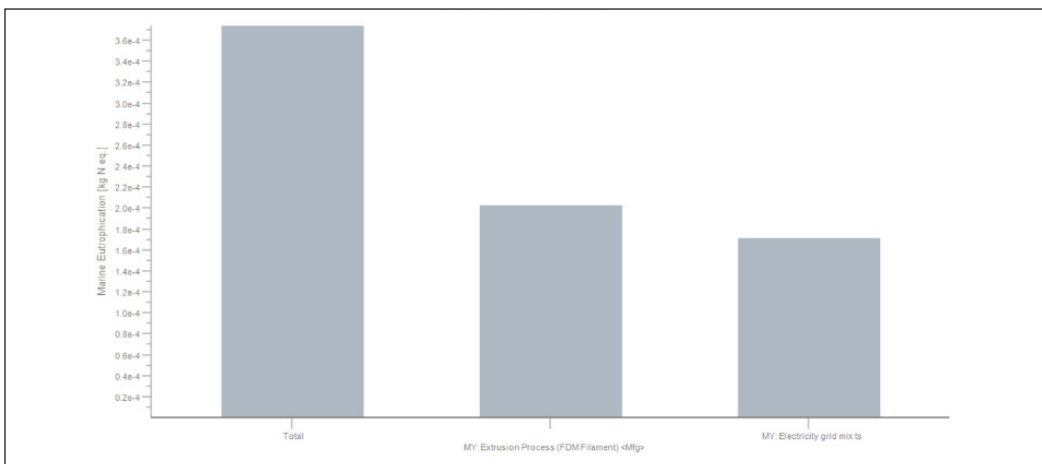


Figure 7. Results of particulate matter formation

the materials used for the processing would exhibit the concentration of the particle emissions and how dangerous they were. Chemical composition is a major concern in PM emissions, which will be released during fabrication, especially under certain high temperatures, such as more than 200 °C (Wojnowski et al., 2022). Some reports highlighted the hazardous emissions from Acrylonitrile Butadiene Styrene (ABS) that formed toxic fumes known as volatile organic carbon (VOC) (Farcas et al., 2020; Manoj et al., 2021; Stefaniak et al., 2017; Wojtyła et al., 2017). However, PLA may also emit VOCs that are harmful to young operators, especially children. A study by Zhang et al. (2017) showed that VOCs might condense throughout the printing process, resulting in bigger particles later in the print cycle. With the presence of wood fiber in the PLA composite, the PM emissions were reduced as the content of PLA was reduced. PM emissions are improved and will become less harmful if natural fiber, such as wood fiber, is employed in the feedstock of FDM.

CONCLUSION

Interest in FDM 3D printers, especially from researchers, has raised concerns about the environmental impact of the technology. Therefore, the study was conducted to evaluate the environmental impact of this technology using GaBi software. The investigation on the environmental impact of processing the bio-composite filament considered it environmentally friendly. It shows that the highest environmental impacts from this process are only contributed by electricity consumption. 138.7 kg CO₂ eq. and 1.71 x 10⁻⁴ kg N eq. were found for the global warming potential and fine particulate matter emissions, respectively. Both impacts were caused by the carbon content of coal, as electricity in Malaysia is mainly generated by coal. Moreover, fine particulate matter emissions were found from the production of PLA polymer as much as 0.393 x 10⁻⁴ kg N eq. The recommendation to change power generation resources is not under the scope of the FDM user. Therefore, the employment of wood fiber in the composite PLA filament of FDM could be the solution to reduce emissions. Hence, the amount of PLA used for this process is reduced, and consequently, the fine particulate matter emissions will be reduced. Further study is suggested to be conducted to compare the significant impact of this technology with the conventional manufacturing process using the same bio-composites. Energy efficiency should be constructed to reduce toxic and greenhouse gas emissions.

ACKNOWLEDGEMENT

The Ministry of Higher Education (MOHE) of Malaysia funded the study through the Fundamental Research Grant Scheme (FRGS), No. FRGS/1/2020/TK0/UTEM/02/26. The authors thank Universiti Teknikal Malaysia Melaka for the support.

REFERENCES

- Anderson, I. (2017). Mechanical properties of specimens 3D printed with virgin and recycled polylactic acid. *3D Printing and Additive Manufacturing*, 4(2), 110–115. <https://doi.org/10.1089/3dp.2016.0054>
- Farcas, M. T., Mckinney, W., Qi, C., Mandler, K. W., Battelli, L., Friend, S. A., Stefaniak, A. B., Jackson, M., Orandle, M., Winn, A., Kashon, M., Lebouf, R. F., Russ, K. A., Hammond, D. R., Burns, D., Ranpara, A., Thomas, T. A., Matheson, J., Qian, Y., ... & Commission, S. (2020). Pulmonary and systemic toxicity in rats following inhalation exposure of 3-D printer emissions from acrylonitrile butadiene styrene (ABS) filament Mariana. *Inhalation Toxicology*, 32(11-12), 403–418. <https://doi.org/10.1080/08958378.2020.1834034>
- Herianto, Atsani, S. I., & Mastriswadi, H. (2020). Recycled polypropylene filament for 3D printer: Extrusion process parameter optimization. *IOP Conference Series: Materials Science and Engineering*, 722(1), Article 012022. <https://doi.org/10.1088/1757-899X/722/1/012022>
- Hopkins, N., Jiang, L., & Brooks, H. (2021). Energy consumption of common desktop additive manufacturing technologies. *Cleaner Engineering and Technology*, 2, Article 100068. <https://doi.org/10.1016/j.clet.2021.100068>
- Khaki, S., Duffy, E., Smeaton, A. F., & Morrin, A. (2021). Monitoring of particulate matter emissions from 3D printing activity in the home setting. *Sensors*, 21(9), Article 3247. <https://doi.org/10.3390/s21093247>
- Khosravani, M. R., & Reinicke, T. (2020). On the environmental impacts of 3D printing technology. *Applied Materials Today*, 20, Article 100689.
- Manoj, A., Bhuyan, M., Banik, S. R., & Sankar, M. R. (2021). Review on particle emissions during fused deposition modeling of acrylonitrile butadiene styrene and polylactic acid polymers. *Materials Today: Proceedings*, 44, 1375–1383. <https://doi.org/10.1016/j.matpr.2020.11.521>
- Nyika, J., Mwema, F. M., Mahamood, R. M., Akinlabi, E. T., & Jen, T. C. (2022). Advances in 3D printing materials processing-environmental impacts and alleviation measures. *Advances in Materials and Processing Technologies*, 8(Sup3), 1275–1285. <https://doi.org/10.1080/2374068X.2021.1945311>
- Papong, S., Malakul, P., Trungkavashirakun, R., Wenunun, P., Chom-In, T., Nithitanakul, M., & Sarobol, E. (2014). Comparative assessment of the environmental profile of PLA and PET drinking water bottles from a life cycle perspective. *Journal of Cleaner Production*, 65, 539–550. <https://doi.org/10.1016/j.jclepro.2013.09.030>
- Pinho, A. C., Amaro, A. M., & Piedade, A. P. (2020). 3D printing goes greener: Study of the properties of post-consumer recycled polymers for the manufacturing of engineering components. *Waste Management*, 118, 426–434. <https://doi.org/10.1016/j.wasman.2020.09.003>
- Rashid, N. A. (2021, December 15). Power sector boosted by better demand for electricity. *Bernama*. <https://www.bernama.com/en/business/news.php?id=2033764>
- Stefaniak, A. B., Lebouf, R. F., Yi, J., Ham, J., Nurkewicz, T., Schwegler-Berry, D. E., Chen, B. T., Wells, J. R., Duling, M. G., Lawrence, R. B., Martin, S. B., Johnson, A. R., & Virji, M. A. (2017). Characterization of chemical contaminants generated by a desktop fused deposition modeling 3-dimensional printer. *Journal of Occupational and Environmental Hygiene*, 14(7), 540–550. <https://doi.org/10.1080/15459624.2017.1302589>

- Suárez, L., & Domínguez, M. (2020). Sustainability and environmental impact of fused deposition modelling (FDM) technologies. *The International Journal of Advanced Manufacturing Technology*, 106(3–4), 1267–1279. <https://doi.org/10.1007/s00170-019-04676-0>
- Ulkir, O. (2023). Energy-consumption-based life cycle assessment of additive-Manufactured product with different types of materials. *Polymers*, 15(6), Article 1466. <https://doi.org/10.3390/polym15061466>
- Vlachopoulos, J., & Polychronopoulos, N. D. (2019). *Understanding Rheology and Technology of Polymer Extrusion*. Polydynamics Inc.
- Wojnowski, W., Kalinowska, K., Majchrzak, T., & Zabiegała, B. (2022). Real-time monitoring of the emission of volatile organic compounds from polylactide 3D printing filaments. *Science of the Total Environment*, 805, Article 150181. <https://doi.org/10.1016/j.scitotenv.2021.150181>
- Wojtyła, S., Klama, P., & Baran, T. (2017). Is 3D printing safe? Analysis of the thermal treatment of thermoplastics: ABS, PLA, PET, and nylon. *Journal of Occupational and Environmental Hygiene*, 14(6), D80–D85. <https://doi.org/10.1080/15459624.2017.1285489>
- Yi, J., LeBouf, R. F., Duling, M. G., Nurkiewicz, T., Chen, B. T., Schwegler-Berry, D., Virji, M. A., & Stefaniak, A. B. (2016). Emission of particulate matter from a desktop three-dimensional (3D) printer. *Journal of Toxicology and Environmental Health - Part A: Current Issues*, 79(11), 453–465. <https://doi.org/10.1080/15287394.2016.1166467>
- Zhang, Q., Wong, J. P. S., Davis, A. Y., Black, M. S., & Weber, R. J. (2017). Characterization of particle emissions from consumer fused deposition modeling 3D printers. *Aerosol Science and Technology*, 51(11), 1275–1286. <https://doi.org/10.1080/02786826.2017.1342029>
- Zhou, Y., Kong, X., Chen, A., & Cao, S. (2015). Investigation of ultrafine particle emissions of desktop 3D printers in the clean room. *Procedia Engineering*, 121, 506–512. <https://doi.org/10.1016/j.proeng.2015.08.1099>

A Study on the Thermal Distribution of the Thermoforming Process for Polyphenylene Sulfite (Polyphenylene Sulfide) PPS Composites Towards Out of Autoclave Activity

Bushra Rashid¹, Nadlene Razali^{2,3*}, Mohamad Shukri Zakaria^{2,3}, Muhammad Zaid Harith Ramlan², Hasanudin Hamdan², Emy Aqillah Sharif², Noryani Muhammad^{2,3} and Syazwan Ahmad Rashidi⁴

¹*Institute of Technology, Middle Technical University, Alzafaranya, Baghdad 29008, Iraq*

²*Fakulti Kejuruteraan Mekanikal, Universiti Teknikal Malaysia Melaka, 76100 Durian Tunggal, Melaka, Malaysia*

³*Centre for Advanced Research on Energy (CARE), Universiti Teknikal Malaysia Melaka, 76100 Durian Tunggal, Melaka, Malaysia*

⁴*Aerospace Malaysia Innovation Centre, German Malaysian Institute, Selangor, Malaysia*

ABSTRACT

The thermoforming process is a widely utilized manufacturing technique for shaping thermoplastic materials into various products. Achieving uniform and controlled thermal distribution within the material during thermoforming is crucial to ensure high-quality products and minimize defects. This study investigates and enhances the understanding of thermal distribution in thermoforming processes through simulation analysis before it is done via experiment. This research investigates the thermal distribution in the thermoforming process of Polyphenylene Sulfide composites. The heating element distances were varied during the simulations of the thermoforming process of Polyphenylene Sulfide (PPS) composites, focusing on understanding how different distances affect the material's

deformability, dimensional accuracy, and overall quality. Three heater temperatures with three heater distances are tested. The distance between two heated surfaces is 200, 300 and 500 mm for 320°C, 360°C and 400°C heated surfaces. The desired PPS temperature (320°C) and maximum heater temperature (400°C) are parameters. The test result shows that to achieve 320°C thermoplastic temperature, we can use 385°C IR heater temperature with a heater

ARTICLE INFO

Article history:

Received: 16 August 2023

Accepted: 09 May 2024

Published: 14 June 2024

DOI: <https://doi.org/10.47836/pjst.32.S2.04>

E-mail addresses:

bushrarasheed50@yahoo.com (Bushra Rashid)

nadlene@utem.edu.my (Nadlene Razali)

Mohamad.shukri@utem.edu.my (Mohamad Shukri Zakaria)

mzaidharithofficial@gmail.com (Muhammad Zaid Harith Ramlan)

addinhasan918@gmail.com (Hasanudin Hamdan)

sharif.emyaqillah@gmail.com (Emy Aqillah Sharif)

noryani@utem.edu.my (Noryani Muhammad)

syazwan.rashidi@amic.my (Syazwan Ahmad Rashidi)

* Corresponding author

distance of 200 mm. However, this 200 mm distance might be too close for the operation, and a larger distance might be needed. Using 300 mm or 500 mm can achieve close to 320°C if the heater temperature is set to 400°C. In conclusion, this value is a reference for the distance of the material between the heater during the fabrication process.

Keywords: Polyphenylene Sulfide composites, thermoforming, thermal distribution

INTRODUCTION

Thermoforming, a versatile manufacturing process, has gained recognition as a sustainable solution in various industries (Valente et al., 2023). Thermoforming has emerged as an environmentally friendly method for producing plastic and composite products, focusing on resource efficiency, waste reduction, and recyclability. This process involves the transformation of flat thermoplastic sheets into three-dimensional shapes using heat and pressure (Ekşi et al., 2019). Thermoforming has become essential in pursuing sustainability in modern manufacturing practices by optimizing material usage, minimizing energy consumption, and promoting recycling.

One of the key factors contributing to the sustainability of thermoforming is its inherent material efficiency. Unlike other manufacturing processes that require extensive material removal, thermoforming utilizes sheets of thermoplastic materials with precise dimensions, minimizing waste generation. The ability to mold the sheets into complex shapes using custom-made molds or tooling ensures that the required materials are used effectively without excess or unnecessary scrap. This efficiency helps reduce raw material consumption, conserve natural resources, and lower production costs.

Additionally, thermoforming offers significant advantages in terms of energy efficiency. The process involves heating the thermoplastic sheets to their pliable state, which requires less energy compared to melting and re-molding processes used in other manufacturing techniques. The energy savings are further amplified by the ability to heat only the specific areas of the sheet that need molding, reducing overall heating time and energy consumption. By optimizing energy use, thermoforming minimizes its environmental impact and contributes to a greener and more sustainable manufacturing landscape.

Moreover, thermoformed products have exceptional recyclability, making them ideal for sustainable packaging and product solutions. Thermoplastics used in thermoforming can be easily recycled and reprocessed into new materials, closing the loop and reducing the demand for virgin resources. Additionally, the lightweight nature of thermoformed products contributes to energy savings during transportation and distribution, further reducing the overall carbon footprint. These recyclability and lightweight characteristics make thermoformed products an environmentally responsible choice for industries seeking sustainable packaging and design alternatives.

Thermal distribution in the thermoforming process is critical to achieving high-quality, defect-free products. However, variations in the temperature distribution during heating can lead to inconsistent material behavior and defects in the final formed parts. Understanding and optimizing the thermal distribution in the thermoforming process is essential to improve product quality, reduce waste, and enhance energy efficiency. Thus, in this study, the heat distribution with respect to the heating element distance was studied to understand the optimum process parameter well. It is important to avoid material waste during the thermoforming process.

Literature Review

In aerospace industries, the thermoplastic composite process differs from traditional thermoset composite. In order to fabricate thermoplastic, one of the processes is the thermoforming process (Nadlene et al., 2021). The thermoforming thermoplastic process is mainly different from the curing process, which is Reinforced Thermoplastic Laminate; RTL does not involve any autoclave for curing. On the other hand, thermoplastic composite only needs 5 to 10 minutes to complete the process and undergoes a thermoforming process since thermoplastic composite was supplied in RTL form (Akkerman & Haanappel, 2015).

Thermoforming is the most widely applied processing of thermoplastic prepregs. In some literature, thermoforming is the matched die-forming process (Ropers, 2017). According to Patil et al. (2019a), thermoforming is a technique in which, by imposing sufficient heating and pressure, a thin polymer film is softened and deformed over a mold into the desired shape. Generally, the thermoforming process for suitable mold temperature control involves long cycle times of up to several minutes. Before the forming stage, thermoforming molds should be heated to higher than the softening temperature of the polymer film and then cooled below the softening temperature after the forming stage for proper demolding (Lee et al., 2017).

According to Margossian et al. (2016), thermoforming processes are complex production processes that involve several factors that affect the consistency of the final product. Parameters such as temperature, forming speed and die geometries, stack properties such as original blank dimensions and layout design play an important role in the final result of the forming process (Process temperature seems to be especially significant among these). Thermoplastic composites display very distinct temperature behaviors due to their complex molecular structures.

Once thermoplastic composites become molten, they weaken and act as viscous materials when heated above their melting temperatures. Due to this behavior change, good temperature regulation within the laminate during development is important. Erchiqui et al. (2020) mentioned that the quality and characteristics of the manufactured parts in the plastics industry depend particularly on the heat transfer in the thermoplastics used. The

precision of the results depends on the consistency of the thermo-physical characterization and the kinetics of the plastic crystallization, as well as on the working conditions associated with the shaping process (Figures 1 and 2).

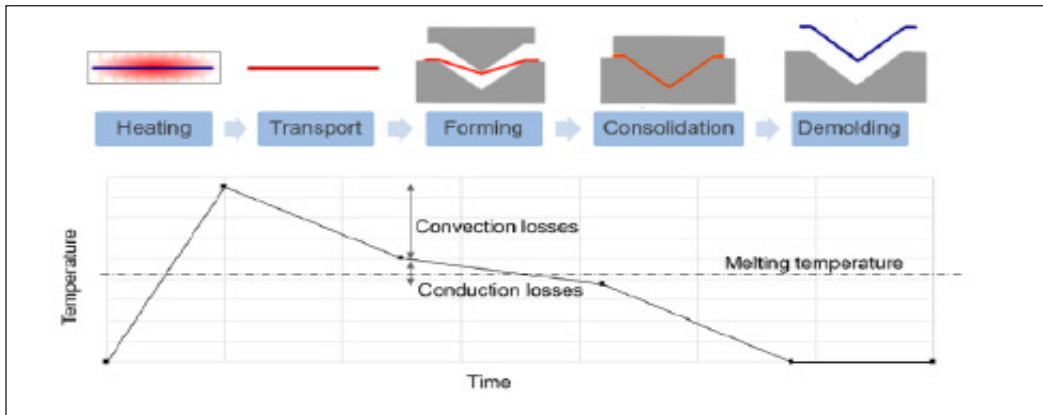


Figure 1. Principal steps of thermoplastic thermoforming process (Xiong et al., 2019)

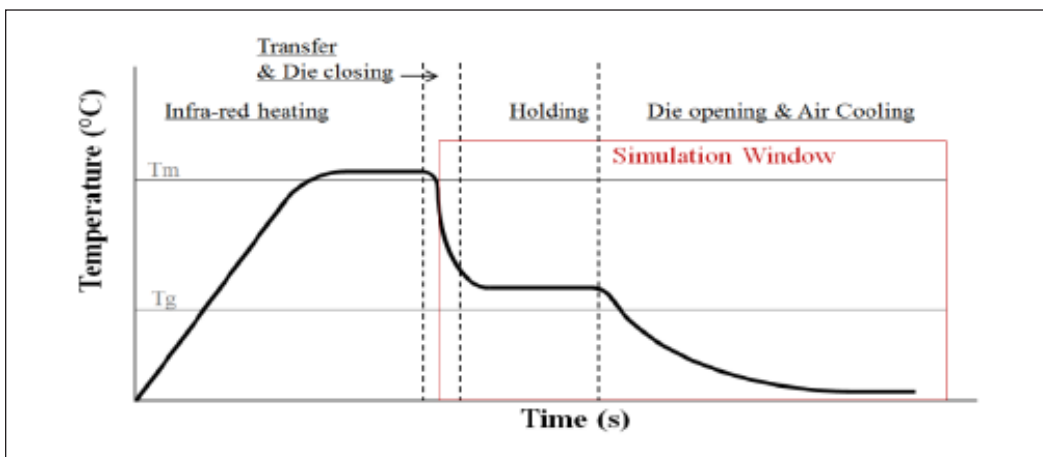


Figure 2. Temperature profile in thermostamping (Ste-marie, 2018)

Note. * T_m : Melting temperature, T_g : Glass Temperature

Shrivastava (2018) states that the amount of crystallinity in the material is affected by the processing technique. During the melt processing time, the plastics with a higher percentage of crystalline regions require longer to solidify. It allows the molecular chains to arrange themselves into crystalline form. However, if it is cooled rapidly, quenching the molecular chains does not receive sufficient time to align themselves properly and freeze as amorphous materials. Therefore, the crystallized plastic varies from material to material.

The sheets need to be heated above their glass transition T_g for the amorphous polymers and slightly below their melting point for the semi-crystalline polymers. It is necessary to

ensure that the form is completed before the sheet temperature falls below these levels to form the thermoplastic composites within the process—the thermoplastic matrices, a very short process over the thermoset. During thermoforming, the temperature influences the formation of a flat laminate into a 3D shape (Günther et al., 2021).

MATERIALS AND METHODS

Thermoforming is an industrial process that involves a heating step before forming. This step is performed in most forming machine machines using an infrared oven containing infrared emitters. In industry, process start-up and control is still based on personal experience and trial and error methods. It leads to varying machine settings, and eventually high start-up times and costs.

This research requires PPS sheet materials to be heated to 320°C within 8 minutes using two infrared (IR) heated surfaces. Therefore, the study aims to determine the heater surface distance and temperature to achieve the requirement. An unsteady numerical radiative transfer method is developed to compute the heat distribution between the heater and a thermoplastic sheet. 3D control-volume software, called ANSYS, has been developed to compute heat transfer during the infrared-heating step. At the end of the simulation, it is hypothesized to determine the heated surface temperature and distance between two heated surfaces.

Table 1 shows the nine case studies investigating the relation between heater distance and temperature to the thermoplastic temperature. Three heater temperatures with three heater distances are tested. The distance between two heated surfaces is 200, 300 and 500 mm for 320°C, 360°C and 400°C heated surfaces. The desired PPS temperature of 320°C and maximum heater temperature of 400°C are parameters. At the same time, the distance of the heater is based on the comfortable movement of the specimen during the process.

The geometry domain in the present task for the heating area is a simple cuboid shape with a 600 mm × 600 mm base area. The domain height that represents distance varies according to the simulated case.

Figures 3 and 4 show the domain geometry of the simulated case for 200 mm and 300 mm heater distance, respectively. The thickness of the plastic plate is constant at 6 mm per PPS sample thickness, and the modeling for the PPS heated process for a 500 mm distance between two heated surfaces in ANSYS can be illustrated in Figure 5.

The maze cell size is 1.0×10^2 m with a minimum of 4.9×10^{-4} m. For this geometry,

Table 1
Summary of the case study

Case number	Heater temperature (°C)	Heater distance (mm)
1	320	200
2	320	300
3	320	500
4	360	200
5	360	300
6	360	500
7	400	200
8	400	300

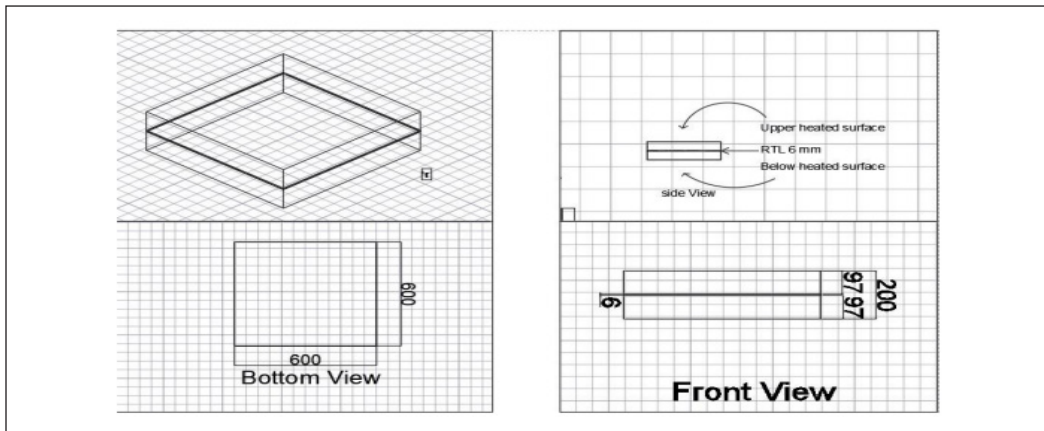


Figure 3. 3D modeling for PPS heating process for 200 mm distance between two heated plates. All units in mm

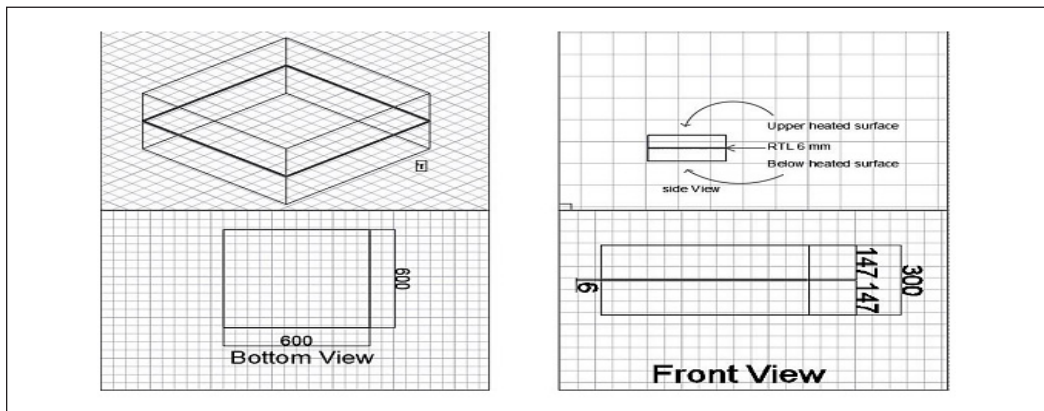


Figure 4. 3D modeling for PPS heating process for 300 mm distance between two heated plates. All units in mm

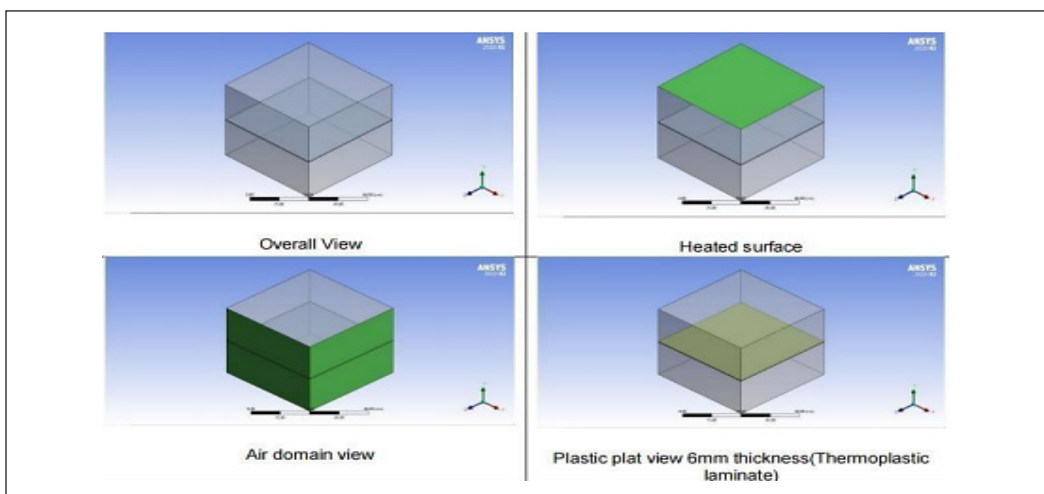


Figure 5. The modeling for the PPS heated process for a 500 mm distance between two heated surfaces in ANSYS

the number of elements is 183,600. All cases have similar face sizes but different elements depending on domain size. A separate study shows that this mesh number achieves the grid-independent test.

The present study's boundary condition comprises two main parts (Figure 6). The first is the heated surface at the domain's upper and bottom. Depending on the case studied, these two heated surfaces imposed free-to-stream and radiative temperatures at either 320°C, 360°C or 400°C. The heat transfer coefficient is 20 W/m²K as the general value for the contacting air undergoing natural convection. The detailed value of the boundary conditions is provided in Table 2. The second part is the side wall of the domain, consisting of four surfaces. All surfaces of this domain are assumed to have zero heat flux, which means no heat loss will occur. Although this assumption is impractical due to non-zero heat loss for real situations, the study's outcome is concerning for the ideal and worst-case scenarios.

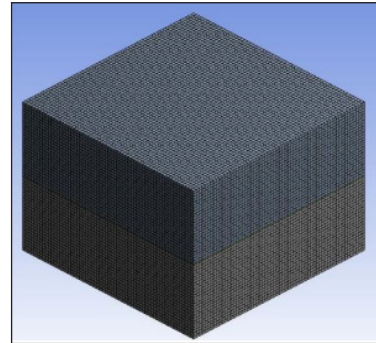


Figure 6. The mesh modeling with a maximum size of 6 mm size element

Table 2

Boundary condition use in the present task

Properties	Heated surface	Domain wall
Mode of heat transfer	Mixed (Rosseland radiation)	Insulation
Free stream temperature (°C)	320/360/400	N/A
Heat Flux	0	0
Heat transfer coefficient (W/m ² K)	20	N/A
External emissivity	0	N/A
External radiation temperature	320/360/400	N/A
Heat generation rate	0	N/A

RESULTS AND DISCUSSION

In this study, steady-state thermal analysis was used in ANSYS Workbench software. It evaluated the thermal achievement target temperature of 320°C (Figure 7) as early as 6 minutes and as high as 360°C (Figure 8) after 8 minutes. Therefore, the choice of 400°C (Figure 9) heater temperature and 20mm heater distance could fulfill the requirement criteria.

Figure 10 shows the temperature distribution of the thermoplastic plate at 8 minutes for the 400°C heater temperature and 200 mm infrared heater distance. As seen, the temperature is uniform with 624 K (351°C).

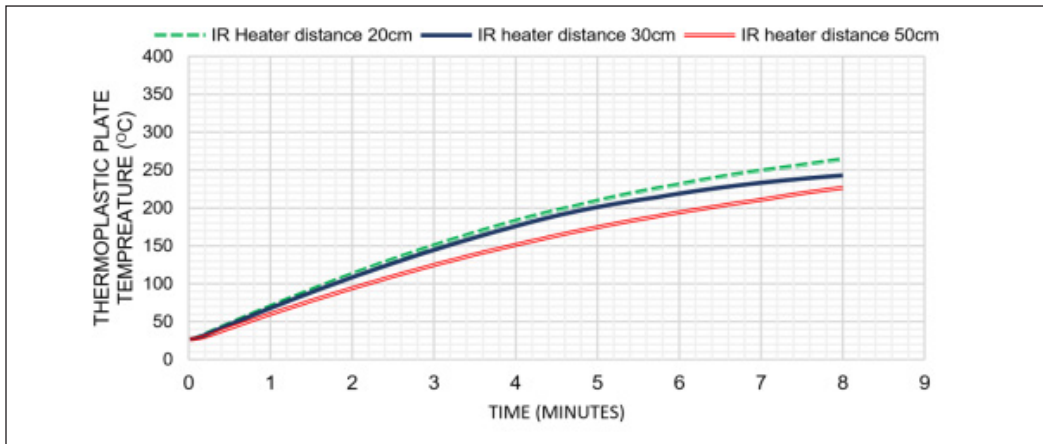


Figure 7. PPS plate temperature at heater temperature 320°C for various infrared (IR) heater distance

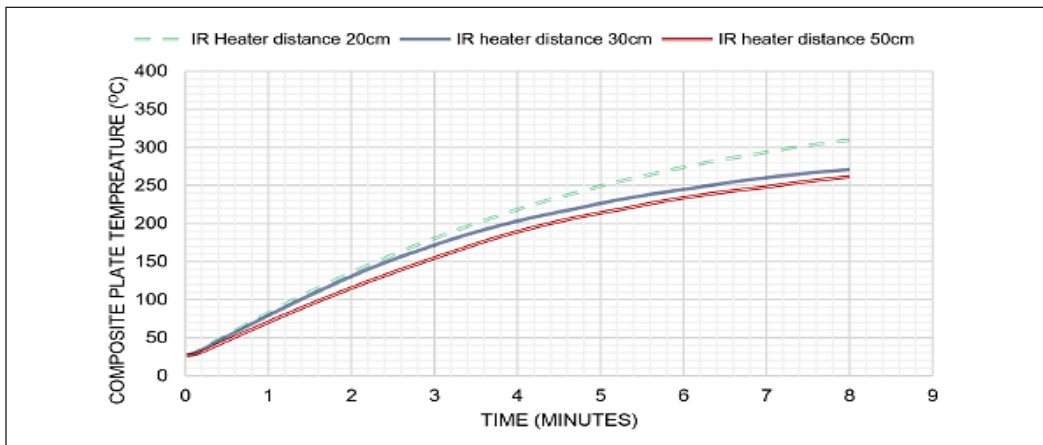


Figure 8. PPS plate temperature at heater temperature 360°C for various infrared (IR) heater distance

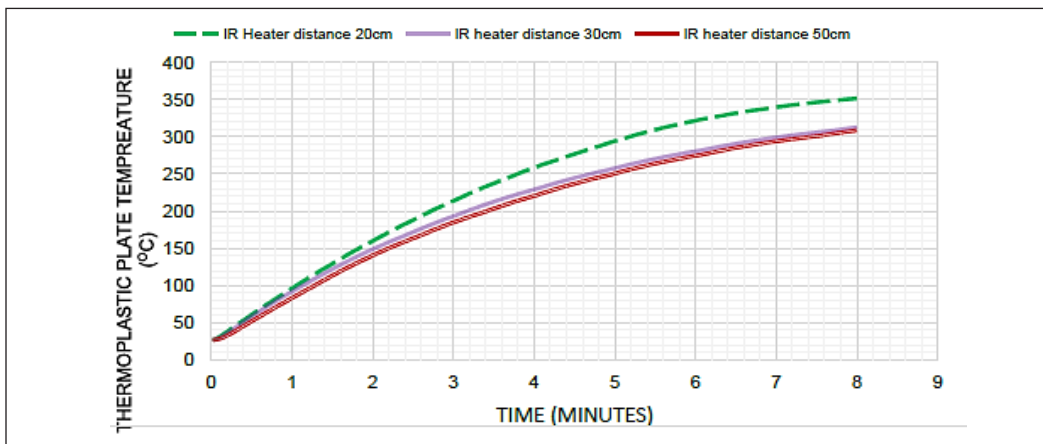


Figure 9. PPS plate temperature at heater temperature 400°C for various infrared (IR) heater distance

Two additional results are present. There is the effect of heater distance at different heater temperatures and effects of heater temperature at different heater distances. These two results could provide estimated data not lying in previous simulated cases.

For example, in Figure 11, which shows the relation of thermoplastic plate temperature against IR heater distance for different heater temperatures, one can predict the thermoplastic temperature at 400 mm heater distance (not in the previous simulated case) and 400°C heater temperature. As can be seen, the maximum thermoplastic temperature that can be achieved is 310°C. Furthermore, if the required temperature of thermoplastic is 320°C, the pre-setting heater distance should be around 275 mm with 400°C heater distance. In addition, the IR heater temperature of 360°C and 400°C did not affect the thermoplastic temperature for the heater distance between 350 mm and 500 mm.

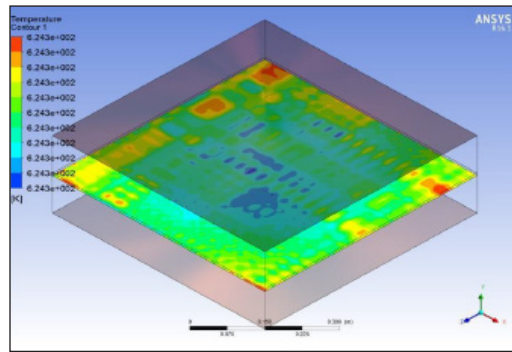


Figure 10. Sample contour shows uniform temperature distribution at 400°C heater and 200mm heater distance

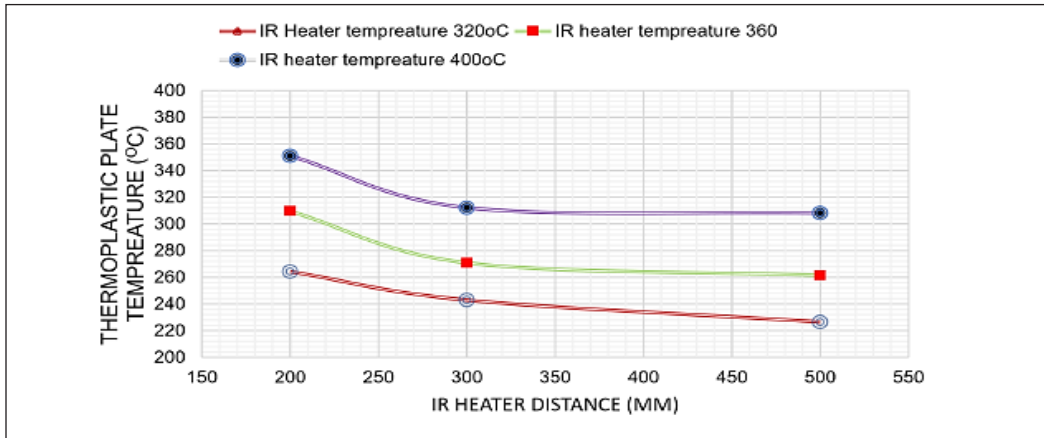


Figure 11. PPS plate temperature at 8 minutes for various infrared (IR) heater temperature

Figure 12 shows the relation of thermoplastic temperature to the IR heater temperature with different IR heater distances. To achieve 320°C thermoplastic temperature, we can use 400°C IR heater temperature with a heater distance of 200 mm. However, this 200 mm distance might be too close for the operation, and a larger distance might be needed. Using 300 mm or 500 mm can achieve close to 320°C if the heater temperature is set to 400°C. The obtained results might not be the same as the experiment in the thermoforming process due to the other environmental factors, machine capabilities, and varieties (Singh et al., 2019). In the simulation process, the thermoforming process is ideal, with perfect

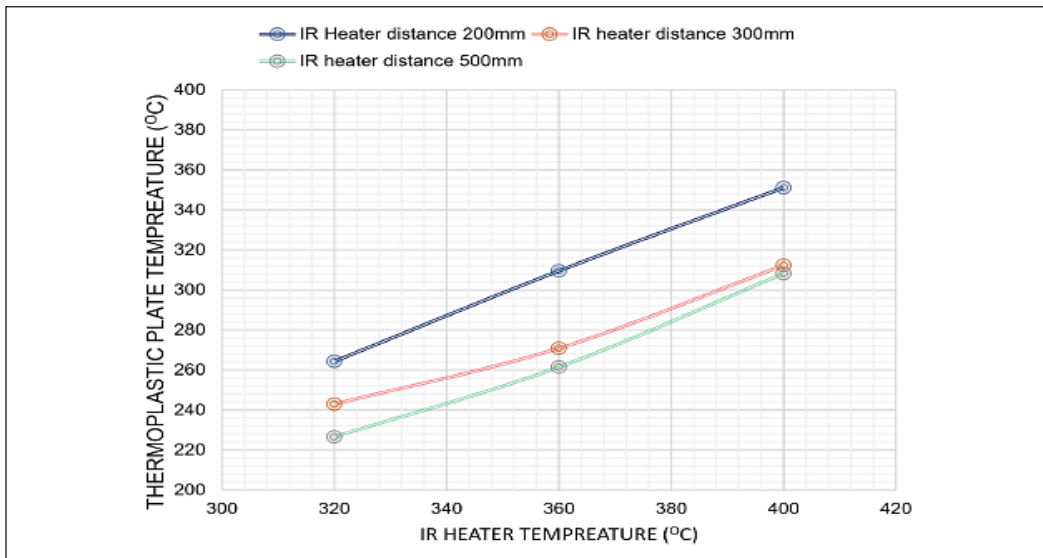


Figure 12. PPS plate temperature at 8 minutes for various infrared (IR) heater distance

heat control by the machine. The significance of finding the reference value in the molding press contributes to reducing the production cycle time and energy saving, enhancing the surface quality requirements and the final mechanical performances of the molded part (Sisca et al., 2020)

The findings of the research have significant implications for the aerospace. The simulation study reduces the uncertainty value and obtains reference value to reduce defect and time consumption during the thermoforming process (Hsiao & Kikuchi, 1999). If the thermoforming process can effectively replicate the mechanical and thermal properties of autoclave-cured PPS composites, it could lead to a paradigm shift in composite manufacturing (Choo et al., 2008; Allard et al., 2018). The potential benefits include reduced energy consumption, shorter cycle times, and improved manufacturing scalability (Nardi & Sinke, 2021). However, challenges related to maintaining consistent temperature distribution, achieving desired curing kinetics, and ensuring adequate fiber-matrix bonding must be addressed (Patil et al., 2019b).

CONCLUSION

This study examines the effect of heater distance at different heater temperatures and the effects of heater temperature at different heater distances. Setting up the maximum temperature of 400°C could achieve a minimum of 320°C for a distance of at least 270 mm. However, a larger distance of up to 500 mm manages to have at least 300°C for the PPS plate temperature. Unfortunately, the PPS plate will not achieve 320°C within 8 minutes if the heater temperature is below 350°C. Ideally, the temperature of 400°C with an IR

heater distance of 250–300 mm could yield the PPS plate to the temperature of 300–320°C. The recommendation for future study might be exploration how different mold designs, including surface textures and cooling channels, affect thermal distribution. It could involve experimental and simulation studies to optimize mold geometry for improved uniformity.

ACKNOWLEDGEMENT

This project has been funded by the grant INDUSTRI(MTUN)/AMIC/2020/FKM-CARE/10050 from Universiti Teknikal Malaysia Melaka (UTeM) and Aerospace Malaysia Innovation Centre (AMIC).

REFERENCES

- Allard, R., Charrier, J. M., Ghosh, A., Marangou, M., Ryan, M. E., Shrivastava, S., & Wu, R. (1986). An engineering study of the thermoforming process: experimental and theoretical considerations. *Journal of Polymer Engineering*, 6(1-4), 363-394. <https://doi.org/10.1515/POLYENG.1986.6.1-4.363>
- Akkerman, R., & Haanappel, S. P. (2015). Thermoplastic composites manufacturing by thermoforming. In P. Boisse (Ed.), *Advances in Composites Manufacturing and Process Design* (pp. 111–129). Woodhead Publishing. <https://doi.org/10.1016/b978-1-78242-307-2.00006-3>
- Choo, H. L., Martin, P. J., & Harkin-Jones, E. M. A. (2008). Measurement of heat transfer for thermoforming simulations. *International Journal of Material Forming*, 1(S1), 1027–1030. <https://doi.org/10.1007/s12289-008-0233-7>
- Ekşi, O., Karabeyoğlu, S. S., & Cinar, K. (2019). Experimental and numerical study on the thermoforming process of amorphous thermoplastic polymers. *Materials Testing*, 61(5), 417-424. <https://doi.org/10.3139/120.111351>
- Erchiqui, F., Annasabi, Z., Kaddami, H., Ben Hamou, K., & Ngoma, G. D. (2021). Effect of the cooling temperature of a PET sheet on the crystallinity and mould removal time for thermoforming applications. *The Canadian Journal of Chemical Engineering*, 99(3), 695-707. <https://doi.org/10.1002/cjce.23906>
- Günther, D., Erhard, P., Schwab, S., & Taha, I. (2021). 3D printed sand tools for thermoforming applications of carbon fiber reinforced composites - A perspective. *Materials*, 14(16), Article 4639. <https://doi.org/10.3390/ma14164639>
- Hsiao, S. W., & Kikuchi, N. (1999). Numerical analysis and optimal design of composite thermoforming process. *Computer Methods in Applied Mechanics and Engineering*, 177(1-2), 1-34. [https://doi.org/10.1016/S0045-7825\(98\)00273-4](https://doi.org/10.1016/S0045-7825(98)00273-4)
- Lee, H. J., Shin, D. J., & Park, K. (2017). Ultrasonic thermoforming of a large thermoplastic polyurethane film with the aid of infrared heating. *Journal of Mechanical Science and Technology*, 31, 5687–5693. <https://doi.org/10.1007/s12206-017-1109-x>
- Margossian, A., Bel, S., & Hinterhoelzl, R. (2016). On the characterisation of transverse tensile properties of molten unidirectional thermoplastic composite tapes for thermoforming simulations. *Composites Part A: Applied Science and Manufacturing*, 88, 48-58. <https://doi.org/10.1016/j.compositesa.2016.05.019>

- Nadlene, R., Mansor, M. R., Omar, G., Kamarulzaman, S. F. S., Zin, M. H., & Razali, N. (2021). Chapter 15 - Out-of-autoclave as a sustainable composites manufacturing process for aerospace applications. In S. M. Sapuan & M. R. Mansor (Eds.), *Design for Sustainability: Green Materials and Processes* (1st ed.: pp. 395-413). Elsevier Inc.
- Nardi, D., & Sinke, J. (2021). Design analysis for thermoforming of thermoplastic composites: Prediction and machine learning-based optimization. *Composites Part C: Open Access*, 5, Article 100126. <https://doi.org/10.1016/j.jcomc.2021.100126>.
- Patil, J. P., Nandedkar, V., Saha, S., & Mishra, S. (2019a). A numerical approach on achieving uniform thickness distribution in pressure thermoforming. *Manufacturing Letters*, 21, 24–27. <https://doi.org/10.1016/j.mfglet.2019.07.003>
- Patil, J. P., Nandedkar, V. M., & Mishra, S. (2019b). Thermal analysis of the heating stage of the thermoforming process. *International Journal of Recent Technology and Engineering (IJRTE)*, 8(2), 2085-2092. <https://doi.org/10.35940/ijrte.b2301.078219>
- Ropers, S. (2017). *Bending Behavior of Thermoplastic Composite Sheets: Viscoelasticity and Temperature Dependency in The Draping Process*. Springer Wiesbaden. <https://doi.org/10.1007/978-3-658-17594-8>
- Shrivastava, A. (2018). *Introduction to Plastics Engineering*. William Andrew Publishing.
- Sisca, L., Locatelli Quacchia, P. T., Messana, A., Airale, A. G., Ferraris, A., Carello, M., Monti, M., Palenzona, M., Romeo, A., Liebold, C., Scalera, S., Festa, A., & Codrino, P. (2020). Validation of a simulation methodology for thermoplastic and thermosetting composite materials considering the effect of forming process on the structural performance. *Polymers*, 12(12), Article 2801. <https://doi.org/10.3390/polym12122801>
- Valente, M., Rossitti, I., & Sambucci, M. (2023). Different production processes for thermoplastic composite materials: sustainability versus mechanical properties and processes parameter. *Polymers*, 15(1), Article 242. <https://doi.org/10.3390/polym15010242>

Material Selection of Natural Fibre Composite Webbing Sling Using Rule of Mixture

Noryani Muhammad^{1,2*}, Nur Ain Fatihah Roslan³ and Mohd Syahril Abd Rahman⁴

¹*Fakulti Teknologi dan Kejuruteraan Mekanikal, Universiti Teknikal Malaysia Melaka, Hang Tuah Jaya, 76100 Durian Tunggal, Melaka, Malaysia*

²*Centre for Advanced Research on Energy, Universiti Teknikal Malaysia Melaka, Hang Tuah Jaya, 76100 Durian Tunggal, Melaka, Malaysia*

³*Bmech Engineering Sdn. Bhd., Kelana Jaya Business Centre, Jalan SS7/2, Kelana Jaya, 47301 Petaling Jaya, Selangor, Malaysia*

⁴*Facility Management Department, Johor Port Berhad, Jalan Pasir Gudang, 81707 Pasir Gudang, Johor, Malaysia*

ABSTRACT

Natural fibre composites have grown in popularity as environmental concerns and knowledge about using eco-friendly materials versus synthetic materials. Furthermore, due to their low density and high strength, natural fibres are suitable for use as lightweight composite and reinforcing materials. Webbing slings are commonly used in many industries to lift loads and are typically made of synthetic fibres such as nylon and polyester. This study analysed the physical and mechanical properties, such as density, tensile strength, and Young's modulus of natural fibre composites. Bananas, pineapple, and jute with polymer matrices such as polypropylene (PP) and epoxy (EP) were used as alternative natural fibre composites for webbing sling application. Furthermore, descriptive statistical analysis was done to summarise the secondary data from the previous study of the physical and mechanical properties of natural fibre and polymer matrix. The rule of mixture (ROM) is

used to identify the optimum fibre loading for manufacturing the webbing sling. This study's volume fractions of fibre were 10%, 30%, and 50%. Using the ROM equation, the results revealed that the higher fibre loading of up to 50% could increase the mechanical properties such as tensile strength and Young's modulus. Based on the results, pineapple/epoxy composite was the best material to manufacture the webbing

ARTICLE INFO

Article history:

Received: 16 August 2023

Accepted: 09 May 2024

Published: 14 June 2024

DOI: <https://doi.org/10.47836/pjst.32.S2.05>

E-mail addresses:

noryani@utem.edu.my (Noryani Muhammad)

fatihahain123@gmail.com (Nur Ain Fatihah Roslan)

mohd.syahril@johorport.com.my (Mohd Syahril Abd Rahman)

* Corresponding author

sling and complied with the requirements of Product Design Specifications of polyester webbing sling compared to banana and jute composites.

Keywords: Material selection, natural fibre composite, webbing sling, ROM

INTRODUCTION

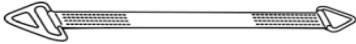
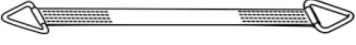


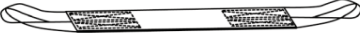
Many industries are struggling to reduce plastic consumption and dispose of bio-waste generated by various plants and trees. Waste management is also an important issue that needs to be overcome to optimise the cost and space in the long term. Many studies published natural fibres and bio-waste utilisation in the current year. Wood, sisal, hemp, coconut, cotton, kenaf, flax, jute, banana, and pineapple are natural fibres. The demand for these materials is increasing due to recent researchers who proved the potential of natural fibre composite (NFC) to replace synthetic or traditional materials (Ilyas et al., 2022). The advantages of these materials are lightweight, low cost, low energy generation, eco-friendly, and biodegradable (Todkar & Patil, 2019).

Moreover, a huge number of researchers reported NFC achieving most of the properties, such as physical, mechanical, thermal, and rheological, of synthetic material based on the applications (Milosevic et al., 2017; Prabhu et al., 2020). Different NFCs have different properties, and many factors influence the characteristics of NFC, such as the type of fibre, reinforcement agent, fibre loading, chemical treatments, and the manufacturing process (Delgado-Aguilar et al., 2017). Aircraft, automotive, construction, food packaging, and textile industries use NFC as their alternative materials to support green technology (Jumaidin et al., 2017). Webbing sling is one of the components used in various industries to lift and secure heavy loads. A webbing sling is a flexible and durable lifting accessory used in ports to transfer cargo or containers. Different webbing slings provide different security and are reliable for lifting and transporting heavy loads, such as cargo containers, onto ships, trucks and other vehicles.

Most webbing slings are currently manufactured from polyester, nylon, and polypropylene, especially in the construction industry (Neto et al., 2018). Multiple factors should be considered to manufacture the webbing sling, such as load capacity, environmental conditions, and chemical resistance. There are many types of webbing slings with different widths and lengths in the market to accommodate different loads and lifting configurations. Table 1 shows six types of webbing slings, describing the market nowadays. The size has to fulfil the applications with adequate support and stability. Choosing the best material to comply with all industry requirements is crucial, particularly safety. Another factor is stitching and reinforcement, in which the webbing sling should have reinforced stitching along its length to ensure durability and strength. It is a good credit to replace this material with the best NFC based on its product design specification

to fulfil the physical and mechanical properties of the webbing sling. Moreover, NFC has reinforcement features that can withstand high wear resistance and non-corrosive nature to enhance longevity (Chang et al., 2014; Dalbehera & Acharya, 2015).

Table 1
Six different types of webbing slings

Types	Description
 Type I	A web sling with a slotted triangle choker fitting on one end and a triangle fitting on the other. Often used in vertical, basket, or choker hitches.
 Type II	Triangle fittings on both ends of a web sling. It is only used with vertical or basket hitches.
 Type III	Each end of the web sling has a flat loop eye, which opens in the same plane as the sling body. A flat eye and eye, or double eye sling, is another name for this sort of sling.
 Type IV	Web Sling with both loop eyes is constructed as in Type III, except that the loop eyes are rotated to produce a loop eye perpendicular to the sling body's plane. A twisted eye sling is the usual name for this sort of sling.
Type V	An endless web sling, often known as a grommet. A load-bearing splice joins the ends of the webbing together to form a continuous loop.
 Type VI	Multiple thicknesses of webbings are held edge to edge to make a return eye (reversed eye) web sling. A worn pad is connected to one or both sides of the web sling body and one or both sides of the loop eyes to produce a loop eye at each end at a right angle to the plane of the web sling body.

Various interesting results indicate the potential of NFC to achieve the performance of traditional or common materials in many industries. There are many tools for multi-criteria decision-making nowadays; the rule of mixture (ROM) is one of the easy and common tools in engineering materials that can provide solutions with minimum time and cost compared to other tools (Tham et al., 2019). ROM is also flexible in multiple applications, such as finance and engineering design (Hine et al., 2014). The properties of individual components in the composite are very important for this method. It provides a way to predict the overall behaviour of the composite by knowing the relative proportions and its constituents. The basic assumption is that the composite material is made up of two materials. Another method is named the rule of hybrid mixture for more than two combinations of materials. Muhammad et al. (2022) validated that the final ROM result was consistent with the experimental data. A previous study also worked on improving the final result by considering the Kelly-Tyson model to estimate the tensile properties of the composite (Summerscales et al., 2019). Monte Carlo simulation was also used with ROM to increase the precision of the final result (Yerbolat et al., 2018).

However, most of the studies in the open literature did not simultaneously examine the analytical analysis of the final material that can replace the synthetic material for webbing slings. Based on the literature, very limited studies are available for webbing sling applications. This present study focuses on estimating physical and mechanical properties using an analytical analysis named ROM to select the best NFC for webbing sling applications. The current study contributes to the industry by addressing three important properties of manufacturing webbing slings in construction and transportation: density, tensile strength, and Young's modulus.

Literature Review

There are three types of natural fibre sources: (1) plant, (2) animal, and (3) mineral. These materials are composed of protein and cellulose, and a current study on plants reported an annual increment of plant fibres compared to animal and mineral natural fibres. The industry trend and forecast for the year 2022 to 2029 based on data year 2021 expected the natural fibre value to reach up to USD 68 447 Million by 2029 (<https://www.databridgemarketresearch.com/reports/global-natural-fibers-market>). Specifically, the forecast is for the automotive, textile, insulation, and medical applications. Pineapple, banana, flax, hemp, bamboo, kenaf, sisal, and jute are natural fibres of plants. Many applications utilise NFC to replace synthetic materials. For example, in the automotive industry, NFC has proved its ability to replace synthetic materials for interior door panels, dashboards, seat backs, and trunk linings (Ishak et al., 2016; Muhammad et al., 2022; Shaharuzaman et al., 2018).

The mechanical properties of this material are reported worldwide to be equivalent to those of metal-based materials. Having lightweight and excellent cost-effectiveness are the other reasons this material is preferable in the automotive industry. NFC is also utilised to produce building materials in the construction industry, such as roofing tiles, window frames, and wall cladding (Das, 2017). They provide thermal and acoustic insulations and are also environmentally friendly for long-term usage (Saba et al., 2016). Its other applications include consumer goods and packaging, where NFC promises an eco-friendly alternative to conventional materials. Examples of these applications are trays, containers, boxes, toys, furniture, sports, and household items. Aerospace and marine industries are the top industries that support plant-based sources that can offer weight reduction benefits, especially in manufacturing the interior components, non-structural parts, boat hulls, and decks (Asim et al., 2018; Pellicer et al., 2017). NFC provides good resistance to water and also reduces environmental impacts, especially in marine vessels (Hawary et al., 2023).

NFC's physical and mechanical properties are very important to be published in research findings. The facts and figures of this material's performance can increase the end users' trustworthiness (Wahab et al., 2015). For example, the user must consider several factors to increase the ability to rely on new cars with parts manufactured from NFC. Strength, stiffness,

impact resistance, fatigue resistance, weight reduction, and thermal expansion are among the vital factors influencing the performance of new cars (Hagnell et al., 2020). Moreover, to ensure the interior components in the car can withstand normal usage and reflect the potential impact forces, it also provides durability and safety in maximum years of usage. Besides that, in the construction industry, the contractor can use NFC to substitute traditional materials based on structural requirements, costs, sustainability, safety, design, and environmental factors (Tezara et al., 2016). It is a crucial task to meet all the requirements. Hence, a current study reported that the strength of kenaf composite is similar to that of synthetic materials (Tholibon et al., 2019). Chemical treatment also increased the performance of the jute-tea leaf fibre-reinforced hybrid composite. The tensile, flexural, and inter-laminar shear strengths were increased, and the morphological properties were improved (Prabhu et al., 2019).

Webbing sling is one of the important tools used in the material handling and lifting industries. Every industry has different requirements for using webbing slings based on the applications that include construction, manufacturing and warehouse facilities, shipping and logistics, utilities and power generation, rigging and offshore operations, and entertainment and events. Tables 2 and 3 show the different sizes and loads based on the types of webbing slings. The minimum width sling is 25mm, and the maximum width is 152mm. Table 3 shows the maximum load of 12 000 kg for 152mm width by vertical basket hitch type. It is important to know the maximum load for every type of webbing sling to prevent accidents or injuries during the lifting process (Nathan et al., 2019). Based on a previous work studying 60 case studies for over 25 years, 87% of sling accident investigations involved synthetic slings (Chi & Lin, 2022). Identifying the best material that fulfils all the factors in multiple applications is difficult. ROM is one of the simplest tools in material selection that minimises cost and time (Noryani et al., 2019). The prediction of the physical and mechanical properties of the webbing sling can reduce the number of failures during the inspection.

Table 2
Different types and sizes of webbing slings (single and two legs)

Sling width (mm)	SINGLE LEG			2 LEGS OR SINGLE BASKET			
	Hitch Types			Horizontal Angles			
	Vertical	Choker	Vertical Basket	Vertical	60°	45°	30°
25	500 kg	400 kg	1 000 kg	1 000 kg	866 kg	707 kg	500 kg
38	725 kg	580 kg	1 450 kg	1 450 kg	1 256 kg	1 025 kg	725 kg
44	850 kg	680 kg	1 700 kg	1 700 kg	1 472 kg	1 202 kg	850 kg
51	1 000 kg	800 kg	2 000 kg	2 000 kg	1 732 kg	1 414 kg	1 000 kg
76	1 500 kg	1 200 kg	3 000 kg	3 000 kg	2 598 kg	2 121 kg	1 500 kg
102	2 000 kg	1 600 kg	4 000 kg	4 000 kg	3 464 kg	2 828 kg	2 000 kg
127	2 500 kg	2 000 kg	5 000 kg	5 000 kg	4 330 kg	3 535 kg	2 500 kg
152	3 000 kg	2 400 kg	6 000 kg	6 000 kg	5 196 kg	4 242 kg	3 000 kg

Source: <https://www.scribd.com>

Table 3
Different types and sizes of webbing slings (hitch and horizontal)

Sling width (mm)	Hitch Types			Horizontal Angles		
	Endless Vertical	Choker	Vertical Basket	60°	45°	30°
25	1 000 kg	800 kg	2 000 kg	1 732 kg	1 414 kg	1 000 kg
38	1 450 kg	1 160 kg	2 900 kg	2 511 kg	2 050 kg	1 450 kg
44	1 700 kg	1 360 kg	3 400 kg	2 944 kg	2 404 kg	1 700 kg
51	2 000 kg	1 600 kg	4 000 kg	3 464 kg	2 828 kg	2 000 kg
76	3 000 kg	2 400 kg	6 000 kg	5 196 kg	4 242 kg	3 000 kg
102	4 000 kg	3 200 kg	8 000 kg	6 928 kg	5 656 kg	4 000 kg
127	5 000 kg	4 000 kg	10 000 kg	8 660 kg	7 070 kg	5 000 kg
152	6 000 kg	4 800 kg	12 000 kg	10 392 kg	8 484 kg	6 000 kg

Source: <https://www.scribd.com>

MATERIALS AND METHODS

Data collection of secondary sources on natural fibre and polymer matrix were identified. Based on the literature review from 2004 to 2022, banana, pineapple and jute are the common natural fibres used for composite applications. Many studies have reported that the properties of this material can achieve the tensile strength of synthetic material for webbing slings. Polypropylene (PP) and epoxy (EP) are considered as the alternatives to select the best material for the webbing sling industry because the properties of PP and EP are almost equal to nylon and polyester, which are the command materials used for webbing slings. Descriptive statistical analysis was used to summarise the properties of the materials. The physical and mechanical properties prediction using the Rule of Mixture (ROM) was compared with the product design specification (PDS) to finalise the composite and identify the best composites for manufacturing the webbing sling. Figure 1 shows the methodology to select the best NFC for webbing slings applications using ROM.

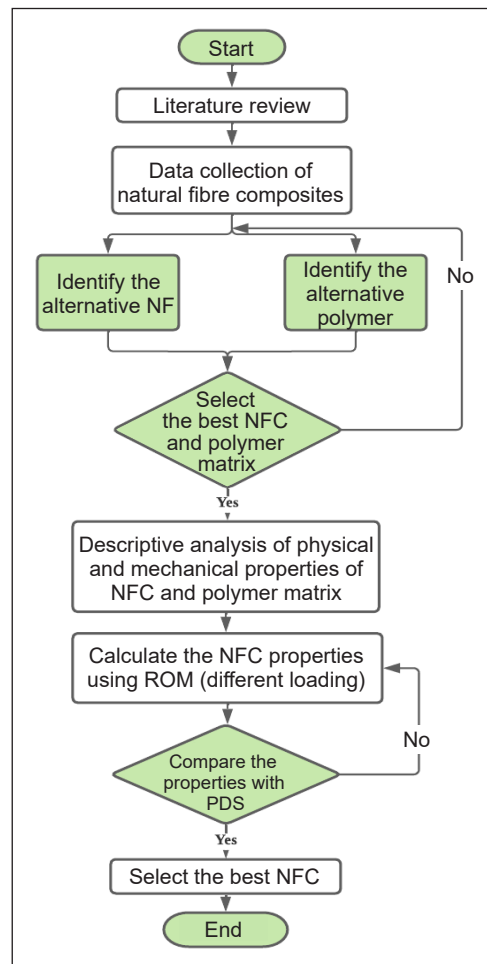


Figure 1. The methodology to identify the best NFC

Descriptive Statistical Analysis of Physical and Mechanical Properties of NFC

The secondary data on the physical and mechanical properties of the material are summarised using descriptive statistical analysis such as minimum, maximum, mean, and standard deviation. These informative values are very important for further estimation analysis using ROM. Equations 1 and 2 were used to calculate the sample mean (\bar{x}) and standard deviation (s), where x_i is the physical and mechanical properties and n is the number of observations.

$$\bar{x} = \frac{\sum x_i}{n} \quad (1)$$

$$s = \left[\frac{1}{n-1} \left(\sum x_i^2 - \frac{(\sum x_i)^2}{n} \right) \right]^{1/2} \quad (2)$$

Rule of Mixture (ROM) of NFC

Analytical analysis using the ROM method was used to estimate the physical and mechanical properties of the composite, such as density (ρ), tensile strength (σ), and Young's modulus (E). Equations 3 to 5 were used to calculate the properties of the composite, where V is the volume for the subscript, f , m , and c are the fibre, matrix, and composite, respectively.

$$\rho_c = \rho_f V_f + \rho_m (1 - V_f) \quad (3)$$

$$E_c = E_f V_f + E_m (1 - V_f) \quad (4)$$

$$\sigma_c = \sigma_f V_f + \sigma_m (1 - V_f) \quad (5)$$

Three types of fibre loading are used based on previous studies, which are 10%, 30% and 50% for the composite materials using ROM (Noryani et al., 2019). The predicted density, tensile strength, and Young's modulus of the composite were compared with the PDS of commercial materials such as polyester and nylon. The density of polyester is 1.39 g/cm³, the tensile strength is 784 MPa, and the Young's modulus is 13.2 GPa (Nathan et al., 2019).

RESULTS AND DISCUSSION

Physical and Mechanical Properties of NFC Using Descriptive Analysis

Table 4 shows the minimum, maximum, mean, and standard deviation of the properties of banana, pineapple, jute, PP, and EP: density, tensile strength, and Young's modulus. These statistical values are used to measure the distribution of the physical and

mechanical properties. The larger the range and standard deviation, the more properties were dispersed, and the distribution was wider from the mean. The standard deviation value for tensile strength was large for all materials compared to density and Young's modulus. For example, the tensile strength of the banana was 135.69 compared to the density of 0.026 and Young's modulus of 23.46 GPa. This pattern was consistent with other materials: pineapple, jute, PP, and EP. PP is a lighter material than other materials. It is widely used in different applications, such as automotive, aircraft, food industry, and construction, due to its lightweight and ease of manufacturing (Altay et al., 2017; Ghasemi et al., 2016; Serrano et al., 2014). Ali et al. (2015) found PP to be the best material used in the material selection, and it complied with the requirements of automotive component manufacturers, compared to polystyrene and polyethylene. Based on tensile strength, pineapple was the highest with 1522.05 MPa, compared to banana and jute with 718.44 MPa and 542.91 MPa, respectively. Asim et al. (2015) reviewed the properties and strength of pineapple leaf fibre (PALF), and its composite revealed that the maximum range of PALF was 1627 MPa. Moreover, the demand and production of this fibre are increasing yearly. Further investigation on the improvement of tensile strength of pineapple by chemical treatment was performed and compared to kenaf fibre (Asim et al., 2016). The average Young's modulus of pineapple also had a higher score of 67.17 GPa, compared to banana with 19.69 GPa and jute with 33.33 GPa. This result is consistent with the ones reported by Shiju et al. (2015), with Young's modulus of pineapple reaching up to 82.5 GPa for 20 to 80 mm fibre diameter.

Table 4
The physical and mechanical properties of natural fibre and polymer

Material	Properties	Mean (\bar{x})	Standard deviation (s)	Maximum	Minimum
Banana	ρ	1.33	0.026	1.37	1.30
	σ	718.44	135.69	914	493
	E	19.69	23.46	32	3.5
Pineapple	ρ	1.44	0.087	1.54	1.32
	σ	1522.05	212.86	1627	898.5
	E	67.17	14.47	82	41
Jute	ρ	1.43	0.167	1.8	1.23
	σ	542.91	214.70	900	190
	E	33.33	15.44	60	15
PP	ρ	0.91	0.0129	0.92	0.89
	σ	34.2	5.89	41.4	26
	E	1.53	0.282	1.8	0.95
EP	ρ	1.15	0.030	1.18	1.096
	σ	64.47	24.02	85	13.7
	E	3.32	0.614	4.4	2.9

Prediction of Physical and Mechanical Properties Using ROM

The expected density, tensile strength, and Young's modulus of NFC are shown in Table 5 for fibre loading of 10%, 30%, and 50% using ROM. All expected properties were increasing with the increase in fibre loading. A previous study reported a positive linear significance of the properties of NFC for hand-brake parking lever application (Noryani et al., 2019). Both pineapple-reinforced polymer composites with 50% fibre loading scored the highest tensile strengths, which are 778.13 MPa and 793.26 MPa, compared to banana/PP, banana/EP, jute/PP, and jute/EP. The tensile strength of single pineapple fibre is highest on average 1522 MPa compared to banana fibre with 718.44 MPa and jute fibre with 542.91 MPa, as shown in Table 4.

The cellulose percentage of pineapple fibre is also high, with 71.6 wt.% compared to banana fibre at 61.5 wt.% and jute fibre at 63.24 wt.% (Venkatachalam et al., 2016). Pineapple leaf is also an interesting material to study nowadays, as this material is a more sustainable, eco-friendly, and alternative fabric-reinforced composite (Mahmud et al., 2022). Moreover, waste management in the agriculture industry will improve and be more cost-efficient in the long term. Based on the calculated density in Table 3, PP with three types of fibre loading is lighter than EP. PP is a common polymer produced in large quantities and has versatile applications in different industries (Altay et al., 2017).

Table 5
The expected density, tensile strength, and Young's modulus of NFC using ROM

Composites	Volume fraction		Expected Properties		
	Vf	Vm	ρ_{11} (g/cm ³)	σ_{11} (MPa)	E11(GPa)
Banana+ PP	0.1	0.9	0.95	102.62	3.35
	0.3	0.7	1.04	239.47	6.98
	0.5	0.5	1.12	376.32	10.61
Pineapple+ PP	0.1	0.9	0.96	182.99	8.09
	0.3	0.7	1.07	480.56	21.22
	0.5	0.5	1.18	778.13	34.35
Jute + PP	0.1	0.9	0.962	85.07	4.71
	0.3	0.7	1.07	186.81	11.07
	0.5	0.5	1.17	288.55	17.43
Banana + EP	0.1	0.9	1.17	129.87	4.96
	0.3	0.7	1.20	260.66	8.23
	0.5	0.5	1.24	391.46	11.51
Pineapple + EP	0.1	0.9	1.18	210.23	9.71
	0.3	0.7	1.24	501.74	22.48
	0.5	0.5	1.30	793.26	35.25
Jute + EP	0.1	0.9	1.18	112.31	6.32
	0.3	0.7	1.23	208	12.32
	0.5	0.5	1.29	303.69	18.33

Physical and Mechanical Properties Compared to PDS of Webbing Slings

Calculated density, tensile strength, and Young’s modulus for six NFCs with the PDS of polyester webbing sling were plotted in Figures 2 to 4. The dashed blue line in Figures 2 to 4 is the PDS of the polyester as the commercial material for webbing sling. Based on the physical properties of density, all composites produced lighter webbing slings based on 1.4g/cm³ as the PDS to manufacture webbing slings. 784 MPa are needed to produce a webbing sling in industry, and Figure 3 shows pineapple/EP composite with 50% fibre loading complied with the requirement of 793.26 MPa. Another important feature is Young’s modulus, with 13.2 GPa, which is the PDS to manufacture a webbing sling. Six different compositions of composites exceeded the PDS, which were 30% and 50% pineapple/PP. EP composite scored more than 13.2 GPa, while only 50% fibre loading of jute/PP and EP scored 17.43 and 18.33 GPa. Based on three PDS for webbing sling, pineapple/ EP is the best material using ROM prediction with the highest strength, low density and good achievement on Young’s modulus.

Another study suggested improving the final result using the hybrid mixture (ROHM) rule, which is believed to generate more alternative materials in different applications (Muhammad et al., 2022). Besides fibre loading, the type of natural fibre is also an important factor in identifying the best material to manufacture webbing slings. Recent studies have shown that potential natural sources for composite materials such as pineapple leaves can optimise the abundance of agriculture. In addition, coconut waste and banana peels in the food industry can be used as recycled material for other end products. In the textile industry, pineapple leaf fibre is the most explored reinforcement component in producing sustainable fabrics that can improve strength, durability, and breathability compared to conventional textiles.

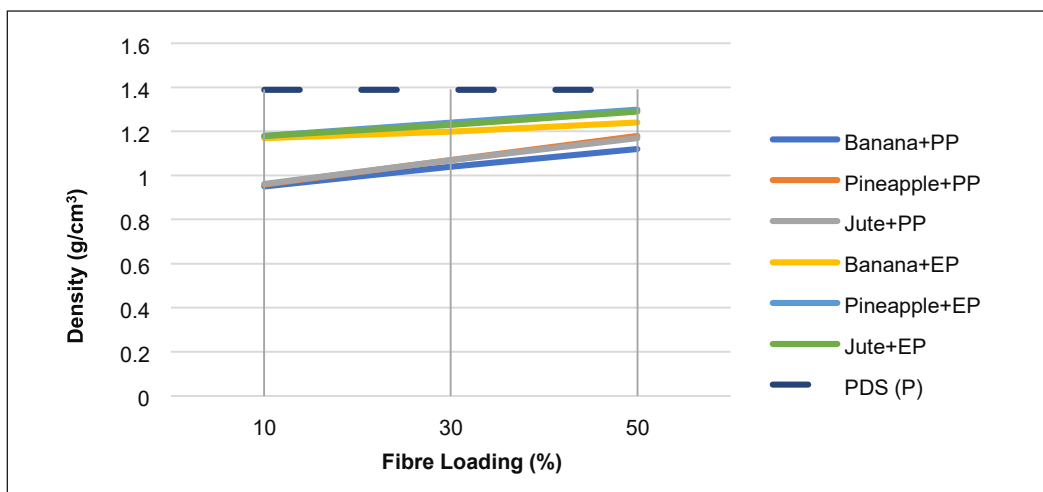


Figure 2. The density of NFC compared with PDS polyester webbing sling

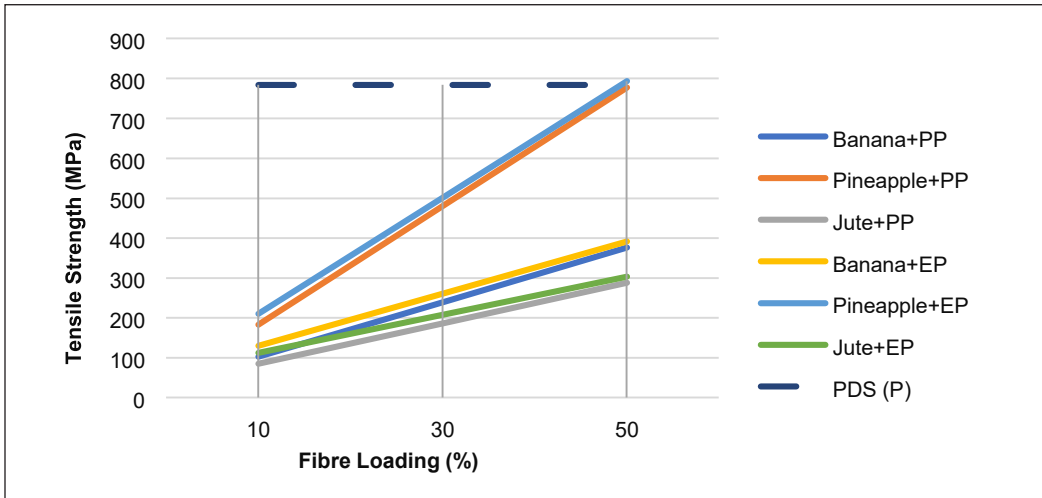


Figure 3. The tensile strength of NFC compared with PDS polyester webbing sling

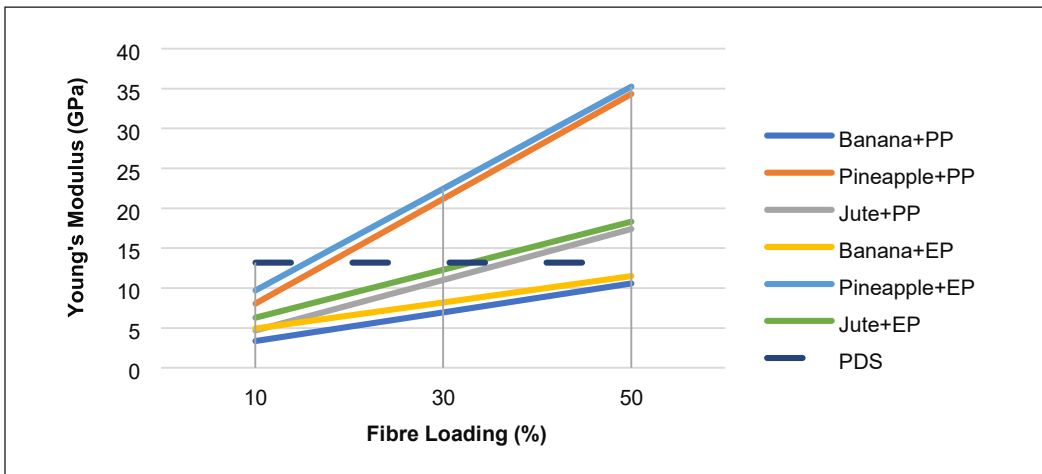


Figure 4. The Young's modulus of NFC compared with PDS polyester webbing sling

CONCLUSION

The analysis and comparison of NFC properties using ROM were performed, and it was found that the combination of pineapple with epoxy was the best material and had the best performance in manufacturing webbing slings at an optimum fibre loading of 50%. The value of tensile strength and Young's modulus were 793.26 MPa and 35.25 GPa, the highest compared to banana and jute composites. The mechanical properties of pineapple/epoxy have achieved comparable PDS as synthetic polyester for the manufacturing of webbing slings. However, the density of pineapple/epoxy did not fulfil the PDS of the polyester webbing sling of 1.30 g/cm^3 at 50% of fibre loading, lacking 0.09 g/cm^3 . From all the results, it has been proved that pineapple epoxy is the most suitable material compared

to other composites for manufacturing webbing slings. As a result, the mechanical and physical properties of pineapple fibre with epoxy, as well as the optimum fibre loading, have been determined and finalised. These findings are based on the approximate prediction by ROM, experimental characterisation, and testing necessary to validate and refine the predicted properties in this study. Further study on the engineering design of the detailed webbing sling structure, including holes, tears, cuts, snags, and burns, could be conducted in the future.

ACKNOWLEDGEMENTS

The authors thank Universiti Teknikal Malaysia, Melaka and the Ministry of Education, Malaysia, for this project's financial support through the FRGS/1/2022/STG06/UTEM/02/1 grant scheme.

REFERENCES

- Ali, B. A., Sapuan, S. M., Zainudin, E. S., & Othman, M. (2015). Implementation of the expert decision system for environmental assessment in composite materials selection for automotive components. *Journal of Cleaner Production*, *107*, 557–567. <https://doi.org/10.1016/j.jclepro.2015.05.084>
- Altay, L., Atagur, M., Akyuz, O., Seki, Y., Sen, I., Sarikanat, M., & Sever, K. (2017). Manufacturing of recycled carbon fiber reinforced polypropylene composites by high speed thermo-kinetic mixing for lightweight applications. *Polymer Composites*, *39*(10), 3656–3665. <https://doi.org/10.1002/pc.24394>
- Asim, M., Abdan, K., Jawaid, M., Nasir, M., Dashtizadeh, Z., Ishak, M. R., & Hoque, M. E. (2015). A review on pineapple leaves fibre and its composites. *International Journal of Polymer Science*, *2015*, 950567. <https://doi.org/10.1155/2015/950567>
- Asim, M., Jawaid, M., Abdan, K., & Ishak, M. R. (2016). Effect of alkali and silane treatments on mechanical and fibre-matrix bond strength of kenaf and pineapple leaf fibres. *Journal of Bionic Engineering*, *13*(3), 426–435. [https://doi.org/10.1016/S1672-6529\(16\)60315-3](https://doi.org/10.1016/S1672-6529(16)60315-3)
- Asim, M., Saba, N., Jawaid, M., & Nasir, M. (2018). Potential of natural fiber/biomass filler-reinforced polymer composites in aerospace applications. In M. Jawaid & M. Thariq (Eds.), *Sustainable Composites for Aerospace Applications* (pp. 253–268). Elsevier Ltd. <https://doi.org/10.1016/B978-0-08-102131-6.00012-8>
- Chang, B. P., Akil, H. M., Affendy, M. G., Khan, A., & Nasir, R. B. M. (2014). Comparative study of wear performance of particulate and fiber-reinforced nano-ZnO / ultra-high molecular weight polyethylene hybrid composites using response surface methodology. *Materials and Design*, *63*, 805–819. <https://doi.org/10.1016/j.matdes.2014.06.031>
- Chi, C. F., & Lin, Y. C. (2022). The development of a safety management system (SMS) framework based on root cause analysis of disabling accidents. *International Journal of Industrial Ergonomics*, *92*, Article 103351. <https://doi.org/10.1016/j.ergon.2022.103351>

- Dalbehera, S., & Acharya, S. K. (2015). Effect of cenosphere addition on erosive wear behaviour of jute-glass reinforced composite using taguchi experimental design. *Materials Today: Proceedings*, 2(4–5), 2389–2398. <https://doi.org/10.1016/j.matpr.2015.07.176>
- Das, S. (2017). Mechanical and water swelling properties of waste paper reinforced unsaturated polyester composites. *Construction and Building Materials*, 138, 469–478. <https://doi.org/10.1016/j.conbuildmat.2017.02.041>
- Delgado-Aguilar, M., Julián, F., Tarrés, Q., Méndez, J. A., Mutjé, P., & Espinach, F. X. (2017). Bio composite from bleached pine fibers reinforced polylactic acid as a replacement of glass fiber reinforced polypropylene, macro and micro-mechanics of the Young's modulus. *Composites Part B: Engineering*, 125, 203–210. <https://doi.org/10.1016/j.compositesb.2017.05.058>
- Ghasemi, F. A., Ghasemi, I., Menbari, S., Ayaz, M., & Ashori, A. (2016). Optimization of mechanical properties of polypropylene/talc/graphene composites using response surface methodology. *Polymer Testing*, 53, 283–292. <https://doi.org/10.1016/j.polymertesting.2016.06.012>
- Hagnell, M. K., Kumaraswamy, S., Nyman, T., & Åkermo, M. (2020). From aviation to automotive - A study on material selection and its implication on cost and weight efficient structural composite and sandwich designs. *Heliyon*, 6(3), Article e03716. <https://doi.org/10.1016/J.HELIYON.2020.E03716>
- Hawary, O. E., Boccarusso, L., Ansell, M. P., Durante, M., & Pinto, F. (2023). An overview of natural fiber composites for marine applications. *Journal of Marine Science and Engineering*, 11(5), Article 1076. <https://doi.org/10.3390/jmse11051076>
- Hine, P., Parveen, B., Brands, D., & Caton-Rose, F. (2014). Validation of the modified rule of mixtures using a combination of fibre orientation and fibre length measurements. *Composites Part A: Applied Science and Manufacturing*, 64, 70–78. <https://doi.org/10.1016/j.compositesa.2014.04.017>
- Ilyas, R. A., Zuhri, M. Y. M., Aisyah, H. A., Asyraf, M. R. M., Hassan, S. A., Zainudin, E. S., Sapuan, S. M., Sharma, S., Bangar, S. P., Jumaidin, R., Nawab, Y., Faudzi, A. A. M., Abral, H., Asrofi, M., Syafri, E., & Sari, N. H. (2022). Natural fiber-reinforced polylactic acid, polylactic acid blends and their composites for advance applications. *Polymers*, 14(1), Article 202. <https://doi.org/10.3390/polym14010202>
- Ishak, N. M., Malingam, S. D., & Mansor, M. R. (2016). Selection of natural fibre reinforced composites using fuzzy VIKOR for car front hood. *International Journal of Materials and Product Technology*, 53(3/4), 267–285. <https://doi.org/10.1504/IJMPT.2016.079205>
- Jumaidin, R., Sapuan, S. M., Jawaid, M., & Ishak, M. R. (2017). Thermal, mechanical, and physical properties of seaweed / sugar palm fibre reinforced thermoplastic sugar palm starch / Agar hybrid composites. *International Journal of Biological Macromolecules*, 97, 606–615. <https://doi.org/10.1016/j.ijbiomac.2017.01.079>
- Mahmud, R. U., Momin, A., Islam, R., Siddique, A. B., & Khan, A. N. (2022). Investigation of mechanical properties of pineapple-viscose blended fabric reinforced composite. *Composites and Advanced Materials*, 31, 1–10. <https://doi.org/10.1177/26349833221087752>
- Milosevic, M., Stoof, D., & Pickering, K. L. (2017). Characterizing the mechanical properties of fused deposition modelling natural fiber recycled polypropylene composites. *Journal of Composites Science*, 1(1), Article 7. <https://doi.org/10.3390/jcs1010007>

- Muhammad, N., Shaharuzaman, M. A., Taha, M. M., & Buniamin, F. F. (2022). Prediction of mechanical and physical properties of hybrid composites using ROHM. In A. S. P. Singh, M. F. Abdollah, H. Amiruddin & M. M. Taha (Eds.), *Proceedings of Mechanical Engineering Research Day 2022* (pp. 95–96). UTeM Press.
- Nathan, S., David, H., & Steven, W. (2019). *Recommended operating and inspection guideline*. Centers for Disease Control and Prevention. <https://www.cdc.gov/infectioncontrol/pdf/guidelines/disinfection/>
- Neto, A. H. P., Geiger, F. P., de Vargas Lisboa, T., & Marczak, R. J. (2018, July 22-25). *Mechanical analysis of polymeric webbing tests with and without preloads*. [Paper presentation]. 4th Brazilian Conference on Composite Materials, Rio de Janeiro, Brazil.
- Noryani, M., Sapuan, S. M., Mastura, M. T., Zuhri, M. Y. M., & Zainudin, E. S. (2019). Material selection of a natural fibre reinforced polymer composites using an analytical approach. *Journal of Renewable Materials*, 7(11), 1165–1179. <https://doi.org/10.32604/jrm.2019.07691>
- Pellicer, E., Nikolic, D., Sort, J., Baró, M. D., Zivic, F., Grujovic, N., Grujic, R., & Pelemis, S. (2017). Marine applications of natural fibre-reinforced Composites: A manufacturing case study. In C. Fragassa (Ed.), *Advances in Applications of Industrial Biomaterials* (pp. 21–47). Springer International Publishing. <https://doi.org/10.1007/978-3-319-62767-0>
- Prabhu, L., Krishnaraj, V., Sathish, S., Gokulkumar, S., & Karthi, N. (2019). Study of mechanical and morphological properties of jute-tea leaf fiber reinforced hybrid composites: Effect of glass fiber hybridization. *Materials Today: Proceedings*, 27, 2372–2375. <https://doi.org/10.1016/j.matpr.2019.09.132>
- Saba, N., Jawaaid, M., Alothman, O. Y., & Paridah, M. T. (2016). A review on dynamic mechanical properties of natural fibre reinforced polymer composites. *Construction and Building Materials*, 106, 149–159. <https://doi.org/10.1016/j.conbuildmat.2015.12.075>
- Serrano, A., Espinach, F. X., Tresserras, J., Pellicer, N., Alcalá, M., & Mutje, P. (2014). Study on the technical feasibility of replacing glass fibers by old newspaper recycled fibers as polypropylene reinforcement. *Journal of Cleaner Production*, 65, 489–496. <https://doi.org/10.1016/J.JCLEPRO.2013.10.003>
- Shaharuzaman, M. A., Sapuan, S. M., Mansor, M. R., & Zuhri, M. Y. M. (2018). Passenger car's side door impact beam: A review. *Journal of Engineering and Technology*, 9(1), 1-22.
- Shiju, C. P., Mathew, C., Viji, T., & Veeramani, S. (2015). Characterization of palf reinforced composites. *International Journal of Engineering Research & Technology (IJERT)*, 3(26), 1–6.
- Summerscales, J., Virk, A. S., & Hall, W. (2019). Enhanced rules-of-mixture for natural fibre reinforced polymer matrix (NFRP) composites (comment on Lau et al. in volume 136). *Composites Part B: Engineering*, 160, 167–169. <https://doi.org/10.1016/j.compositesb.2018.10.021>
- Tezara, C., Siregar, J. P., Lim, H. Y., Fauzi, F. A., Yazdi, M. H., Moey, L. K., & Lim, J. W. (2016). Factors that affect the mechanical properties of kenaf fiber reinforced polymer: A review. *Journal of Mechanical Engineering and Sciences*, 10(2), 2159–2175. <https://doi.org/10.15282/jmes.10.2.2016.19.0203>
- Tham, M. W., Fazita, M. N., Abdul Khalil, H. P. S., Zuhudi, N. Z. M., Jaafar, M., Rizal, S., & Haafiz, M. M. (2019). Tensile properties prediction of natural fibre composites using rule of mixtures: A review. *Journal of Reinforced Plastics and Composites*, 38(5), 211–248. <https://doi.org/10.1177/0731684418813650>

- Tholibon, D., Tharazi, I., Sulong, A. B., Muhamad, N., Farhani Ismail, N., Fadzly, K., Radzi, M., Afiqah, N., Radzuan, M., & Hui, D. (2019). Kenaf fiber composites: A review on synthetic and biodegradable polymer matrix. *Jurnal Kejuruteraan*, 31(1), 65–76. [https://doi.org/10.17576/jkukm-2019-31\(1\)-08](https://doi.org/10.17576/jkukm-2019-31(1)-08)
- Venkatachalam, N., Navaneethkrishnan, P., Rajsekar, R., & Shankar, S. (2016). Effect of pretreatment methods on properties of natural fiber composites: A review. *Polymers and Polymer Composites*, 24(7), 555–566. <https://doi.org/10.1177/096739111602400715>
- Wahab, O. A., Bentahar, J., Otok, H., & Mourad, A. (2015). A survey on trust and reputation models for Web services: Single, composite, and communities. *Decision Support Systems*, 74, 121–134. <https://doi.org/10.1016/j.dss.2015.04.009>
- Yerbolat, G., Amangeldi, S., Ali, M. H., Badanova, N., Ashirbeok, A., & Islam, G. (2019, November 16-18). *Composite materials property determination by Rule of Mixture and monte carlo simulation*. [Paper presentation]. IEEE International Conference on Advanced Manufacturing (ICAM), Yunlin, Taiwan. <https://doi.org/10.1109/AMCON.2018.8615034>

The Influence of MAPP and MAPE Compatibilizers on Physical and Mechanical Properties of 3D Printing Filament Made of Wood Fiber/Recycled Polypropylene

Nuzaimah Mustafa^{1*}, Yusliza Yusuf¹, Syahibudil Ikhwan Abdul Kudus¹, Nadlene Razali², Dwi Hadi Sulistyarini³, Mohd Hafizi Halim¹ and Aenderson Chaong Anak Ujih¹

¹Fakulti Teknologi dan Kejuruteraan Industri dan Pembuatan, Universiti Teknikal Malaysia Melaka, Hang Tuah Jaya, 76100 Durian Tunggal, Melaka, Malaysia

²Fakulti Teknologi dan Kejuruteraan Mekanikal, Universiti Teknikal Malaysia Melaka, Hang Tuah Jaya, 76100 Durian Tunggal, Melaka, Malaysia

³Faculty of Industrial Engineering, Brawijaya University, Malang, 65145, Jawa Timur, Indonesia

ABSTRACT

This study aims to develop 3D printing filament composites that support sustainability and waste reduction goals by utilizing wood waste and recycled polypropylene. This study evaluated the effect of Maleic Anhydride Polyethylene (MAPE) and Maleic Anhydride Polypropylene (MAPP) compatibilizers on the mechanical properties of the filament. The study found that r-WoPPc filament with MAPP and MAPE had higher tensile strength compared to r-WoPPc with significant increments of 13% and 74%, respectively, compared to v-WoPPc. The flexural strength of r-WoPPc increased by 18% and 60% after adding optimum loading MAPP and MAPE, respectively. The finding also reveals a significant enhancement in the tensile and flexural strength of the composite, proportional to the increase in MAPP percentage. In contrast, as the MAPE content increases, the tensile strength and

flexural strength of the r-WoPPc experience a gradual decrease. Consequently, the addition of MAPP and MAPE improved the interfacial adhesion between wood and polypropylene, as revealed by the surface morphology of the r-WoPPc tensile fractured surface. Moreover, the reduced water absorption in r-WoPPc is attributed to the enhanced interfacial adhesion between wood fibers and the r-PP matrix, associated with improved tensile and flexural strength.

ARTICLE INFO

Article history:

Received: 16 August 2023

Accepted: 09 May 2024

Published: 14 June 2024

DOI: <https://doi.org/10.47836/pjst.32.S2.06>

E-mail addresses:

nuzaimah@utem.edu.my (Nuzaimah Mustafa)

yusliza@utem.edu.my (Yusliza Yusuf)

syahibudil@utem.edu.my (Syahibudil Ikhwan Abdul Kudus)

nadlene@utem.edu.my (Nadlene Razali)

dwhiadi@ub.ac.id (Dwi Hadi Sulistyarini)

hafizihalimisa@gmail.com (Mohd Hafizi Halim)

aendersonchaong@gmail.com (Aenderson Chaong Anak Ujih)

* Corresponding author

The highest tensile strength of r-WoPPc with MAPP absorbs 14% water, while the lowest tensile strength absorbs 26%. Likewise, the highest tensile strength of r-WoPPc with MAPE absorbs only 0.8% water, compared to the lowest strength, which absorbs 2% water. This study demonstrated the potential for producing 3D printing filament from recycled polypropylene and wood waste, which benefits sustainability.

Keywords: 3D printing, compatibilizer, filament, wood fiber, recycled polypropylene, MAPP, MAPE, mechanical properties

INTRODUCTION

3D printing has experienced remarkable advancements in recent years, revolutionizing various industries and enabling the production of complex objects with great precision and efficiency. One area of particular interest is the development of 3D printing filament using sustainable and environmentally friendly materials. In this study, an investigation on the influence of compatibilizers, namely Maleic Anhydride Polypropylene (MAPP) and Maleic Anhydride Polyethylene (MAPE), was conducted on the performance and properties of wood fiber/recycled polypropylene filament for 3D printing. In recent years, investigating the effect of maleic anhydride compatibilizer agents on composite properties has gained significant attention in enhancing composite strength. Consequently, this study extends these principles in manufacturing 3D printing filament as they play a crucial role in optimizing the performance of the wood fiber/recycled polypropylene composite filament.

The utilization of wood fiber as reinforcement in polymer composites has gained significant attention due to its desirable properties, such as low cost, abundance, and excellent mechanical performance. On the other hand, recycled polypropylene addresses the crucial concern of plastic waste management while offering favorable thermoplastic characteristics. However, the inherent incompatibility between wood fiber and polypropylene matrix poses challenges in achieving optimal interfacial adhesion and mechanical strength in the composites. Typically, wood fiber exhibits a polar nature, while polymer matrices tend to be non-polar (Zhang et al., 2019). Nonetheless, the introduction of the maleic anhydride coupling enhancing the compatibility between the wood fiber and the polymer matrix, which improved adhesion between these two constituents, resulted in better mechanical properties (Bütün et al., 2019; Khalid et al., 2021). The stronger adhesion primarily resulted from forming hydrogen bonds and covalent linkages between wood fibers and maleic anhydride. Subsequently, the hydroxyl group of the wood fibers establishes a stronger bond with the oxygen atoms in the polymer matrices, further enhancing the adhesion (Billah et al., 2022).

Compatibilizers, such as MAPP and MAPE, have become promising additives that enhance the compatibility and interfacial bonding between materials in polymer composites. Reactive functional groups in these compatibilizers facilitate molecule interaction between

wood fiber and polypropylene, which promotes adhesion. Compatibilizers effectively bridge the interfacial gap between reinforcing wood fiber and polypropylene matrix strong adhesion, resulting in improved mechanical properties of the composites (Aida et al., 2021). The addition of maleic anhydride as a compatibilizer in PP-based composite during the FDM filament extrusion process also improved the friction and wear rate of the PP composite during the extrusion process, improving the mechanical properties of extruded filament (Kristiawan et al., 2021).

This paper aims to investigate the influence of MAPP and MAPE compatibilizers on the physical and mechanical properties of the wood fiber/recycled polypropylene composite (r-WoPPc) filament for 3D printing. The wood dust was pretreated using silane to ensure better enhancement of the wood fiber and polypropylene (PP) matrix in this study. Silanes are efficient coupling experts commonly utilized in fiber-reinforced composites; by forming compound linkages between the silane and the natural fiber surface, the surface morphology of natural fibers was altered (Khalid et al., 2021). The increase in strength is due to silanol (Si-OH) groups forming, creating strong bonds with the -OH groups of the fibers. For the remaining Si-OH groups, condensation occurs with adjacent Si-OH groups (Atiqah et al., 2018). A study by Petchwattana et al. (2019), who developed 3D printing filament using PLA/teak wood flour composite, encountered that composite filament with wood silane treatment had higher tensile strength compared to those without silane treatment. The impact of two different compatibilizers on the printed parts' tensile and flexural strength was assessed. Furthermore, the study also evaluated the effect of compatibilizer on water absorption of the filament and surface characteristics of the filament. Hence, this research could provide valuable insight into the potential of developing sustainable filament materials for 3D printing.

Literature Review

Maleic coupling agents are commonly employed to enhance the properties of polymer composites that incorporate filler or fiber reinforcement (Khalid et al., 2021). The incompatibility between these two constituents can be resolved by reacting anhydride groups in maleated polymer additive and the hydroxyl group of natural fibers. This interaction enhances the tensile properties of the composites. Generally, natural fibers, including wood, are polar, and polymer matrices are non-polar (Zhang et al., 2019). Hence, Maleic Anhydride Polypropylene (MAPP) and Maleic Anhydride Polyethylene (MAPE) are commonly used as polymer blend compatibilizers to improve mechanical properties and compatibility. When used as compatibilizers in 3D printing, fused deposition modeling (FDM) filaments made of wood fiber/recycled polypropylene can influence the properties of the resulting material. The MAPP and MAPE help in improving the compatibility between the polar surface of wood fiber and the non-polar surface of the PP matrix (Bütün et al., 2019; Khalid et al., 2021).

To begin with, the addition of MAPP and MAPE can improve the adhesion of wood fiber to recycled polypropylene. It can result in a more uniform distribution of the wood fiber within the polymer matrix, improving the mechanical properties of the resulting material. Improved adhesion reduces the likelihood of delamination during printing, improving the printed parts' quality (Razak et al., 2018). MAPP was used as a compatibilizer to competently enhance fiber-matrix bonding because of the formation of hydrogen bonds and covalent linkages between the hydroxyl groups of the fiber and maleic anhydride. The hydroxyl group of wood fiber, a chemical functional group of lignin, creates a strong hydrogen bond with the oxygen atom of MAPP (Billah et al., 2022).

Composite reinforced with wood is generally developed using raw wood fiber without any treatment or modification. Wood is alkali-treated to remove impurities, enhance properties, or improve compatibility with the matrix material. Wood is impregnated with a compatibilizer that helps to improve its compatibility with the matrix material. Also, silane is a coupling agent that enhances interfacial adhesion between fiber and matrix. The purpose of using these compatibilizers is to enhance the overall performance of the composites (Baykus et al., 2016). Keener et al. (2004) mentioned that adding maleated compatibilizing agents with a balance of maleic anhydride and molecular mass helps provide composites with the best performance. This is due to its function of enhancing the effectiveness of the oxidation of the polymer matrices with the fiber (Hao et al., 2021). Their work found that adding 1%–5 % MAPE or MAPP to the WPC improved mechanical properties by 30%–100 %.

Maleated coupling agents are commonly preferred in the literature for various polymer and fiber systems. Although maleated coupling agents are most utilized directly during the mixing process, they can also be grafted on hydroxyl groups of fiber or pre-impregnated with fiber prior to manufacturing. The physical and mechanical features of the wood particles, as well as the chemical interaction between wood particles and polymers, affect the quality of WPCs. Couplers like maleated anhydride grafted polyethylene and maleated anhydride grafted polypropylene are commonly used to improve the compatibility between hydrophilic cellulosic materials and a hydrophobic polymer (Mu et al., 2018). Moreover, high compatibility aids particle dispersion and adequate wetting in matrices, resulting in strong contact adhesion. Because ester linkages promote fiber-matrix contact, stress can be transferred more easily from the matrix to the reinforcing particles, improving mechanical characteristics. Furthermore, adequate contact adhesion lowers WPC water absorption (Dhanalakshmi et al., 2017).

MATERIALS AND METHODS

The wood dust used in this study was sourced from a local furniture workshop. The wood dust was treated using silane ((3-aminopropyl) triethoxysilane with CAS 919-30-2) from

Sigma-Aldrich. The recycled PP, a byproduct of plastic products, was supplied by a plastic factory in Ayer Keroh, Melaka.

Preparation of r-WoPPc

The wood dust was sieved to obtain 125 μm size, thoroughly washed with distilled water to eliminate impurities, and then dried in a hot air oven at 60°C for 24 hours. The wood dust was soaked in 2 wt% silane solution for 3 hours and dried at 80°C for 72 hours (Atiqah et al., 2018). The sample of treated wood dust was ready to mix with polypropylene after three days in the oven. The loadings of MAPP and MAPE used were 1%, 3%, and 5% respectively. Meanwhile, wood dust loading was fixed at 3%.

Silane-treated wood dust was mixed with recycled PP pellets, pressed using a hot press, and later crushed into pellets prior to making the filament. r-WoPPc pellet was then fed into a single screw extruder to produce filament. The filament of the composite material was extruded using a single screw extruder equipped with a die nozzle of 1.75 mm. The screw speed was set into range (18–20 rpm). To produce a 3D printed product, the dumbbell for tensile and flexural models, according to ASTM D638 and ASTM D790, was made using SolidWorks Software. The 3D modeling files were converted into STL files, which were later printed using the Ender 3D printing machine, as shown in Figure 1.

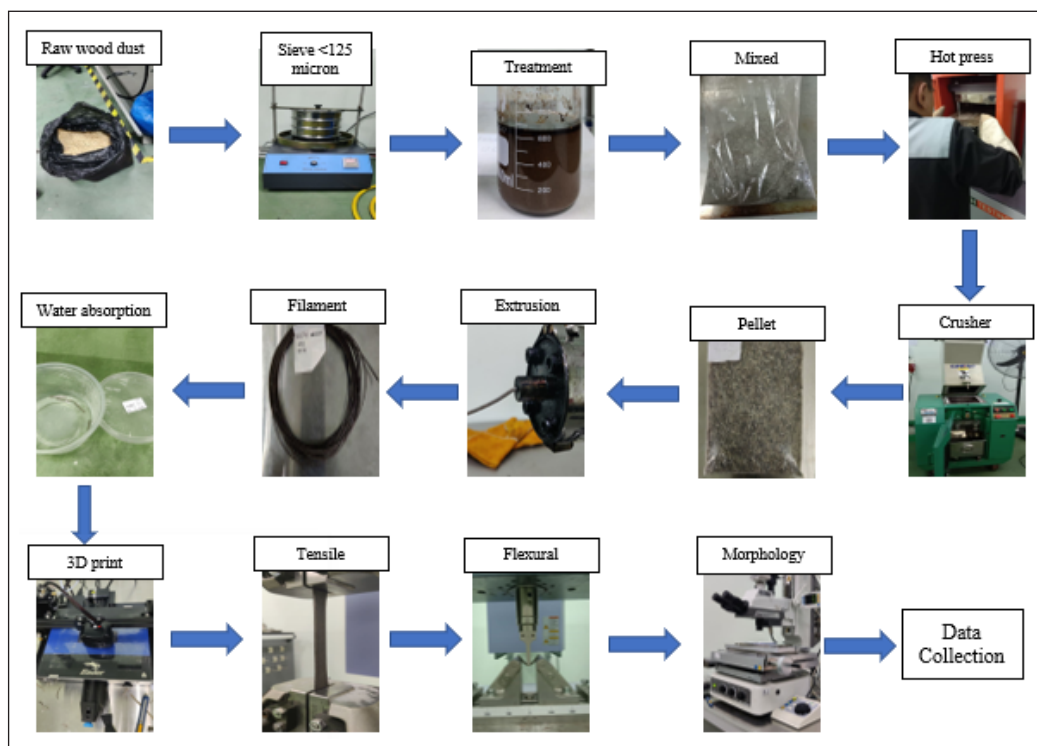


Figure 1. Production of 3D printing filament of r-WoPPc

Tensile and Flexural Tests of r-WoPPc

Tensile and flexural tests were conducted in accordance with ASTM D638 and ASTM D790 standards using Shimadzu AGS-X Universal Testing Machine. The following conditions were used: 5 mm/s displacement with a 30mm/min crosshead speed.

Surface Morphology r-WoPPc Tensile Fracture Surface

Surface morphological analyses of the tensile fractured surface were conducted using a Nikon MM-800N high-precision microscope.

Water Absorption of r-WoPPc

The water absorption of r-WoPPc was evaluated according to ASTM D570-98 to assess the hydrophilicity of the composite. The r-WoPPc filament was cut into 20 mm lengths and soaked in distilled water for 30 days. The weight of samples was recorded before and after immersion using the analytical balance model JA203P with ± 0.002 g accuracy. The water absorption of the composites was determined using Equation 1.

$$\text{Water Absorption (\%)} = \frac{W_1 - W_0}{W_0} \times 100\% \quad (1)$$

where w_0 (g) is the weight of composites after drying and w_1 (g) is the weight after water immersion.

RESULTS AND DISCUSSION

The mechanical properties of 3D printed parts are crucial for their function performance in various applications. This study investigated the influence of MAPP and MAPE compatibilizers on the tensile and flexural strength of 3D printed parts made of wood fiber/recycled polypropylene filaments. Polypropylene matrix with low melt viscosity can penetrate the wood fiber cellulose, which decreases the number of voids. Fewer voids resulted in higher density composite with improved mechanical properties (Yuan et al., 2008). Adding maleic anhydride polypropylene or polyethylene as a compatibilizer significantly enhanced the interfacial adhesion between the wood fiber and the polypropylene matrix. As a result, the composite strength improved considerably (Aida et al., 2021).

Effect of MAPE Compatibilizer Concentrations on Mechanical Properties

Figure 2 shows the variation of tensile strength with different compatibilizer concentrations. It can be observed that the addition of MAPE improved the tensile strength of the 3D-printed part produced from the r-WoPPc filament. The tensile strength of the r-WoPPc composite with MAPE compatibilizer was 74% higher than without compatibilizer. The composite's tensile strength was improved due to the enhanced bonding between the wood fiber and

the polypropylene matrix facilitated by the compatibilizer. Compatibilizer helped create stronger connections at the interface between the wood fiber and the polypropylene, leading to an overall enhancement in the mechanical properties of the composite. Introducing the compatibilizer into the mixture initiates the reaction of the anhydride group with the alcohol hydroxyl group within the wood fiber, thereby decreasing the fiber's polarity and hydrophilicity. This reduction in polarity strengthens the compatibility between the wood fiber and polypropylene.

Additionally, this process improves compatibility between the wood fiber and polymer surfaces. However, a higher compatibilizer concentration beyond the optimum point decreased tensile strength, indicating a possible plasticization effect. It can be observed that when loading MAPE was further increased to 3 wt% and 5 wt%, the tensile strength of the composite started to decrease, indicating the optimum MAPE value for the r-WoPPc 3D filament was 1 wt%. This finding was comparable with a study by Zhou et al. (2022), as adding MAPE into the wood fiber composite improved the tensile and flexural strengths because MAPE enhanced the interfacial adhesion between wood fiber and polymer matrix. This resulted in efficient stress transfer from the polymer to the wood fiber (Mu et al., 2018; Ou et al., 2014).

This study assessed the flexural strength of the 3D printed parts fabricated using r-WoPPc filament to measure their resistance to bending and deformation. Figure 3 shows the relationship between the flexural strength of the WoPPc 3D-printed part and compatibilizer concentration. Like the tensile strength, the flexural strength improved by adding MAPE. MAPE promoted better stress transfer between the wood fiber and polypropylene, resulting in increased flexural strength of approximately 60% than without a compatibilizer. However, the addition of excessive amounts of compatibilizer at concentrations of 3wt% and 5wt% showed decrement in tensile strength, indicating 1% as the optimum value of MAPE for the r-WoPPc filament.

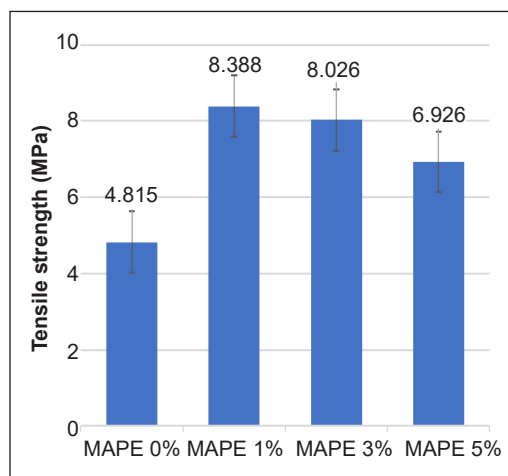


Figure 2. Tensile strength of r-WoPPc with MAPE

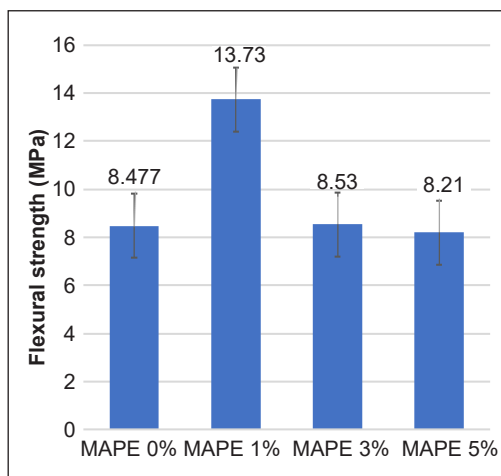


Figure 3 Flexural strength of r-WoPPc with MAPE

Effect of MAPP Compatibilizer Concentrations on Mechanical Properties

Figure 4 illustrates the effect of varying percentages of MAPP on the tensile and flexural strength of the r-WoPPc composite part. Notably, the introduction of MAPP led to an enhancement in the tensile strength of the composite by 13% compared to v-WoPPc. Furthermore, the tensile strength of the composite increased proportionally with a higher percentage of MAPP compatibilizer. The result indicates a notable enhancement in the tensile strength of the r-WoPPc as the MAPE content increased to 3 wt% with an increase of tensile strength from 13% to 20%. Furthermore, the highest amount of 5wt% MAPP resulted in a remarkable 40% increase in tensile strength. However, the rWoPPc flexural strength decreased by adding MAPE of 1 wt%. However, it improved proportionally with the addition of 3 wt% and 5 wt% of MAPP, with 5 wt% MAPP resulting in the highest flexural strength with an increment of 17.8% compared to v-WoPPc (Figure 5). It is concurrent with a study by Silva et al. (2021) and Petchwattana et al. (2019).

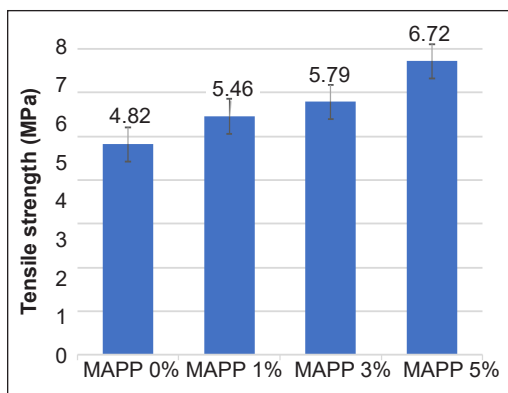


Figure 4. Tensile strength of r-WoPPc with MAPP

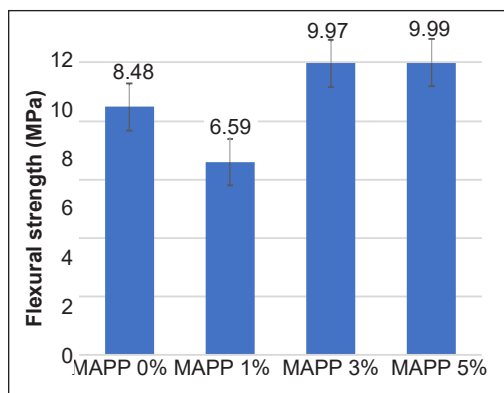


Figure 5. Flexural strength of r-WoPPc with MAPP

Effects of MAPE Compatibilizer on r-WoPPc Tensile Fracture Surface and Filament Surface Morphology

Figure 6 shows the SEM micrograph of the r-WoPPc tensile fracture surface with various MAPE loadings. In the absence of MAPE compatibilizer, there was inadequate adhesion between the wood fibers and the r-PP matrix, resulting in the wood fiber easily fractured and pulled out from the matrix (Figure 6a). Meanwhile, Figure 6(b) demonstrates strong adhesion between the wood fiber and r-PP matrix when MAPE was incorporated in r-WoPPc. The evidence of the wood fiber impregnated well in the r-PP matrix was enhanced interfacial bond, resulting in higher tensile and flexural strengths (Hao et al., 2021). Contrary to this, incorporating higher quantities of MAPE did not improve adhesion between the wood fiber and r-PP matrix, as evidenced by the SEM micrographs. Figures 6(c) and (d) show poor interfacial adhesion between the wood fiber and PP matrix in the r-WoPPc was incorporated with 3 wt% and 5 wt% MAPE.

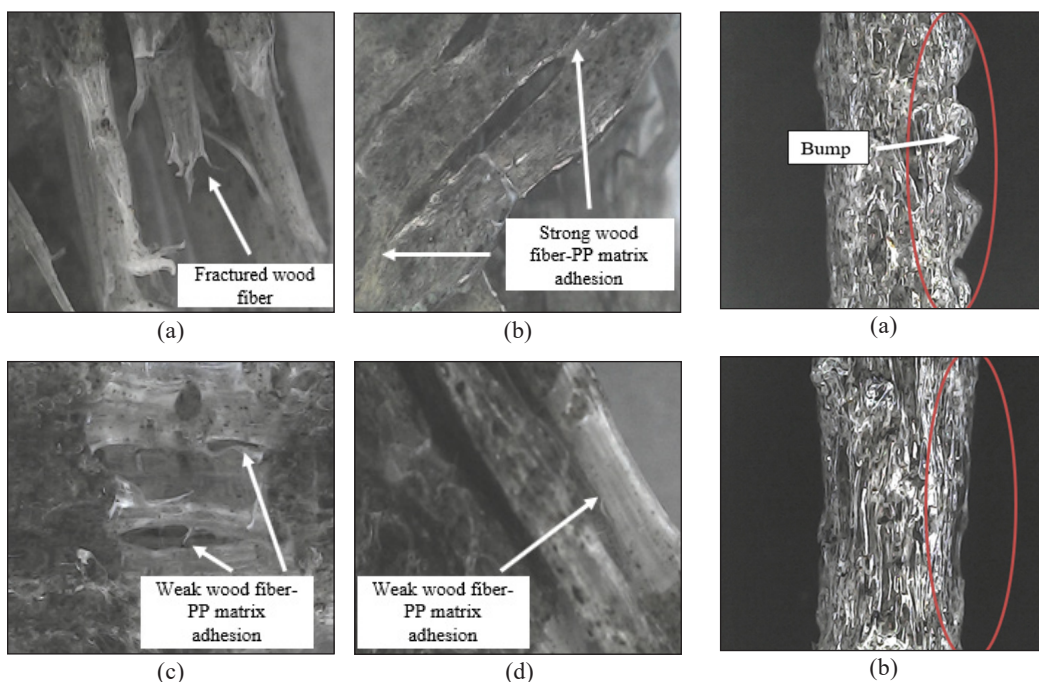


Figure 6. High precision micrograph with 10 \times magnification of r-WoPPc tensile fracture surface: (a) without MAPE; (b) 1 wt% MAPE; (c) 3 wt% MAPE; and (d) 5 wt% MAPE

Figure 7 shows the filament surface morphology with various MAPE loadings taken using a high-precision microscope. For filament without MAPE in Figure 7(a), the filament's surface was uneven, possibly lacking bonding between wood and r-PP matrix. Meanwhile, r-WoPPc with 1 wt% MAPE produced a smooth and even filament, as shown in Figure 7(b). However, adding more than 1 wt% loading of MAPE seemed to tamper the optimum interfacial adhesion between wood and r-PP, as the filament surface appeared uneven and not smooth, as shown in Figures 7(c) and (d) for r-WoPPc with 3 wt% and 5 wt% MAPE, respectively.

Effects of MAPP Compatibilizer on r-WoPPc Tensile Fracture Surface Morphology

Similarly, incorporating MAPP into the r-WoPPc improved the interfacial adhesion between the wood fiber and the r-PP matrix, much like the effect observed with MAPE. Figure 8 shows the r-WoPPc filament surface morphology without

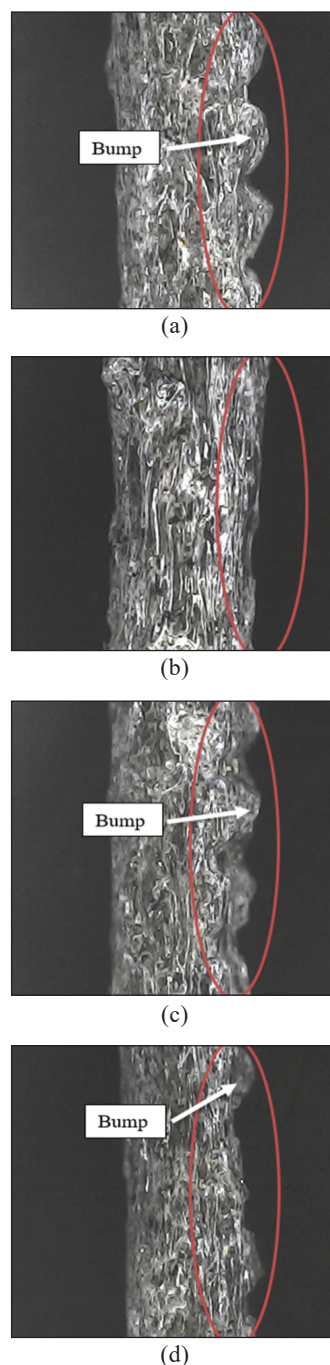


Figure 7. r-WoPPc filament surface morphology: (a) without MAPE; (b) 1 wt% MAPE; (c) 3 wt% MAPE; and (d) 5 wt% MAPE

MAPP (0 wt%), with 1 wt%, 3 wt%, and 5 wt% of MAPP loadings, respectively. Figure 8(a) demonstrates that the absence of MAPP in the r-WoPPc composite affected the integrity of the composite; having more fiber pull-out led to more holes (Çavuş, 2020). A noticeable wood fiber rupture and fiber pull-out from the matrix were observed. The surface morphology of r-WoPPc with 1% MAPP showed slightly better adhesion compared to composite without MAPP, showing that compatibilizer helped enhance the wood and PP matrix (Amir et al., 2017). Meanwhile, it can be observed that the r-WoPPc containing 3 wt% MAPP loading, as depicted in Figure 8(c), showed better interfacial adhesion between wood and PP.

Moreover, with 5 wt% MAPP loading, as shown in Figure 8(d), significantly improved interfacial adhesion between the wood and r-PP matrix, which demonstrated the highest tensile and flexural strengths of the r-WoPPc were found. Additionally, 5 wt% MAPP significantly enhanced the composites' interfacial adhesion between wood and r-PP matrix. This improvement reduced void formation, effectively minimizing stress concentration points that could potentially compromise the strength of the composites (Sosiati et al., 2018). Adding maleic anhydride as a compatibilizer in PP-based composite also improved PP's friction and wear rate during the FDM extrusion process, which produced improved mechanical properties of the extruded part (Kristiawan et al., 2021).

Effects of MAPE Compatibilizer on Water Absorption of r-WoPPc.

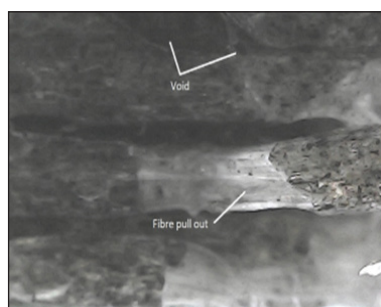
The amount of water uptake or absorption in the composite indicates the composite structural integrity. Higher water absorption is associated with more voids in the composites, leading to a detrimental effect on the composite mechanical properties. Thus, the quantification of water uptake in the r-WoPPc provided significant information regarding the presence of voids and their impact on the tensile and flexural strengths. A lower number of r-WoPPc water



(a)



(b)



(c)



(d)

Figure 8. High precision micrograph with $10\times$ magnification of r-WoPPc tensile fracture surface: (a) without MAPP; (b) 1 wt% MAPP; (c) 3 wt% MAPP; and (d) 5 wt% MAPP

absorption signified that the r-WoPPc had a more compact structure and fewer voids, typically associated with improved tensile and flexural strengths. In contrast, voids were present when r-WoPPc absorbed a higher amount of water. These voids caused detrimental effects on the tensile and flexural strengths due to additional stress concentration points.

The water absorption of r-WoPPc with different MAPE loadings provides significant proof of the influence of compatibilizer on composites' structure. Figure 9 presents the water absorption result of r-WoPPc. It is apparent from the data that the incorporation of 1 wt% MAPE in r-WoPPc led to significantly reduced water absorption. The r-WoPPc with 1% MAPE absorbs a smaller amount of water, which was 0.8%, compared to a higher absorption rate for 3 wt% MAPE addition and 5 wt% MAPE addition, which are 2% and 1.1% water absorbed, respectively. The lower water absorption value of r-WoPPc was attributed to the improved interfacial adhesion between the wood fiber and PP matrix, which signified the composite's tensile and flexural strength. This result was similar to the finding of (Zhou et al., 2022). These water absorption results aligned with the tensile and flexural strengths of the r-WoPPc composites with 1 wt% MAPE, obtaining the highest strength among all tested composites. Meanwhile, water absorption of composites containing 3 wt% MAPE was higher than 1 wt% and 5 wt% MAPE loadings, which evidenced that the composite had more voids compared to the composite with 1 wt% MAPE. The reduction in water absorption of the r-WoPPc was confirmed by the morphology results that showed strong adhesion between the wood and r-PP matrix.

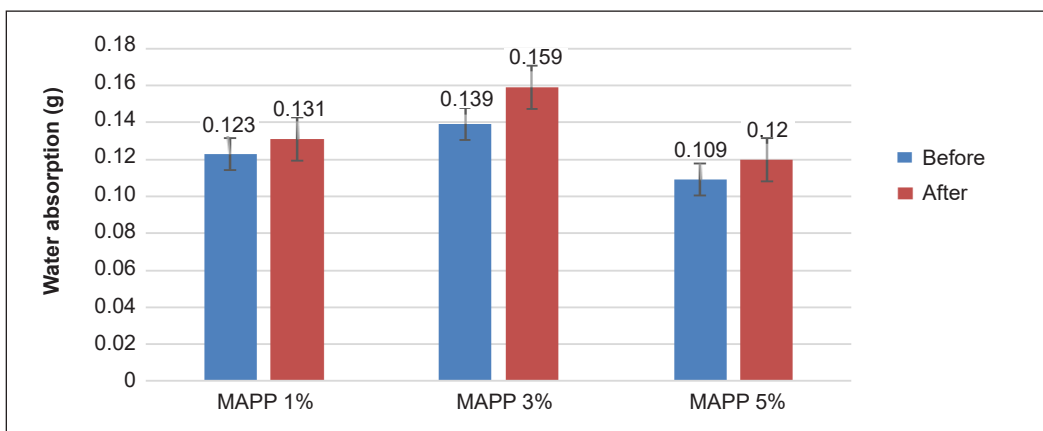


Figure 9. r-WoPPc water absorption values with varying MAPE loadings

Effects of MAPP Compatibilizer on Water Absorption of r-WoPPc

The study of water absorption in r-WoPPc with varying MAPP loadings provides substantial evidence of the influence of the compatibilizer in improving interfacial adhesion between wood and PP, as shown in Figure 10. Composite with 5 wt% MAPP absorbed the least water compared to 1 wt% and 3 wt% MAPP, respectively. This finding validated the smaller

number of voids in the composites, as observed in filament morphology resulting from improved interfacial adhesion of wood and PP, subsequently improved composite strength. The finding was similar to the study conducted by Petchwattana et al. (2019), who showed that using a compatibilizer significantly reduced water absorption compared to without a compatibilizer (Billah et al., 2022).

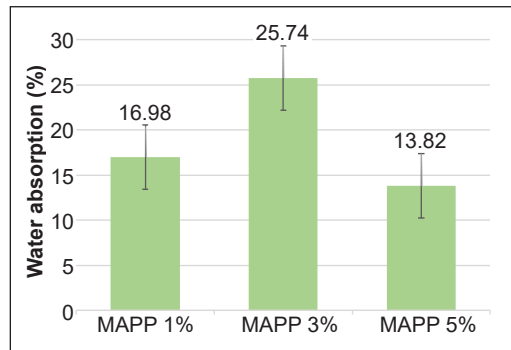


Figure 10. r-WoPPc water absorption values with varying MAPP loadings

CONCLUSION

In conclusion, adding MAPP and MAPE compatibilizers improved the mechanical properties of the wood fiber/recycled polypropylene (r-WoPPC) 3D printing filaments. The addition of MAPP improved the tensile and flexural strength of the composite by 13% and 18%, respectively, and the addition of MAPE enhanced the composite tensile and flexural strength by 74% and 60%, respectively. This study identified that the optimal MAPP content for achieving the highest mechanical performance of the r-WoPPc was 5 wt%, whereas for MAPE, it was 1 wt%. A significant improvement in r-WoPPc mechanical performance was observed as the percentage of MAPP in the composite increased. The tensile and flexural strength increased proportionally with the percentage of MAPP amount.

In contrast, as the MAPE percentage increases, the mechanical performance of the composite decreases gradually. This observation is likely attributed to the nature of the coupling agent-based and their compatibility with the polypropylene matrix. As PP- a based compound- MAPP provides more effective intermolecular or intramolecular coupling between the r-PP molecules and wood fibers. Therefore, increasing the MAPP percentage strengthens the interfacial adhesion between the wood fibers and the r-PP matrix. This finding highlights the importance of selecting a suitable coupling agent for achieving desired composite performance. Moreover, the increasing proportion of maleic anhydride coupling agents is shown to enhance the structural integrity of the composite, provided that the basis of the coupling agent is compatible with the composite matrix. The enhanced mechanical properties of r-WoPPc 3D printing filament were ideal for prototyping parts and products to produce architectural and structural models, furniture, and consumer goods.

ACKNOWLEDGEMENT

The authors thank Universiti Teknikal Malaysia Melaka for the financial support from the Short-Term Grant (PJP/2020/FKM/PP/S01736) to the principal author to carry out this research project.

REFERENCES

- Aida, H. J., Nadlene, R., Mastura, M. T., Yusriah, L., Sivakumar, D., & Ilyas, R. A. (2021). Natural fibre filament for fused deposition modelling (FDM): A review. *International Journal of Sustainable Engineering*, *14*(6), 1988–2008. <https://doi.org/10.1080/19397038.2021.1962426>
- Amir, N., Abidin, K. A. Z., & Shiri, F. B. M. (2017). Effects of fibre configuration on mechanical properties of banana fibre/PP/MAPP Natural fibre reinforced polymer composite. *Procedia Engineering*, *184*, 573–580. <https://doi.org/10.1016/j.proeng.2017.04.140>
- ASTM [American Society for Testing and Materials]. (2017). *ASTM D570-98 Standard test method for water absorption of plastics*. ASTM International.
- ASTM [American Society for Testing and Materials]. (2022). *ASTM D638 Standard test method for tensile properties of plastics*. ASTM International.
- ASTM [American Society for Testing and Materials]. (2017). *ASTM D790 Standard test methods for flexural properties of unreinforced and reinforced plastics and electrical insulating materials*. ASTM International.
- Atiqah, A., Jawaid, M., Ishak, M. R., & Sapuan, S. M. (2018). Effect of alkali and silane treatments on mechanical and interfacial bonding strength of sugar palm fibers with thermoplastic polyurethane. *Journal of Natural Fibers*, *15*(2), 251–261. <https://doi.org/10.1080/15440478.2017.1325427>
- Baykus, O., Mutlu, A., & Dogan, M. (2016). The effect of pre-impregnation with maleated coupling agents on mechanical and water absorption properties of jute fabric reinforced polypropylene and polyethylene biocomposites. *Journal of Composite Materials*, *50*(2), 257–267. <https://doi.org/10.1177/0021998315573>
- Billah, M. M., Rabbi, M. S., & Hasan, A. (2022). Injection molded discontinuous and continuous rattan fiber reinforced polypropylene composite: Development, experimental and analytical investigations. *Results in Materials*, *13*, Article 100261. <https://doi.org/10.1016/j.rinma.2022.100261>
- Bütün, F. Y., Sauerbier, P., Militz, H., & Mai, C. (2019). The effect of fibreboard (MDF) disintegration technique on wood polymer composites (WPC) produced with recovered wood particles. *Composites Part A: Applied Science and Manufacturing*, *118*, 312–316. <https://doi.org/10.1016/j.compositesa.2019.01.006>
- Çavuş, V. (2020). 1 Selected-properties of mahogany wood flour filled polypropylene composites: The effect of maleic anhydride-grafted polypropylene (MAPP). *BioResources*, *15*(2), 2227–2236. <https://doi.org/10.15376/biores.15.2.2227-2236>
- Dhanalakshmi, S., Ramadevi, P., & Basavaraju, B. (2017). A study of the effect of chemical treatments on areca fiber reinforced polypropylene composite properties. *Science and Engineering of Composite Materials*, *24*(4), 501–520. <https://doi.org/10.1515/secm-2015-0292>
- Hao, X., Xu, J., Zhou, H., Tang, W., Li, W., Wang, Q., & Ou, R. (2021). Interfacial adhesion mechanisms of ultra-highly filled wood fiber/polyethylene composites using maleic anhydride grafted polyethylene as a compatibilizer. *Materials and Design*, *212*, Article 110182. <https://doi.org/10.1016/j.matdes.2021.110182>
- Keener, T. J., Stuart, R. K., & Brown, T. K. (2004). Maleated coupling agents for natural fibre composites. *Composites Part A: Applied Science and Manufacturing*, *35*(3), 357–362. <https://doi.org/10.1016/j.compositesa.2003.09.014>

- Khalid, M. Y., Imran, R., Arif, Z. U., Akram, N., Arshad, H., Rashid, A. A., & Márquez, F. P. G. (2021). Developments in chemical treatments, manufacturing techniques and potential applications of natural-fibers-based biodegradable composites. *Coatings*, *11*(3), Article 293. <https://doi.org/10.3390/coatings11030293>
- Kristiawan, R. B., Imaduddin, F., Ariawan, D., Ubaidillah, & Arifin, Z. (2021). A review on the fused deposition modeling (FDM) 3D printing: Filament processing, materials, and printing parameters. *Open Engineering*, *11*(1), 639–649. <https://doi.org/10.1515/eng-2021-0063>
- Mu, B., Wang, H., Hao, X., & Wang, Q. (2018). Morphology, mechanical properties and dimensional stability of biomass particles/high density polyethylene composites: Effect of species and composition. *Polymers*, *10*(3), Article 308. <https://doi.org/10.3390/polym10030308>
- Ou, R., Xie, Y., Wolcott, M. P., Sui, S., & Wang, Q. (2014). Morphology, mechanical properties, and dimensional stability of wood particle/high density polyethylene composites: Effect of removal of wood cell wall composition. *Materials and Design*, *58*, 339–345. <https://doi.org/10.1016/j.matdes.2014.02.018>
- Petchwattana, N., Channuan, W., Naknaen, P., & Narupai, B. (2019). 3D printing filaments prepared from modified poly(lactic acid)/teak wood flour composites: An investigation on the particle size effects and silane coupling agent compatibilisation. *Journal of Physical Science*, *30*(2), 169–188. <https://doi.org/10.21315/jps2019.30.2.10>
- Razak, Z., Sulong, A. B., Muhamad, N., Haron, C. H. C., Mohd Khairol, M. K. F., Tholibon, D., Tharazi, I., & Ismail, N. F. (2018). The effects of maleic anhydride grafted PP (MAPP) on the mechanical properties of injection moulded kenaf/CNTs/PP composites. *Sains Malaysiana*, *47*(6), 1285–1291. <https://doi.org/10.17576/jsm-2018-4706-25>
- Silva, N. F. I., Filho, J. E. S., Santos, T. G. C., Chagas, J. D. S., Medeiros, S. A. S. L. D., Santos, E. B. C., Wellen, R. M. R., Silva, L. B. D., Carvalho, L., Nunes, M. A. B. S., & Santos, A. S. F. E. (2021). Biocomposites based on poly(hydroxybutyrate) and the mesocarp of babassu coconut (*Orbignya phalerata* Mart.): Effect of wax removal and maleic anhydride-modified polyethylene addition. *Journal of Materials Research and Technology*, *15*, 3161–3170. <https://doi.org/10.1016/j.jmrt.2021.09.008>
- Sosiati, H., Nahyudin, A., Wijayanti, D. A., Triyana, K., & Sudarisman. (2018). Effect of alkali treatment and MAPP addition on tensile strength of sisal/polypropylene composites. *Journal of Advanced Manufacturing Technology*, *12*(2), 65–78.
- Yuan, Q., Wu, D., Gotama, J., & Bateman, S. (2008). Wood fiber reinforced polyethylene and polypropylene composites with high modulus and impact strength. *Journal of Thermoplastic Composite Materials*, *21*(3), 195–208. <https://doi.org/10.1177/0892705708089472>
- Zhang, J., Li, Y., Xing, D., Wang, Q., Wang, H., & Koubaa, A. (2019). Reinforcement of continuous fibers for extruded wood-flour/HDPE composites: Effects of fiber type and amount. *Construction and Building Materials*, *228*, Article 116718. <https://doi.org/10.1016/j.conbuildmat.2019.116718>
- Zhou, H., Li, W., Hao, X., Zong, G., Yi, X., Xu, J., Ou, R., & Wang, Q. (2022). Recycling end-of-life WPC products into ultra-high-filled, high-performance wood fiber/polyethylene composites: A sustainable strategy for clean and cyclic processing in the WPC industry. *Journal of Materials Research and Technology*, *18*, 1–14. <https://doi.org/10.1016/j.jmrt.2022.02.091>

Mechanical Properties of Thermoplastic Cassava Starch/ Coconut Fibre Composites: Effect of Fibre Size

Ridhwan Jumaidin^{1*}, Ainin Sofiya Gazari¹, Zatil Hafila Kamaruddin^{2,3}, Zatil Hazrati Kamaruddin³, Nazri Huzaimi Zakaria¹, Syahibudil Ikhwan Abdul Kudus¹, Mohd Shukri Yob², Fudhail Abd Munir⁴ and Meysam Keshavarz⁵

¹Fakulti Teknologi dan Kejuruteraan Industri dan Pembuatan, Universiti Teknikal Malaysia Melaka, Hang Tuah Jaya, 76100 Durian Tunggal, Melaka, Malaysia

²Fakulti Teknologi dan Kejuruteraan Mekanikal, Universiti Teknikal Malaysia Melaka, Hang Tuah Jaya, 76100 Mel76100 Durian Tunggal Melaka, Malaysia

³German-Malaysian Institute, Jalan Ilmiah Taman Universiti, Kajang 43000, Malaysia

⁴Department of Mechanical Engineering, Faculty of Engineering, Universiti Teknologi PETRONAS, 32610 Seri Iskandar Perak Malaysia

⁵The Hamlyn Centre, Institute of Global Health Innovation, Imperial College London, Bessemer Building, South Kensington Campus, Exhibition Road, London, SW7 2AZ, United Kingdom

ABSTRACT

This research aims to study the thermal and mechanical properties of biodegradable thermoplastic cassava starch (TPCS) reinforced with various sizes of coconut husk fibre (CHF). The range of fibre sizes used was 125, 200, and 300 μm . These CHF were integrated into a thermoplastic cassava starch matrix to make bio-composites. After integrating all components, the bio-composites were hot-pressed at 155°C for 60 minutes to produce thermoplastic sheets. Tensile and flexural tests were carried out to examine the mechanical characteristics of TPCS/CHF composites. The samples were also characterised

using Thermogravimetric Analysis (TGA), X-ray diffraction (XRD), Fourier Transform Infrared Spectroscopy (FTIR), and Scanning Electron Microscopy (SEM). The findings demonstrated that a smaller 125 μm CHF improved the mechanical properties higher than other fibre sizes. Fibre with 300 μm showed more voids, which led to lower material strength. TGA results showed that 300 μm fibres enhanced the crystallinity and thermal stability of the material. FTIR and TGA showed that CHF incorporation

ARTICLE INFO

Article history:

Received: 16 August 2023

Accepted: 09 May 2024

Published: 14 June 2024

DOI: <https://doi.org/10.47836/pjst.32.S2.07>

E-mail addresses:

ridhwan@utem.edu.my (Ridhwan Jumaidin)

aininsof@gmail.com (Ainin Sofiya Gazari)

zatihafila@gmail.com (Zatil Hafila Kamaruddin)

hazrati88@gmail.com (Zatil Hazrati Kamaruddin)

nazrihuzaimi@utem.edu.my (Nazri Huzaimi Zakaria)

syahibudil@utem.edu.my (Syahibudil Ikhwan Abdul Kudus)

mshukriy@utem.edu.my (Mohd Shukri Yob)

fudhail.munir@utp.edu.my (Fudhail Abd Munir)

keshavarz.meyssam@gmail.com (Meysam Keshavarz)

* Corresponding author

increased intermolecular interactions and thermal stability. Overall, a smaller fibre size of 125 μm showed a better reinforcement effect than the larger fibre sizes, which enhanced the materials' tensile and flexural properties. This study demonstrated that modified TPCS/CHF has shown enhanced functionality than neat TPCS.

Keywords: Cassava starch, coconut husk fibre, fibre size, thermoplastic starch

INTRODUCTION

Plastic trash and pollution are pervasive across the water (oceans, rivers, lakes), land (soils, sediments, animal biomass), and air (atmosphere) (Hazrol et al., 2021; Madhumitha et al., 2018; Syafiq et al., 2020). As environmental impediments, e.g., non-biodegradable and plant wastes, as well as mounting garbage mountains, are documented, current environmental challenges become more apparent (Ilyas et al., 2022; Pradeep et al., 2022). There are limited disposal spaces and expanding incineration capacity that necessitate substantial capital expenditures and increased environmental dangers. These issues have influenced the design and development of ecologically sustainable and renewable materials as alternatives to non-biodegradable materials (Ilyas & Sapuan, 2020b, 2020a). Packaging is crucial in preserving food quality and controlling the interaction between food and the environment. It is vital to produce biodegradable packaging to prevent recycling and environmental pollution challenges caused by synthetic plastics.

Estrada-Monje et al. (2021) state that starches are crucial raw ingredients for generating bio-based blends and composites. Also, they are natural, and numerous biopolymers come from grains, e.g., cassava, maize, rice, and potato. The amylose and amylopectin contents in starch vary depending on their sources. The bioplastics' tensile properties improved as the materials' amylose content increased (Ceseracciu et al., 2015; Marichelvam et al., 2019). Starch, among the most significant industrial raw materials, is a versatile substance with a variety of applications. According to Tharanathan (2005), starch is the most common hydrocolloid in the food business, providing various functional qualities.

Thermoplastic starch (TPS) is a native starch-derived biopolymer following its granular structure modification that uses a plasticiser, such as water, glycerol, and sorbitol, among many others (Rivadeneira-Velasco et al., 2021; Mina et al., 2009). Another statement by Weerapoprasit and Prachayawarakorn (2019) is that glycerol is the ideal plasticiser for making TPS because it breaks starch granules and forms an amorphous structure. Studies have been done by Mo et al. (2010) employing thermoplastic cassava starch and reported cellulose fibre demonstrating changes in the thermoplastic starch that enhanced the material's characteristics. Hot compression moulding was used to treat the starch, plasticiser, and fibre reinforcement to make this TPS material (Jumaidin et al., 2021; Zhang et al., 2014). Furthermore, starch plays a crucial role in bio-composite structures as a matrix

or resin during the production of biopolymers. Over the years, researchers have explored various types of natural starch, including corn, sugar palm, *Dioscorea hispida*, cassava, and many others. Table 1 illustrates the utilisation of cassava starch as a thermoplastic material in bio-composites and their potential applications.

Table 1

Thermoplastic cassava starch composites and their potential applications

Thermoplastic starch blends	Potential application	Reference
Thermoplastic cassava starch/kraft	Biodegradable tray	Campos et al., 2018
Thermoplastic cassava starch/cassava bagasse	Food packaging plastic	Travalini et al., 2019
Thermoplastic cassava starch/cogon grass	Biodegradable tray	Jumaidin et al., 2020
Thermoplastic cassava starch/ <i>Cymbopogon citratus</i>	Biodegradable material	Kamaruddin et al., 2022

Malaysia produces abundant agricultural waste materials, including rice husk, coconut, and oil palm frond fibre. Around 25 % of the nut is made up of coir, a challenging and rigid lignocellulosic fibre obtained from the fibrous mesocarp part of coconut fruits, as shown in Figure 1. Due to their high lignin concentration, coir fibres are resilient, weather-resistant, somewhat waterproof, and may be chemically altered. The fibres also have a high elongation at break, allowing for stretching over their elastic limit without rupturing. Among the benefits of these fibres are that they are renewable, nonabrasive, inexpensive, plentiful, and pose fewer health and safety risks during handling and processing (Abdullah et al., 2011). According to Jusoh et al. (2021), coconut fibres possess the maximum toughness of all-natural fibres. Hence, further research and development of these materials to generate the most recent polymer sources include using fibre as an amplifier in polymer composites.



Figure 1. Coconut husk

It is evident from the literature that a few research have been published on cassava starch development and the effect size of CHF. Thus, the main objective of this work is to evaluate the mechanical and thermal properties of the influence of fibre size on biodegradable thermoplastic cassava starch reinforced with coconut husk fibre composite.

MATERIALS AND METHODS

Materials

Antik Sempurna Sdn. Bhd. Malaysia supplies the cassava starch. The plasticiser in this study was glycerol purchased from QReC (Asia) Sdn. Bhd., while palm wax was acquired

from Green & Natural Industries Sdn. Bhd. (Selangor, Malaysia). Coconut husk fibre was supplied from Negeri Sembilan, Malaysia. The husk and shell were separated from the coconut by hand. Coconut fibre was prepared by crushing the long coconut fibres (Figure 2). Shredded coconut fibre was sieved and retained using 125, 200, and 300 μm circular stainless steel sievers.



Figure 2. Coconut husk fibre

Preparation of Samples

Thermoplastic cassava starch (TPCS), glycerol, palm wax, and CHF were weighed according to the (%) ratio. Before pre-mixing the TPCS samples, glycerol, palm wax, and CHF were added to a dry mixer at 120 rpm for 5 min at room temperature. The resultant mixture was then thermo-pressed at 155°C for 60 min using a Plastic Hydraulic Moulding Press under 10 tonnes to create 3 mm thick sheets. Before the conditioning, samples were immediately put in a silica gel-filled desiccator to prevent undesired moisture absorption. Thermoplastic cassava starch with palm wax and coconut husk fibre prepared earlier was kept in an airtight container to prevent it from absorbing moisture from the surrounding environment. The integration of coconut husk fibre in this portion was determined by the fibre sizes of 125, 200, and 300 μm . The process flow is shown in Figure 3.

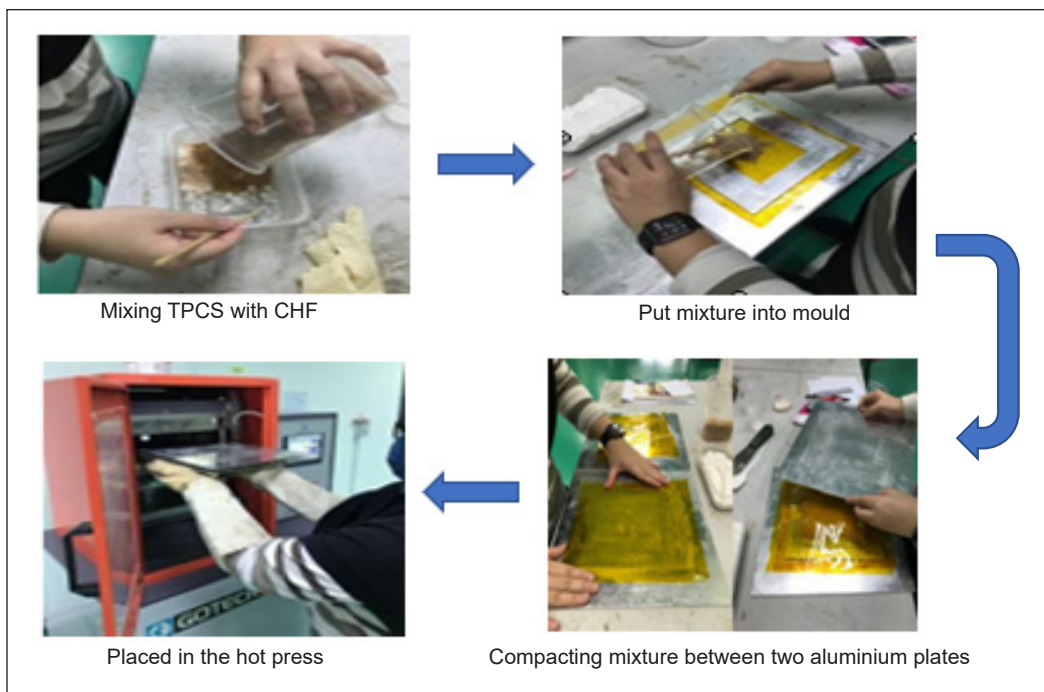


Figure 3. Fabrication of TPCS-reinforced coconut husk fibre

Tensile Testing

The tensile strength, strain, and modulus were determined using tensile testing. This test measures the required force to fracture the specimen and its length. Referencing ASTM D638 as a standard, the specimens were used to draw five samples. The samples were examined using an INSTRON 5969 Universal Testing Machine (United States) with a 5 mm/min crosshead speed of a 50 kN load cell. In addition, this test was conducted at a temperature of 24.0°C and relative humidity (RH) of 50%. The results of the tensile properties were determined by calculating the data mean.

Flexural Testing

Flexural tests were performed according to ASTM D790 at a relative humidity (RH) of 50 ± 5 % and a temperature of 23 ± 1°C. Five (5) samples with dimensions of 130 mm (L) × 13 mm (W) × 3 mm (T) each were produced. A Universal Testing Machine (INSTRON 5969) from INSTRON (United States) with a 2 mm/min crosshead speed and a 50 kN load cell was employed during the testing.

Thermo-gravimetric Analysis (TGA)

A thermogravimetric evaluation of the material's deterioration and stability was conducted. TGA was conducted using a Q-series thermal analysis instrument, namely the Mettler-Toledo AG, Analytical (Switzerland), to examine the thermal stability of the samples. The study was conducted in aluminium pans at 10°C min⁻¹ at temperatures ranging from 25 to 900°C in a nitrogen environment with dynamic pressure. The weight of the sample was around 102 mg.

Fourier Transform Infrared (FT-IR) Spectroscopy

The FT-IR test assessed whether coconut husk fibre contains functional groups. This test is to determine the material's functional group and chemical characteristics. An IR spectrometer was used to get the material's spectrum (JASCO FTIR-6100 Spectrometer (Japan)). A sample of FT-IR spectra was gathered between 4000 and 500 cm⁻¹. The material was mixed with potassium bromide (KBr) to make a 1 mm thick disc weighing 2 mg in powder form.

Scanning Electron Microscope (SEM)

The morphological traits of fractured tensile samples were observed under a scanning electron microscope (SEM), Zeiss Evo 18 Research (Jena, Germany), at the pre-set 10 kV acceleration voltage. The samples were reduced to comparable sizes, and gold coating was applied to their surfaces before the observation. The tensile-analysed specimens were saved in zip-locked packing containers and characterised through SEM.

X-ray Diffraction (XRD)

The structure of the coconut husk fibre solid waste was assessed using an X-ray diffractometer (APD 2000, Italy) with Cu K- α radiation at 0.15406 nm, 40 kV, and 30 mA of wavelength, voltage, and current, respectively. The samples underwent scanning at a rate of 2° min⁻¹ at room temperature across the diffraction angle range of 2 θ = 5 to 60°. The crystallinity index calculation of the samples CI (%) was done referring to Equation 1:

$$CI = \frac{I - am}{I} \times 100\% \quad CI = \frac{I - am}{I} \times 100\% \quad (1)$$

where crystalline (I) and amorphous (am) are the total area under the crystalline peaks and the amorphous halo, respectively.

Statistical Analysis

The mechanical characteristics were analysed statistically using a one-way analysis of variance (ANOVA). Using Duncan's multiple range tests, the significance of each mean property value was determined ($p < 0.05$). This test was used to measure the significance of the difference between the two groups.,

RESULT AND DISCUSSION

Tensile Testing

Figure 4 depicts the tensile strength of TPCS/CHF composites for fibre sizes of 125, 200, and 300 μm . The tensile strength for size ranges of 125, 200, and 300 μm were 6.5, 4.1, and 2.3 MPa, respectively. The results have shown increments with the use of CHF reinforcement substantially in tensile strength with the addition of a CHF size of 125 μm . Then, the strength dropped with the increased CHF sizes of 200 and 300 μm . The smaller fibre size composites of 125 μm demonstrated superior tensile performance compared to the larger fibre composites, with fibres widely scattered throughout the matrix. The increased fibre-matrix surface contact led to reduced fibre aggregation. It indicates that solid interfacial adhesion was obtained between the components of hybrid composites, which increased stress-transfer efficiency in the TPCS/CHF matrix. Similarly, identical findings were noted by Diyana et al. (2021a). Using larger 300 μm fibre contents considerably reduced the composites' strength qualities. In spite of this fact, this contrasts with Mohamed et al. (2018) findings that extending fibre length enhances tensile strength. Consequently, it was determined that an increase in fibre size decreased the absorption of specific energy of hot-pressed fibre composite materials with a 300 μm fibre size. This outcome can be attributed to the fact that despite using a small fibre size, it still offers a larger surface area for interaction with TPS. Consequently, the greater aspect ratio of the fibre promotes stress transmission to the matrix (Santos et al., 2018).

In this study, the measured mechanical strength fracture exhibited ductile features. Figure 5 presents the results of the tensile modulus of CHF composites with different fibre sizes of 0%, 125, 200, and 300 μm . Including CHF fibre increased the tensile modulus of 0% fibre from 5.8 to 880.8 MPa, the optimum tensile modulus obtained at 125 μm . Thus, the smaller the fibre size of the CHF, the greater the tensile modulus, and vice versa. When the chopped fibre length or diameter was smaller, weaker tensile strength and stiffness were determined. This statement is aligned with previous work by Jacob et al. (2005). Specifically, fibre packing is much improved for smaller fibre sizes, reducing modulus for larger ones.

With an increase in fibre sizing of 200 and 300 μm , the tensile modulus decreased to 395.7 and 172.3 MPa, respectively. The reason is that increasing fibre size decreases matrix content while decreasing ductility results in a stiffer composite. Moreover, at this fibre size, there was less fibre-matrix interaction. It is due to the decreased intermolecular contact between starch molecules, which results in a larger free volume and greater chain mobility (Aji et al., 2011).

Figure 6 shows the tensile strain of fibre sizes 0%, 125, 200, and 300 μm at break. It was shown that with the addition of CHF, the tensile strain at failure dropped simultaneously from 35.7 to 1.5%, decreasing the composite's stiffness. It was ascribed to the poor internal contact of larger

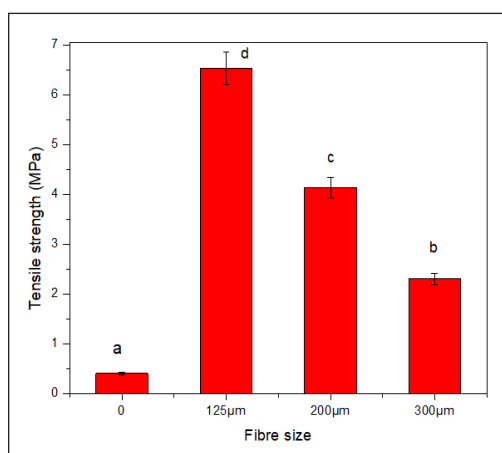


Figure 4. Tensile strength of coconut fibre composites with different fibre sizes (MPa)

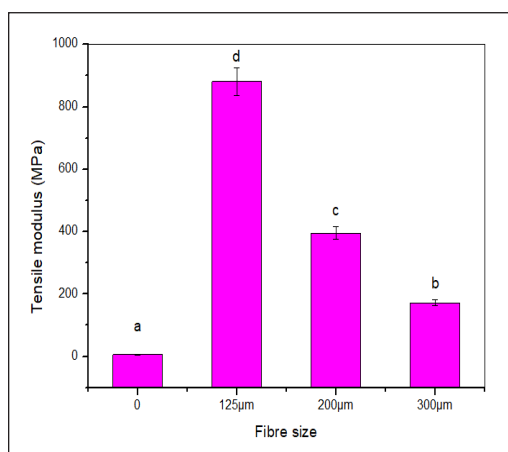


Figure 5. Tensile modulus of coconut fibre composition with different fibre sizes (MPa)

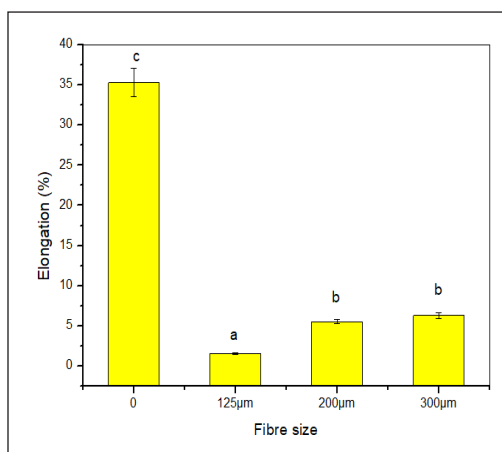


Figure 6. The tensile strain of coconut fibre composition with different fibre sizes (MPa)

fibres and the incapacity of larger fibres to bear the matrix-transferred strain (Prakash et al., 2021). According to Prasad et al. (2019), integrating natural fibre's fragility impeded the polymer chains' mobility in the matrix. The composites became stiffer when the elasticity ratio of matrix phases was substituted by increased fibre size content. For 125 μm fibre size, the composites demonstrated elongation at 1.5% fibre. According to Wollerdorfe and Bader (1998) and Yokesahachart et al. (2021), the size of the fibres affects the stress concentration at the ends of the fibres, which results in less elongation at fibre breaks for bigger fibres since the force cannot sustain local failure. Meanwhile, the tensile strain increased with the addition of larger fibre sizes of 200 and 300 μm to 5.5% and 6.3%, respectively. Decreasing the size diameter of the CHF led to greater stress on the composites.

Flexural Testing

Figure 7 shows the flexural strength of composite with CHF sizes 0%, 125, 200, and 300 μm , respectively. With fibre addition, the flexural strength rose to the highest strength of 13.8 MPa at 125 μm from 2.4 MPa, indicating the fibre-matrix interfacial adhesion facilitating increased stress transmission. It suggested the degree of cross-linking between molecular chains in the blends. The cross-linking of palm wax had favourably influenced the flexural strength and elasticity modulus, as indicated by a prior study describing the enhancement in flexural strength of corn starch mixed with kaolin and beeswax (Polat et al., 2013). The improvement in the flexural characteristics of the TPCS/CHF composites could be attributable to identical causes in the tensile findings.

Afterwards, the strength slightly decreased to 9.8 MPa at 200 μm before increasing again to 12.0 MPa at 300 μm . Owing to the low interfacial adhesion between reinforcement and matrix, an increase in fibre sizes of 200 μm diminished both strength and modulus attributes. It could be because the TPCS's palm wax failed to act as a reinforcing agent due to agglomerates and an uneven distribution. Additionally, because of the excess palm wax content associated with forming large agglomerates and phase separation, poor particle distribution resulted in poor mechanical distribution, similar to the tensile results reported by Ilyas et al. (2018).

As presented in Figure 8, the maximum flexural modulus of the CHF-reinforced TPCS composite was raised from 16.5 MPa at 0% fibre to 118.8 MPa at 125 μm . Then, the

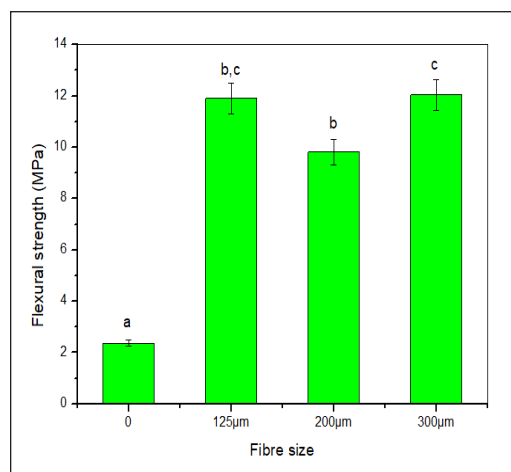


Figure 7. Flexural strength of TPCS/CHF composites with different fibre sizes (MPa)

particle reinforcement strength decreased to 320.8 MPa for 200 μm before rising to 532.2 MPa for 300 μm . This decrease was caused by the presence of voids or the formation of cracks at the composite's interface, the inability of the particle to endure the stresses transferred from the matrix, and the ineffective particle-matrix interfacial bonding, which resulted in a weak structure. However, the excessive fibre sizes of 300 μm elevated fibre elasticity and matrix to transmit stress. It enhanced the flexural modulus of the composites due to the composites' higher stiffness, including CHF in the matrix, and reduced polymeric chain mobility.

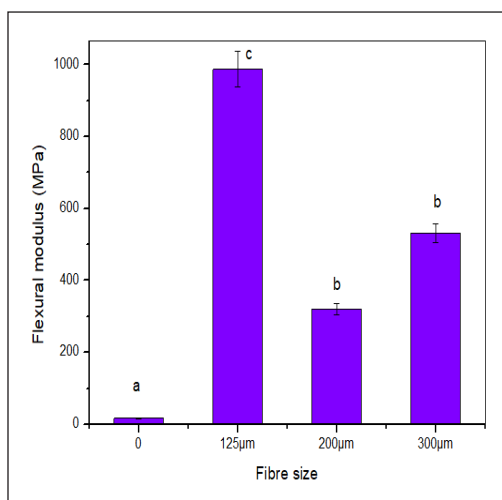


Figure 8. Flexural modulus of TPCS/CHF composites with different fibre sizes (MPa)

Seth et al. (2018), who researched the influence of particle size and loading on polypropylene-reinforced doum palm shell particle composites, obtained similar results. Literature documented a composite's properties improvement with decreasing particle size because smaller particles have greater compaction and reduced porosity, which results in effective stress transfer between the matrix and the particles. The tensile and flexural test results were subjected to statistical analysis using one-way ANOVA, and the results are presented in Table 2. The test's p-value was less than 0.05, showing statistically significant differences in the mixtures' average thermoplastic blend values for tensile and flexural strengths.

Table 2

Analysis of variance (ANOVA) summary of tensile and flexural properties

Variables	df	Tensile strength	Tensile strain	Tensile modulus	Flexural strength	Flexural modulus
Mixture	4	0.00*	0.00*	0.00*	0.00*	0.00*

Thermal Properties

The thermal properties and stability of TPCS-reinforced CHF composites were assessed by plotting the TGA curves as the percentage of sample weight loss versus temperature ($^{\circ}\text{C}$), as shown in Figure 9(a). As the temperature rose, the weight percentage decreased, indicating continual mass changes due to thermal treatment. The three-step deterioration process was distinguished for all composites and their constituent materials. At about 100 and 160 $^{\circ}\text{C}$, the weight losses were due to the evaporation of water and glycerol, respectively. Relative to Sanyang et al. (2015), the earliest stage of degradation that occurs

at temperatures below 100°C is in relation to the dehydration of loosely bound water and low molecular weight compounds.

The mixtures of TPCS and CHF composites altered the thermal decomposition of the composites in numerous ways. At 250°C, the native TPCS began to degrade, representing the temperature at which samples started to deviate from the baseline and weight loss was ready to commence. The highest weight loss rate was reported at 318°C, according to the curve in Figure 9(a). Following Abral et al. (2019), when the temperature hits 180 to 360°C, the second phase of weight loss occurs due to starch’s volatile breakdown. It was discovered that adding CHF to CFC1, CFC2, and CFC3 composites increased their onset and maximum degradation temperatures, as shown in Table 3. The composites’ heat conductivity decrement with coir fibre addition was due to TPCS having more lignocellulose than CHF, which increased thermal stability. Besides, the CHF is less hydrophilic than the matrix, allowing quicker moisture evaporation when heated (Jumaidin et al., 2020). Parallel outcomes were discovered by Sarifuddin et al. (2012) and M. Hasan et al. (2020). At 350°C, CHF entered its final phase of disintegration.

Based on the graph in Figure 9(a), composites with 125 µm fibre size (CFC1) needed a lower temperature compared to larger-size CFC2 and CFC3 before losing weight percentage due to water loss. It is also reported that the maximum temperature value observed was 291°C, lower than the 336°C provided in the study by Diyana et al. (2021b). The discrepancies may be attributable to the varied parameter conditions during testing. According to Prachayawarakorn et al. (2012), using a variable fibre size may raise the temperature at which TPCS begins to degrade.

Furthermore, the thermal degradation of TPCS/CHF composites that led to the weight loss was found between 280 and 352°C. Figure 9(a) shows that the water weight loss percentage dropped significantly by including larger fibre. Hence, the larger the size of the fibre, the higher the temperature needed to lose water percentage. Adding larger CHF caused the CFC3 degradation temperature to drop when 300 µm fibres were used. This study suggested that larger-size CHF may enhance the thermal stability of composites through hydrogen bond interactions between the fibre and matrix, which corresponded to Javaid et al. (2020). At this point, the increase in fibre-size content from 125 to 300 µm has suggested that CHF is primarily responsible for the increase in degradation rate.

The thermal degradation and stability of TPCS/CHF composites were assessed by plotting the DTG curves as the derivative weight loss (mg °C⁻¹ versus temperature (°C), as shown in Figure 9(b). The curves denote that the most significant breakdown temperature of the native TPCS was around 318°C. It could be explained by the

Table 3
TGA findings of TPCS/CHF composites on the onset temperature, T_{on} (°C)

Samples	Ton (°C)
TPCS (reference)	318
CFC 1 (125 µm)	304
CFC 2 (200 µm)	305
CFC 3 (300 µm)	305

interactions between the polar side groups in the starch (e.g., hydroxyl carbonyl) and wax fraction in native TPCS, which has a high initial breakdown temperature (Halal et al., 2016).

With fibre inclusion in Figure 9(b), the highest DTG peak was observed between the temperature range of 250 and 350°C. However, when the fibre was added, the DTG peaks decreased, and only very slight variations were found (Sahari et al., 2013). A rapid weight loss took place due to the decomposition of fibre, starch, and glycerol, creating volatile matters, e.g., carbon monoxide (CO) and carbon dioxide (CO₂) (Hassan et al., 2019). Monteiro et al. (2012) reported that the initial phase of the DTG peak is related to moisture release. The breakdown of fibre began in the second phase, as represented by the primary DTG peak. Cellulose degradation is indicated at the peak, whereas hemicellulose and lignin decompositions occur at the shoulder and tail peaks. The residue at the end of the process might be ascribed to the solid char from the degradation events. The DTG curve is crucial for better insight into the composite material's thermal decomposition behaviour.

This observation is in accordance with research done by Tajvidi and Takemura (2010), who investigated the heat deterioration of natural fibre reinforced with polypropylene (PP), wool flour composites, and kenaf fibre. The wood flour composites and kenaf fibre had high breakdown rates in three phases. The initial step began at the temperature range of 250 and 300°C and was linked to hemicellulose and PP breakdown. The second stage was initiated at 300°C and continued up to 400°C, describing cellulose degradation. The ultimate decomposition was detected at about 450°C.

Razali et al. (2015) previously studied char as the residue after the pyrolysis of all volatile matter in a substance. The char residue concentration of TPCS/CHF composites rose with the addition of CHF, with CFC3 containing the most char residue at 49.33% (7.94 mg). Based on the TGA study, it is summarised that the CHF inclusion enhanced the charring and thermal stability of the TPCS/CHF composite.

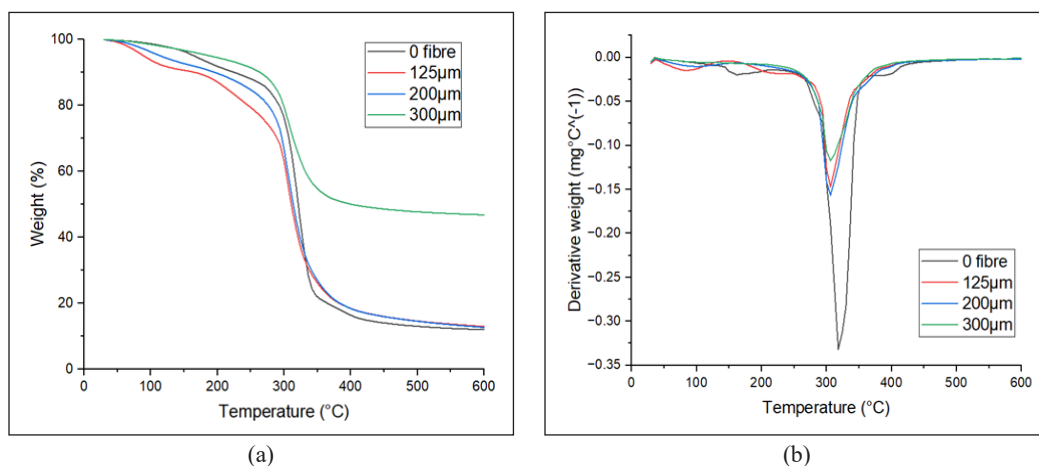


Figure 9. (a) TGA and (b) DTG curves on TPCS/CHF composites

FTIR Analysis

The Fourier transform infrared (FT-IR) analysis revealed the high content of chemical components in coir materials. The FT-IR findings for TPCS/CHF composites from 0 to 300 μm of fibre size contents are shown in Figure 10. All spectra of TPCS composites displayed comparable patterns, demonstrating that the TPCS was unaffected by the size of the coconut husk fibre in all composite samples. A broad wavelength range between 3000 and 3700 cm^{-1} matched the hydroxyl group (-OH) stretching vibrations ascribed with the complicated vibrational stretching of free-, inter-, and intra-molecularly bonded hydroxyl groups (AL-Hassan & Norziah, 2017; Hafila et al., 2022). This discovery demonstrated new matrix-fibre hydrogen bond formations that relate to fibre addition. Notably, the slightly smaller C-O stretching peak in TPCS compared to TPCS/CHF at 1338 cm^{-1} is probably due to the reorganisation of hydrogen bonds between starch and fibre (Sariffuddin et al., 2012). Changes in the IR spectrum revealed a specific interaction and compatibility between polymer chains.

In Figure 10, the band at around 2916 cm^{-1} was attributed to C-H stretching from CH_2 or CH_3 or conjugated bending vibrations, which were present in all composite samples. Like Barkoula et al. (2008), this band coincided with natural fibre's cellulose and hemicellulose constituents. The existence of hydroxyl groups led to the starch being very sensitive to water molecules (Ilyas et al., 2018; Sahari et al., 2013). It was also linked to the hydroxyl groups stretching due to the molecules' hydrogen bonds. Pursuant to Dang and Yoksan (2021), the peak around 2916 cm^{-1} corresponds to C-H stretching ($-\text{CH}_2$) of the anhydroglucose ring (Zullo & Iannace, 2009), while the peak at around 3277 cm^{-1} is associated to the firmly bound water exist in the starch structure (Zhang & Han, 2006) owing to its hygroscopic nature.

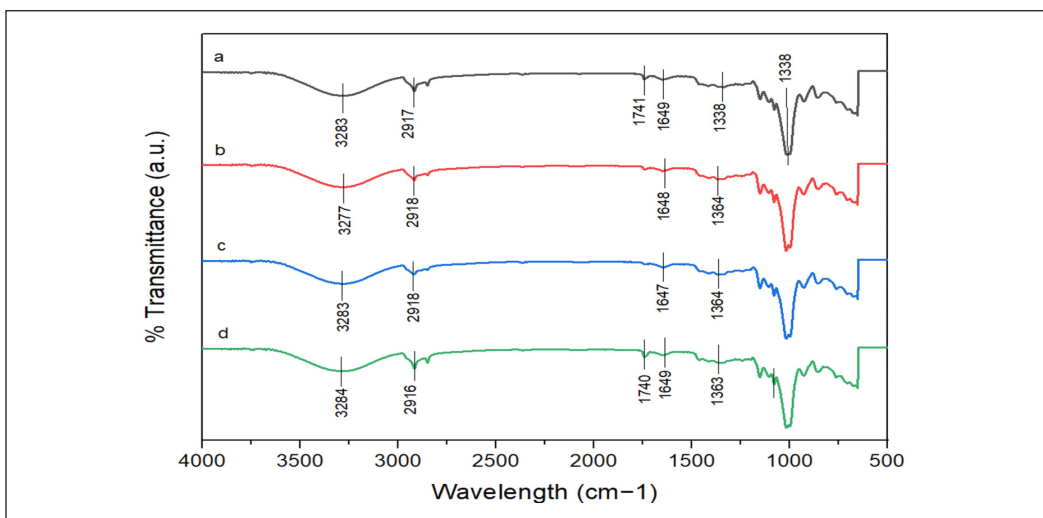


Figure 10. FTIR spectrum of TPCS with (a) 0%, (b) 125 μm , (c) 200 μm , and (d) 300 μm fibre

According to Lomelí-Ramírez et al. (2014), the band at around 1725 cm^{-1} may correspond to stretching vibrations of carbonyl groups ($\text{C}=\text{O}$). However, when the larger fibre was used, the $\text{O}-\text{H}$ bond peak moved to a lower wavenumber before arising to a higher frequency, indicating an increase in the average strength of hydrogen bonds. Sample with no fibre (Figure 10 a) reached a maximum peak of 3283 cm^{-1} , whereas specimens with the largest fibre size, $300\text{ }\mu\text{m}$ (Figure 10 (d), reached a maximum peak of 3284 cm^{-1} . In a prior Prachayawarakorn et al. (2011) study, TPCS/kapok and TPCS/jute fibres exhibited a comparable $\text{O}-\text{H}$ pattern.

It is related to starch containing hydroxyl (OH) functional groups in their basic structure. The tensile result was substantiated at the OH peak regions at 3277 and 3284 cm^{-1} . Meanwhile, the decrease in elongation following fibre addition might be due to starch-fibre matrix bonding, which precluded considerable material elongation. As a result, the composite matrix lost some of its ductility. It may be assumed that the resulting bio-composite became tougher, more brittle, and less flexible as the diameter was increased.

XRD Analysis

The presence of cellulose and amorphous fractions in the fibre was verified by XRD analysis. Figure 11 illustrates the diffraction patterns of the three native starches employed. Starch granules display, in general, two primary kinds of X-ray diffraction patterns called A and B crystal structures. These two allomorphs assume that the crystalline domains are generated for the short terminal segments of amylopectin molecules with identical double-helical shapes but distinct packing arrangements and differing intercrystalline water content. The A-type structure is usually present in cereal starches, whereas the B-type structure is prevalent in starches from tubers or rich amylose carbohydrates (Montero et al., 2017).

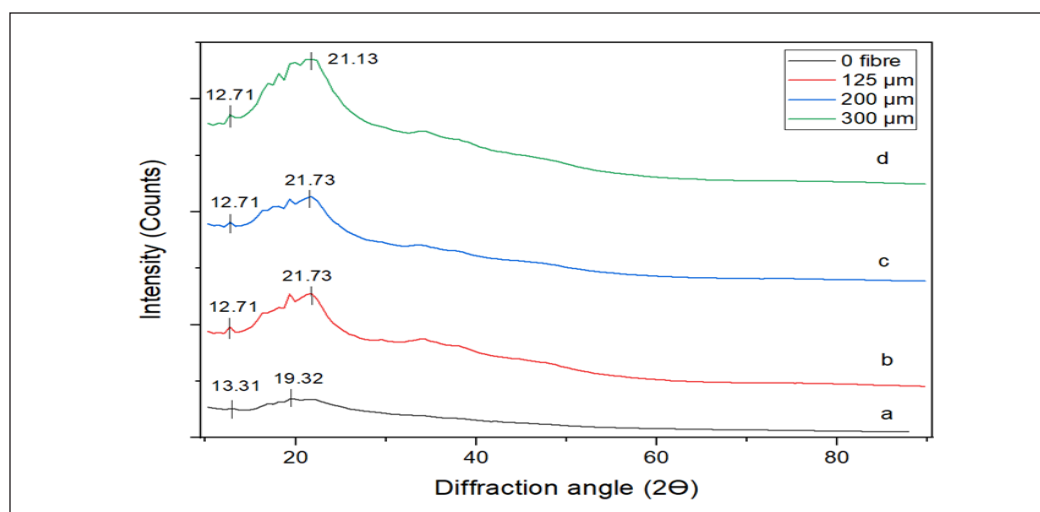


Figure 11. XRD analysis on TPCS/CHF with (a) 0%, (b) $125\text{ }\mu\text{m}$, (c) $200\text{ }\mu\text{m}$, and (d) $300\text{ }\mu\text{m}$ fibre

The study by Moura et al. (2019) compared the composites reinforced with larger-sized and small-sized fibres. The smaller fibre-reinforced composites exhibited a higher crystallinity and melting temperature. According to the XRD analysis, the fibre diameter and crystallinity dropped and increased during the bleaching or heating of the raw coir fibres. Abraham et al. (2013) stated that it would cause the fibre to inflate, leading to an increase in the fibre's reactive surface area. Consequently, it was verified by Dong et al. (2014) that coir fibres performed an efficient nucleating function to expedite the polylactic acid (PLA) crystallisation process, thus increasing the crystal growth rate.

XRD patterns of all samples are shown in Figure 11. The spectrum of TPCS revealed only a semi-crystalline substance with small crystalline peaks at 2-theta values between 13.31 and 19.32°, which corresponded to the processing-induced crystal of amylose-glycerol complexes of the Vh-type (Kaewtatip & Tanrattanakul, 2012; Yokesahachart et al., 2021). The TPCS/CHF matrices displayed prominent diffraction peaks at $2\theta = 21.73^\circ$ (300 μm), suggesting a typical A-type pattern (Kamaruddin et al., 2022). It may be related to the unstable single helix structure complexation of amylose and plasticiser containing a low quantity of water. Relative to Agyei-Tuffour et al. (2021), the higher the composite's crystallinity, the harder and more brittle it becomes.

The diffraction peaks of TPCS rose after the inclusion of CHF, primarily exhibiting a V-type crystal as the CHF sizes continued to rise (Liu et al., 2022). Thus, the percentage crystallinity of TPCS-based composites increased as CHF fibre size increased. After the gelatinisation process, the crystalline structure of TPCS was created by the fast retrogradation or recrystallisation of starch molecules. However, with further mixing with a larger fibre size of 300 μm , the diffractograms peak at 2θ dropped to 39.85% due to the aggregation of CHFs, resulting in a less heterogeneous nucleation action and slowed starch molecule movements (Yokesahachart et al., 2021).

Besides, the analysis revealed that the inclusion of the CHF particle sizes of 125 and 200 μm increased most of the crystallinity of the TPCS/CHF composite. The crystallinity of the sample was enhanced when the TPCS was reinforced with fibres of a larger diameter. It was likely attributable to the larger CHF size exhibiting a smaller surface area ratio. Hence, it was predicted that raising the size diameter of CHF in the samples would enhance their relative crystallinity. Similar findings were noted by Liu et al. (2022). According to Dang and Yoksan (2021), the crystallinity also increased with increasing temperature and pressure during extrusion owing to the amylose release resulting from the more significant disruption of the starch granule structure. Moreover, the total crystallinity of the TPCS/CHF composites rose with rising CHF sizes, perhaps owing to the high CHF crystallinity. A parallel conclusion was reported for thermoplastic cassava starch/cassava bagasse composites reinforced with sugar palm fibre by Edhirej et al. (2017) and TPCS/PLA blend reinforced with coir fibres by Chotiprayon et al. (2020).

It could be described by the heterogeneous nucleation impact of CHF on starch recrystallisation. Nevertheless, the composites containing CHF revealed a lower peak intensity at 2θ of 12.71° due to the aggregation of CHFs generating a declined heterogeneous nucleation effect and the slowed movements of starch molecules. The computed crystalline index content in the TPCS matrix was 31.11% (Table 4).

Table 4
Index crystallinity of TPCS/CHF composites

Samples	Crystallinity Index (%)
TPCS	31.11
CFC 125	41.51
CFC 200	41.51
CFC 300	39.85

SEM Analysis

The surface morphology of the tensile fractured surface was examined using scanning electron microscopy (SEM). The porosity of samples was determined by the voids present, which are the result of fibre packing. The coconut husk fibres (CHF) and the matrix demonstrated good compatibility and adhesion. According to Prachayawarakorn et al. (2011), the size, chemical composition, and shape of the fibre directly impact the interfacial adhesion between the fibre and polymer matrix, homogenisation in the distribution with the polymer matrix, and subsequently, the affinity between the two materials. These characteristics are essential for the composite's mechanical performance.

Figure 12 arrays the SEM images of the fractured surface microstructures with various fibre sizes: 0%, 125, 200, and 300 μm . Figure 12(a) demonstrates the TPCS matrix exhibiting a continuous surface without voids, creasers, or distinct starch portions. No starch aggregates or inflated granules were visible on this surface; hence, the plasticiser was thought to have broken the inter- and intra-molecular hydrogen bonding in native cassava starch, appropriately completing the plasticisation process. Then, the CHF was effectively encoded into the TPCS matrix. It is feasible to see fibres emerging from the composite's fracture surface in Figures 12 (b, c, and d).

The fracture surfaces' microstructure demonstrated ductile tearing with some fibre breakings. It is attributable to poor fibre-matrix interface adhesion. These observations aligned with the tensile results reported by Diyana et al. (2021a). Meanwhile, in Figure 12(d), it was noticed that the samples' surfaces displayed decreased homogeneity, yielding a non-uniform and stiff structure with an uneven surface and the presence of voids. It can be linked to the starch-CHF interaction that was comparatively low due to the inclusion of larger-size fibres and the lack of appropriate hydrophilic starch mixed with a hydrophobic fibre matrix (Hafila et al., 2022). Due to discontinuity in the matrix and agglomeration, it started at a larger fibre content.

Figure 13 depicts the focused SEM images of TPCS/CHF composites. The close-up detail of native cassava starch granules can be seen with 150 μm magnification, as

presented in Figure 13(a). Cassava starch granules are spherical with a truncated end and a well-defined hilum. The granule sizes are between 5 and 35 μm . The existence of starch granules indicated the efficiency of shear- and thermo-processing at gelatinising the starch granules. However, the starch granules were not noticeably visible, indicating the starch was well plasticised in Figures 13 (b, c, d, and e).

Fragmentation of the fibres was seen in all composites as a consequence of tensile fracture caused by the reinforcing effect of the matrix's stress transmission to the fibres (Jumaidin et al., 2021). Meanwhile, including CHF in TPCS composites produced a rough structure with CHF on its surface. It can be shown in Figure 13(e) that CHF and TPCS are highly compatible, as evidenced by the matrix's adequate fibre wetting. A previous study reported that the length of the fibres impacts the stress concentration at the fibre ends, resulting in less elongation at fibre breaks for longer fibres since the system cannot withstand local failure (Delli et al., 2021). In addition, more fibre-size ends are present in composites, leading to failure at lower stresses. It is also in perfect accord with the previously disclosed Young's modulus and yield strength values. Parallel findings were discovered by Khalaf et al. (2021) and Salasinska et al. (2015). The morphological examination indicated excellent interfacial adhesion, demonstrating the matrix's inherent affinity with the reinforcement without using chemicals that harm the environment.

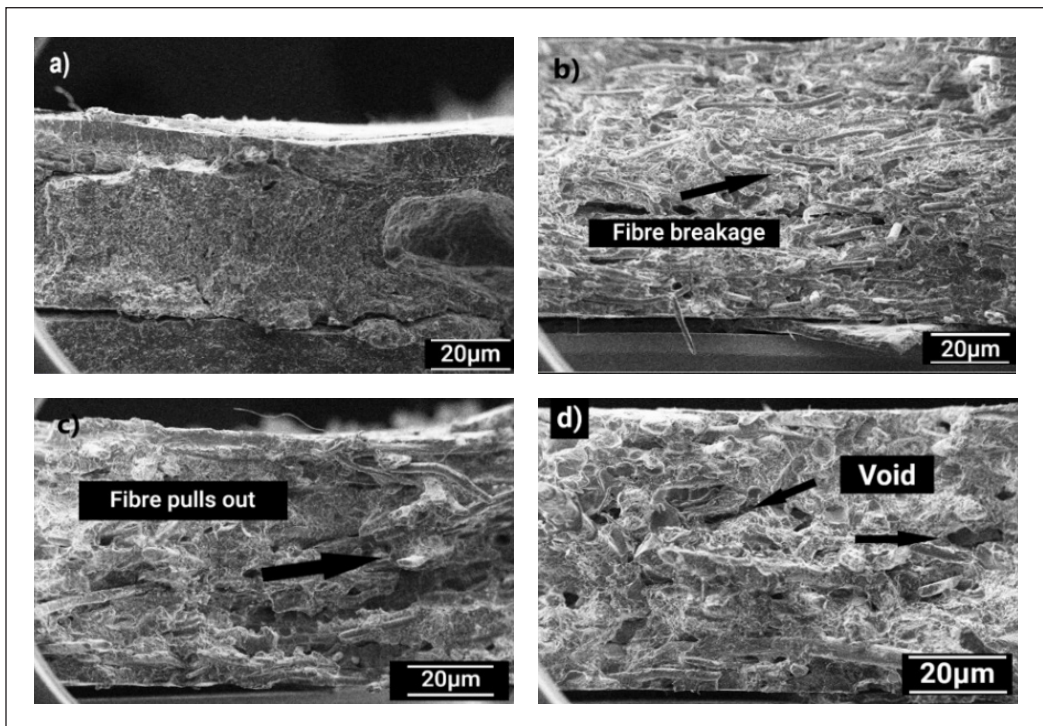


Figure 12. SEM images of fracture surfaces of TPCS/CHF with different fibre sizes: (a) 0 fibre, (b) 125 μm , (c) 200 μm , and (d) 300 μm

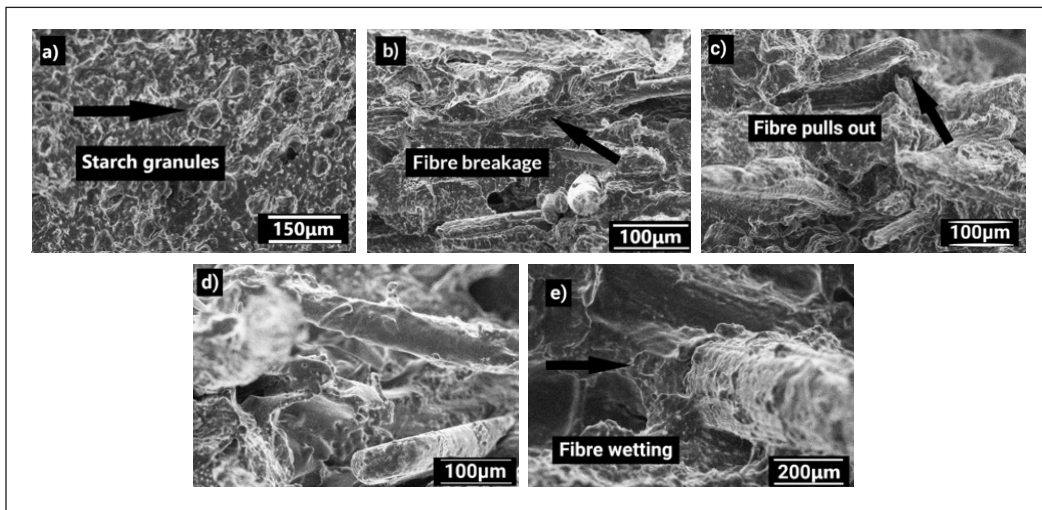


Figure 13. SEM images of shattered surface microstructures with various fibre sizes

CONCLUSION

The biodegradable TPCS reinforced with coconut husk fibre composite has been successfully prepared at 125, 200, and 300 µm fibre using dry mixing and hot-pressed methods. The addition of fibre increased tensile and flexural strength as well as modulus. Composites with a fibre size of 125 µm showed the highest tensile of 6.5 MPa and flexural strength of 13.8 MPa. In general, mixing the cassava starch with the fibre improved the thermal stability of the composites, while smaller fibre sizes led to better mechanical properties. The FTIR and SEM results also depict that cassava starch and coconut husk fibre were compatible and could form a homogenous structure. Overall, TPCS-reinforced coconut husk fibre has shown promise as an alternative to non-environmentally friendly polymers.

ACKNOWLEDGEMENTS

The authors thank Universiti Teknikal Malaysia Melaka and the Ministry of Higher Education Malaysia for the financial support through research grant FRGS/1/2023/FTKIP/F00548.

REFERENCES

- Abdullah, A., Jamaludin, S. B., Noor, M. M., & Hussin, K. (2011). Composite cement reinforced coconut fibre: Physical and mechanical properties and fracture behaviour. *Australian Journal of Basic and Applied Sciences*, 5(7), 1228–1240.
- Abraham, E., Deepa, B., Pothen, L. A., Cintil, J., Thomas, S., John, M. J., Anandjiwala, R., & Narine, S. S. (2013). Environmental friendly method for the extraction of coir fibre and isolation of nanofibre. *Carbohydrate Polymers*, 92(2), 1477–1483. <https://doi.org/10.1016/j.carbpol.2012.10.056>

- Abral, H., Basri, A., Muhammad, F., Fernando, Y., Hafizulhaq, F., Mahardika, M., Sugiarti, E., Sapuan, S. M., Ilyas, R. A., & Stephane, I. (2019). A simple method for improving the properties of the sago starch films prepared by using ultrasonication treatment. *Food Hydrocolloids*, *93*, 276–283. <https://doi.org/10.1016/j.foodhyd.2019.02.012>
- Agyei-Tuffour, B., Asante, J. T., Nyankson, E., Dodoo-Arhin, D., Oteng-Pepurah, M., Azeko, S. T., Azeko, A. S., Oyewole, O. K., & Yaya, A. (2021). Comparative analyses of rice husk cellulose fibre and kaolin particulate reinforced thermoplastic cassava starch biocomposites using the solution casting technique. *Polymer Composites*, *42*(7), 3216–3230. <https://doi.org/10.1002/pc.26052>
- Aji, I. S., Zainudin, E. S., Khalina, A., Sapuan, S. M., & Khairul, M. D. (2011). Studying the effect of fibre size and fibre loading on the mechanical properties of hybridized kenaf/PALF-reinforced HDPE composite. *Journal of Reinforced Plastics and Composites*, *30*(6), 546–553. <https://doi.org/10.1177/0731684411399141>
- AL-Hassan, A. A., & Norziah, M. H. (2017). Effect of transglutaminase induced crosslinking on the properties of starch/gelatin films. *Food Packaging and Shelf Life*, *13*, 15–19. <https://doi.org/10.1016/j.fpsl.2017.04.006>
- ASTM [American Society for Testing and Materials]. (2022). *ASTM D638 Standard test method for tensile properties of plastics*. ASTM International.
- ASTM [American Society for Testing and Materials]. (2017). *ASTM D790 Standard test methods for flexural properties of unreinforced and reinforced plastics and electrical insulating materials*. ASTM International.
- Barkoula, N. M., Alcock, B., Cabrera, N. O., & Peijs, T. (2008). Flame-retardancy properties of intumescent ammonium poly(Phosphate) and mineral filler magnesium hydroxide in combination with graphene. *Polymers and Polymer Composites*, *16*(2), 101–113. <https://doi.org/10.1002/pc>
- Campos, A., Sena Neto, A. R., Rodrigues, V. B., Luchesi, B. R., Mattoso, L. H. C., & Marconcini, J. M. (2018). Effect of raw and chemically treated oil palm mesocarp fibres on thermoplastic cassava starch properties. *Industrial Crops and Products*, *124*, 149–154. <https://doi.org/10.1016/j.indcrop.2018.07.075>
- Ceseracciu, L., Heredia-Guerrero, J. A., Dante, S., Athanassiou, A., & Bayer, I. S. (2015). Robust and biodegradable elastomers based on corn starch and polydimethylsiloxane (PDMS). *ACS Applied Materials and Interfaces*, *7*(6), 3742–3753. <https://doi.org/10.1021/am508515z>
- Chotiprayon, P., Chaisawad, B., & Yoksan, R. (2020). Thermoplastic cassava starch/poly(lactic acid) blend reinforced with coir fibres. *International Journal of Biological Macromolecules*, *156*, 960–968. <https://doi.org/10.1016/j.ijbiomac.2020.04.121>
- Dang, K. M., & Yoksan, R. (2021). Thermoplastic starch blown films with improved mechanical and barrier properties. *International Journal of Biological Macromolecules*, *188*, 290–299. <https://doi.org/10.1016/j.ijbiomac.2021.08.027>
- Delli, E., Giliopoulos, D., Bikiaris, D. N., & Chrissafis, K. (2021). Fibre length and loading impact on the properties of glass fibre reinforced polypropylene random composites. *Composite Structures*, *263*, Article 113678. <https://doi.org/10.1016/j.compstruct.2021.113678>
- Diyana, Z. N., Jumaidin, R., Selamat, M. Z., Alamjuri, R. H., & Yusof, F. A. M. (2021a). Extraction and characterization of natural cellulosic fibre from pandanus amaryllifolius leaves. *Polymers*, *13*(23), Article 4171. <https://doi.org/10.3390/polym13234171>

- Diyana, Z. N., Jumaidin, R., Selamat, M. Z., & Suan, M. S. M. (2021b). Thermoplastic starch/beeswax blend: Characterization on thermal mechanical and moisture absorption properties. *International Journal of Biological Macromolecules*, *190*, 224–232. <https://doi.org/10.1016/j.ijbiomac.2021.08.201>
- Dong, Y., Ghataura, A., Takagi, H., Haroosh, H. J., Nakagaito, A. N., & Lau, K. T. (2014). Polylactic acid (PLA) biocomposites reinforced with coir fibres: Evaluation of mechanical performance and multifunctional properties. *Composites Part A: Applied Science and Manufacturing*, *63*, 76–84. <https://doi.org/10.1016/j.compositesa.2014.04.003>
- Edhirej, A., Sapuan, S. M., Jawaid, M., & Zahari, N. I. (2017). Preparation and characterization of cassava bagasse reinforced thermoplastic cassava starch. *Fibers and Polymers*, *18*(1), 162–171. <https://doi.org/10.1007/s12221-017-6251-7>
- Estrada-Monje, A., Alonso-Romero, S., Zitzumbo-Guzmán, R., Estrada-Moreno, I. A., & Zaragoza-Contreras, E. A. (2021). Thermoplastic starch-based blends with improved thermal and thermomechanical properties. *Polymers*, *13*(23), Article 4263. <https://doi.org/10.3390/polym13234263>
- Hafila, K. Z., Jumaidin, R., Ilyas, R. A., Selamat, M. Z., & Yusof, F. A. M. (2022). Effect of palm wax on the mechanical, thermal, and moisture absorption properties of thermoplastic cassava starch composites. *International Journal of Biological Macromolecules*, *194*, 851–860. <https://doi.org/10.1016/j.ijbiomac.2021.11.139>
- Halal, S. L. M. E., Zavareze, E. D. R., Rocha, M. D., Pinto, V. Z., Nunes, M. R., Luvielmo, M. D. M., & Prentice, C. (2016). Films based on protein isolated from croaker (*Micropogonias furnieri*) and palm oil. *Journal of the Science of Food and Agriculture*, *96*(7), 2478–2485. <https://doi.org/10.1002/jsfa.7368>
- Hasan, M., Gopakumar, D. A., Olaiya, N. G., Zarlaida, F., Alfian, A., Aprinasari, C., Alfatah, T., Rizal, S., & Khalil, H. P. S. A. (2020). Evaluation of the thermomechanical properties and biodegradation of brown rice starch-based chitosan biodegradable composite films. *International Journal of Biological Macromolecules*, *156*, 896–905. <https://doi.org/10.1016/j.ijbiomac.2020.04.039>
- Hassan, M. M., Le Guen, M. J., Tucker, N., & Parker, K. (2019). Thermo-mechanical, morphological and water absorption properties of thermoplastic starch/cellulose composite foams reinforced with PLA. *Cellulose*, *26*(7), 4463–4478. <https://doi.org/10.1007/s10570-019-02393-1>
- Hazrol, M. D., Sapuan, S. M., Zainudin, E. S., Zuhri, M. Y. M., & Wahab, N. I. A. (2021). Corn starch (*Zea mays*) biopolymer plastic reaction in combination with sorbitol and glycerol. *Polymers*, *13*(2), Article 242. <https://doi.org/10.3390/polym13020242>
- Ilyas, R. A., & Sapuan, S. M. (2020a). Biopolymers and biocomposites: Chemistry and technology. *Current Analytical Chemistry*, *16*(5), 500–503. <https://doi.org/10.2174/157341101605200603095311>
- Ilyas, R. A., & Sapuan, S. M. (2020b). The preparation methods and processing of natural fibre bio-polymer composites. *Current Organic Synthesis*, *16*(8), 1068–1070. <https://doi.org/10.2174/157017941608200120105616>
- Ilyas, R. A., Sapuan, S. M., Ishak, M. R., & Zainudin, E. S. (2018). Development and characterization of sugar palm nanocrystalline cellulose reinforced sugar palm starch bionanocomposites. *Carbohydrate Polymers*, *202*, 186–202. <https://doi.org/10.1016/j.carbpol.2018.09.002>

- Ilyas, R. A., Zuhri, M. Y. M., Norrrahim, M. N. F., Misenan, M. S. M., Jenol, M. A., Samsudin, S. A., Nurazzi, N. M., Asyraf, M. R. M., Supian, A. B. M., Bangar, S. P., Nadlene, R., Sharma, S., & Omran, A. A. B. (2022). Natural fiber-reinforced polycaprolactone green and hybrid biocomposites for various advanced applications. *Polymers*, *14*(1), Article 182. <https://doi.org/10.3390/polym14010182>
- Jacob, G. C., Starbuck, J. M., Fellers, J. F., & Simunovic, S. (2005). Effect of fibre volume fraction, fibre length and fibre tow size on the energy absorption of chopped carbon fibre-polymer composites. *Polymer Composites*, *26*(3), 293–305. <https://doi.org/10.1002/pc.20100>
- Javaid, M. A., Zia, K. M., Zafar, K., Khosa, M. K., Akram, N., Ajmal, M., Imran, M., & Iqbal, M. N. (2020). Synthesis and molecular characterisation of chitosan/starch blends based polyurethanes. *International Journal of Biological Macromolecules*, *146*, 243–252. <https://doi.org/10.1016/j.ijbiomac.2019.12.234>
- Jumaidin, R., Diah, N. A., Ilyas, R. A., Alamjuri, R. H., & Yusof, F. A. M. (2021). Processing and characterisation of banana leaf fibre reinforced thermoplastic cassava starch composites. *Polymers*, *13*, Article 1420. <https://doi.org/10.3390/polym13091420>
- Jumaidin, R., Khiruddin, M. A. A., Asyul Sutan Saidi, Z., Salit, M. S., & Ilyas, R. A. (2020). Effect of cogon grass fibre on the thermal, mechanical and biodegradation properties of thermoplastic cassava starch biocomposite. *International Journal of Biological Macromolecules*, *146*, 746–755. <https://doi.org/10.1016/j.ijbiomac.2019.11.011>
- Jusoh, M. S. M., Nordin, M. N., & Ahamad, W. M. A. W. (2021). Comparison study on fibre and cocopeat from young coconut husks and old coconut husks. *Advances in Agricultural and Food Research Journal*, *2*(2), Article a0000216. <https://doi.org/10.36877/aafrij.a0000216>
- Kaewtatip, K., & Tanrattanakul, V. (2012). Structure and properties of pregelatinized cassava starch/kaolin composites. *Materials and Design*, *37*, 423–428. <https://doi.org/10.1016/j.matdes.2011.12.039>
- Kamaruddin, Z. H., Jumaidin, R., Ilyas, R. A., Selamat, M. Z., Alamjuri, R. H., & Yusof, F. A. M. (2022). Biocomposite of cassava starch-cymbopogon citratus fibre: Mechanical, thermal and biodegradation properties. *Polymers*, *14*(3), Article 514. <https://doi.org/10.3390/polym14030514>
- Khalaf, Y., El Hage, P., Dimitrova Mihajlova, J., Bergeret, A., Lacroix, P., & El Hage, R. (2021). Influence of agricultural fibres size on mechanical and insulating properties of innovative chitosan-based insulators. *Construction and Building Materials*, *287*, Article 123071. <https://doi.org/10.1016/j.conbuildmat.2021.123071>
- Liu, Y., Liang, Z., Liao, L., & Xiong, J. (2022). Effect of sisal fibre on retrogradation and structural characteristics of thermoplastic cassava starch. *Polymers and Polymer Composites*, *30*, Article 09673911221080363. <https://doi.org/10.1177/09673911221080363>
- Lomelí-Ramírez, M. G., Kestur, S. G., Manríquez-González, R., Iwakiri, S., De Muniz, G. B., & Flores-Sahagun, T. S. (2014). Bio-composites of cassava starch-green coconut fibre: Part II - Structure and properties. *Carbohydrate Polymers*, *102*(1), 576–583. <https://doi.org/10.1016/j.carbpol.2013.11.020>
- Madhumitha, G., Fowsiya, J., Mohana Roopan, S., & Thakur, V. K. (2018). Recent advances in starch-clay nanocomposites. *International Journal of Polymer Analysis and Characterisation*, *23*(4), 331–345. <https://doi.org/10.1080/1023666X.2018.1447260>

- Marichelvam, M. K., Jawaid, M., & Asim, M. (2019). Corn and rice starch-based bio-plastics as alternative packaging materials. *Fibres*, 7(4), Article 32. <https://doi.org/10.3390/fib7040032>
- Mina, J. H., Valadez, A., Franco, P. J. H., & Toledano, T. (2009). Influencia del tiempo de almacenamiento en las propiedades estructurales de un almidón termoplástico de yuca (TPS) [Influence of storage time on the structural properties of a cassava thermoplastic starch (TPS)]. *Ingeniería y Competitividad*, 11(2), 1-26. <https://doi.org/10.25100/iyc.v11i2.2461>
- Mohamed, W. Z. W., Baharum, A., Ahmad, I., Abdullah, I., & Zakaria, N. E. (2018). Effects of fibre size and fibre content on mechanical and physical properties of *Mengkuang* reinforced thermoplastic natural rubber composites. *BioResources*, 13(2), 2945–2959. <https://doi.org/10.15376/biores.13.2.2945-2959>
- Mo, X. Z., Zhong, Y. X., Liang, C. Q., & Yu, S. J. (2010). Studies on the properties of banana fibers-reinforced thermoplastic cassava starch composites: Preliminary results. *Advanced Materials Research*, 87–88, 439–444. <https://doi.org/10.4028/www.scientific.net/AMR.87-88.439>
- Monteiro, S. N., Calado, V., Rodriguez, R. J. S., & Margem, F. M. (2012). Thermogravimetric behaviour of natural fibres reinforced polymer composites-An overview. *Materials Science and Engineering A*, 557, 17–28. <https://doi.org/10.1016/j.msea.2012.05.109>
- Montero, B., Rico, M., Rodríguez-Llamazares, S., Barral, L., & Bouza, R. (2017). Effect of nanocellulose as a filler on biodegradable thermoplastic starch films from tuber, cereal and legume. *Carbohydrate Polymers*, 157, 1094–1104. <https://doi.org/10.1016/j.carbpol.2016.10.073>
- Moura, A. D. S., Demori, R., Leão, R. M., Frankenberg, C. L. C., & Santana, R. M. C. (2019). The influence of the coconut fiber treated as reinforcement in PHB (polyhydroxybutyrate) composites. *Materials Today Communications*, 18, 191–198. <https://doi.org/10.1016/j.mtcomm.2018.12.006>
- Polat, S., Uslu, M. K., Aygün, A., & Certel, M. (2013). The effects of the addition of corn husk fibre, kaolin and beeswax on cross-linked corn starch foam. *Journal of Food Engineering*, 116(2), 267–276. <https://doi.org/10.1016/j.jfoodeng.2012.12.017>
- Prachayawarakorn, J., Limsiriwong, N., Kongjindamunee, R., & Surakit, S. (2012). Effect of agar and cotton fiber on properties of thermoplastic waxy rice starch composites. *Journal of Polymers and the Environment*, 20(1), 88–95. <https://doi.org/10.1007/s10924-011-0371-8>
- Prachayawarakorn, J., Ruttanabus, P., & Boonsom, P. (2011). Effect of cotton fiber contents and lengths on properties of thermoplastic starch composites prepared from rice and waxy rice starches. *Journal of Polymers and the Environment*, 19(1), 274–282. <https://doi.org/10.1007/s10924-010-0273-1>
- Pradeep, M., Binoy, R. F., Yaswanth, S., Pullan, T. T., & Joseph, M. (2022). Investigations on chitin and coconut fibre reinforcements on mechanical and moisture absorption properties of corn starch bioplastics. *Materials Today: Proceedings*, 58, 65-70. <https://doi.org/10.1016/j.matpr.2021.12.585>
- Prakash, K. B., Fageehi, Y. A., Saminathan, R., Manoj Kumar, P., Saravanakumar, S., Subbiah, R., Arulmurugan, B., & Rajkumar, S. (2021). Influence of fiber volume and fibre length on thermal and flexural properties of a hybrid natural polymer composite prepared with banana stem, pineapple leaf, and s-glass. *Advances in Materials Science and Engineering*, 2021, Article 6329400. <https://doi.org/10.1155/2021/6329400>

- Razali, N., Salit, M. S., Jawaid, M., Ishak, M. R., & Lazim, Y. (2015). A study on chemical composition, physical, tensile, morphological, and thermal properties of roselle fibre: Effect of fibre maturity. *BioResources*, 10(1), 1803–1823. <https://doi.org/10.15376/biores.10.1.1803-1824>
- Rivadeneira-Velasco, K. E., Utreras-Silva, C. A., Díaz-Barrios, A., Sommer-Márquez, A. E., Tafur, J. P., & Michell, R. M. (2021). Green nanocomposites based on thermoplastic starch: A review. *Polymers*, 13(19), Article 3227. <https://doi.org/10.3390/polym13193227>
- Sahari, J., Sapuan, S. M., Zainudin, E. S., & Maleque, M. A. (2013). Mechanical and thermal properties of environmentally friendly composites derived from sugar palm tree. *Materials and Design*, 49, 285–289. <https://doi.org/10.1016/j.matdes.2013.01.048>
- Salasinska, K., & Ryszkowska, J. (2015). The effect of filler chemical constitution and morphological properties on the mechanical properties of natural fibre composites. *Composite Interfaces*, 22(1), 39–50. <https://doi.org/10.1080/15685543.2015.984521>
- Santos, B. H. D. Prado, K. D. S. D., Jacinto, A. A., & Spinace, M. A. D. S. (2018). Influence of sugarcane bagasse fiber size on biodegradable composites of thermoplastic starch. *Journal of Renewable Materials*, 6(2), 176–182. <https://doi.org/10.7569/JRM.2018.634101>
- Sanyang, M. L., Sapuan, S. M., Jawaid, M., Ishak, M. R., & Sahari, J. (2015). Effect of plasticizer type and concentration on tensile, thermal and barrier properties of biodegradable films based on sugar palm (*Arenga pinnata*) starch. *Polymers*, 7(6), 1106–1124. <https://doi.org/10.3390/polym7061106>
- Sarifuddin, N., Ismail, H., & Ahmad, Z. (2012). Effect of fibre loading on properties of thermoplastic sago starch/kenaf core fibre biocomposites. *BioResources*, 7(3), 4294–4306. <https://doi.org/10.15376/biores.7.3.4294-4306>
- Seth, S. A., Aji, I. S., & Tokan, A. (2018). Effects of particle size and loading on tensile and flexural properties of polypropylene reinforced doum palm shell particles composites. *Technology, and Sciences (ASRJETS) American Scientific Research Journal for Engineering*, 44(1), 231–239.
- Syafiq, R., Sapuan, S. M., Zuhri, M. Y. M., Ilyas, R. A., Nazrin, A., Sherwani, S. F. K., & Khalina, A. (2020). Antimicrobial activities of starch-based biopolymers and biocomposites incorporated with plant essential oils: A review. *Polymers*, 12(10), Article 2403. <https://doi.org/10.3390/polym12102403>
- Tajvidi, M., & Takemura, A. (2010). Thermal degradation of natural fibre-reinforced polypropylene composites. *Journal of Thermoplastic Composite Materials*, 23(3), 281–298. <https://doi.org/10.1177/0892705709347063>
- Tharanathan, R. N. (2005). Starch - Value addition by modification. *Critical Reviews in Food Science and Nutrition*, 45(5), 371–384. <https://doi.org/10.1080/10408390590967702>
- Travalini, A. P., Lamsal, B., Magalhaes, W. L. E., & Demiate, I. M. (2019). Cassava starch films reinforced with lignocellulose nanofibers from cassava bagasse. *International Journal of Biological Macromolecules*, 139, 1151–1161. <https://doi.org/10.1016/j.ijbiomac.2019.08.115>
- Weerapoprasit, C., & Prachayawarakorn, J. (2019). Characterization and properties of biodegradable thermoplastic grafted starch films by different contents of methacrylic acid. *International Journal of Biological Macromolecules*, 123, 657–663. <https://doi.org/10.1016/j.ijbiomac.2018.11.083>

- Wollerdorfer, M., & Bader, H. (1998). Influence of natural fibres on the mechanical properties of biodegradable polymers. *Industrial Crops and Products*, 8(2), 105–112. [https://doi.org/10.1016/S0926-6690\(97\)10015-2](https://doi.org/10.1016/S0926-6690(97)10015-2)
- Yokesahachart, C., Yoksan, R., Khanonkon, N., Mohanty, A. K., & Misra, M. (2021). Effect of jute fibres on morphological characteristics and properties of thermoplastic starch/biodegradable polyester blend. *Cellulose*, 28(9), 5513–5530. <https://doi.org/10.1007/s10570-021-03921-8>
- Zhang, Y., & Han, J. H. (2006). Plasticisation of pea starch films with monosaccharides and polyols. *Journal of Food Science*, 71(6), 253–261. <https://doi.org/10.1111/j.1750-3841.2006.00075.x>
- Zhang, Y., Rempel, C., & Liu, Q. (2014). Thermoplastic starch processing and characteristics: A review. *Critical Reviews in Food Science and Nutrition*, 54(10), 1353–1370. <https://doi.org/10.1080/10408398.2011.636156>
- Zullo, R., & Iannace, S. (2009). The effects of different starch sources and plasticizers on film blowing of thermoplastic starch: Correlation among process, elongational properties and macromolecular structure. *Carbohydrate Polymers*, 77(2), 376–383. <https://doi.org/10.1016/j.carbpol.2009.01.007>

Design Ideation and Selection of Under-Piston Door for a Two-stroke Marine Engine Using Hybrid TRIZ-biomimetic and MCDM Methods

Yiow Ru Vern¹, Muhd Ridzuan Mansor^{1*}, Mohd Adrinata Shaharuzaman¹ and Basori²

¹*Fakulti Teknologi dan Kejuruteraan Mekanikal, Universiti Teknikal Malaysia Melaka, Hang Tuah Jaya, 76100 Durian Tunggal, Melaka, Malaysia*

²*Department of Mechanical Engineering, Faculty of Engineering and Science, Universitas Nasional, Sawo Manila, Pasar Minggu, Jakarta, 12520, Indonesia*

ABSTRACT

Design ideation and selection of a two-stroke marine engine under-piston door employing Theory of Inventive Problem Solving (TRIZ), biomimetics, Analytical Hierarchy Process (AHP) and Technique for Order of Preference by Similarity to Ideal Solution (TOPSIS) is presented in this paper. The study is motivated by exploring bio-composites as potentially suitable substitutes for conventional steel in engine component manufacture. As bio-composites possess lower mechanical properties compared to steel, the geometrical redesign was deemed necessary for any potential material substitution to take place. New under-piston door designs were ideated through the synergy between TRIZ and biomimetics. Computational models were developed, inspired by the Amazon waterlily, the tortoiseshell and the spider web. Mechanical simulation was performed for maximum stress (von Mises), total deformation and volume. With the simulated results of these designs, AHP and TOPSIS provided the solution's capabilities to decide the best design overall. The design inspired by the Amazon waterlily proved the best and showed lower stress and deformation values compared to the original by 45.25% and 4.5%, respectively. This research provided conclusive evidence that with refined scrutiny of the TRIZ and biomimetic methods, along with AHP and TOPSIS, potential

alternatives to conventional materials that offer environmental friendliness without compromising operational requirements can be realised.

Keywords: Biomimetics, design ideation, multi-criteria decision-making methods, two-stroke marine engine, TRIZ

ARTICLE INFO

Article history:

Received: 16 August 2023

Accepted: 09 May 2024

Published: 14 June 2024

DOI: <https://doi.org/10.47836/pjst.32.S2.08>

E-mail addresses:

yiowrv@gmail.com (Yiow Ru Vern)

muhd.ridzuan@utem.edu.my (Muhd Ridzuan Mansor)

adrinata@utem.edu.my (Mohd Adrinata Shaharuzaman)

basori@civitas.unas.ac.id (Basori)

* Corresponding author

INTRODUCTION

The growth of consciousness across humanity has brought about a common realisation of the importance of a sustainable way of life (Sapuan & Mansor, 2021). An increase in global awareness of the plight of human society has driven the launch of initiatives now known as the United Nations Sustainability and Development Goals (UNSDG) (United Nations, 2023). The marine industry, like others, has made strides to reduce its environmental impact with various initiatives spearheaded by the International Maritime Organization (IMO). Stringency in environmental protection has been on the increase, particularly with regard to emission control from ships as well as other forms of pollution, ranging from the discharge of pollutants into the sea to garbage and sewage management (<https://tinyurl.com/4azfj6ca>).

In keeping with sustainability, research has been published on the potential of alternative naturally sourced materials over conventional synthetics presently used across industries (Claverie et al., 2020; Moudood et al., 2019; Girijappa et al., 2019). These materials are generally categorised as natural fibre composites (NFC), made of bio-polymers reinforced by natural fibres (Pingulkar et al., 2021). In the marine industry, particularly in marine engineering, limited work has been found on using NFC as a potential substitute for conventional structural materials, particularly steel. Some literature on NFC involved its use in pleasure vessel hull construction (Ansell, 2014; Fragassa, 2017; Mouritz et al., 2001).

This paper investigates the idea generation and design selection processes of envisaging a new geometrical concept of a two-stroke marine engine under-piston door. Brief backgrounds will be presented on the topics of marine engines, the ideation tools of the Theory of Inventive Problem Solving (TRIZ) and biomimetics, and the decision-making methods of Technique for Order of Preference by Similarity to Ideal Solution (TOPSIS) and Analytical Hierarchy Process (AHP). A new under-piston door design is presented using these tools and methods in synergy.

Two-stroke Marine Engine

The two-stroke marine engine is responsible for powering a large percentage of the world tonnage transported across the oceans in modern times (Bilousov et al., 2020). Traditionally, these engines were run on marine diesel oil and, later, marine heavy fuel oil. These days, cleaner alternative fuels are being researched as we aim to reduce the impact of global warming (Latarche, 2021). These are slow-speed engines, with the piston assembly connected to the connecting rod via a crosshead arrangement. Cylinder aspiration is achieved by passing the turbocharged air through a scavenging space below the piston assembly, commonly known as the uniflow scavenging method. The space underneath the pistons is the scavenging or under-piston space within the marine engineering circle. Access to this scavenging space for maintenance and inspection is permitted through manhole doors, aptly called the under-piston door. The location of the under-piston door is highlighted in Figure 1.

The scavenge space is often subjected to low scavenging air pressure and temperature. Based on the ISO 3046-1:2002E (Reciprocating Internal Combustion Engines-Performance-Part 1: Declarations of Power, Fuel and Lubricating Oil Consumptions, and Test Methods - Additional Requirements for Engines for General Use), these values are placed at 25°C and 1 bar respectively. From the author's experience working with these engines while serving on board merchant ships, these values can rise to 42°C and 1.6 bar for a 60 cm bore engine charged by a single turbocharger. It has also been reported that higher scavenge pressures of up to 3.6 bar for a 90 cm bore engine equipped with three turbochargers (Livanos et al., 2003). These values may differ depending on the setup, but the variation would be minimal.

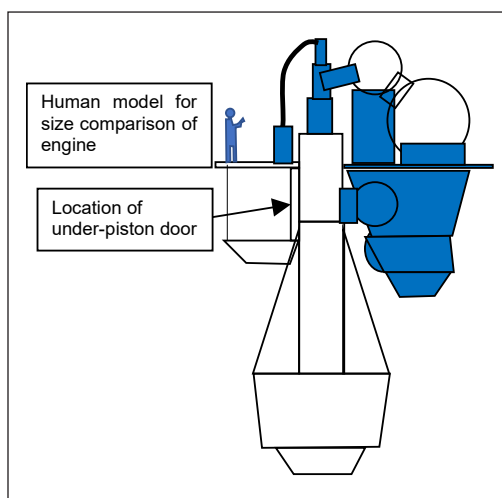


Figure 1. Location of the under-piston door on a two-stroke marine engine

Theory of Inventive Problem Solving (TRIZ)

Teoriya Resheniya Izobretatelskikh Zadatch (TRIZ) is a problem-solving method that Russian scientist Genrikh Saulovich Altshuller introduced after studying vast numbers of patents (Ekmecki & Nebati, 2019; Sheu et al., 2020). TRIZ provides different perspectives on problem-solving and idea innovation by tapping into past strategies. In recent years, TRIZ has closely been associated with eco-design in the proposed development of green products and processes (Russo & Spreafico, 2020) and improvements in the selection of greener materials (Spreafico, 2022). A sustainable innovation model was proposed based on TRIZ with an ecological innovation tool (Boavida et al., 2020). One study suggested that TRIZ provided solutions in investment strategies involving green nuclear energy (Yuan et al., 2021). TRIZ innovations have also positively influenced various environmental impact categories (Spreafico, 2021). A point has also been made that applying TRIZ in language classes improved the proficiency of students in English classes (Alkasem & Tilfarlioğlu, 2022).

Biomimetics

How living organisms evolve to adapt to their respective environments has often inspired human beings in our development of engineering solutions (Kunzmann et al., 2023). The concept of copying nature's ingenuity has been documented and is broadly categorised as "biomimetics" (Fayemi et al., 2014; Wanieck et al., 2020). Several notable innovations

that can be seen today thanks to biomimetics include hook and loop fasteners, inspired by the tiny hooks on dried burdock seeds and the Shinkansen bullet train nose profile, inspired by the kingfisher's beak (Primrose, 2020). In recent times, the design of wind turbines has mimicked the profile of humpback whale flippers. Modern antifouling paints on ships adopt similar hydrophobic properties to the lotus leaf, preventing barnacles and other microorganisms from staying attached to the ship's hull (Han et al., 2021), merging TRIZ with biomimetics allowed for new valve designs with improved erosion resistance and increased service life (Cheng et al., 2019; Zhang et al., 2019).

The Analytical Hierarchy Process (AHP) and Technique for Order of Preference by Similarity to Ideal Solution (TOPSIS)

Multi-Criteria Decision-Making (MCDM) models such as AHP and TOPSIS have long established the foundation for ranking and selection involving multiple attributes (Sahoo & Goswami, 2023) and have remained among the most preferred methods reported (Taherdoost & Madanchian, 2023). Where AHP compares each criterion and alternative pairwise (Saaty, 1987), TOPSIS measures the distance of each alternative to the derived ideal solution (Hwang & Yoon, 1981). Recent studies have demonstrated the benefits of both methods working in series.

The hybridisation of AHP-TOPSIS has successfully selected unmanned aircraft models (Djukic et al., 2022) and bus chassis designs (James et al., 2021). A risk assessment model was based on AHP-TOPSIS, providing a decision-making method in hazard mitigation involving oil and gas pipelines (Wang & Duan, 2019). Other examples demonstrating the effectiveness of this tandem strategy include selecting the best base oil for biodiesel application (Abdulvahitoglu & Kilic, 2022) and suitable software for the study of solar radiation (Ahmad et al., 2022). Additionally, the ideal configuration of a geothermal energy system was decided using this synergistic strategy (Arslan et al., 2021). Although integrated AHP-TOPSIS strategies have been applied in various fields, limited work has been found regarding design selection in marine engines.

METHODOLOGY

The two-stroke marine engine under-piston door's design ideation and selection process can be broken down into three sub-sections. In the first, design specifications are listed to aid in developing new ideas for the under-piston door geometry. These include physical parameters as well as any regulatory requirements stated by governing bodies. The second step is to envisage ideas using a combination of TRIZ and biomimetics. Digital models of these ideas will then be drawn up and simulated with the aid of the ANSYS software. Lastly, from the simulation data, the best design will be selected using AHP and TOPSIS. Figure 2 visually represents the flow and details of these three sub-sections.

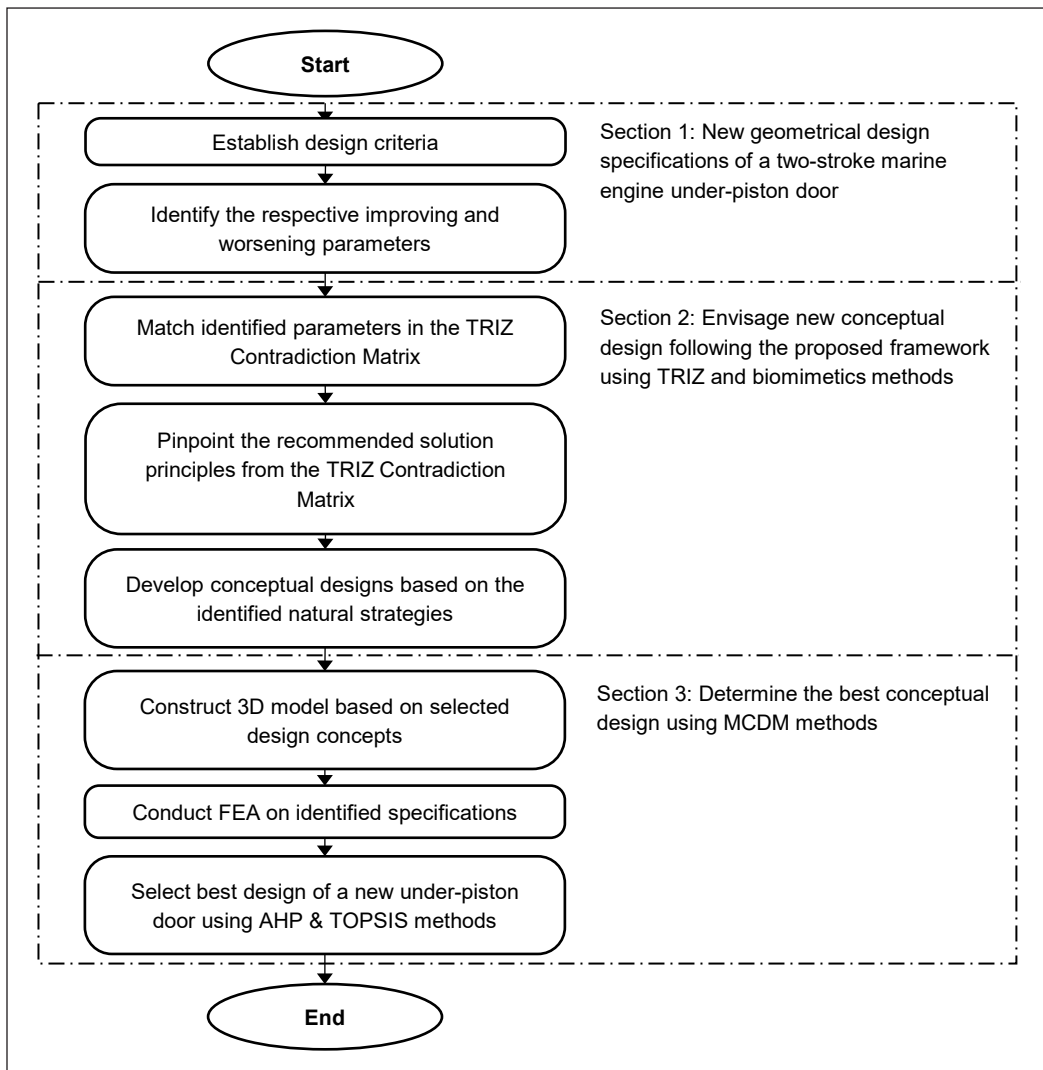


Figure 2. Flowchart of the design selection process

Establish Design Specifications

The specifications of the intended new under-piston door design can be divided into several parts. All regulatory requirements for marine engines were referenced, and guidance was sought from industry experts. From a general perspective, the main regulating body in the marine industry falls under the jurisdiction of the International Maritime Organization (IMO) (<https://www.imo.org/>). The International Convention for the Safety of Life at Sea (SOLAS) is the main international treaty focused on all aspects of the safety of merchant ships (<https://tinyurl.com/2p9593az>). SOLAS provides the framework and details involving all aspects of safety at sea, including those for the construction of seagoing vessels.

However, the authors did not come across any specific standards for applying non-metallic material in marine engine manufacturing or other related standards on engine component testing from SOLAS.

Another key aspect of safety in the marine industry is covered by the International Association of Classification Societies (IACS), which provides recommendations on the details of shipbuilding. They publish rules for the design, material selection, manufacturing methods, testing, and so on for ships and other related equipment, including marine machinery (<https://iacs.org.uk/>). Under IACS rules, Unified Requirements-Machinery Installations (UR M), M71 (Type Testing of Internal Combustion Engines) and M72 (Certification of Engine Components) provide details on engine certification and tests and specify the need for declaration of chemical composition and mechanical properties of materials used as well as witness of tests conducted on material samples (IACS, 2006). Another document, Unified Interpretations-SOLAS (UI SC), provides clarification on the use of non-metallic materials under SC282 (Application of Materials Other than Steel on Engine, Turbine and Gearbox Installations), in which it is mentioned that components not likely to cause release of flammable fluid to machinery and meet fire test criteria under ISO 19921:2005/19922:2005 can be manufactured using non-metallic materials (IACS, 2016).

Additionally, standards set by the International Standards Organization (ISO) were referred to in this research (<https://www.iso.org/home.html>). ISO 3046-1:2002E (Reciprocating Internal Combustion Engines - Performance - Part 1: Declarations of Power, Fuel and Lubricating Oil Consumptions, and Test Methods - Additional Requirements for Engines for General Use) defines the ambient conditions for engine aspiration at a temperature of 25°C and 1 bar gauge pressure. This standard has also been mentioned in the manuals of major marine engine makers (MAN Diesel & Turbo, 2010; Winterthur Gas & Diesel, 2023).

Incidentally, the initial motivation for the new under-piston door design was so that it could be made lighter, making it easier for removal and reinstallation during maintenance. The most obvious way to design a lighter object is to replace the material with something lighter or less dense. In line with the current drive for sustainability worldwide (United Nations, 2023), this new design for the under-piston door was intended to be made with NFC. Hence, there is a need for ingenuity in design to compensate for the loss of material strength due to the substitution of NFC. It should be highlighted that this research focuses only on the design selection. Material selection for NFC, including fibre, polymer, and fire retardant, shall be presented in a separate publication. Additionally, the physical dimensions of the under-piston door for a MAN B&W S60MC-C engine were measured and detailed in Figure 3.

Hence, for the ideation of a new under-piston door design, the criteria mainly provide setting values for the later simulation stage and the physical dimensions. The standards

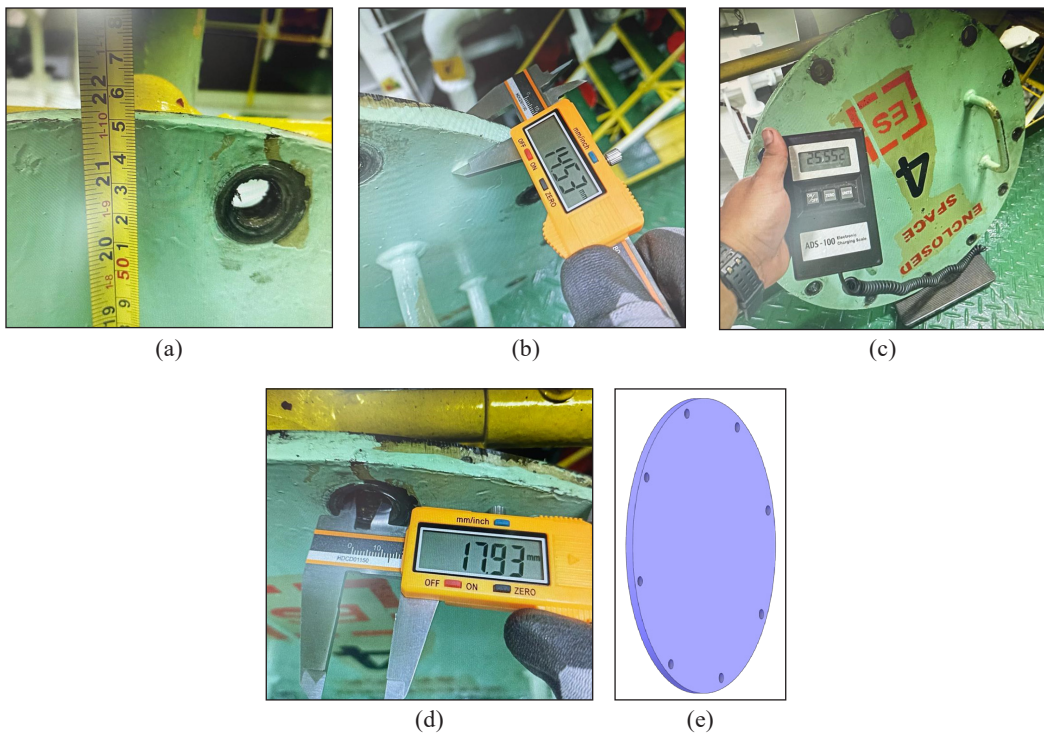


Figure 3. Measurements of an actual under-piston door for a MAN B&W 60MC-C marine engine with dimensions (a) diameter: 550 mm, (b) thickness: 15 mm, (c) weight: 25.5 kg, (d) bolt hole diameter: 18 mm, (e) CAD model of original under piston door

described were to verify that alternative materials were allowed for use in marine engines, where further tests would have to be performed, which would not be part of this research since the area of interest is limited only to the geometrical design of the said component. The details are summarised in Table 1.

Table 1
Design criteria for two-stroke marine engine under-piston door

Criteria	Description
Standard	Operating temperature: 25C
ISO 3046-1:2002E	Operating pressure: 1 bar
Dimensions	Diameter: 550 mm
	Thickness: 15 mm
	Bolt holes: 18 mm (diameter) × 8 nos

Design Ideation Using TRIZ and Biomimetics Methods

The intended purpose of the process was to reimagine the design of the under-piston door so that an improved and robust design could be envisioned. Although not part of this paper, the new design of the under-piston door is crucial in the wider scope of studying the potential of substituting steel with natural fibre composites. Hence, the process involves reimaging the simple bolted cover of the scavenge space of a two-stroke marine diesel engine, otherwise known commonly as the under-piston door, from

a different perspective. The door is not subjected to high physical or thermal load levels, it was selected for this exercise.

The under-piston door had clearly defined parameters such as dimensions, weight, and strength. Considering these parameters carefully, two were applied to the TRIZ Contradiction Matrix (San, Jin and Li, 2009), those being “durability of a stationary object” and “strength”. This line of thought revolves around substituting steel, which has high strength, with composite material, which is of a lower strength, without losing its durability. Thus, the “durability of a stationary object” is the improving parameter, while “strength” is the worsening parameter to be applied in the Contradiction Matrix. Recommendations in the matrix are then referred to for potential solutions. However, in this case, no recommendation is specified in the matrix for these two parameters, suggesting that a wide choice of solutions can be considered for this problem.

Since no recommendations were given, a careful study of all the TRIZ 40 Inventive Principles was carried out. Of the listed solutions, the decision was made to choose “Local quality”. This solution made the most sense for solving our problem, giving the idea that modifying the geometry of the under-piston door would improve its durability even if it was manufactured using material of lower strength. This solution pointed towards possible designs but still needed to suit the specifics of the under-piston door geometry. This stage demonstrates the generalised TRIZ process, whereby the specific problem is made into a generic TRIZ problem to find a generic TRIZ solution, which would then be adapted to a specific solution. It was then understood that fortifying the geometry was the way forward.

Specific solutions on structural fortification were then searched for in AskNature.org (Asknature, 2023). After going through the website’s large database of biological strategies, three strategies were identified as potential solutions for an improved under-piston door design. The first was the Amazon water lily, with its ribbed structure spanning its large leaves (Box et al., 2022). The second was the tortoiseshell, made of a sutured outer carapace and internally padded and reinforced with packings of twisted plywood-like fibrils (Achrai & Wagner, 2017). The third was the spider’s web, which is light but highly capable of absorbing the impact of flying insects that tangle in its intricate trap (Jyoti et al., 2019).

Six designs were drawn up from the biological strategies selected using ANSYS Discovery, as listed in Table 2. Design A1 has hollowed-out cylindrical sections radiating from the middle of the door. If this design was viewed externally, the observer could not tell any differences from the original design. On the other hand, A2 has a reduced thickness except for the flange area and is reinforced with cylindrical rod-like ribs radiating from the centre on the inside of the door. For B1, the internal structure of the door is made up of two rows of square-sectioned bars layered perpendicularly. Design B2 employs a similar arrangement as B1 but spreads across the whole door except for the flange. Similar to A1, both B designs are internal with no notable external difference from the original. Design

C1 and C2 have reduced door thickness with reinforcements similar to A2. C1 has eight ribs from the centre with additional randomly placed lattice reinforcements. C2, instead, has six ribs and is reinforced by random hexagonal rings. These were then simulated to obtain maximum stress (Von Mises), deformation, and volume. The simulation was performed using ANSYS Mechanical with a fixed edge support and a pressure of 4 bar on one side. These simulation results were then used in the next stage, where the best design was selected.

Design Selection Using the AHP-TOPSIS Hybrid Method

With the obtained simulation results (Table 3), the selection process could then be performed. Through simulation with the ANSYS Mechanical software, results for each design were obtained for maximum stress (Von Mises), maximum deformation and volume. These three parameters and shape complexity would be the determinants for selecting the best design. For the shape complexity, the size of each file was taken as a reference, whereby a larger file size would represent a more complex design. The reasoning behind this is that the dimensions

Table 2
Designs of under-piston doors inspired by biomimetic strategies

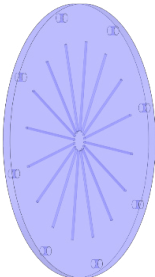
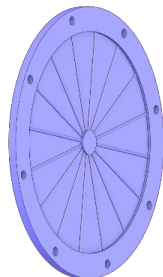
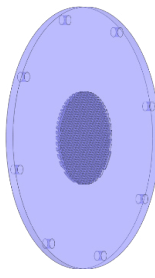
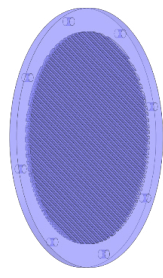
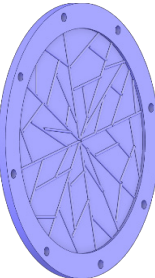
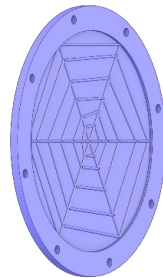
Biomimetic strategy	Design	
Amazon waterlily		
	A1	A2
Tortoiseshell		
	B1	B2
Spider web		
	C1	C2

Table 3
Data from simulation results for input into the TOPSIS method

Design	Maximum stress (von Mises) (MPa)	Volume ($\times 10^6 \text{ mm}^3$)	Maximum deformation (mm)	Shape complexity
A1	70.506	5.47	0.361	395
A2	405.130	4.77	0.864	449
B1	89.497	5.36	0.457	1262
B2	225.950	4.73	0.809	5262
C1	413.460	4.78	0.907	689
C2	245.270	4.78	0.883	688

for the under-piston door model were the same for all designs. However, the complexity of each respective design increased the file size proportionately. Hence, it was taken as a fair representation of the design complexity suited as the fourth determining criterion.

Weightage Determination Using the Analytical Hierarchy Process (AHP)

The TOPSIS weightage for each criterion was first determined using the AHP process. AHP uses a pairwise comparison matrix, whereby each criterion is compared against the others. It has been used in previous decision-making exercises. Each pair is judged and graded based on a fundamental scale, as shown in Table 4. A decision is made based on the priority between the two compared criteria. A numerical value is given based on the decided judgment. If the comparison is found to be in between any of the stated priority levels, the corresponding numerical value is selected.

The first step in AHP is to establish the pairwise comparison and the priority vector values, w :

$$A = (a_{ij})_{n \times n} = \begin{bmatrix} a_{11} & \dots & a_{1n} \\ \vdots & \ddots & \vdots \\ a_{n1} & \dots & 1 \end{bmatrix} \tag{1}$$

where $a_{ji} = 1/k$ is the reciprocal value of $a_{ij} = k$, and $i, j = 1, 2, \dots, n$.

$$w = \frac{1}{n} \sum_{j=1}^n \frac{a_{ij}}{\sum_{i=1}^n a_{ij}}, \tag{2}$$

where $i, j = 1, 2, \dots, n$.

a_{ij} is the scale of importance.

In step two, the principal eigenvalue, λ_{max} is determined:

$$\lambda_{max} = \sum_{i=1}^n \frac{\sum_{j=1}^n a_{ij} \times w_j}{w_i}, \tag{3}$$

where $i, j = 1, 2, \dots, n$.

In step three, the principal eigenvalue is then used to determine the consistency index, CI :

$$CI = \frac{(\lambda_{max} - n)}{(n - 1)}, \tag{4}$$

Table 4
Fundamental scale for pairwise comparison

Priority level	Numerical value
Extremely less important	1/9
	1/8
Very strongly less important	1/7
	1/6
Strongly less important	1/5
	1/4
Moderately less important	1/3
	1/2
Equal importance	1
	2
Moderately more important	3
	4
Strongly more important	5
	6
Very strongly more important	7
	8
Extremely more important	9

Step four is where the consistency ratio is determined:

$$CR = \frac{CI}{RI} \quad [5]$$

where RI is the random index that is selected based on the matrix size (Asadabadi et al., 2019), the Consistency Ratio, CR , should be 0.1 or less. It indicates that the results are consistent and acceptable (AL-Oqla et al., 2015; Al-Subhi, 2001).

Selection of Best Design with Technique for Order of Preference by Similarity to Ideal Solution (TOPSIS) Method

TOPSIS, as a Multi-Criteria Decision-Making (MCDM) tool, was chosen due to its suitability in engineering faculties where alternatives and evaluations can be generated (Opricovic & Tzeng, 2004). The main determining factor in TOPSIS is that the best alternative is closest to the positive ideal solution (PIS) and farthest from the negative ideal solution (NIS).

The TOPSIS method first begins with formulating the decision matrix:

$$D = \begin{bmatrix} & C_1 & C_2 & \dots & C_n \\ A_1 & X_{11} & X_{12} & \dots & X_{1n} \\ A_2 & X_{21} & X_{22} & \dots & X_{2n} \\ \vdots & \vdots & \vdots & \ddots & \vdots \\ A_m & X_{m1} & X_{m2} & \dots & X_{mn} \end{bmatrix} \quad [6]$$

where:

A_1, A_2, \dots, A_m are potential alternatives that the decision maker has to select:

C_1, C_2, \dots, C_n are the criteria from which the potential alternative performances are measured:

X_{ij} is the rating of alternative A_i with reference to criterion C_j , where w_j is the weightage assigned to criterion C_j and $w_1 + w_2 + \dots + w_n = 1$ (Roszkowska, 2011).

In step two, the normalised matrix, n_{ij} , is calculated:

$$n_{ij} = \frac{x_{ij}}{\sqrt{\sum_{i=1}^m x_{ij}^2}} \quad [7]$$

where $i = 1, 2, \dots, m; j = 1, 2, \dots, n$.

Thirdly, the weighted normalised decision matrix, v_{ij} , is obtained:

$$v_{ij} = w_j n_{ij} \quad [8]$$

where $i = 1, 2, \dots, m; j = 1, 2, \dots, n$.

w_j is the weight of the j th criterion and $\sum_{j=1}^n w_j = 1$.

It is then followed by the fourth step to determine the ideal best, A^+ and ideal worst, A^- values, respectively:

$$A^+ = \{v_1^+, v_2^+ \dots, v_n^+\} = \left\{ \left(\max_i v_{ij} \mid j \in I \right), \left(\min_i v_{ij} \mid j \in J \right) \right\} \tag{9}$$

$$A^- = \{v_1^-, v_2^- \dots, v_n^-\} = \left\{ \left(\min_i v_{ij} \mid j \in I \right), \left(\max_i v_{ij} \mid j \in J \right) \right\} \tag{10}$$

Where I is associated with the beneficial criterion, and J is associated with the cost criterion.

The fifth step calculates the separation measures using the n -dimension Euclidian distance. Each alternative distance is defined as:

$$d_i^+ = \sqrt{\sum_{j=1}^n (v_{ij} - v_i^+)^2} \tag{11}$$

where $i = 1, 2, \dots, m$.

$$d_i^- = \sqrt{\sum_{j=1}^n (v_{ij} - v_i^-)^2} \tag{12}$$

where $i = 1, 2, \dots, m$.

The sixth step is to calculate the relative closeness to the ideal solution, A_j , with respect to A^+ :

$$R_i = \frac{d_i^-}{(d_i^- + d_i^+)} \tag{13}$$

where $0 \leq R_i \leq 1, i = 1, 2, \dots, m$.

The alternatives are ranked in descending order based on the obtained R_i values.

RESULTS AND DISCUSSION

The weightage of each criterion was determined first with AHP. The first step was establishing the pairwise comparison matrix of the four determining criteria (Table 5). It established the hierarchy of importance across the selected criterion in Table 3. The following steps were then simply to obtain the respective values for the principal eigenvalue, λ_{max} , consistency index, CI , and consistency ratio, CR (Table 6). The determined consistency ratio is 0.01997, which is less than 0.1. Hence, the results obtained are verified as acceptable. The final determined weightage of the selected criteria is reflected in Table 7, which will be used in the next phase of the design selection.

From here, the design selection process moves on to the TOPSIS method. The values obtained from the simulation (Table 3) are first normalised to bring all values under a common scale in the matrix shown in Table 8. These normalised values are then weighted

Table 5

Pairwise comparison matrix

Criteria	Maximum stress (von Mises)	Total deformation	Volume	Complexity
Maximum stress (von Mises)	1	2	5	6
Total deformation	1/2	1	4	5
Volume	1/5	1/4	1	1
Shape complexity	1/6	1/5	1	1

Table 6

Principle eigenvalue, λ_{max} , consistency index, CI, and consistency ratio, CR

Principle eigenvalue, λ_{max}	4.054
Consistency index, CI	0.01797
Consistency ratio, CR	0.01997

Table 7

Weightage values for selected criteria obtained through the AHP method

Criteria	Maximum stress (von Mises)	Volume	Total deformation	Shape complexity
Weightage	0.508	0.087	0.326	0.079

Table 8

Normalised matrix

Design	Maximum Stress (Von Mises) (MPa)	Volume (mm ³)	Maximum Deformation (mm)	Shape complexity
A1	0.104	0.447	0.197	0.071
A2	0.598	0.390	0.473	0.081
B1	0.132	0.438	0.250	0.228
B2	0.333	0.387	0.443	0.951
C1	0.610	0.391	0.496	0.125
C2	0.362	0.391	0.483	0.124

using the weightage obtained from the AHP exercise for the respective criterion (Table 9). Now that the weightage has been included, the positive ideal solution (PIS) and negative ideal solution (NIS) are determined (Table 10). The purpose of obtaining PIS and NIS is to define the range or scale of measurement for the criteria. It allows for ranking each envisioned design according to the respective criterion. Once the rankings are calculated, the Euclidean distance determines the ranking for all six designs (Table 11).

The results obtained from this research showed that the best design is A1, which was inspired by the Amazon waterlily. For comparison, the simulated data was put side by side with that of the original design of the under-piston door, as depicted in Table 12.

Table 9

Weighted normalised matrix

Design	Maximum Stress (Von Mises) (MPa)	Volume (mm ³)	Maximum Deformation (mm)	Shape complexity
A1	0.053	0.039	0.064	0.006
A2	0.304	0.034	0.154	0.006
B1	0.067	0.038	0.082	0.018
B2	0.169	0.034	0.144	0.075
C1	0.310	0.034	0.162	0.010
C2	0.184	0.034	0.157	0.010

Table 10

Positive and negative ideal solution matrix

	Maximum Stress (Von Mises) (MPa)	Volume (mm ³)	Maximum Deformation (mm)	Shape complexity
PIS	0.053	0.034	0.064	0.006
NIS	0.310	0.039	0.162	0.075

Table 11

Overall ranking of designs

Design	Positive ideal solution	Negative ideal solution	Relative closeness to the ideal solution	Ranking
A1	0.005	0.284	0.982	1
A2	0.266	0.070	0.207	5
B1	0.026	0.262	0.910	2
B2	0.158	0.142	0.474	3
C1	0.275	0.066	0.192	6
C2	0.161	0.142	0.469	4

Table 12

Comparison of simulated data of new designs with original under-piston design

Design	Maximum stress (von Mises) (MPa)	Volume ($\times 10^6$ mm ³)	Maximum deformation (mm)	Shape complexity
A1	70.506	5.47	0.361	395
A2	405.130	4.77	0.864	449
B1	89.497	5.36	0.457	1262
B2	225.950	4.73	0.809	5262
C1	413.460	4.78	0.907	689
C2	245.270	4.78	0.883	688
Original	128.80	5.53	0.378	294

Compared to the original, A1 also showed reductions in maximum stress (von Mises), volume, and deformation by 45.25%, 0.97% and 4.61%, respectively. However, there was an increase in shape complexity by 34.35%. The values of maximum stress (von Mises) and deformation provide information on the design's ability to withstand mechanical load without damage to the structure. The reduction in these two parameters for A1 indicates that this design can be better than the original when exposed to normal working conditions. Furthermore, the volume reduction directly translates to a reduced weight of the under-piston door. At the start of this research, it was not expected that new designs could have obtained better readings than the original.

The results of designs A1 and A2 indicate that hollowed-out cylindrical sections in A1 greatly reduce the stress experienced by the under-piston door compared to the added external ribs in A2. The reduced thickness in A2 can also cause an increase in deformation compared to A1 and the original. It can be suggested that the reduction in thickness of the under-piston door, as seen in designs A2, C1 and C2, led to these three designs recording the highest maximum stress (von Mises) and deformation. Design B1 ranked second place, showed improvement in maximum stress (von Mises) compared to the original. However, it did not provide ample support and instead showed an increase in deformation compared to the original. In B2, where the two rows of square bars extended across the whole door within the flange, the maximum stress (von Mises) and deformation increased greatly by 150.47% and 77.00%, respectively, compared to B1. It indicates that the extensive reduction in B2 material contributed to the weakening of the structure, considering that B2 registered the lowest volume. Furthermore, B2 was also the most complex among the simulated designs. As for designs C1 and C2, which we ranked sixth and fourth, respectively, indicate that external ribs did not provide the necessary structural compensation for the reduction in thickness, as previously justified when discussing design A2.

CONCLUSION

Six designs were evaluated across four criteria. The determined weightage calculated using the AHP method for the four criteria from highest to lowest were maximum stress (von Mises) (0.508), maximum deformation (0.326), volume (0.087) and shape complexity (0.079). Through the TOPSIS method, the best design was determined to be design A1, with relative closeness to the ideal solution of 0.982, followed by B1 (0.910), B2 (0.474), C2 (0.469), A2 (0.207) and C1 (0.192). The results obtained from the simulation exercise showed positive proof of the potential of applying TRIZ with biomimetics to improve an existing design of an under-piston door for a two-stroke marine diesel engine. When combined symbiotically, these ideation tools promote creative thinking and can push the barriers to creativity in problem-solving. As it is common today to see many applications using a combination of MCDM methods, the demonstration where AHP and TOPSIS

complemented each other proved a successful collaboration. This design ideation and selection process brought together the four methods of TRIZ, biomimetics, AHP and TOPSIS to decide on an improved design of the under-piston door for a two-stroke marine engine. Future work on this subject will include the selection of the best NFC, which shall comprise natural fibre, polymer matrix and fire retardant.

ACKNOWLEDGEMENT

The authors would like to extend their gratitude to Universiti Teknikal Malaysia Melaka for the opportunity to conduct this research and write this paper.

REFERENCES

- Abdulvahitoglu, A., & Kilic, M. (2022). A new approach for selecting the most suitable oilseed for biodiesel production; The integrated AHP-TOPSIS method. *Ain Shams Engineering Journal*, 13(3), Article 101604. <https://doi.org/10.1016/j.asej.2021.10.002>
- Achrai, B., & Wagner, H. D. (2017). The turtle carapace as an optimized multi-scale biological composite armor – A review. *Journal of the Mechanical Behavior of Biomedical Materials*, 73, 50–67. <https://doi.org/10.1016/j.jmbbm.2017.02.027>
- Ahmad, S., Parvez, M., Khan, T. A., & Khan, O. (2022). A hybrid approach using AHP–TOPSIS methods for ranking of soft computing techniques based on their attributes for prediction of solar radiation. *Environmental Challenges*, 9, Article 100634. <https://doi.org/10.1016/j.envc.2022.100634>
- Al-Oqla, F. M., Sapuan, S. M., Ishak, M. R., & Nuraini, A. A. (2015). Predicting the potential of agro waste fibers for sustainable automotive industry using a decision making model. *Computers and Electronics in Agriculture*, 113, 116–127. <https://doi.org/10.1016/j.compag.2015.01.011>
- Al-Subhi, K. (2001). Application of the AHP in project management. *International Journal of Project Management*, 19(1), 19–27.
- Alkasem, B., & Tilfarlioğlu, F. Y. (2022). TRIZ as innovative method in english language teaching. *Journal of Education and Training Studies*, 11(1), 37-45. <https://doi.org/10.11114/jets.v11i1.5823>
- Ansell, M. P. (2014). Natural fibre composites in a marine environment. In A. Hodzic & R. Shanks (Eds.), *Natural Fibre Composites: Materials, Processes and Applications* (pp. 365–374). Woodhead Publishing Limited. <https://doi.org/10.1533/9780857099228.3.365>
- Arslan, A. E., Arslan, O., & Kandemir, S. Y. (2021). AHP–TOPSIS hybrid decision-making analysis: Simav integrated system case study. *Journal of Thermal Analysis and Calorimetry*, 145(3), 1191–1202. <https://doi.org/10.1007/s10973-020-10270-4>
- Asadabadi, M. R., Chang, E., & Saberi, M. (2019). Are MCDM methods useful? A critical review of analytic hierarchy process (AHP) and analytic network process (ANP). *Cogent Engineering*, 6(1), Article 1623153. <https://doi.org/10.1080/23311916.2019.1623153>
- Asknature. (2023). *Innovation inspired by nature*. Asknature. <https://asknature.org/>

- Bilousov, I., Bulgakov, M., & Savchuk, V. (2020). *Modern Marine Internal Combustion Engines*. Springer International Publishing. <https://doi.org/10.1007/978-3-030-49749-1>
- Boavida, R., Navas, H., Godina, R., Carvalho, H., & Hasegawa, H. (2020). A combined use of TRIZ methodology and eco-compass tool as a sustainable innovation model. *Applied Sciences*, *10*(10), Article 3535. <https://doi.org/10.3390/app10103535>
- Box, F., Erlich, A., Guan, J. H., & Thorogood, C. (2022). Gigantic floating leaves occupy a large surface area at an economical material cost. *Science Advances*, *8*(6), Article eabg3790. <https://doi.org/10.1126/sciadv.abg3790>
- Cheng, M., Xu, H., Sun, F., Jiao, L. and Yu, F. (2019, September 11-14). *Study on erosion resistance of control valve cage based on TRIZ and bionics*. [Paper presentation]. The 15th International Conference TRIZfest, Heilbronn, Germany.
- Claverie, M., McReynolds, C., Petitpas, A., Thomas, M., & Fernandes, S. C. M. (2020). Marine-derived polymeric materials and biomimetics: An overview. *Polymers*, *12*(5), Article 1002. <https://doi.org/10.3390/polym12051002>
- Djukic, Đ., Petrovic, I., Bozanic, D., & Delibasic, B. (2022). Selection of unployed aircraft for training of small-range aircraft defense system AHP - TOPSIS optimization methods. *Yugoslav Journal of Operations Research*, *32*(3), 389–406. <https://doi.org/10.2298/YJOR211125007D>
- Ekmekci, I., & Nebati, E. E. (2019). Triz methodology and applications. *Procedia Computer Science*, *158*, 303–315. <https://doi.org/10.1016/j.procs.2019.09.056>
- Fayemi, P. E., Maranzana, N., Aoussat, A., & Bersano, G. (2014). Bio-inspired design characterisation and its links with problem solving tools. In D. Marjonavic, S. Marion, P. Neven & B. Nenad (Eds.), *Proceedings of International Design Conference* (pp. 173–182). Design.
- Fragassa, C. (2017). Marine applications of natural fibre-reinforced composites: a manufacturing case study. In E. Pellicer, D. Nikolic, J. Sort, M. D. Baro, F. Zivic, N. Grujovic, R. Grujic & S. Pelemis (Eds.), *Advances in Applications of Industrial Biomaterials* (pp. 21-47). Springer. https://doi.org/10.1007/978-3-319-62767-0_2
- Girijappa, Y. G. T., Ragappa, S. M., Parameswaranpillai, J., & Siengchin, S. (2019). Natural fibers as sustainable and renewable resource for development of eco-friendly composites: A comprehensive review. *Frontiers in Materials*, *6*, 1–14. <https://doi.org/10.3389/fmats.2019.00226>
- Han, X., Wu, J., Zhang, X., Shi, J., Wei, J., Yang, Y., Wu, B., & Feng, Y. (2021). The progress on antifouling organic coating: From biocide to biomimetic surface. *Journal of Materials Science and Technology*, *61*, 46–62.
- Hwang, C. L., & Yoon, K. (1981). Basic concepts and foundations. In *Multiple Attribute Decision Making* (pp. 16-57). Springer. https://doi.org/10.1007/978-3-642-48318-9_2
- IACS. (2016). *Application of materials other than steel on engine, turbine and gearbox installations*. International Association of Classification Societies. <https://iacs.org.uk/publications/unified-interpretations/ui-sc/?page=14>
- IACS. (2006). *Requirements concerning machinery installations*. International Association of Classification Societies. http://www.iacs.org.uk/media/3773/ur_m_pdf2793.pdf

- James, A. T., Vaidya, D., Sodawala, M., & Verma, S. (2021). Selection of bus chassis for large fleet operators in India: An AHP-TOPSIS approach. *Expert Systems with Applications*, 186, Article 115760. <https://doi.org/10.1016/j.eswa.2021.115760>
- Jyoti, J., Kumar, A., Lakhani, P., Kumar, N., & Bhushan, B. (2019). Structural properties and their influence on the prey retention in the spider web. *Philosophical Transactions of the Royal Society A*, 377(2138), 20180271. <https://doi.org/10.1098/rsta.2018.0271>
- Kunzmann, C., Aliakbarpour, H., & Ramezani, M. (2023). Biomimetics design of sandwich-structured composites. *Journal of Composites Science*, 7(8), Article 315. <https://doi.org/10.3390/jcs7080315>
- Latarche, M. (2021). *Pounder's Marine Diesel Engines and Gas Turbines* (10th ed.). Butterworth-Heinemann.
- Livanos, A. G., Theotokatos, G., & Kyrtatos, N. P. (2003). Simulation of large marine two-stroke diesel engine operation during fire in the scavenging air receiver. *Journal of Marine Engineering and Technology*, 2(2), 9–16. <https://doi.org/10.1080/20464177.2003.11020170>
- MAN Diesel & Turbo. (2010). *MAN B&W 98-50 ME/ME-C-TII Type Engines, Engine Selection Guide* (1st ed.). MAN Energy Solutions.
- Moudood, A., Rahman, A., Khanlou, H. M., Hall, W., Öchsner, A., & Francucci, G. (2019). Environmental effects on the durability and the mechanical performance of flax fiber/bio-epoxy composites. *Composites Part B: Engineering*, 171, 284-293. <https://doi.org/10.1016/j.compositesb.2019.05.032>
- Mouritz, A. P., Gellert, E., Burchill, P., & Challis, K. (2001). Review of advanced composite structures for naval ships and submarines. *Composite Structures*, 53(1), 21–42. [https://doi.org/10.1016/S0263-8223\(00\)00175-6](https://doi.org/10.1016/S0263-8223(00)00175-6)
- Opricovic, S., & Tzeng, G. H. (2004). Compromise solution by MCDM methods: A comparative analysis of VIKOR and TOPSIS. *European Journal of Operational Research*, 156(2), 445–455. [https://doi.org/10.1016/S0377-2217\(03\)00020-1](https://doi.org/10.1016/S0377-2217(03)00020-1)
- Pingulkar, H., Mache, A., Munde, Y., & Siva, I. (2021). A comprehensive review on drop weight impact characteristics of bast natural fiber reinforced polymer composites. *Materials Today: Proceedings*, 44, 3872–3880. <https://doi.org/10.1016/j.matpr.2020.12.925>
- Primrose, S. B. (2020). *Biomimetics: Nature-Inspired Design and Innovation*. John Wiley & Sons.
- Roszkowska, E. (2011). Multi-criteria decision making models by applying the TOPSIS method to crisp and interval data. *International Scientific Journal*, 6(1), 200–230.
- Russo, D., & Spreafico, C. (2020). TRIZ-Based guidelines for eco-improvement. *Sustainability*, 12(8), Article 3412. <https://doi.org/10.3390/su12083412>
- Saaty, R. W. (1987). The analytic hierarchy process - What it is and how it is used. *Mathematical Modelling*, 9(3–5), 161–176. [https://doi.org/10.1016/0270-0255\(87\)90473-8](https://doi.org/10.1016/0270-0255(87)90473-8)
- Sahoo, S. K., & Goswami, S. S. (2023). A comprehensive review of multiple criteria decision-making (MCDM) methods: Advancements, applications, and future directions. *Decision Making Advances*, 1(1), 25–48. <https://doi.org/10.31181/dma1120237>
- San, Y. T., Jin, Y. T., & Li, S. C. (2009). *TRIZ: Systematic Innovation in Manufacturing*. Firstfruits Publishing.

- Sapuan, S. M., & Mansor, M. R. (2021). *Design for Sustainability: Green Materials and Processes*. Elsevier.
- Sheu, D. D., Chiu, M. C., & Cayard, D. (2020). The 7 pillars of TRIZ philosophies. *Computers and Industrial Engineering*, 146(101), Article 106572. <https://doi.org/10.1016/j.cie.2020.106572>
- Spreafico, C. (2021). Quantifying the advantages of TRIZ in sustainability through life cycle assessment. *Journal of Cleaner Production*, 303, Article 126955. <https://doi.org/10.1016/j.jclepro.2021.126955>
- Spreafico, C. (2022). Can TRIZ (Theory of Inventive Problem Solving) strategies improve material substitution in eco-design? *Sustainable Production and Consumption*, 30, 889–915. <https://doi.org/10.1016/j.spc.2022.01.010>
- Taherdoost, H., & Madanchian, M. (2023). Multi-criteria decision making (MCDM) methods and concepts. *Encyclopedia*, 3(1), 77–87. <https://doi.org/10.3390/encyclopedia3010006>
- United Nations. (2023). *The 17 Goals*. United Nations. <https://sdgs.un.org/goals>
- Wang, X., & Duan, Q. (2019). Improved AHP–TOPSIS model for the comprehensive risk evaluation of oil and gas pipelines. *Petroleum Science*, 16(6), 1479–1492. <https://doi.org/10.1007/s12182-019-00365-5>
- Wanieck, K., Ritzinger, D., Zollfrank, C., & Jacobs, S. (2020). Biomimetics: Teaching the tools of the trade. *FEBS Open Bio*, 10(11), 2250–2267. <https://doi.org/10.1002/2211-5463.12963>
- Winterthur Gas & Diesel. (2023). *Marine installation manual (X62-S2.0)*. WIN GD. chrome-extension://efaidnbmninnibpcjpcglclefindmkaj/[https://www.wingd.com/en/documents/x62-s2-0/engine-installation/mim/marine-installation-manual-\(mim\)/](https://www.wingd.com/en/documents/x62-s2-0/engine-installation/mim/marine-installation-manual-(mim)/)
- Yuan, G., Xie, F., Dinçer, H., & Yüksel, S. (2021). The theory of inventive problem solving (TRIZ)-based strategic mapping of green nuclear energy investments with spherical fuzzy group decision-making approach. *International Journal of Energy Research*, 45(8), 12284–12300. <https://doi.org/10.1002/er.6435>
- Zhang, Y., Xu, H., Wang, H., Chen, S., Zhao, Z., & Pooneeth, V. (2019). Innovative design of the anti-erosion structure in a water hydraulic valve based on TRIZ combining with bionics and fractal theory. In V. Souchkov & O. Mayer (Eds.), *The 15th International Conference TRIZfest-2019*. (pp. 206–217). International TRIZ Association.

Effect of Cutting Speed and Feed per Tooth on the Trimmed Surface Roughness and Tool Wear During Milling of CFRP: Aerostructural Part

Syahrul Azwan Sundi^{1*}, Izzat Afandi Abdul Hakim¹, Mohd Farid Mahadi¹, Noramin Nazar Shah¹, Raja Izamshah¹, Intan Sharhida Othman¹, Mohd Shahir Kasim² and Mohd Nor Hafizi Noordin³

¹Faculty of Industrial and Manufacturing Engineering Technology, Universiti Teknikal Malaysia Melaka (UTeM), Hang Tuah Jaya, 76100 Durian Tunggal, Melaka, Malaysia

²Faculty of Design of Innovative and Technology, Universiti Sultan Zainal Abidin (UNISZA), Kampung Gong Badak, 21300, Terengganu, Malaysia

³Defense Research Institute (DRI), Universiti Pertahanan Nasional Malaysia, Kem Sungai Besi 57000 Kuala Lumpur, Malaysia

ABSTRACT

The machining quality plays a pivotal role in determining the service life of components. In this context, the primary focus of the experimental investigation is centered on the impact of cutting conditions during edge trimming of carbon fiber reinforced plastics (CFRP) material. The ultimate objective of this experiment is to pinpoint the most effective machining parameters, specifically the cutting speed, V_c and the feed per tooth, f_z , to minimize damages during the edge trimming process using actual aerostructural sample components composed of CFRP material. Furthermore, the study took into account the issue of tool wear

on cutting tools. The Design of Experiment (DoE) technique, specifically the Taguchi L_9 orthogonal arrays method, was used to conduct this research. It was shown that the feed per tooth, f_z , and the cutting speed, V_c , had the biggest effects on the trimmed surface quality as the longitudinal surface roughness increased. It was demonstrated that the fracture of the pyramidal tooltips in router-type tools happened more frequently at higher cutting speeds, V_c . The optimal machining parameters for minimizing damages during CFRP edge trimming were

ARTICLE INFO

Article history:

Received: 16 August 2023

Accepted: 09 May 2024

Published: 14 June 2024

DOI: <https://doi.org/10.47836/pjst.32.S2.09>

E-mail addresses:

syahrul.azwan@utem.edu.my (Syahrul Azwan Sundi)
m052220004@student.utem.edu.my (Izzat Afandi Abdul Hakim)
m052220002@student.utem.edu.my (Mohd Farid Mahadi)
m052220034@student.utem.edu.my (Noramin Nazar Shah)
izamshah@utem.edu.my (Raja Izamshah)
intan_sharhida@utem.edu.my (Intan Sharhida Othman)
shahirkasim@unisza.edu.my (Mohd Shahir Kasim)
mohdhafizi@upnm.edu.my (Mohd Nor Hafizi Noordin)

* Corresponding author

the combination of the feed per tooth, f_z at 0.05 mm and cutting speed, V_c at 50 m/min. The most significant element influencing the tool's wear was the cutting speed, V_c .

Keywords: Carbon fiber reinforced plastics (CFRP), machining conditions, milling, surface quality, tool wear

INTRODUCTION

Due to a few benefits, like being lightweight and having high modulus, specific strength, and corrosion resistance, carbon fiber reinforced plastics (CFRP) are becoming a more significant and vital material in the aerospace sector. The usage of CFRP materials has been on an upward trend over the past year. For instance, the weight of the composite structure in the Boeing 777, which entered service in 1995, was only 10 %, whereas the aircraft A350 XWB began using over 50 % of the composite structure in 2010 (Hashish, 2013). This outcome unmistakably demonstrates the interest and demand for the use of CFRP by the aerospace sector.

Comprehending the complicated phenomenon of composite behavior, including its inhomogeneity and interaction with the cutting tool during machining, is crucial. The quality of the machined composite part, such as delamination, cracking, fiber pull-out, and burned matrices, may be caused by the machining process. The abrasive character of the reinforcement fibers and the necessity of neatly shearing them impose additional demands and limitations on the choice of optimal tool materials and shape (Sheikh Ahmed, 2009). Surface roughness is one of the measurable factors that significantly affect dimensional accuracy, the functioning of the machined composite's mechanical properties, and the overall cost of manufacture. Understanding the kinetics of machining operations and the mechanics of material removal is essential to achieving the appropriate surface roughness of the machined surface.

Literature Review

Numerous difficulties arise while attempting to determine the proper machining parameters for cutting the edges of CFRP material. When milling CFRP, problems with integrity and surface finish are common (Sheikh-Ahmed & Shahid, 2013). Surface finish and damage are the two characteristics that define the surface quality produced by finish machining CFRP. When two panels are assembled in the aerospace industry, a higher degree of surface roughness will impact the CFRP's quality since it cannot bond the two together. On the other side, while milling CFRP material, the rapid tool wear brought on by the abrasive nature of composite materials provides another challenge—the imperfect machining at a faster transverse causes rapid tool wear. The rise in feed rate during machining is widely thought to be the primary driver of this issue. The overall tool wear rate is also influenced by the depth of the cut (Halim et al., 2017).

Bi et al. (2022) investigated the wear characteristics of uncoated multiple flutes for milling operations. Their research encompassed a range of feeds per tooth, spanning from 0.01 to 0.15 mm/tooth while keeping spindle speed constant at 3000 rpm. Through a combination of theoretical analysis and practical experimentation, the authors proved the influence of tool wear on machining performance. They uncovered that the top ply exhibited less burr damage, primarily due to the dominance of SLHCE in the top ply cutting process, which resulted in less pronounced tool wear, thanks to clearance. In contrast, the bottom ply experienced greater cutting dominance by SRHCE, leading to increased damage.

Duboust et al. (2016, 2017) substantiated that surface quality was most significantly affected by the feed rate and the type of tool used. Fiber orientation emerged as a crucial factor in the chip removal mechanism and surface damage. Can (2017) indicated that inclined machining positions consistently yielded superior along and cross-directional surface trimmed quality compared to vertical machining across all cutting conditions. Furthermore, in a study by Khairusshima et al. (2017), an optimization study on CFRP material milling employing the Response Surface Method (RSM) revealed that the most substantial impact on trimmed surface roughness and delamination of the CFRP material was the feed rate when deployed helical helix end mill tool. The quality of the trimmed surface finish along the machining direction is correlated with a higher feed rate and lower spindle speed, which is caused by the increase in the effectiveness of chip thickness (Sheikh-Ahmed & Shahid, 2013).

Wang et al. (2016) established that cutting speed played a pivotal role in influencing the cutting temperature during CFRP composite material milling. Following cutting speed, feed rate and radial depth of cut were identified as secondary factors. In two separate studies, Sundi et al. (2019) highlighted that the geometric features of tools, particularly the number of teeth or flutes in router-type tools, had a notable impact on the resulting surface quality when performing edge trimming on specific CFRP materials.

More recently, Cunningham et al. (2018) conducted a comparative analysis of Multi-tooth (MT) or burr tools and Up-Down or Compression Routers (UD) under cryogenic conditions. They found that cryogenic machining improved both tool geometries' average surface roughness and delamination length. In a separate study by Kuo et al. (2021), various cutting scenarios were modeled during the trimming of composite materials, mainly the CFRP. This simulation investigated the impact of cutting circumstances on delayed tool wear, vibrations, and the consequent surface integrity while accounting for the deflections caused in the cutting tools by bending moments. The study's conclusions provided an overview of the underlying cutting mechanisms in charge of cutting forces and tool flank wear, as well as information on how they affect the texture, roughness, and topography of machined surfaces.

In contrast to previous research efforts, the current study analyzes a specific type of CFRP material that exhibits distinct characteristics. Notably, this material adheres to

aerospace standards. Moreover, the study introduces a unique range of cutting parameters distinct from existing literature. The primary objective is to investigate the impact of the cutting speed, V_c and the feed per tooth, f_z , on the quality of trimmed surfaces when using a burr tool for edge trimming this particular CFRP material. The trimmed surfaces underwent thorough examination using a surf-tester apparatus to quantify the average surface roughness, denoted as Ra. Additionally, microscopy tools were employed to analyze the machined surfaces in detail to better understand the underlying processes. The study also monitored tool wear rates using appropriate equipment to establish a correlation between surface damage and tool wear.

MATERIALS AND METHODS

Methodology Overview

The cutting speed, V_c , and the feed per tooth, f_z , were the primary cutting conditions chosen for the current work-study. On a real sample of an aerostructural composite panel with the specifications stated in the next paragraph, experimental work was done using a router tool type. At the conclusion of the research milestone, longitudinal surface roughness and tool wear observation were the principal analyses performed. The overall structure of the current research work is summarized in Figure 1.

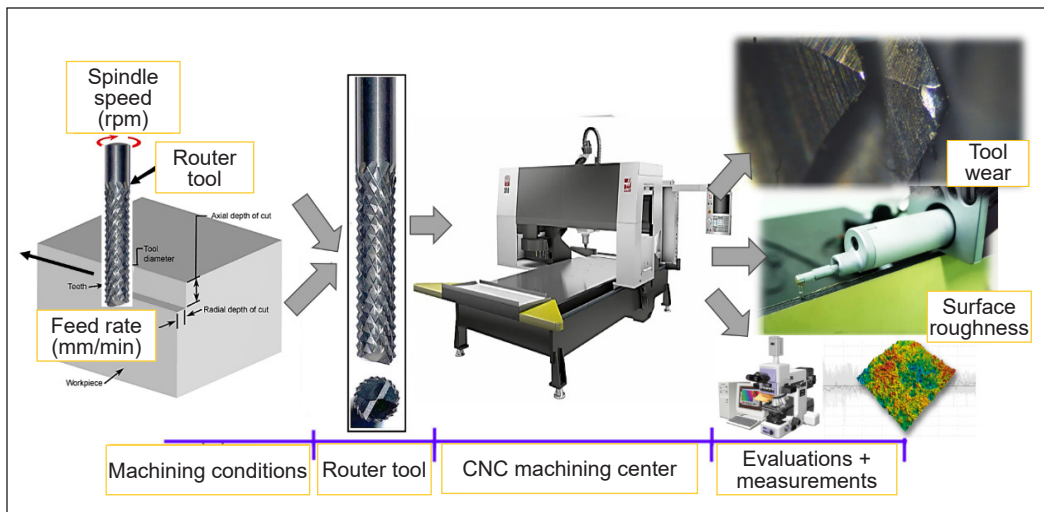


Figure 1. Illustration of the research methodology overview

Materials

The thickness of the CFRP specimen used in this work was 3.25 mm, made of unidirectional (UD) fabric. It contained 26 plies, including two thin layers of woven glass/epoxy textiles. The Hexcel Composite Company's carbon/epoxy prepreg created the 26 unidirectional

plies. The composite was stacked in the following order: [45/135/90₂/0/90/0/90/0/135/45₂/135]s. The areal density of the carbon plywood was 203 g/m², compared to 107 g/m² for the glass. While the glass ply was woven, the carbon ply had a single-directional (UD) fiber arrangement. The CFRP was compacted using a vacuum pump under controlled atmospheric conditions during curing. The laminate was prepared in a mold and then placed inside an autoclave. The curing cycle involved heating the temperature to 180°C at 3°C/min and maintaining it for 120 minutes. Subsequently, the temperature gradually lowered to room temperature at the same rate. The cycle occurred under a pressure of 700 kPa within the autoclave while being vacuum-bagged and evacuated to 70 kPa. The glass had a cured ply thickness (CPT) of 0.08, while the carbon had a CPT of 0.125. Employing this curing recipe yields a nominal fiber volume fraction of 60%.

Cutting Tool

Table 1 describes the cutting tool utilized in this project, which has a 6.35 mm diameter. It is an uncoated tungsten carbide router or burr tool. The specific tool geometries used during the current work's experimental phases are detailed in Figure 2. There were nine tools in total were used, one for each run.

Table 1
Cutting tool geometries/details

	Diameter (mm)	Number of teeth	Number of helix		Angle of the helix (°)		Length (mm)
			Right	Left	Right	Left	
Burr/Router	6.35	10	10	10	30	30	75

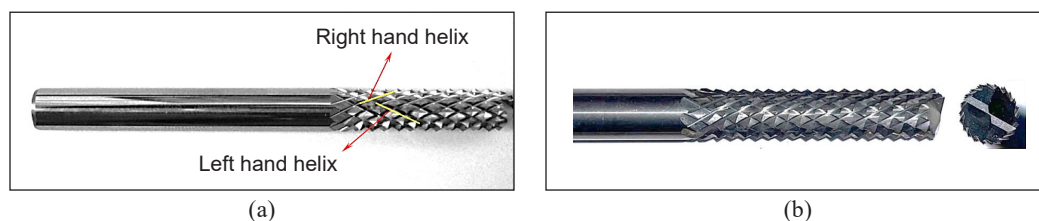


Figure 2. Geometry information for the burr or router tool; (a) geometric specifics; and (b) physical representation of the tool

Design of Experiment

One of the statistical methods, the Taguchi method (Orthogonal Array L₉), was used to arrange the entire experiment. This investigation focused on two machining parameters: the cutting speed, V_c and the feed per tooth, f_z . The cutting speed, V_c settings were 50 m/min (low), 100 m/min (medium), and 150 m/min (high), with feed per tooth, f_z set to 0.05 mm (low), 0.1 mm (medium), and 0.15 mm (high). In the following formulas, the correlations

between cutting speed (V_c), spindle speed (N), feed per tooth (f_z), and feed rate (V_f) are illustrated. On the other hand, Table 2 provides the edge-trimming parameters that were used in this research.

$$V_c = \frac{\pi \times D \times N}{1000} \tag{1}$$

$$f_z = \frac{V_f}{N} \quad f_z = \frac{V_f}{N} \tag{2}$$

where V_c = cutting speed, D = diameter of cutting tool, N = spindle speed, f_z = feed per tooth, V_f = feed rate.

Table 2
Machining settings

Run (R)	Cutting Speed, V_c (m/min)	RPM	Feed per Tooth, F_z (mm)	V_f (mm/min)
1	50	2526	0.05	125
2	100	5053	0.15	752
3	50	2526	0.1	251
4	100	5053	0.05	251
5	100	5053	0.1	501
6	150	7579	0.1	752
7	150	7579	0.05	376
8	50	2526	0.15	376
9	150	7579	0.15	1128

Taguchi Method

The Taguchi method represents a structured approach essential in experimental design and data analysis, particularly concerning Taguchi L_9 orthogonal arrays. It is carefully crafted to conduct controlled experiments to gain valuable insights into process behavior. Through the utilization of this method, researchers concentrate on fine-tuning process parameters to achieve optimal output characteristics across diverse materials. At the heart of this approach lies the optimization of crucial output attributes such as material surface quality, tool wear, and surface roughness (R_a). These attributes play a pivotal role in determining the quality and performance of machined components.

Signal-to-Noise (SN) ratios—a crucial component in assessing performance and variability—are integrated into the Taguchi approach. SN ratios are useful for evaluating the desired output’s quality in terms of noise components and provide a thorough understanding of process behavior. When applied with L_9 orthogonal arrays, this methodical technique promotes a comprehensive understanding of the process under study. It gives researchers the ability to maximize parameters and provide better-than-average results. In the end, this

approach greatly advances the field overall, improves efficiency, and refines operations (Pang et al., 2014; Ramnath et al., 2017).

Surface Roughness Measurement and Tool Wear Observation

The workpiece's surface finish was measured using a Mitutoyo Surftest SJ-410 surface roughness tester. In this study, the assessment of surface roughness was referred to as Ra (Arithmetical mean deviation). Longitudinal surface roughness was assessed with each measurement's stylus traveling a distance set to 4 mm. Each machined surface was assessed at five measurement sites, and the ultimate average Ra value was computed to quantify the level of surface smoothness for each specimen. Figure 3 displays the measurement apparatus for determining the quality of the surface roughness.

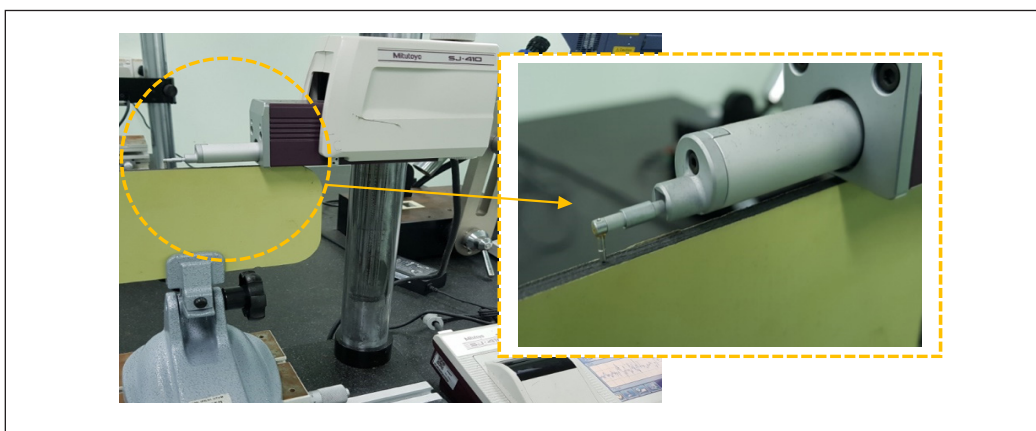


Figure 3. Mitutoyo SJ-410 surf tester equipment for surface quality evaluation

An optical microscope, Nikon MM-800, was also used to check each cutting tool's tool wear and learn how each machined surface was finished. With a magnification range of $1\times$ to $100\times$, this microscope made it easier to spot tool wear or damage and provided a sharper picture of what was happening on the trimmed surfaces. E-max software attached to a personal computer eased the image capturing and data processing when the specimen was under the microscope. Both surface damage observations and tool wear assessments were made with the Nikon MM-800 microscope, as shown in Figures 4 and 5. The burr tooltip, which is the primary area of engagement during the machining process, was the focus of the evaluation of the tool wear following the CFRP trimming.

RESULTS AND DISCUSSION

When specifying the surface quality of machined CFRP material in production, surface roughness plays a significant impact. The surface layer can be quickly altered during manufacturing, which alters the composite's mechanical characteristics.

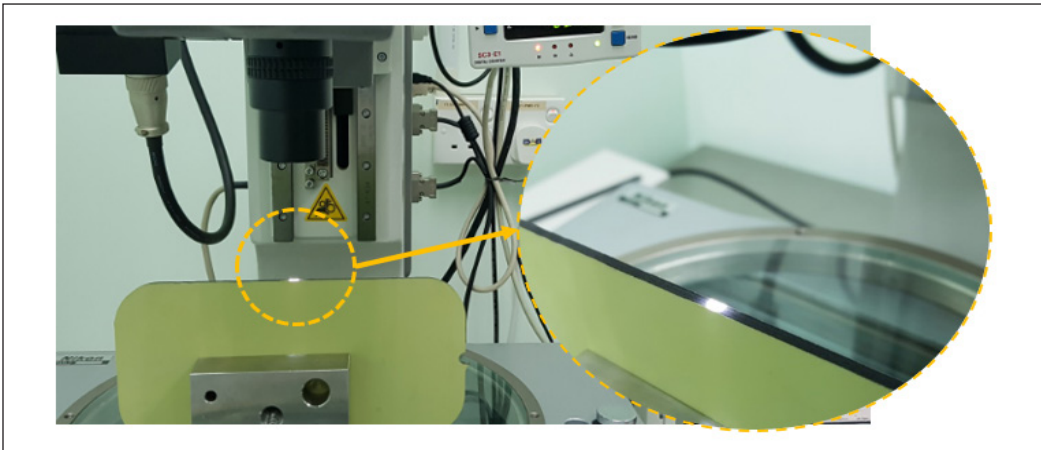


Figure 4. Examination of surface damage on trimmed surfaces using the Nikon MM-800

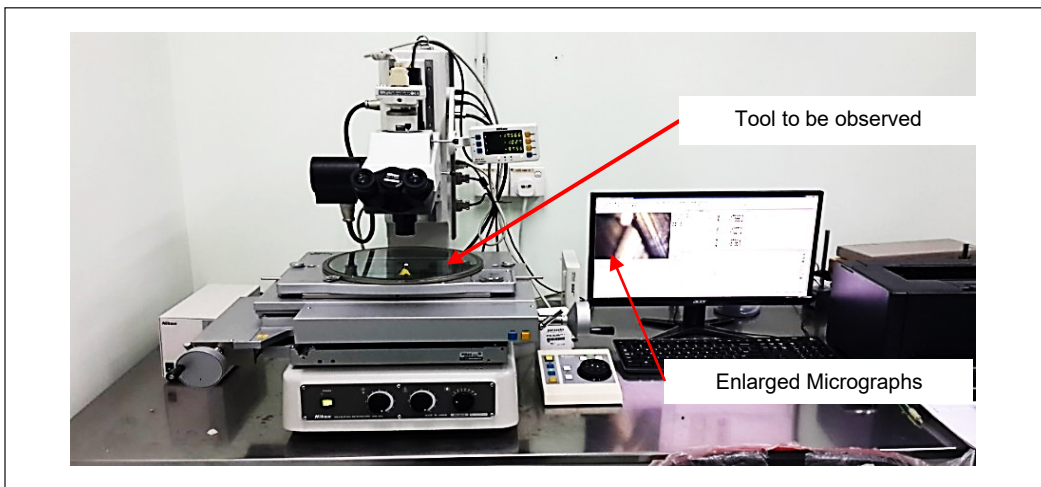


Figure 5. Observation of tool wear using the Nikon MM-800 optical microscope

In general, Figure 6 demonstrates that an increase in the feed per tooth, f_z , will cause an increase in the Ra value of surface roughness for all three cutting speeds, V_c applied. Surface roughness rises proportionately as the feed per tooth, f_z , rises. The lowest average Ra value of surface roughness was seen in run 8, which has a cutting speed, V_c at 50 m/min and the feed per tooth, f_z , at 0.15 mm. The surface roughness measurement, Ra, generated the maximum value for the highest cutting speed, V_c at 150 m/min and the highest feed per tooth, f_z , at 0.15 mm, represented by run 9.

A rougher finish on the trimmed surface resulted from increased cutting speed, V_c and the feed per tooth, f_z . This finding is consistent with a prior study by Karataş and Gökkaya (2018), who found that greater feed rates, V_f , were associated with increased trimmed or milled surface quality. In contrast, higher cutting speeds, V_c , were associated with a

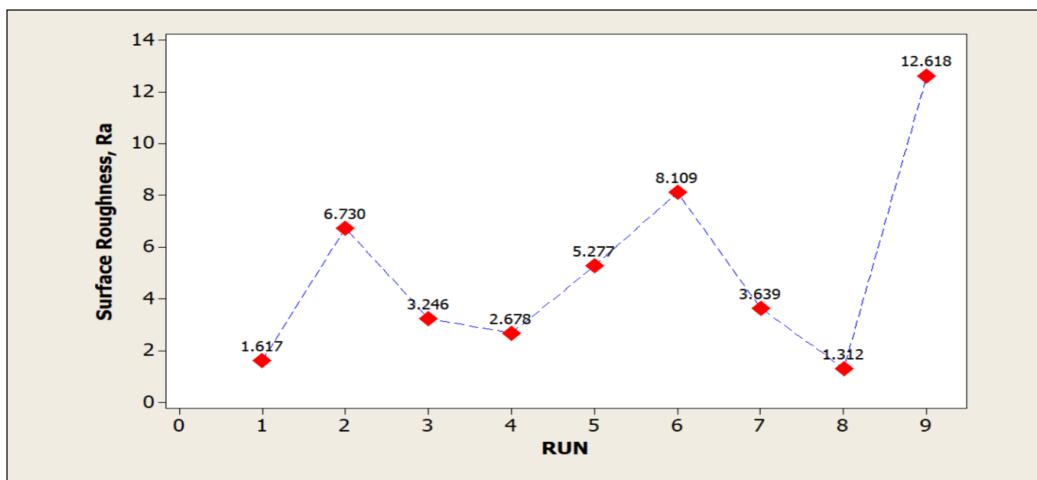


Figure 6. Average surface roughness, Ra value vs. number of Runs (refer to Table 2)

similar decrease. In contrast, Bi et al. (2022) findings showed that lower feed rates, V_f (0.01 mm/tooth) or lower feed per tooth, f_z (0.01 mm/tooth), led to more severe tool wear and lower-quality machining.

Taguchi—Signal to Noise (SN) Ratio Analysis

The means of the SN ratio for the smaller, better qualities of surface roughness, as determined by Minitab software, are shown in Figure 7. The graphs' slope unequivocally demonstrates that feed per tooth, f_z , is the second most important element influencing the trimmed surface quality after cutting speed, V_c . Of all the cutting settings examined, the best combination for achieving the best surface roughness was 50 m/min of cutting speed, V_c and 0.05 mm of feed per tooth, f_z . Both settings were the first or the smallest settings overall.

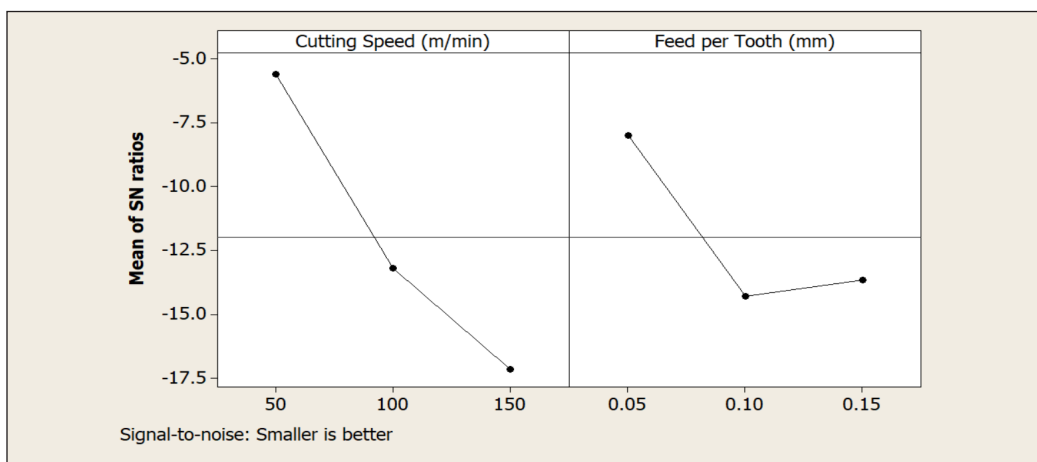


Figure 7. Main effects plot for signal-to-noise (SN) ratio (data means)

Microscopy Evaluation

From looking at the microscopic photos of the machined surface in run 3 operated at a cutting speed, V_c of 50 m/min and a feed per tooth, f_z of 0.10 mm, some areas had experienced fiber pull-out (Figure 8a). A clear illustration of a well-machined surface with no obvious flaws is shown in Figure 8(d). However, Figure 8(b) reveals some areas exhibiting matrix smearing and visible signs of matrix burnout. Notably, the extent of damage increased with higher spindle speeds and feed rates.

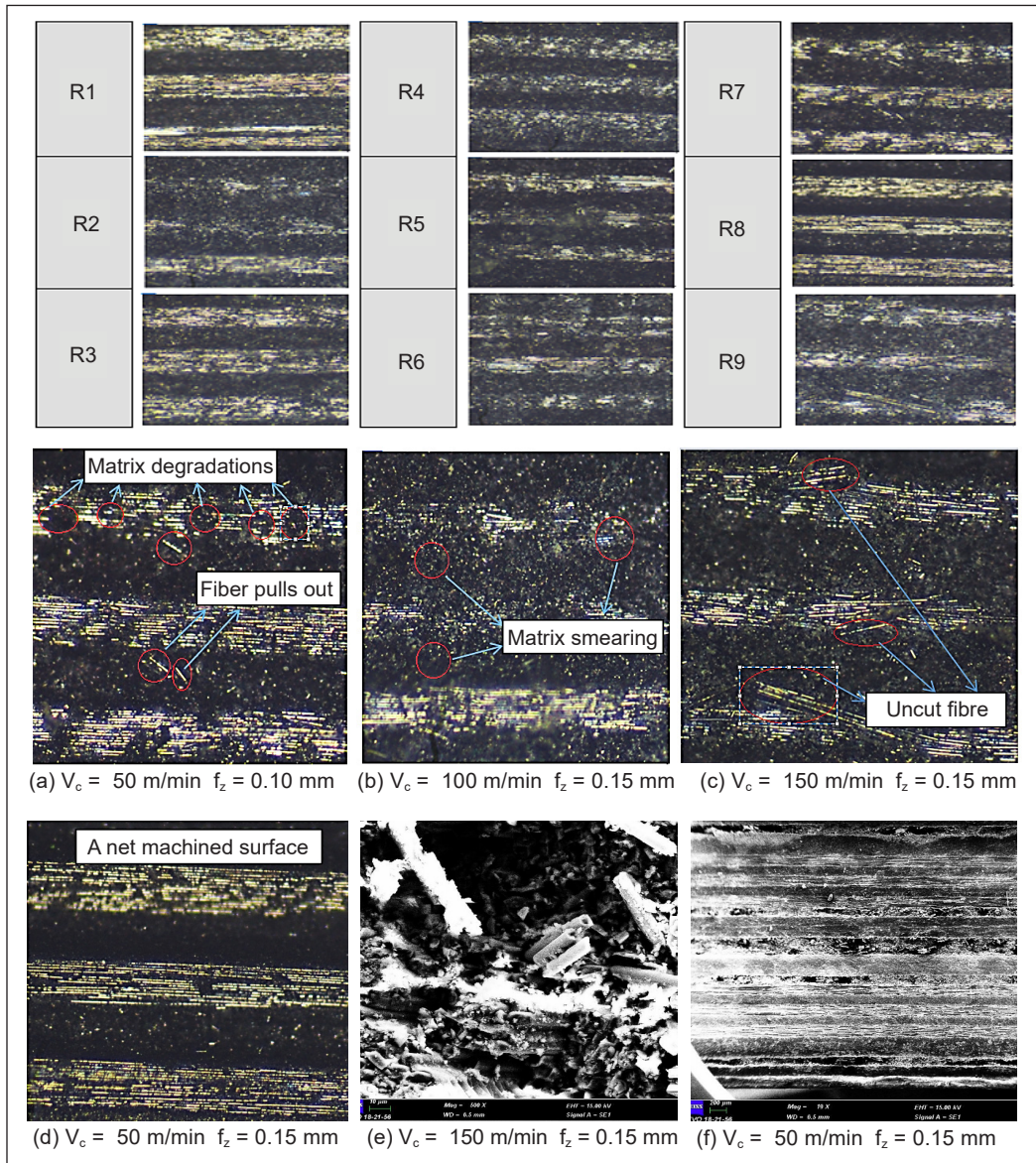


Figure 8. Overall microscopic images and SEM images of the trimmed surface

Conversely, the combination of trimming parameters featuring a cutting speed, V_c of 150 m/min and a feed per tooth, f_z of 0.15 mm in run 9 resulted in the most severe surface damage, as evident from the microscopic and SEM images in Figure 8(e). These images depict most fibers remaining uncut and illustrate the poorest surface integrity among all the tested conditions.

Tool Wear Observation

The examination of the burrs tool after the CFRP trimming process revealed fractures in the tooltip, and the corresponding data is presented in Table 3. It is evident that the cutting tool was subjected to a lower cutting speed, and V_c exhibited minimal damage compared to the others. Runs 2, 4, and 5, where moderate cutting speed, V_c , at 100 mm/min, was utilized, showed moderate damage to the tools. However, the most significant tool fractures were observed in runs 6, 7, and 9, where the damage to the tooltip was notably pronounced. This underscored the relationship between higher cutting speed, V_c and increased tool tip fractures. Additionally, it became apparent that the tool's wear condition influenced surface roughness values, with higher tool wear correlating with elevated surface roughness readings. Figure 9 depicts the photomicrograph of run 9, which appeared to align with the observed surface finish.

Furthermore, the variation in applied feed rates also generally impacted tool wear. These findings aligned with those of Cunningham et al. (2018), who reported that surface

Table 3
Images of tooth fracture

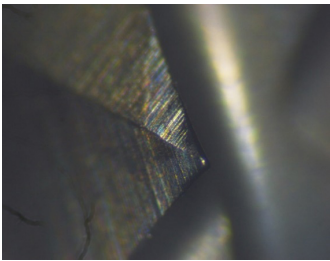
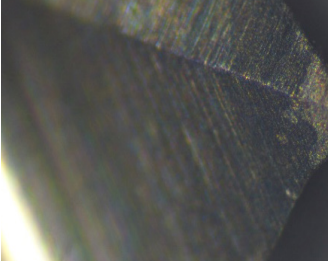
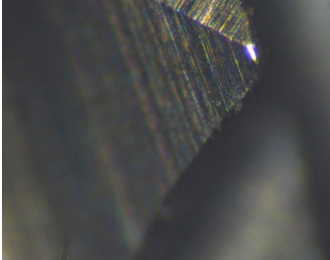
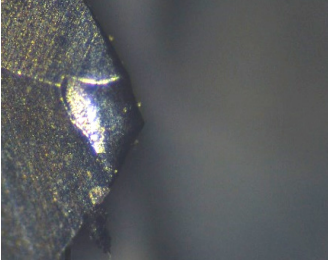
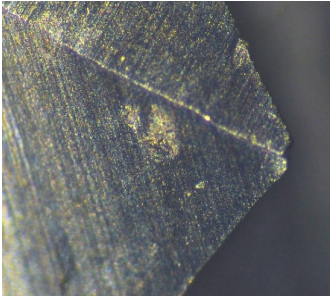
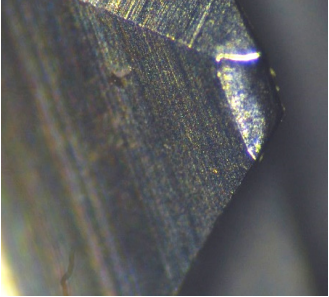
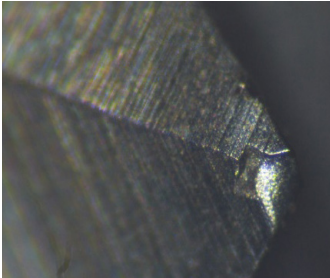
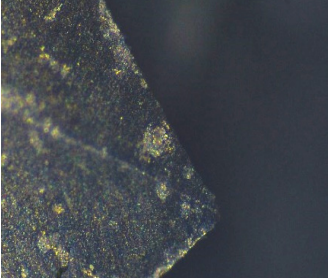
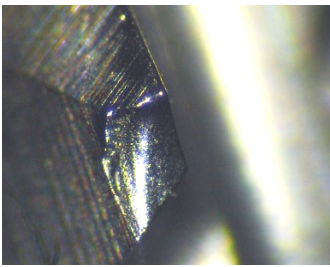
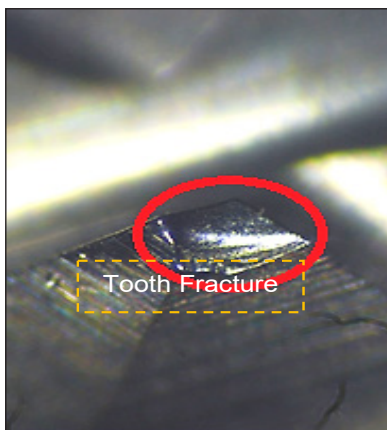
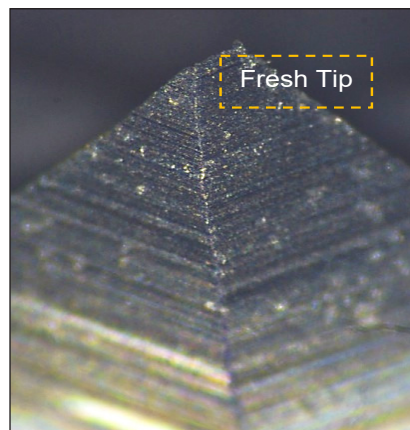
RUN No.	Tooth Fracture	RUN No.	Tooth Fracture
(1)		(2)	
(3)		(4)	

Table 3 (continue)

RUN No.	Tooth Fracture	RUN No.	Tooth Fracture
(5)		(6)	
(7)		(8)	
(9)			



(a)



(b)

Figure 9. (a) Fractured tooth; and (b) tooltip of pyramid tooth still obviously seen

roughness worsened with increasing tool wear, primarily affecting the CFRP panel. In a separate study by Devan et al. (2022) and Urresti et al. (2022), it was noted that tool wear was primarily influenced by abrasive wear and the rounding of the cutting edge, attributed to the hard abrasion of carbide grains. The study also concluded that tool life is inversely proportional to cutting speed, V_c feed speed, V_f and depth of cut.

CONCLUSION

This study clarifies the effect of the cutting speed, V_c and the feed per tooth, f_z , on the edge-trimming of CFRP material during the machining process.

1. The cutting speed, V_c , as the longitudinal surface roughness rose with greater feed per tooth, f_z , was shown to have the greatest influence on the trimmed surface quality.
2. It was shown that at greater cutting speed, V_c , the fracturing of the pyramidal tooltips in router-type tools occurred more frequently.
3. Based on the SN ratio study, it was determined that the combination of the cutting speed, V_c and the feed per tooth, f_z at level 1 (50 m/min and 0.05 mm) resulted in the best machining parameters for reducing damages during CFRP edge trimming.
4. The cutting speed, V_c , has been shown to have the greatest influence on the effect of the tool damage during CFRP edge trimming.

ACKNOWLEDGEMENTS

The authors appreciate the financial support from the Ministry of Education (MOE), Malaysia, and Universiti Teknikal Malaysia Melaka (UTeM). Short-term Grant, PJP/2022/FTKMP/S01896 and Industrial Matching Grant, INDUSTRI(URMG)/EISSB/FTKMP/2023/I00078 were utilized to fund the project.

REFERENCES

- Bi, G., Wang, F., Fu, R., & Chen, P. (2022). Wear characteristics of multi-tooth milling cutter in milling CFRP and its impact on machining performance. *Journal of Manufacturing Processes*, 81, 580-593. <https://doi.org/10.1016/j.jmapro.2022.07.008>
- Can, A. (2017). Effect of edge trimming parameters on surface quality of C carbon fiber reinforced polymer composites. *Journal of Science Engineering*, 17(1), 302–311. <https://doi.org/10.5578/fmbd.54017>.
- Karataş, M. A., & Gökkaya, H. (2018). A review on machinability of carbon fiber reinforced polymer (CFRP) and glass fiber reinforced polymer (GFRP) composite materials. *Defence Technology*, 14(4), 318–326. <https://doi.org/10.1016/j.dt.2018.02.001>
- Kuo, C., Liu, J., Chang, T., & Ko, S. (2021). The effects of cutting conditions and tool geometry on mechanics, tool wear and machined surface integrity when routing CFRP composites. *Journal of Manufacturing Processes*, 64, 113-129. <https://doi.org/10.1016/j.jmapro.2021.01.011>

- Cunningham, C. R., Shokrani, A. and Dhokia, V. (2018). Edge trimming of carbon fiber reinforced plastic. *Procedia CIRP*, 77, 199-202. <https://doi.org/10.1016/j.procir.2018.08.285>
- Devan, D. J., Almaskari, F., Sheikh-Ahmad, J., & Hafeez, F. (2022). A study on tool wear of tungsten carbide cutters in edge trimming of CFRP. *Journal of Mechanical Science and Technology*, 36(5), 2499-2510. <https://doi.org/10.1007/s12206-022-0432-z>
- Duboust, N., Melis, D., Pinna, C., Ghadbeigi, H., Collis, A., Ayvar-Soberanis, S., & Kerrigan, K. (2016). Machining of carbon fiber : Optical surface damage characterisation and tool wear study. *Procedia CIRP*, 45, 71–74. <https://doi.org/10.1016/j.procir.2016.02.170>
- Duboust, N., Ghadbeigi, H., Pinna, C., Ayvar-Soberanis, S., Collis, A., Scaife, R., & Kerrigan, K. (2017). An optical method for measuring surface roughness of machined carbon fiber-reinforced plastic composites. *Journal of Composite Materials*, 51(3), 289–302. <https://doi.org/10.1177/0021998316644849>.
- Halim, N. F. H. A., Ascroft, H. & Barnes, S. (2017). Analysis of tool wear, cutting force, surface roughness and machining temperature during finishing operation of ultrasonic assisted milling (UAM) of carbon fiber reinforced plastic (CFRP). *Procedia Engineering*, 184, 185–191. <https://doi.org/10.1016/j.proeng.2017.04.084>.
- Hashish, M. (2013, September 9-11). *Trimming of CFRP aircraft components*. [Paper presentation]. WJTA-IMCA Conference and Expo, Texas, USA.
- Khairusshima, M. K. N., Aqella, A. K. N., & Sharifah, I. S. S. (2017). Optimization of milling carbon fiber reinforced plastic using RSM. *Procedia Engineering*, 184, 518–528. <https://doi.org/10.1016/j.proeng.2017.04.122>.
- Pang, J. S., Ansari, M. N. M., Zaroog, O. S., Ali, M. H., & Sapuan, S. M. (2014). Taguchi design optimization of machining parameters on the CNC end milling process of halloysite nanotube with aluminium reinforced epoxy matrix (HNT/Al/Ep) hybrid composite. *HBRC Journal*, 10(2), 138-144. <https://doi.org/10.1016/j.hbrj.2013.09.007>
- Ramnath, B. V., Sharavanan, S., & Jeykrishnan, J. (2017). Optimization of process parameters in drilling of fibre hybrid composite using Taguchi and grey relational analysis. *IOP Conference Series: Materials Science and Engineering* 183(1), Article 012003. <https://doi.org/10.1088/1757-899X/183/1/012003>
- Sheikh-Ahmad, J., & Shahid, A. H. (2013). Effect of edge trimming on failure stress of carbon fiber polymer composites. *International Journal of Machining and Machinability of Materials*, 13(2-3), 331-347. <https://doi.org/10.1504/IJMMM.2013.053231>
- Sundi, S. A., Izamshah, R., Kasim, M. S., & Abdullah, M. K. A. (2019). Effect of machining parameters on surface quality during edge trimming of multi-directional CFRP material: Taguchi method. *IOP Conference Series, Materials Science and Engineering*, 469(1), Article 012095. <https://doi.org/10.1088/1757-899X/469/1/012095>.
- Sundi, S. A., Izamshah, R., Kasim, M. S., Amin, A. M., & Kumaran, T. (2019). Influence of router tool geometry on surface finish in edge trimming of multi-directional CFRP material. *IOP Conference Series: Materials Science and Engineering*, 469(1), Article 012026. <https://doi.org/10.1088/1757-899X/469/1/012026>.

- Urresti, I., Llanos, I., de Lacalle, L. L., & Zelaieta, O. (2022) Study of the surface integrity during CFRP trimming: Tool material and geometry, fiber orientation and tool wear effect analysis. *Procedia CIRP*, 108, 660-664. <https://doi.org/10.1016/j.procir.2022.03.102>
- Wang, H., Sun, J., Li, J., Lu, L., & Li, N. (2016). Evaluation of cutting force and cutting temperature in milling carbon fiber-reinforced polymer composites. *International Journal of Advanced Manufacturing Technology*, 82(9–12), 1517–1525. <https://doi.org/10.1007/s00170-015-7479-2>.

The Mechanical and Physical Properties of 3D Printing Filament made from Recycled Polypropylene and Ground Tyre Rubber Treated with Alkali

Yusliza Yusuf^{1*}, Nuzaimah Mustafa¹, Yusra Fitri Yusoff¹ and Dwi Hadi Sulistyarini²

¹*Fakulti Teknologi dan Kejuruteraan Industri dan Pembuatan, Universiti Teknikal Malaysia Melaka, Hang Tuah Jaya, 76100, Durian Tunggal, Melaka, Malaysia*

²*Faculty of Industrial Engineering, Brawijaya University, Malang, 65145, Jawa Timur, Indonesia*

ABSTRACT

When molten, used vehicle tyres are unable to decompose or be recycled. Despite global efforts to find new uses for these materials, many worn tyres are still dumped in landfills. Therefore, this study proposes using ground tyre rubber (GTR) as a fill material for recycled polypropylene 3D printing filament. The filament composite's physical and mechanical properties will be assessed in this investigation. GTR is expected to give the filament elastic characteristics, which could lead to rubber-like filaments. This study filled recycled polypropylene (rPP) polymer matrix composites with GTR to make filament. The mechanical and physical properties of a 3D-printed specimen made from rPP and GTR filament with varying compositions were analysed. Compared to pure rPP, rPP/GTR samples with 3 wt% GTR had a maximum tensile strength of 716.76 MPa. The flexural test findings showed that rPP/GTR with 3 wt% GTR had the highest flexural strength at 80.53 MPa, followed by rPP/1 wt% GTR at 65.38 MPa. In physical tests, the rPP/GTR at 5 wt% GTR had the highest water absorption at 5.41 %, and the wt% of GTR connected directly with water absorption. This study has shown that affordable, environmentally friendly rPP/GTR filaments can be developed with less amount of GTR content (3 wt%) and used for

3D printing applications, helping to lessen the impact of plastic and waste while having valuable mechanical and physical properties that are comparable to those of the pure polypropylene material produced.

Keywords: 3D printing filament, ground tyre rubber, mechanical properties, physical properties, recycled polypropylene, waste management

ARTICLE INFO

Article history:

Received: 16 August 2023

Accepted: 09 May 2024

Published: 14 June 2024

DOI: <https://doi.org/10.47836/pjst.32.S2.10>

E-mail addresses:

yusliza@utem.edu.my (Yusliza Yusuf)

nuzaimah@utem.edu.my (Nuzaimah Mustafa)

B091910109@utem.edu.my (Yusra Fitri Yusoff)

dwhadi@ub.ac.id (Dwi Hadi Sulistyarini)

*Corresponding author

INTRODUCTION

Ground tyre rubber (GTR) is a form of recycled material composed of tyres that have been shredded and ground into fine particles. GTR has been utilised in an expanding number of applications, including construction, roads, and sporting surfaces. In addition, using GTR in these applications reduces the number of tyres that wind up in landfills or the environment, thereby promoting sustainable waste management (Fazli et al., 2020). As interest in sustainability increases, GTR will likely become more widespread.

On the other hand, recycled polypropylene (rPP) is a plastic made from post-consumer and post-industrial waste. It is a thermoplastic polymer used in a variety of products, including food packaging, automotive components, and domestic goods. Recycled polypropylene is an environmentally preferable alternative to virgin plastic because it reduces waste sent to landfills and conserves natural resources. In the coming years, the demand for rPP is projected to increase significantly due to the world's ongoing emphasis on sustainability and waste reduction (Pandey et al., 2023).

Utilising recycled materials to produce 3D printing filament is a manufacturing strategy that is gathering popularity in the 3D printing industry. Filament for 3D printing is the material utilised by 3D printers to produce three-dimensional objects. Historically, 3D printing filament has been manufactured from non-biodegradable virgin materials such as ABS or PP, contributing to the growing plastic waste problem. 3D printing filament can be manufactured environmentally using recycled materials such as PP bottles or industrial waste (Zander et al., 2019). Compared to the production of virgin filament, the procedure conserves resources, reduces waste, and has a smaller carbon footprint.

It is currently impossible to 3D print with natural rubber, ethylene propylene diene monomer (EPDM) rubber, or other rubber materials that do not readily liquify or transform into a cured state. Depending on the ultimate applications, this poses limitations for 3D-printable rubber products (Drossel et al., 2020). At the moment, thermoplastic polyurethane (TPU) and thermoplastic elastomer (TPE) are the most effective rubber-like materials for 3D printing (Leon-Calero et al., 2021). TPE, for example, is a rubber-like filament used to make flexible and durable objects. It is resistant to stress and impact, unlike PLA and ABS. Its qualities allow it to be employed in 3D printing automobile parts, toys, and medical supplies, to mention a few applications. Nevertheless, TPE filaments exhibit certain drawbacks. First, they are not recyclable. Second, they are not user-friendly for beginners, as printer settings must be precise to achieve the desired results (Musa et al., 2022). In addition, TPE is more temperature-sensitive than other materials, and almost every printed model requires a rework procedure.

Thus, this study aims to develop a new filament composite for 3D printing applications incorporating rPP and GTR as fillers. This study intends to evaluate the mechanical and physical properties of the completed filament composite. The usage of GTR in this study is expected to impart elastic qualities to the created filament, providing a new option for

the creation of rubber-based filaments while also assisting in the utilisation of GTR in new applications.

LITERATURE REVIEW

Rapid growth in the automotive industry generates an increasing quantity of waste rubber, especially from worn-out tyres. The natural and synthetic rubbers in used tyres can be used as strengthening materials in composite manufacture. Incorporating used tyres into virgin matrices reduces the final product's cost and lowers the quantity of virgin materials needed. Ground tyre rubber (GTR) is a substance that is derived from the process of recycling and repurposing waste tyres. The GTR recycling process occurs due to its positive environmental and economic impacts. Alkadi et al. (2019) and Tri et al. (2022) stated that the production of GTR is environmentally friendly and economically advantageous, as it eliminates some of the operations required to recycle natural rubber.

The utilisation of GTR as a filler in diverse fundamental materials also contributes to reducing final product costs. According to Alkadi et al. (2019) and Nguyen et al. (2022), it has been observed that GTR additions have improved characteristics such as lightweight composition, improved thermal and acoustic capabilities, and resistance to booth ageing and severe weather conditions. Rapidly, it became evident that there was a need to assess and ensure the quality of GTR. The two primary quality attributes of tyre rubber (GTR) that are of utmost importance are the particle size range, also known as particle size distribution, and the level of contamination.

According to Alkadi et al. (2019), a correlation exists between the amount of filler in a matrix and the mechanical characteristics of composite materials, including tensile strength, compression strength, and abrasion resistance. Furthermore, the interplay between polymer molecules and the surface of additives can substantially influence the composite materials' mechanical properties. In order to obtain the appropriate composite for a specific application, it is imperative to take into account the composition, properties (such as particle size), and processing (including manufacturing method and pre-treatment) of tyre rubber GTR when it is used as a filler in the rubber matrix.

According to previous research by Kociuszko et al. (2022), highly filled PP/GTR compounds can be mass-produced using a fine portion of tyre rubber GTR with an ordinary particle size of 400 μm as the filler. Standard injection moulding machines can produce thermoplastic compounds when rubber powder is adequately prepared. The PP/GTR90 and PP/GTR90-P compositions have a positive cohesion despite excessive filling. Additionally, Hernandez et al. (2017) introduced a GTR/PP composite material and investigated the impact of sulfuric acid treatment on its mechanical and thermal properties. The study found that exposing the rubber particles to an acidic treatment enhanced their surface roughness and porosity, improving the mechanical characteristics of GTR/PP composites.

GTR can be a filler in the polymer matrix to create composite materials suitable for printing ink using the direct-printing method. The findings indicate that 3D-printed samples exhibit similar tensile strength to moulded samples. Additionally, surface modification of GTR, such as chemical modification, has been demonstrated to enhance the tensile strength of the 3D-printed samples (Alkadi et al., 2017). Nguyen et al. (2022) also developed GTR-based composite materials by incorporating up to 50 wt% rubber fillers into ABS as the main matrix. The study found that adding rubber from 0 wt% to 50 wt% in the 3D-printed GTR-based composite led to a 260% enhancement in damping capabilities. Additionally, specimens containing larger rubber particles had longer contact lines with the host polymeric matrix.

As a result, the energy dissipation is increased, leading to improved overall damping characteristics of the 3D printed composites. Another work by Laoutid et al. (2021) included GTR into ABS at 15 wt% and 30 wt% to produce filaments suitable for 3D printing with FDM. Using a compatibilizing agent to create composite materials with improved mechanical characteristics is advisable. A compatibilizing agent decreases the interfacial tension between incompatible tyre and polymeric phases, serving as a barrier to hinder the coalescence of GTR particles.

Polypropylene (PP) is categorised as a thermoplastic material. Unlike thermosets, thermoplastics can be heated and reshaped indefinitely (Satya & Sreekanth, 2020). Thermoplastics are lightweight and durable and can be manufactured with high precision. Polypropylene exhibits a notable glass transition temperature or softening point, demonstrating a strong resistance to bending stress, exhibiting minimal water absorption, displaying great electrical resistance, maintaining dimensional stability, possessing high impact strength, and being non-toxic.

Polypropylene (PP) has been employed as the matrix material. Polymers exhibiting low melting, such as PP, are widely employed within the 3D printing industry sector owing to their advantageous characteristics, including reduced weight, cost-effectiveness, and versatile processing capabilities. The wide-ranging uses of 3D-printed polymer products are hindered by their limited mechanical strength and functionality, notwithstanding their geometric complexity. Table 1 demonstrates the benefits and drawbacks of some of the 3D printing filaments currently available and commonly used in FDM-based 3D printing.

Integrating diverse materials to achieve specific mechanical and functional properties presents a viable strategy for addressing mechanical performance and functioning challenges. There has been a notable surge in curiosity over the past few years regarding the advancement of composite materials that can be effectively utilised with currently available printers (Wang et al., 2017). Composite 3D printing has utilised numerous materials, including thermoplastics based on nylon and continuous fibres, such as fibreglass, carbon fibre, high-temperature and high-strength fibreglass, and Kevlar materials. Fibreglass with

Table 1

Existing 3D printing filament advantages and drawbacks (Flynt, 2020)

Filament Material	Advantage	Disadvantage
Polylactic acid (PLA)	<ol style="list-style-type: none"> 1. Easy to use. 2. Biodegradable and made from sustainable sources. 3. Inexpensive. 4. Do not produce fumes while printing. 5. Does not warp. 	<ol style="list-style-type: none"> 1. Poor mechanical characteristics. 2. Low heat resistance 3. Tend to deform easily. 4. Naturally, it disintegrates over time. 5. Absorbs moisture easily.
Acrylonitrile Butadiene (ABS)	<ol style="list-style-type: none"> 1. Superior toughness. 2. Excellent impact resistance. 3. Chemical stability. 4. Good thermal stability. 5. Can be finished via an acetone vapour bath. 6. Inexpensive. 	<ol style="list-style-type: none"> 1. Non-biodegradable. 2. Highly prone to warping and stringing. 3. Gives off toxic fumes while printing. 4. Very irritating and noxious.
Nylon	<ol style="list-style-type: none"> 1. Very strong and flexible. 2. Thermally and chemically stable. 3. Abrasion resistant. 4. Takes up dyes easily. 	<ol style="list-style-type: none"> 1. Prints at very high temperatures. 2. Prone to warping and stringing. 3. Degrades under UV radiation. 4. Absorbs moisture easily.
Thermoplastic Polyurethane (TPU)	<ol style="list-style-type: none"> 1. Rubber-like flexibility. 2. Excellent layer-to-layer adhesion. 3. Impact resistant. 4. Resilient against solvents and oils. 	<ol style="list-style-type: none"> 1. Difficult to handle. 2. Poor bridging performance. 3. Cannot be smoothed or polished. 4. Prone to blobs and stringing.
Polycarbonate (PC)	<ol style="list-style-type: none"> 1. Excellent strength and impact resistance. 2. Flexible. 3. High tensile strength. 4. Heat-stable. 	<ol style="list-style-type: none"> 1. It requires a very high temperature for printing. 2. Prone to abrasion. 3. Resistance to scratches. 4. Difficult to work with.

high-temperature and high-strength properties has exceptional heat resistance, rendering it well-suited for various applications such as 3D-printed thermoforms, thermoset moulds, and welding fixtures. Consequently, this investigation aims to develop a new filament composite using rPP and GTR as reinforcements. This investigation aims to assess the physical and mechanical properties of the completed filament composite. The use of GTR in this study is expected to contribute elastic properties to the produced filament and may offer an alternative for producing rubber-based filaments.

MATERIALS AND METHODS

Raw Materials Preparation

The GTR particles, produced by mechanical pulverising tyre rubber in an ambient environment, were obtained from the waste processing industry in Selangor, Malaysia and used as received. The recycled rubber particles exhibited a particle size distribution ranging from 10 to 600 μm as determined by the Malvern particle size analyser. Prior to that, the

GTR powder was alkaline-treated using 6 wt% sodium hydroxide (NaOH) in water (Ismail et al., 2021). This treatment process is necessary to modify the surface properties of the rubber particles, which can improve their compatibility with other materials and enhance their performance in various applications.

The GTR was stirred evenly in 6 wt% NaOH solution to ensure it was mixed thoroughly and later soaked for 40 minutes to ensure that all the rubber particles were in contact with the solution (Nuzaimah et al., 2020). Afterwards, the GTR was washed and rinsed with distilled water to eliminate any leftover NaOH solution and other impurities and dried for 24 hours at 60°C using an oven. The recycled polypropylene (rPP) used in this study was post-manufacturer recycled polymer obtained from San Miguel Plastic Melaka in granulated form. Figure 1 depicts this study's overall process flow for raw material preparation.

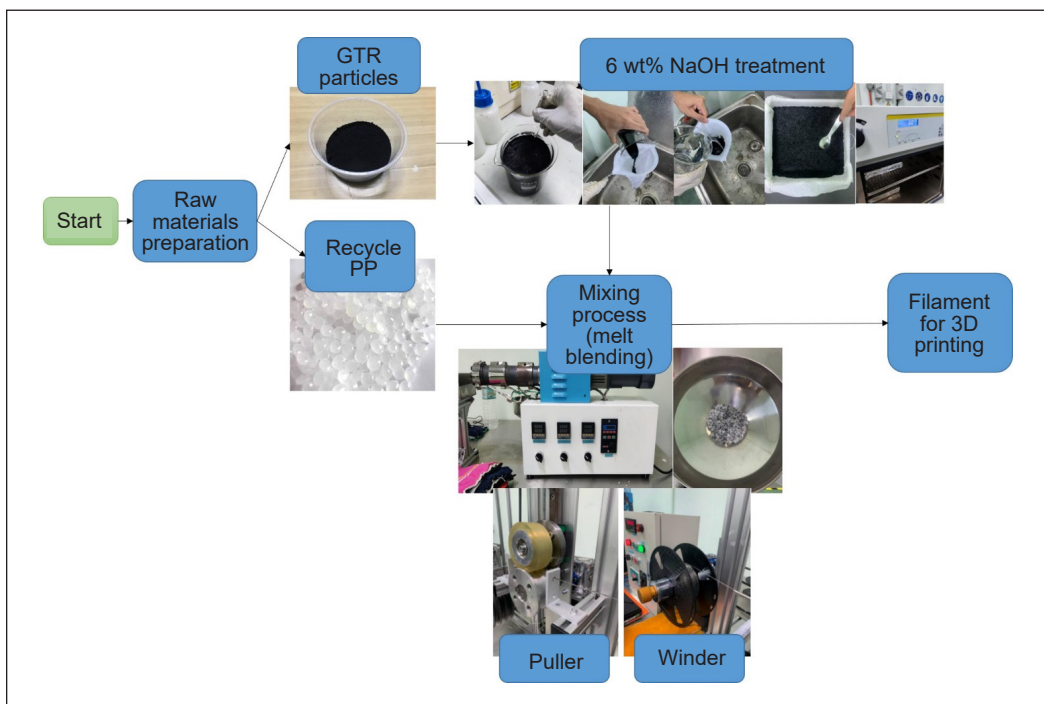


Figure 1. Overall process flow of raw material preparation in this study

Filament Production

The rPP and GTR were compounded by melt blending at various compositions, as shown in Table 2, using a single screw extruder (Figure 2). The study utilised GTR content of 1%, 3%, and 5%, with a 0% GTR sample as the control. The low weight percentage of GTR utilised in this study is determined by the researcher's assessment of the performance of rPP filament in combination with a natural fibre blend deemed more appropriate and of superior quality with reduced fibre content. Hence, the weight percentage content of GTR is considered appropriate

for the first study at lower levels to assess its compatibility with rPP and its potential usage as filament material. The barrel and nozzle zones of the extruder were pre-heated to 170°C and 180°C, respectively, prior to the feeding material process. The speed of the screw and side feeder was set to 18-20 rpm. Table 3 displays the overall extrusion process parameter. The filament was then cooled in a water bath and was coiled up and spooled on the spooler to maintain the acceptable filament diameter ranges.



Figure 2. Single screw extruder machine used in this study

Specimens Printing with 3D Printer

Samples were 3D printed using an FDM 3D printer utilising the produced filaments. The required (.stl) files for printing were created using the open-source Ultimaker Cura 4.8.0 software. The printed samples were the typical Type 1 ASTM D638 tensile test specimens and ASTM D790 rectangular shape. The printing process parameters used, which include a printing strategy of [0, 90] degrees and an infill percentage of 100 %, are shown in Table 4. The nozzle and bed of the printer printed the filament at 180–220°C and 85°C, respectively. The molten filament was fed via a 1 mm nozzle with a 0.32 mm layer thickness at 20 mm per minute.

Table 2
Various compositions of mixed rPP and GTR

	rPP (g)	GTR (g)	wt % of GTR
A	200	0	0
B	198	2	1
C	194	6	3
D	190	10	5

Table 3
Filament extrusion processing parameters

Parameter	Value
Barrel Temperature (°C)	170
Die/ Nozzle Temperature (°C)	180
Die/ Nozzle diameter (mm)	1.75
Screw extrusion speed (rpm)	18–20
Speed of Filament pulling roller (mm/s)	300
Speed of Filament winding roller (mm/s)	200

Table 4
3D printing process parameter

Parameters	Value
Printing temperature (°C)	190
Printing temperature, initial layer (°C)	200
Build plate/ bed temperature (°C)	85
Build plate temperature, initial layer (°C)	95
Infill pattern	Lines
Infill flow (%)	110
Layer height (mm)	0.3
Line width (mm)	0.38
Top and bottom layers (layers)	2
Print speed (mm/s)	25
Initial layer speed (mm/s)	15
Build plate adhesion type	Brim

Mechanical Testing

Tensile tests were performed at ambient temperature in accordance with the ASTM D638 standard, utilising a 500N load cell and a strain rate of 10 mm/min on a Shimadzu Universal Tensile machine. A minimum of five dog bone specimens, each having a thickness of 3 mm, were utilised for every formulation. The averaged values of the tensile strength (σ_Y), tensile modulus (E), and yield strength (ϵ_b) were presented alongside their corresponding standard deviations.

The flexural tests were conducted using a Shimadzu Universal Tensile machine equipped with a 50N load cell, following the guidelines in ASTM D790 at ambient temperature. The experiment involved testing rectangular specimens of 60×12.7 mm². Each formulation was tested five times using a three-point bending mode with a span length of 60 mm. The specimens were tested at a speed of 2 mm/min.

Physical Testing

A water absorption test was also carried out to monitor the capacity of produced filaments to absorb moisture from their environment. A water absorption test was carried out according to ASTM D570 standards, with 3 samples for each parameter submerged in water for 24 hours, and the average value was calculated. Water absorption is expressed as an increase in weight per cent or % weight gain of a plastic specimen, as shown in Equation 1.

$$\text{Increase in weight, \%} = (\text{wet weight} - \text{conditioned weight} / \text{conditioned weight}) \times 100 \quad (1)$$

RESULTS AND DISCUSSION

Mechanical Properties

Tensile Properties. Figure 3 illustrates the variations in the tensile strength, yield strength, and elastic modulus of rPP/ GTR composites with respect to the percentage of GTR content. Incorporating GTR enhanced the tensile strength, yield strength, and elastic modulus of rPP compared to a control sample consisting of only rPP. For instance, increasing the GTR content by 1% and 3% increased the tensile strength by 528.19 N/m² and 716.76 N/m², respectively, compared to the tensile strength of pure rPP, which was 498.64 N/m². The rising trend relates to tensile strength properties, yield strength, and elastic modulus value. At 3 wt% GTR, the sample exhibited the highest values for tensile strength, yield strength, and elastic modulus; at 5 wt% GTR, the tensile properties exhibited a reducing trend.

The reduced tensile strength, yield strength, and elastic modulus properties observed in the presence of 5 wt% of GTR can be attributed to increased agglomeration and particle-matrix interaction caused by a higher quantity of GTR. It led to stress concentration points and weak interfacial adhesion, ultimately increasing the likelihood of crack

initiation and premature failure due to easier crack propagation (Fazli et al., 2020). In agreement with Shaker et al. (2019) and Wang et al. (2018) for recycled PE/GTR, it is evident that less GTR content contributes to increased tensile and yield strengths as well as elastic modulus. At lower GTR content, the effect of filler on tensile properties was found to be more significant, whereas at higher GTR content, poor interaction was the primary factor regulating tensile properties (Fazli et al., 2021). The optimal specific surface area of the filler promoted better interfacial stress transfer and interaction between GTR and rPP, making a quantity that was not excessive the most important factor for producing filament with good tensile strength.

Flexural Properties. Figure 4 depicts the flexural characteristics. The flexural strength of the material increased to 65.38 MPa and 80.53 MPa, respectively, when the GTR content was increased by 1 wt% and 3 wt%, respectively, in comparison to the flexural strength of pure rPP, which was 57.83 MPa. Additionally, the flexural modulus values improved to 1070.63 MPa and 1557.82 MPa, respectively, compared to the flexural modulus characteristics of pure rPP, which was 887.40 MPa. On the other hand, when the GTR concentration is about 5%, both flexural properties decline. This study showed a strong relationship between the mechanical properties of the filler dispersion (GTR) and the interfacial interaction, which is controlled by the concentration of the GTR. In addition, the flexural characteristics of the material are diminished when a significant quantity of GTR is utilised. This finding is consistent with the results for the previously tensile properties. Once more, the enhanced contact between GTR particles and thermoplastic molecules is responsible for the higher flexural characteristics, reducing structural flaws (Fazli et al., 2023).

An additional factor contributing to a reduction in flexural strength with increasing weight per cent GTR is the deterioration of the polymer matrix. In addition to disrupting the polymer matrix's homogeneity and integrity, introducing GTR particles may also introduce a

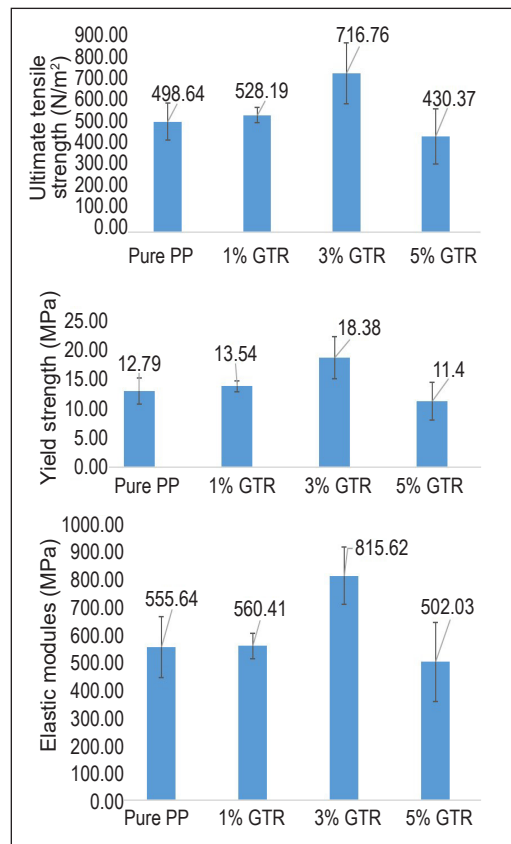


Figure 3. Tensile properties result

vulnerable point into the filament, rendering it more prone to deformation and stress-induced failure (Celestino & Aboelkheir, 2022). Furthermore, including rubber particles could potentially disrupt the intermolecular forces between the chains of polymers, resulting in a degradation of the material’s overall strength (Allegra et al., 2008). Consequently, the flexural strength may be diminished due to the compromised resistance of the polymer molecules to deformation.

Physical Properties

Water Absorption Properties. Figure 5 depicts the water absorption behaviour of the rPP/GTR filament generated. The GTR

addition boosted the water absorption characteristics of the filament in general. The presence of GTR particles, which increases the composite’s hydrophilic behaviour, and the presence of filler particles in the matrix, which can cause voids at the interface and increase the capacity of water molecules to penetrate the composite via capillary transport, are the two main causes of water absorption in composites (Mohammed et al., 2022). Both mechanisms were expected to become less active when the phases were suitably compatible. It suggested that water molecule diffusion through microscopic gaps between polymer macromolecules is the primary mechanism of water absorption inside composites.

CONCLUSION

Using recycled rubber particles, also called GTR, in a recycled thermoplastic matrix (rPP) improved mechanical qualities, even though a lower percentage of GTR was used. The presence of a significant amount of filler material led to a decrease in the mechanical properties of the composite material. It is primarily attributed to insufficient interfacial adhesion and inadequate contact between the cross-linked rubber particles and the thermoplastic chains. This study involved

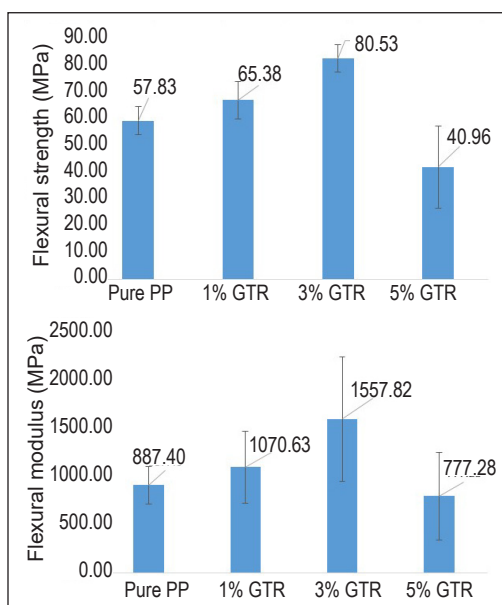


Figure 4. Flexural properties

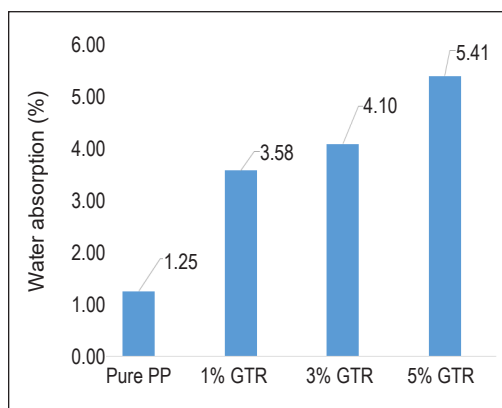


Figure 5. Percentage of water absorption in various compositions of rPP/ GTR and pure rPP

the production of samples by a 3D printing process, utilising a filament composed of a combination of recycled rubber particles (GTR) and recycled thermoplastic matrix (rPP). The samples were prepared with varying concentrations of GTR, specifically 1, 3, and 5 wt% GTR. The study's findings confirm that including GTR at a concentration of 3 wt% led to enhancements in tensile and flexural properties. Nevertheless, it was shown that the sample exhibited a higher water absorption rate with an increased quantity of GTR.

ACKNOWLEDGEMENT

The research conducted in this study received financial support from the Ministry of Higher Education Malaysia and an internal grant from Universiti Teknikal Malaysia Melaka (PJP/2020/FTKMP/PP/S01737).

REFERENCES

- Alkadi, F., Lee, J., Yeo, J. S., Hwang, S. H., & Choi, J. W. (2019). 3D printing of ground tyre rubber composites. *International Journal of Precision Engineering and Manufacturing - Green Technology*, 6(2), 211–222. <https://doi.org/10.1007/s40684-019-00023-6>
- Allegra, G., Raos, G., & Vacatello, M. (2008). Theories and simulations of polymer-based nanocomposites: From chain statistics to reinforcement. *Progress in Polymer Science*, 33(7), 683-731. doi.org/10.1016/j.progpolymsci.2008.02.003
- Celestino, R., & Aboelkheir, M. G. (2022). Recovery of tire rubber waste after UV treatment as a recycled aggregate in cementitious composites. *Materials Today: Proceedings*, 58, 1476-1479. doi.org/10.1016/j.matpr.2022.02.552.
- Drossel, W. G., Ihlemann, J., Landgraf, R., Oelsch, E., & Schmidt, M. (2020). Basic research for additive manufacturing of rubber. *Polymers*, 12(10), Article 2266. <https://doi.org/10.3390/polym12102266>
- Fazli, A., & Rodrigue, D. (2020). Recycling waste tyres into ground tyre rubber (GTR) / rubber compounds: A review. *Journal of Composites Science*, 4(3), Article 103. <https://doi.org/10.3390/jcs4030103>
- Fazli, A., & Rodrigue, D. (2021). Effect of ground tyre rubber (GTR) particle size and content on the morphological and mechanical properties of recycled high-density polyethylene (rHDPE)/GTR blends. *Recycling*, 6(3), Article 44. <https://doi.org/10.3390/recycling6030044>
- Fazli, A., & Rodrigue, D. (2023). Thermoplastic elastomers based on recycled high-density polyethylene/ground tyre rubber/ethylene vinyl acetate: Effect of ground tyre rubber regeneration on morphological and mechanical properties. *Journal of Thermoplastic Composite Materials*, 36(6), 2285-2310. <https://doi.org/10.1177/08927057221095388>
- Flynt, J. (2020, July 22). *The pros and cons of every 3D printing filament material*. 3Dinsider. <https://3dinsider.com/pros-and-cons-3d-printing-filaments/>
- Hernández, E. H., Gámez, J. F. H., Cepeda, L. F., Muñoz, E. J. C., Corral, F. S., Rosales, S. G. S., Velázquez, G. N., Morones, P. G., & Martínez, D. I. S. (2017). Sulfuric acid treatment of ground tire rubber and its

- effect on the mechanical and thermal properties of polypropylene composites. *Journal of Applied Polymer Science*, 134(21), Article 44864. <https://doi.org/10.1002/app.44864>
- Ismail, N. F., Radzuan, N. A. M., Sulong, A. B., Muhamad, N., & Haron, C. H. C. (2021). The effect of alkali treatment on physical, mechanical and thermal properties of kenaf fibre and polymer epoxy composites. *Polymers*, 13(12), Article 2005. <https://doi.org/10.3390/polym13122005>
- Kościuszko, A., Sykutera, D., Czyżewski, P., Hoyer, S., Kroll, L., & Szczupak, B. (2022). Processing and mechanical properties of highly filled PP/GTR compounds. *Materials*, 15(11), Article 3799. <https://doi.org/10.3390/ma15113799>
- Leon-Calero, M., Vales, S.C.R., Marcos-Fernandez, A., Rodriguez-Hernandez, J. (2021). 3D printing of thermoplastic elastomers: roles of the chemical composition and printing parameters in the production of parts with controlled energy absorption and damping capacity. *Polymers*, 13(20), Article 3551. <https://doi.org/10.3390/polym13203551>
- Laoutid, F., Lafqir, S., Toncheva, A., & Dubois, P. (2021). Valorization of recycled tire rubber for 3D printing of ABS- and TPO-based composites. *Materials*, 14(19), Article 5889. <https://doi.org/10.3390/ma14195889>
- Mohammed, M., Rahman, R., Mohammed, A. M., Adam, T. O. Betar, B., F., Osman, A. S., & Dahham, O. (2022). Surface treatment to improve water repellence and compatibility of natural fibre with polymer matrix: Recent advancement. *Polymer Testing*, 115, Article 107707. <https://doi.org/10.1016/j.polymertesting.2022.107707>
- Musa, L., Kumar, N. K., Abd Rahim, S. Z., Rasidi, M. S. M., Rennie, A. E. W., Rahman, R., Kanani, A. Y., & Azmi, A. A. (2022). A review on the potential of polylactic acid based thermoplastic elastomer as filament material for fused deposition modelling. *Journal of Materials Research and Technology*, 20, 2841–2858. <https://doi.org/10.1016/j.jmrt.2022.08>
- Nguyen, H. T., Crittenden, K., Weiss, L., & Bardaweel, H. (2022). Recycle of waste tyre rubber in a 3D printed composite with enhanced damping properties. *Journal of Cleaner Production*, 368, Article 133085. <https://doi.org/10.1016/j.jclepro.2022.133085>
- Nuzaimah, M., Sapuan, S. M., Nadlene, R., & Jawaid, M. (2020). Sodium hydroxide treatment of waste rubber crumb and its effects on properties of unsaturated polyester composites. *Applied Sciences*, 10(11), Article 3913. doi.org/10.3390/app10113913
- Pandey, P., Dhima M., Kansai, A., & Subudhi, S. P. (2023). Plastic waste management for sustainable environment: Techniques and approaches. *Waste Disposal & Sustainable Energy*, 5, 205–222. <https://doi.org/10.1007/s42768-023-00134-6>.
- Satya, S. K., & Sreekanth, P. S. R. (2020). An experimental study on recycled polypropylene and high-density polyethylene and evaluation of their mechanical properties. *Materials Today: Proceedings*, 27, 920–924. <https://doi.org/10.1016/j.matpr.2020.01.259>
- Shaker, R., & Rodrigue, D. (2019). Rotomolding of thermoplastic elastomers based on low-density polyethylene and recycled natural rubber. *Applied Science*, 9(24), Article 5430. <https://doi.org/10.3390/app9245430>
- Wang, X., Jiang, M., Zhou, Z., Gou, J., & Hui, D. (2017). 3D printing of polymer matrix composites: A review and prospective. *Composites Part B: Engineering*, 110, 442–458. <https://doi.org/10.1016/j.compositesb.2016.11.034>

- Wang, Y. H., Chen, Y. K., & Rodriguw, D. (2018). Production of thermoplastic elastomers based on recycled PE and ground tyre rubber: Morphology, mechanical properties and effect of compatibilizer addition. *International Polymer Processing*, 33(4), 525-534. <https://doi.org/10.3139/217.3544>
- Zander, N. E., Gillian, M., Burchhard, Z., & Gardea, F. (2019). Recycled polypylene blends as npovel 3D printing materials. *Additive Manufacturing*, 25, 122-130. <https://doi.org/10.1016/j.addma.2018.11.009>

REFEREES FOR THE PERTANIKA JOURNAL OF SCIENCE & TECHNOLOGY

Vol. 32 (S2) 2024

The Editorial Board of the Pertanika Journal of Science and Technology wishes to thank the following:

Ahmad Ilyas bin Rushdan
(UTM, Malaysia)

Mohd Zuhri Mohamed Yusoff
(UPM, Malaysia)

Arjulizan Rusli
(USM, Malaysia)

Muhammad Hafiz Hassan
(USM, Malaysia)

Atiqah Mohd Afdzaluddin
(UKM, Malaysia)

Muhammed Nafis Osman Zahid
(UMPSA, Malaysia)

Heru Suryanto
(UM, Indonesia)

Nasrul Hadi Johari
(UMPSA, Malaysia)

Izwan Ismail
(UMPSA, Malaysia)

Razaina Mat Taib
(USM, Malaysia)

Mohd Azaman Md Deros
(UniMAP, Malaysia)

Reni Dwi Astuti
(UAD, Indonesia)

Mohd Rizal Alkahari
(UTeM, Malaysia)

Suhad Dawood Salman
(Mustansiriyah University, Baghdad)

Mohd Supian Abu Bakar
(UNITEN, Malaysia)

UAD - Universitas Ahmad Dahlan
UKM - Universiti Kebangsaan Malaysia
UM - Universitas Negeri Malang
UniMAP - Universiti Malaysia Perlis
UNITEN - Universiti Tenaga Nasional

UMPSA - Universiti Malaysia Pahang Al-Sultan Abdullah
UPM - Universiti Putra Malaysia
USM - Universiti Sains Malaysia
UTeM - Universiti Teknikal Malaysia Melaka
UTM - Universiti Teknologi Malaysia

While every effort has been made to include a complete list of referees for the period stated above, however if any name(s) have been omitted unintentionally or spelt incorrectly, please notify the Chief Executive Editor, *Pertanika* Journals at executive_editor.pertanika@upm.edu.my

Any inclusion or exclusion of name(s) on this page does not commit the *Pertanika* Editorial Office, nor the UPM Press or the university to provide any liability for whatsoever reason.

Mechanical Properties of Thermoplastic Cassava Starch/Coconut Fibre Composites: Effect of Fibre Size	91
<i>Ridhwan Jumaidin, Ainin Sofiya Gazari, Zatil Hafila Kamaruddin, Zatil Hazrati Kamaruddin, Nazri Huzaimi Zakaria, Syahibudil Ikhwan Abdul Kudus, Mohd Shukri Yob, Fudhail Abd Munir and Meysam Keshavarz</i>	
Design Ideation and Selection of Under-Piston Door for a Two-stroke Marine Engine Using Hybrid TRIZ-biomimetic and MCDM Methods	115
<i>Yiow Ru Vern, Muhd Ridzuan Mansor, Mohd Adrinata Shaharuzaman and Basori</i>	
Effect of Cutting Speed and Feed Per Tooth on the Trimmed Surface Roughness and Tool Wear During Milling of CFRP: Aerostructural Part	135
<i>Syahrul Azwan Sundi, Izzat Afandi Abdul Hakim, Mohd Farid Mahadi, Noramin Nazar Shah, Raja Izamshah, Intan Sharhida Othman, Mohd Shahir Kasim and Mohd Nor Hafizi Noordin</i>	
The Mechanical and Physical Properties of 3D Printing Filament made from Recycled Polypropylene and Ground Tyre Rubber Treated with Alkali	151
<i>Yusliza Yusuf, Nuzaimah Mustafa, Yusra Fitri Yusoff and Dwi Hadi Sulistyarini</i>	

Sustainable Design and Manufacturing

Preface	i
<i>Mastura Mohammad Taha</i>	
Flow Analysis and Shear Rate Comparison of Counter-rotating and Co-rotating Intermeshing Twin-screw Extruders for Filament Extrusion of Polypropylene-based Biocomposites	1
<i>Abdul Munir Hidayat Syah Lubis, Syahibudil Ikhwan Abdul Kudus, Ammar Syafi Amran, Nuzaimah Mustafa, Mastura Mohammad Taha and Mohd Adrinata Shahraruzaman</i>	
Conceptual Design and Materials Selection of the FDM Composites for Passenger Vehicle's Spoiler	21
<i>Mohd Adrinata Shahraruzaman, Syed Muhammad Ayyub Sayed Idros, Mastura Mohammad Taha, Muhd Ridzuan Mansor, Ridhwan Jumaidin and Hilmi Senan</i>	
Environmental Assessment on Fabrication of Bio-composite Filament Fused Deposition Modeling Through Life Cycle Analysis	37
<i>Muhammad Farhan, Mastura Mohammad Taha, Yusliza Yusuf, Syahrul Azwan Sundi and Nazri Huzaimi Zakaria</i>	
A Study on the Thermal Distribution of the Thermoforming Process for Polyphenylene Sulfite (Polyphenylene Sulfide) PPS Composites Towards Out of Autoclave Activity	49
<i>Bushra Rashid, Nadlene Razali, Mohamad Shukri Zakaria, Muhammad Zaid Harith Ramlan, Hasanudin Hamdan, Emy Aqillah Sharif, Noryani Muhammad and Syazwan Ahmad Rashidi</i>	
Material Selection of Natural Fibre Composite Webbing Sling Using Rule of Mixture	61
<i>Noryani Muhammad, Nur Ain Fatimah Roslan and Mohd Syahril Abd Rahman</i>	
The Influence of MAPP and MAPE Compatibilizers on Physical and Mechanical Properties of 3D Printing Filament Made of Wood Fiber/ Recycled Polypropylene	77
<i>Nuzaimah Mustafa, Yusliza Yusuf, Syahibudil Ikhwan Abdul Kudus, Nadlene Razali, Dwi Hadi Sulistyarini, Mohd Hafizi Halim and Aenderson Chaong Anak Ujih</i>	



Pertanika Editorial Office, Journal Division,
Putra Science Park,
1st Floor, IDEA Tower II,
UPM-MTDC Center,
Universiti Putra Malaysia,
43400 UPM Serdang,
Selangor Darul Ehsan
Malaysia

<http://www.pertanika.upm.edu.my>
Email: executive_editor.pertanika@upm.edu.my
Tel. No.: +603- 9769 1622

PENERBIT
UPM
UNIVERSITI PUTRA MALAYSIA
P R E S S

<http://www.penerbit.upm.edu.my>
Email: penerbit@upm.edu.my
Tel. No.: +603- 9769 8851

